Investigation of Corticotropin-Releasing Hormone Receptor Signalling Properties

By

Danijela Markovic

BSc.

A thesis submitted in fulfillment of the requirements for the degree of Doctor of Philosophy.

University of Warwick, Warwick Medical School,

Division of Clinical Sciences

July 2007

To Vlad

CONTENTS

List of Figures ..... **IX**

List of Tables ..... **XIII**

Acknowledgements ..... **XIV**

Declaration ..... **XV**

Publications ..... **XV**

Summary ..... **XVI**

Abbreviations ..... **XVII**

1 INTRODUCTION 1
1.1 The corticotropin-releasing hormone (CRH) 1
1.1.1 The family of CRH-related peptides 1
1.1.2 The action of CRH and CRH-related peptides 3
1.1.2.1 The pituitary and extrapituitary action of CRH and CRH-related peptides 3
1.1.2.2 CRH and CRH-related peptides action in pregnancy 5
1.1.2.3 CRH and CRH-related peptide action in metabolism and energy homeostasis 6
1.2 CRH-Binding Protein (CRH-BP) 7
1.3 The CRH receptor (CRH-R) 9
1.3.1 The CRH-R type 1 (CRH-R1) 10
1.3.2 The CRH-R type 2 (CRH-R2) 14
1.4 Intracellular signalling of GPCRs 17
1.4.1 CRH-R coupling to G-proteins, second messengers and downstream signals 18
1.5 Termination of GPCRs signalling 21
1.5.1 Receptor desensitization 21
1.5.1.1 G-protein coupled receptor kinases 22
1.5.1.2 The arrestin family 23
1.5.2 Receptor internalization 25
1.5.3 Receptor down-regulation 27
1.5.4 Receptor resensitization 28
1.5.5 CRH-R desensitization and internalization 28
1.6 GTPase Rho and Rho-dependent response 30
1.7 Nuclear factor kappa B (NF-κB) 33
1.7.1 NF-κB activation 36
1.8 Brown adipose tissue 38
1.8.1 Lipolysis and proteins involved in lipolysis 39
1.8.2 Thermogenesis in BAT 41
1.8.3 BAT and regulation of total body fat 43
1.9 Aim of the study 45

2 MATERIALS AND METHODS 46
2.1 LIST OF BUFFERS AND CHEMICALS 46
2.1.1 Chemicals 51
2.2 PATIENTS 52
2.3 TISSUE CULTURE METHODS 53
2.3.1 Primary myometrial cell cultures 53
2.3.1.1 Digestion and primary culture 53
2.3.1.2 Subculture of the human myometrial smooth muscle cells (HMSM cells) 54
2.3.1.3 Stimulation of HMSM cells 54
2.3.2 Culture of HEK 293 cell line 55
2.3.3 Transient transfection in HEK293 cells and HMSM cells 56
2.3.4 Transient transfection of HEK293 with the pBudCE.4.1 mammalian expression plasmid 57
2.3.5 Stable transfection in HEK293 cells (st293 R2β) 58
2.3.5.1 MTT assay 60

2 MATERIALS AND METHODS 46
2.1 LIST OF BUFFERS AND CHEMICALS 46
2.1.1 Chemicals 51
2.2 PATIENTS 52
2.3 TISSUE CULTURE METHODS 53
2.3.1 Primary myometrial cell cultures 53
2.3.1.1 Digestion and primary culture 53
2.3.1.2 Subculture of the human myometrial smooth muscle cells (HMSM cells) 54
2.3.1.3 Stimulation of HMSM cells 54
2.3.2 Culture of HEK 293 cell line 55
2.3.3 Transient transfection in HEK293 cells and HMSM cells 56
2.3.4 Transient transfection of HEK293 with the pBudCE.4.1 mammalian expression plasmid 57
2.3.5 Stable transfection in HEK293 cells (st293 R2β) 58
2.3.5.1 MTT assay 60
2.3.6 Clathrin siRNA transfection to st.293-R2β 60
2.3.7 Culture of T37i cells 60
2.3.7.1 Oil Red O staining 61
2.3.7.2 Stimulation of T37i cells 61
2.3.7.3 Cell proliferation assay 62
2.3.7.4 Glycerol release assay 62
2.4 SECOND MESSENGER STUDIES: cAMP PRODUCTION 63
2.4.1 Stimulation of cells 63
2.4.2 Receptor desensitization/ cAMP production 64
2.4.3 cAMP measurement 64
2.5 MAPK ACTIVATION STUDIES 65
2.5.1 Stimulation of cells 65
2.6 MOLECULAR BIOLOGY TECHNIQUES 65
2.6.1 Gel electrophoresis of DNA and RNA 65
2.6.2 Gel purification of DNA fragments 65
2.6.3 RNA isolation 66
2.6.3.1 RNA extraction from BAT 66
2.6.4 Determination of DNA and RNA concentration 66
2.6.5 RT-PCR (reverse transcription polymerase chain reaction) 67
2.6.6 Primers design 67
2.6.7 Polymerase chain reaction (PCR) 68
2.6.8 Real time PCR performed on a Light Cycler system 69
2.6.9 Semi-quantitative RT-PCR analysis 70
2.6.10 Real time PCR performed on a TaqMan System 71
2.7 MUTAGENESIS AND CLONING TECHNIQUES 73
2.7.1 PCR mutagenesis of 14 amino acids within the 7th transmembrane domain (TMD) of CRH-R1 73
2.7.2 Digestion and ligation of CRH-R1α and CRH-R1d mutant inserts into pcDNA.3.1(+) 76
2.7.3 PCR mutagenesis of 4 amino acids in the C-terminus of CRH-R2β 77
2.8 DUAL EXPRESSION VECTOR 78
2.9 BACTERIAL METHODS 80

2.11 IMMUNOCYTOCHEMISTRY AND CONFOCAL MYCROSCOPY ...91
2.11.1 Preparation of cover slips ... 91
2.11.2 Plating cells on the cover slips ... 91
2.11.3 Stimulation of cells ... 91
2.11.4 Fixing the cells ... 92
2.11.5 Immunostaining ... 92
2.11.6 Fixing and immunostaining for RhoA translocation ... 94
2.11.7 Confocal microscopy ... 95
2.11.8 Quantitative analysis of protein localization ... 96
2.12 STATISTICS ... 96

3 EXPRESSION AND INTERNALIZATION PROPERTIES OF CRH-R1 SPLICE VARIANTS IN TRANSIENTLY TRANSFECTED HEK293 CELLS ... 98
3.1 INTRODUCTION ... 98
3.2 RESULTS ... 101
3.2.1 The cellular expression of CRH-R1 variants ... 101
3.2.2 Internalization characteristics of CRH-R1α ... 103
3.2.3 Internalization of CRH-R1α leads to β-arrestin recruitment to the plasma membrane ... 105
3.2.4 Internalization characteristics of CRH-R1β ... 108
3.2.5 Internalization of CRH-R1α leads to β-arrestin recruitment to the plasma membrane ... 109
3.2.6 Internalization characteristics of CRH-R1d ... 110
3.2.7 Heterologous internalization of CRH-R1α and CRH-R1β ... 113
3.3 DISCUSSION ... 117

4 STRUCTURAL AND FUNCTIONAL CHARACTERISTICS OF CRH-R1d ... 123
4.1 INTRODUCTION ... 123
4.2 RESULTS ... 125
4.2.1 Expression of CRH-R1d in over-expressing systems ... 125
4.2.2 Prediction of transmembrane domains and loops using the transmembrane helix prediction (TMHMM) algorithm ... 127
4.2.3 The C-terminus of CRH-R1d is in the extracellular space ... 128
4.2.4 Identification of amino acids encoded from the exon 13 that are necessary for the membrane expression of the receptor ... 130
4.2.5 Co-expression of CRH-R1d and CRH-R2β in HEK293 cells ... 134
4.2.5.1 Characterisation of cellular localisation of CRH-R2β-V5, CRH-R1α-myc, and CRH-R1d-myc ... 134
4.2.5.2 The effect of CRH-R1d on the CRH-R2β receptor internalization properties ... 139
4.2.5.3 The effect of CRH-R1d on CRH-R2β-mediated cAMP production ... 143
4.2.5.4 The effect of CRH-R1d on CRH-R2β-medaiated MAP kinase activation ... 145
4.3 DISCUSSION ... 146

5 SIGNALLING AND INTERNALIZATION CHARACTERISTICS OF CRH-R2β RECEPTOR 154
5.1 INTRODUCTION 154
5.2 RESULTS 156
5.2.1 Characterisation of st.293-R2β cells 156
5.2.2 Agonist induced cAMP production in st.293-R2β 163
5.2.3 CRH-R2β desensitization is dependent on the agonist potency 164
5.2.4 The effect of different growth conditions on UCN-II induced ERK1/2 and p38 MAPK phosphorylation in st.293-R2β 165
5.2.5 The ERK1/2 and p38 MAPK activation depends on type and dose of the agonists 167
5.2.6 Agonist-induced ERK1/2 and p38 MAPK phosphorylation is transient 170
5.2.7 The spatio-temporal characteristics of MAPK activation following UCN-II stimulation 171
5.2.8 UCN-II induced ERK1/2 phosphorylation, but not p38 MAPK phosphorylation, is protein kinase A (PKA) dependent 173
5.2.9 UCN-II induced ERK1/2 phosphorylation, but not p38 MAPK phosphorylation, is PI(3) kinase dependent 177
5.2.10 Internalisation characteristics of CRH-R2β 178
5.2.11 Internalization of CRH-R2β is β-arrestin and clathrin dependent . 181
5.2.12 UCN-II induced MAPK activation is independent of CRH-R2β endocytosis 186
5.2.13 UCN-II induced CRH-R2β desensitization is dependent on the CRH-R2β endocytotic machinery 190
5.2.14 UCN-II induced ERK1/2 phosphorylation negatively regulates CRH-R2β endocytosis via β-arrestin1 phosphorylation 192
5.2.15 The effect of ERK1/2 on CRH-R2β internalization 196
5.2.16 The role of C-terminus of CRH-R2β in the receptor mediated signalling 198
5.2.16.1 The role of CRH-R2β C-terminus in UCN-II induced cAMP production and CRH-R2β desensitization 199
5.2.16.2 The role of CRH-R2β C-terminus in UCN-II induced CRH-R2β internalization 200
5.2.16.3 The role of CRH-R2β C-terminus in UCN-II induced ERK1/2 and p38 MAPK phosphorylation 203
5.3 DISCUSSION 205

6 THE REGULATION OF EXPRESSION AND SIGNALLING CHARACTERISTICS OF ENDOGENOUS CRH-Rs IN HUMAN PREGNANT MYOMETRIAL CELLS 214
6.1 INTRODUCTION 214
6.2 RESULTS 219
6.2.1 CRH-R mRNA and protein expression in primary myometrial smooth muscle cells 219
6.2.2 Effects of IL-1β on PGHS-2 mRNA and protein expression in primary myometrial smooth muscle cells. 222

6.2.3 Effects of IL-1β on CRH-R1 mRNA and protein expression in primary myometrial smooth muscle cells 225
6.2.4 Signalling pathways mediating IL-1β effects in myometrial cells 229
6.2.5 Effects of IL-1β on CRH-induced myometrial cAMP response 232
6.2.6 The effect of UCN-II on cAMP production 234
6.2.7 The effect of UCN-II on MAPK activation 235
6.2.8 CRH-R2 mediated RhoA translocation 238
6.2.9 Methods for monitoring UCN-II induced RhoA translocation and activation 239
6.2.10 UCN-II induced CRH-R internalization 242
6.3 DISCUSSION 243

7 CHARACTERISATION OF CRH RECEPTOR SIGNALLING AND BIOLOGICAL PROPERTIES IN BROWN ADIPOCYTES 251
7.1 INTRODUCTION 251
7.2 RESULTS 254
7.2.1 Expression of CRH-R in T37i cells 254
7.2.2 Agonist induced cAMP production in T37i adipocytes 257
7.2.3 Agonist induced MAPK activation in T37i adipocytes 259
7.2.4 The involvement of PKA and PI(3)-kinase in UCN-II induced MAPK activation 263
7.2.5 Agonists induced proliferation of T37i fibroblasts 264
7.2.6 Agonist induced lipolysis in T37i adipocytes 265
7.2.7 The effect of CRH on perilipin and HSL translocation in T37i adipocytes 267
7.3 DISCUSSION 270

8 CONCLUSION 275

9 BIBLIOGRAPHY 279

List of Figures

Figure 1. 1 Schematic representation of POMC prohormone..... 3
Figure 1.2 CRH-R1 isoforms. 13
Figure 1.3 CRH-R2 isoforms. 16
Figure 1.4 The G-protein cycle. 18
Figure 1.5 Structural and functional domains of β-arrestin1 and β-arrestin2. 25
Figure 1.6 RhoA activation cycle. 32
Figure 1.7 NF-κB activation pathway. 37
Figure 1.8. PKA-stimulated lipolysis in adipocytes. 40
Figure 1.9.Thermogenesis in brown adipocytes 43

Figure 2.1. Confocal micrograph of HMSM cells shows α-actin and vimentin distribution 55
Figure 2.2. Transfection efficiency. 58
Figure 2.3. Cell viability in the presence of G418 59
Figure 2.4. Schematic diagram of CRH-R1 gene splicing pattern and the annealing position of PCR primers and probes relative to the structure of CRH-R1 alternative spliced variants. 72
Figure 2.5. Schematic representation of OE-PCR. 75
Figure 2.6. Products of PCR reactions 75
Figure 2.7. Map of pBudCE4.1. 79
Figure 2.9. Characterisation of CRH-R1 and β-arrestin antibody specificity……...94

Figure 3.1. The cellular expression of CRH-R1 variants visualised by confocal microscopy 102
Figure 3.2. Internalization of CRH-R1α in st-293-R1α- agonist-dose dependency. 104
Figure 3.3. Internalization of CRH-R1α in st-293-R1α- time course 105
Figure 3.4. Cellular distribution of CRH-R1α and β-arrestin following CRH stimulation of st.293-R1α cells. 107
Figure 3.5. Internalization of CRH-R1β in tr-293-R1β- time course. 108
Figure 3.6. Cellular distribution of CRH-R1β and β-arrestin following CRH stimulation of tr.293-R1β cells 109
Figure 3.7. Western blot analysis of plasma membrane fraction of HEK293 transiently expressing CRH-R1α and CRH-R1d. 111
Figure 3.8. Cellular distribution of CRH-R1d in tr-293-R1d- time course. 112
Figure 3.9. The involvement of β-arrestin in CRH-R1d internalization 113
Figure 3.10. Effect of PMA on cellular redistribution of CRH-R1α and CRH-R1β 115
Figure 3.11. Relative quantification of intracellular CRH-R1α and CRH-R1β..... 115
Figure 3.12. The effect of PMA treatment on β-arrestin distribution 116

Figure 4.1. Visualization of over-expressed CRH-R1α and CRH-R1d distribution in HEK293 and HMSM cells by indirect immunofluorescent confocal microscopy. 126

Figure 4.2. TMHMM prediction of TMD and loops 128
Figure 4.3. Orientation of the C-terminus of CRH-R1. 130
Figure 4.4. The cellular localisation of CRH-R1α wild type and mutant constructs. 132
Figure 4.5. The cellular localisation of CRH-R1d wild type and mutant constructs 133
Figure 4.6. Quantitative analysis of CRH-R1 intracellular fluorescent intensity in HEK293 cells over-expressing different CRH-R1 constructs. 134
Figure 4.7. Expression of CRH-R1α-myc, CRH-R1α-V5, CRH-R1d-myc, CRH-R2β-V5 in HEK293 cells 136
Figure 4.8. Co-expression of two types of CRH-Rs in HEK293 cells 137
Figure 4.9. The cellular localisation pattern of CRH-R1d is dependent on the expression levels of CRH-R2β and CRH-R1d..... 138
Figure 4.10. Cellular distribution of CRH-R2β-V5 in HEK293 cells: agonist time course. 140
Figure 4.11. Internalization characteristics of CRH-R2β-V5 co-expressed with CRH-R1d-myc in HEK293 cells: time course 141
Figure 4.12. Internalization characteristics of CRH-R2β-V5 co-expressed with CRH-R1α-myc in HEK293 cells: time course 142
Figure 4.13. CRH-R2β mediated cAMP production 144
Figure 4.14. The effect of CRH-R1d on CRH-R2β mediated MAPK activation. . 146
Figure 4.15. Secondary structure prediction. 149

Figure 5.1. Characterisation of CRH-R2β cellular expression 157
Figure 5.2. Characterisation of mRNA CRH-R2β expression..... 158
Figure 5.3. Characterisation of protein CRH-R2β expression 158
Figure 5.4. cAMP production in HEK293 and CRH-R2β clones. 161
Figure 5.5. ERK1/2 phosphorylation in HEK293 and CRH-R2β clones. 162
Figure 5.6. Agonist-induced cAMP production in st.293-R2β cells..... 163
Figure 5.7. CRH-R2β desensitization characteristics in st.293-R2β cells 164
Figure 5.8. The effect of media on UCNII-induced ERK1/2 phosphorylation. 166
Figure 5.9. The effect of media on UCNII-induced p38 MAPK phosphorylation. 167
Figure 5.10. Agonist-induced and dose-dependent ERK1/2 phosphorylation in st.293-R2β. 168
Figure 5.11. Agonist-induced and dose-dependent p38 MAPK phosphorylation in st.293-R2β. 169
Figure 5.12. Time-dependent ERK1/2 activation by UCN-II in 293-R2β cells. ... 170
Figure 5.13. Time-dependent p38 MAPK activation by UCN-II in 293-R2β cells. 171
Figure 5.14. CRH-R2β and phospho-ERK1/2 or phospho-p38 MAPK subcellular distribution induced by UCN-II in st.293-R2β cells: visualization by confocal microscopy. 173
Figure 5.15. The effect of PKA inhibition on UCN-II induced ERK1/2 and p38 MAPK activation 175
Figure 5.16. Time course: the effect of PKA inhibition on UCN-II induced ERK1/2 176
Figure 5.17. The effect of PI(3)-kinase inhibition on UCN-II induced ERK1/2 and p38 MAPK activation 177

Figure 5.18. Internalization of CRH-R2β in st293-R2β 179
Figure 5.19. Quantification of CRH-R2β expression on the plasma membrane. .. 181
Figure 5.20. CRH-R2β, β-arrestin and clathrin subcellular distribution following CRH or UCN-II treatment: 184
Figure 5.21. Agonist-dependent β-arrestin recruitment to the plasma membrane. 185
Figure 5.22. Recruitment of β-arrestin by the agonist-activated CRH-R2β in st.293-R2β. 186
Figure 5.23. Effect of DN β-arrestin and conconavalin A on UCN-II induced CRH-R2β endocytosis 187
Figure 5.24. Effect of CHC siRNA on UCN-II induced CRH-R2β internalization 188
Figure 5.25. Verification of clathrin silencing by CHC siRNA in st.293-R2β cells. 189
Figure 5.26. Effect of concanavalin A, DN β-arrestin and CHC siRNA on UCN-II induced ERK1/2 and p38MAPK activation in 293-R2β cells 190
Figure 5.27. Effect of DN β-arrestin and CHC siRNA on UCN-II induced CRH-R2β desensitization in st.293-R2β cells 191
Figure 5.28. UCN-II induced ERK1/2 phosphorylation is MEK dependent. 192
Figure 5.29. Regulation of β-arrestin1 membrane translocation by ERK1/2 in 293-R2β cells 194
Figure 5.30. Characterisation of phospho-β-arrestin1 (Ser412) antibody. 195
Figure 5.31. Regulation of β-arrestin1 phosphorylation by ERK1/2 in 293-R2β cells 196
Figure 5.32. The effect of ERK1/2 on CRH-R2β endocytocis. 197
Figure 5.33. Schematic representation of the created CRH-R2β mutant receptors 198
Figure 5.34. Role of CRH-R2β C-terminus amino acid cassette TAAV on receptor expression in the plasma membrane 199
Figure 5.35. Role of CRH-R2β C-terminus amino acid cassette TAAV on UCN-II induced cAMP production and receptor desensitization. 200
Figure 5.36. Role of CRH-R2β C-terminus amino acid cassette TAAV on receptor endocytosis 201
Figure 5.37. Role of CRH-R2β C-terminus amino acid cassette, TAAV, on UCN-II induced β-arrestin recruitment visualization by fluorescent confocal microscopy 202
Figure 5.38. Time course of UCN-II stimulated p38 MAPK phosphorylation in HEK293 cells transiently expressing wild type or mutant CRH-R2β. 203
Figure 5.39. Time course of UCN-II stimulated ERK1/2 phosphorylation in HEK293 cells transiently expressing wild type or mutant CRH-R2β. 204
Figure 5.40. Schematic representation of signal transduction pathways activated by CRH-R2β. 212

Figure 6.1. Visualization of endogenous CRH-R distribution in primary myometrial cells. 220
Figure 6.2. Detection of CRH-Rs in HMSM cells. 221
Figure 6.3. Time course of the IL-1β effects on PGHS-2 mRNA expression. 223
Figure 6.4. Time course of the IL-1β effects on PGHS-2 protein expression 224
Figure 6.5. The effect of IL-1β on PGHS-2 protein expression monitored by indirect immunofluorescence confocal microscopy. 225

Figure 6.1. Visualization of endogenous CRH-R distribution in primary myometrial cells. 220
Figure 6.2. Detection of CRH-Rs in HMSM cells. 221
Figure 6.3. Time course of the IL-1β effects on PGHS-2 mRNA expression. 223
Figure 6.4. Time course of the IL-1β effects on PGHS-2 protein expression 224
Figure 6.5. The effect of IL-1β on PGHS-2 protein expression monitored by indirect immunofluorescence confocal microscopy. 225
Figure 6.6. The IL-1β effect on CRH-R1 mRNA expression 227
Figure 6.7. The effect of IL-1β on CRH-R protein expression 228
Figure 6.8. IL-1β-induced p65 translocation 229
Figure 6.9. IL-1β-induced degradation of IκBα 230
Figure 6.10. The inhibitory effect of IKK inhibitor II on IL-1β induced IκBα degradation and p65 translocation 231
Figure 6.11 Effect of IKK, ERK1/2 and p38 MAPK inhibitors on IL-1β-induced effects on myometrial PGHS-2 and CRH-R1 gene expression 232
Figure 6.12. Effect of IL-1β on CRH-induced cAMP production 233
Figure 6.13. The effect of UCN-II on cAMP production in HMSM cells 234
Figure 6.14. UCN-II-induced ERK1/2 and p38MAPK phosphorylation 235
Figure 6.15. Time-dependent ERK1/2 activation by UCN-II in HMSM cells. 236
Figure 6.16. Phospho-ERK1/2 subcellular distribution induced by UCN-II in HMSM cells 237
Figure 6.17. Agonist induced RhoA translocation to the plasma membrane in HMSM 239
Figure 6.18. UCN-II induced RhoA translocation in HMSM cells 241
Figure 6.19. UCN-II induced RhoA activation in HMSM cells 241
Figure 6.20. UCN-II induced CRH-R internalization in HMSM cells 242

Figure 7.1. Differentiation of T37i fibroblast into adipocytes. 254
Figure 7.2. RT-PCR analysis of CRH-Rs and UCP-1 mRNA expression 255
Figure 7.3. Western blot analysis of CRH-R1/2 protein expression 256
Figure 7.4 Visualization of CRH-Rs and perilipin A in T37i adipocytes by indirect confocal microscopy 256
Figure 7.5 Validation of CRH-R immunoreactive in T37i adipocytes by indirect confocal microscopy. 257
Figure 7.6. Agonist induced cAMP production in T37i adipocytes 258
Figure 7.7. Agonist dose dependent MAPK activation in T37i adipocytes. 260
Figure 7.8. Time course of UCN-II induced MAPK activation in T37i adipocytes. 261
Figure 7.9. Phospho-ERK1/2 MAPK subcellular distribution induced by UCN-II in T37i adipocytes: 262
Figure 7.10. The role of PKA, AKAP and PI(3)-kinase on UCN-II induced ERK1/2 and p38 MAPK activation in T37i adipocytes 264
Figure 7.11. Effect of CRH and UCN-II on T37i fibroblasts numbers. 265
Figure 7.12. CRH and UCN-II induced lipolysis in T37i adipocytes. 266
Figure 7.13. CRH and UCN-II induced lipolysis in T37i adipocytes is PKA dependent 267
Figure 7.14. Visualization of perilipin A/B distribution in T37i adipocytes by indirect confocal microscopy. 268

Figure 7.15. Visualization of HSL distribution in T37i adipocytes by indirect confocal microscopy 269

List of Tables

Table 1.1. Structural and splicing characteristics of CRH-R1 subtypes..... 12

Table 2.1: PCR reaction components used for majority of PCR reaction.. 68
Table 2.2: PCR reaction components used to generate CRH-R1α and CRH-R1d mutants..... 75
Table 2.3: PCR conditions used for the two first rounds of the overlap extension PCR and for the overlapping PCR..... 76
Table 2.4: Nucleotide sequences of primers used to created CRH-R1α and CRH-R1d mutants..... 76
Table 2.5. Nucleotide sequences of primers used to create CRH-R2β mutant receptors..... 78
Table 2.6. Primer sequences used to insert CRH-Rs cDNA into pBudCE4.1..... 79
Table 2. 7. The antibody and conditions used for immunodetection of proteins by western blotting..... 88
Table 2. 8. The antibody and conditions used for immunodetection of proteins by confocal microscopy. 93

Table 4.1.CRH-R1α and CRH-R1d mutant receptors. 131

Table 5.1. The IR signal characteristics..... 180

Table 8.1. Internalization characteristics of CRH-R1 splice variants..... 276
Table 8.2. Internalization and signalling characteristics of CRH receptors type 1 and 2..... 276

Acknowledgements

I would like to express my appreciation to my supervisors Professors Dimitris Grammatopoulos and Hendrik Lehnert for giving me the opportunity to carry out this project. I am grateful to Prof. Grammatopoulos for his advice and guidance throughout the course of my study and during the writing up of my thesis. I would also like to thank Prof. Jeffery Pessin and his group at the SUNY at Stony Brook, USA, for helping and guiding me during the time that I spent in his laboratory. I am indebted to Dr. Janet Digby for helping me with adipocyte cells and providing me with cDNA from adipose tissues, and for being a good friend. I am grateful to Dr Rosemary Bland for teaching me various experimental techniques, and Dr Andy Blanks for teaching me confocal microscopy technique. Also, I would like to thank Dr Mei Gu for performing Real-Time PCR analysis, and Miss Helen Bennett for proofreading my thesis.

I am grateful to Mrs Jeanette Bennett for being such a great friend and lunch/coffee buddy, without whose kind words and encouragement the lab life would have been much harder. Also I owe a thankyou to everyone in the student's office for being there during the ups and downs of research, especially a big thanks to Yati and Tina.

Most of all, I would like to express the greatest appreciation to my husband, Vlad, for the tremendous support, encouragement, and endless patience during the course of my study and the marriage. I am grateful to him for being there for me during my worst moments. At last, but not at least, I am thankful to him for showing me what a real devotion to science means and for being a scientist role model for me.

Declaration

I hereby declare that all the work reported in this thesis is my own unless stated otherwise in the text. None of this work has been previously submitted for any other degree or at any other institution. However, some of results obtained during the course of the project have been published (see Publications). All sources of information used in the preparation of this thesis are indicated by references.

Publications

Teli T*, **Markovic D***, Hewitt ME, Levine MA, Hillhouse EW, Grammatopoulos DK.(2007) Structural domains determining signalling characteristics of the CRH-receptor type 1 variant R1beta and response to PKC phosphorylation. *Cell Signal.* 2007 Aug 28; [Epub ahead of print]

Markovic D, Vatish M, Gu M, Slater D, Newton R, Lehnert H, Grammatopoulos DK (2007). The onset of labour alters corticotropin-releasing hormone type 1 receptor (CRH-R1) variant expression in human myometrium: putative role of IL-1β. *Endocrinology 148(7):3205-13*

Markovic D, Papadopoulou N, Teli T, Levine MA, Hillhouse EW, Grammatopoulos DK (2006). Differential responses of CRH receptor type 1 variants to PKC phosphorylation. *J Pharmacol Exp Ther 319(3):10032-42*

Teli T, **Markovic D**, Levine MA, Hillhouse EW, Grammatopoulos (2005). Regulation of corticotropin-releasing hormone receptor type 1α signalling: structural determinants for G protein coupled receptor kinase-mediated phosphorylation and agonist-mediated desensitization. *Mol Endocrinol. 19(2):474-90*

Summary

Besides the well-known role of CRH and CRH-related peptides in controlling the HPA axis, the peptides have been implicated as important mediators in various physiological processes including those of reproduction, the endocrinology of pregnancy and energy homeostasis. Diverse functions of CRH and UCNs are governed via activation of two types of CRH receptors, R1 and R2.

Since tissue sensitivity to agonists is determined by the availability of receptors in the plasma membrane and speed of signal termination, one of the goals of this project was to investigate the cellular expression of CRH-R1 variants (α, β, d and β/d), and internalization characteristics of the receptors following homologous and heterologous activation of the receptor. Also, the structural and functional characteristics of the CRH-R1d receptor, a splice variant that contains deletion of 14 amino acids within the 7th TMD were investigated. The co-expression studies utilizing HEK293 cells expressing CRH-R1d and CRH-R2β demonstrated attenuation of CRH-R2β mediated cAMP production and MAPK activation in the presence of CRH-R1d. This could be of potential importance in human peripheral tissues which express both types of CRH receptors, such as the uterus. Additionally, the signalling and internalization characteristics of CRH-R2β were studied and the possible link between the CRH-R2 internalization and MAPK activation was investigated. The analysis of the spatio-temporal characteristics of MAPK activation revealed important differences between CRH-R1 and R2 mediated signalling cascades. Immunofluorescence analysis demonstrated that activation of both types of CRH receptors led to a recruitment of β-arrestin to the plasma membrane; however the internalization pathways of the receptors were different.

Since human pregnancy is associated with changes in the myometrial CRH-R variant expression profile and functional activity, as a part of the study, the effect of IL-1β (an important mediator of the onset of labour) on the regulation of CRH-R1 gene expression and the functional properties of the CRH-R was investigated. Data showed that IL-1β can potentially target CRH-R1 gene transcription and splicing mechanisms of the CRH-R1 gene; these interactions appeared to involve two members of the MAPK family of proteins, ERK1/2 and p38 MAPK and NF-κB activation. Interestingly, increased CRH-R1 gene transcription and generation of receptor splice variants was not associated with increased CRH-R protein levels and CRH signalling activity. Furthermore, the signalling characteristics of CRH-R activated by UCN-II (CRH-R2 specific agonist) were investigated. The data showed that activation of CRH-R2 did not lead to cAMP production which is associated with the quiescent state of the uterus, but the MAPK signalling cascade was activated, which has been implicated in mediating pathways that promote contractility.

During the course of this project the biological role of CRH receptors was investigated in T37i cells. RT-PCR analysis showed the presence of CRH-R1 and R2 mRNA in mice brown adipose tissue and T37i cells. Immunofluorescence and western blot analysis demonstrated the presence of CRH-Rs in T37i cells. The functional capacity of adipose CRH-Rs to activate adenylyl cyclase and MAPK signalling cascade was assessed. Low concentration of agonists (close to receptors Kd=1 nM) stimulated activation of the adenylyl cyclase/cAMP/PKA signalling cascade resulting in lipolysis. However; higher concentrations (10-100 nM) of agonists activated MAPK signalling cascades.

Abbreviations

A Kinase Anchoring Protein (Protein Kinase A Anchoring Protein)	AKAP
Adenosine Triphosphate	ATP
Adenylyl Cyclase	AC
Adrenocorticotropic Hormone	ACTH
Alanine	Ala
Ammonium Persulfate	APS
Base pair	Bp
Bicinchoninic Acid	BCA
Bovine Serum Albumin	BSA
Brown Adipose Tissue	BAT
Carnitine Palmitoytransferase	CPT
Central Nervous System	CNS
Clathrin Heavy Chain	CHC
CoenzymeA	CoA
Complementary Deoxyribonucleic Acid	cDNA
Corticotropin Releasing Hormone Binding Protein	CRH-BP
Corticotropin Releasing Hormone Receptor	CRH-R
Corticotropin-Releasing Hormone	CRH
Cyclic Adenosine Monophosphate	cAMP
Cyclic Guanosine Monophosphate	cGMP
Cyclooxygenase-2	Cox-2
Dehydroepiandrostenedione Sulfate	DHEAS
Deoxyribonuclease	DNase
Deoxyribonucleic Acid	DNA
Diacylglycerol	DAG
Distilled Water	dH_2O
Dithiothreitol	DTT
Dominant Negative	DN
Dulbecco's Modified Eagle's Medium	DMEM
Enhanced chemiluminescence	ECL
Ethylenediamine Tetraacetic Acid	EDTA
Extracellular signal Regulated Kinase	ERK
Fetal Calf Serum	FCS
Filter Sterilised	F/S
Flavin Adenine Dinucleotide H	FADH
Free Fatty Acids	FFA
Glyceraldehyde-3-phosphate dehydrogenase	GAPDH
Guanine nucleotide exchange factor	GEF
GDP dissociation inhibitor	GDI
G-Protein Coupled Receptor	GPCR
G-protein coupled Receptor Kinase	GRK
Gram	G
Guanosine Diphosphate	GDP
Guanosine Triphosphate	GTP

Hank's Balanced Salt Solution	HBSS
Hormone Sensitive Lipase	HSL
Horse-radish Peroxidase	HRP
Human Embryonic Kidney Cells-293	HEK-293
Human Myometrial Smooth Muscle cells	HMCM
Human/rat	h/r
Hour	H
Interleukin-1β	IL-1β
Inhibitory Kappa B	IκB
Inhibitory Kappa Kinase	IKK
Inositol 1,4,5 triphosphate	IP3
International Units	IU
Kilodalton	kDa
Knockout	KO
Messenger RNA	mRNA
Microgram	Mg
Microlitre	µl
Micromolar	µM
Milliamper	mA
Milligram	Mg
Millilitre	ml
Millimeter	mm
Millimolar	mM
Minimum Essentials Medium	MEM
Minute	min
Mitogen Activated Protein Kinase	MAPK
Myosin Light Chain	MLC
Molar	M
Molecular Weight	MWt
Myristoylated Protein Kinase A inhibitor	myrPKAi
N, N, N^1, N^1-tetramethylethylenediamine	TEMED
Nanogram	ng
Nanomolar	nM
National Centre for Biotechnology Information	NCBI
Nicotinamide Adenine Dinucleotide (reduced)	NADH
Nitric Oxide	NO
Nuclear Factor Kappa B	NF-κB
Nuclear Localization Signal	NLS
Oxytocin	OT
Paraventricular nucleus	PVN
Phenylmethylsulphonyl Fluoride	PMSF
Phorbol-12-myristate-13-acetate	PMA
Phosphate Buffer Saline	PBS
Phosphatidylinositol-3 OH kinase	PI3-K
Phospholipase A2	PLA2
Picomolar	pM
Polyacrylamide Gel Electrophoresis	PAGE
Polymerase Chain Reaction	PCR
Polyvinylidene Fluoride	PVDF

Plasma Membrane	PM
Pro-opiomelanocortin	POMC
Prostaglandins	PG
Prostaglandin H Synthase	PGHS
Protein Kinase A	PKA
Protein Kinase C	PKC
Paraventricular Nuclei	PVN
Reverse Transcriptase Polymerase Chain Reaction	RT-PCR
Ribonucleic Acid	RNA
Room Temperature	RT
Sauvagine	Svg
Seconds	secs
Serine	Ser
Small interference RNA	siRNA
Sodium Dodecyl Sulphate	SDS
Standard Error of Means	SEM
Sympathetic Nervous System	SNS
Tetramethyl Rodamine isothiocyanate	TRITC
Threonine	Thr
Transmembrane Domain	TMD
Triiodothyronine	T3
Tris Buffered Saline-0.1% Tween-20	TBS-T
Tris (hydroxymethyl) aminomethane	Tris
Tris Buffer EDTA	TBE
Tris Buffered Saline	TBS
Tyrosine	Tyr
Ultraviolet	UV
Uncoupling Protein-I	UCP-I
Urocortin	UCN
Urocortin-II	UCN-II
Urocortin-III	UCN-III
Volts	V
Volume per volume ratio	v/v
Weight per volume ratio	w/v
White Adipose Tissue	WAT
α-Melanocyte Stimulating Hormone	α-MSH
β-arrestin	β-arr
β-Lipoprotein	β-LPH
1-(3-dimethylaminopropyl)-3-2- ethanesulphonic acid	HEPES
3-(aminopropyl)triethoxy silane	APES
3-isobutyl-1-methylxanthine	IMBX
3-[4,5-dimetylthiazol-2yl]-2,5 diphenyl tetrazolium bromide)	MTT
4', 6'-diamino-2-phenylindole	DAPI

1 INTRODUCTION

1.1 The corticotropin-releasing hormone (CRH)

Since the discovery of corticotropin releasing hormone or factor (CRH or CRF), a 41-amino acid peptide, in the early 1980s (Vale W *et al*, 1981), it has become evident that the physiological role of CRH is much wider than initially thought. The primary function of CRH is to stimulate the secretion of adrenocorticotropinc hormone (ACTH) from the anterior pituitary, which induces the release of adrenal glucocorticoids. The release of glucocorticoids represents the final stage in the hypothalamic-pituitary-adrenal axis (HPA axis) which mediates the endocrine response to stress (Swanson LW *et al*., 1986). Furthermore, CRH has been linked with chronic anxiety disorder, melancholic and atypical depression, chronic pain and fatigue states, sleep disorders, addictive behaviour, acute and chronic neurodegeneration, allergic and autoimmune inflammatory disorders, the metabolic syndrome, gastrointestinal diseases, and pre-term labour (Grammatopoulos DK & Chrousos G, 2002).

1.1.1 The family of CRH-related peptides

Since the early 1980s, the family of CRH-related peptides has rapidly expanded to include mammalian urocortin (UCN), urocortin II (UCN-II) (also known as stresscopin-related peptide-SRP), and urocortin III (UCN-III) (also

known as stresscopin-SCP), as well as fish urotensin I and frog sauvagine (Svg) (Vaughan J *et al*., 1995; Reyes TM *et al*., 2001; Lewis K *et al*., 2001; Hsu SY & Hsueh AJ, 2001). All of these peptides appear to share an ancestral peptide precursor. Mammalian CRH shares approximately 50% homology to sauvagine and urotensin I. UCN is a 40 amino acid peptide with 45% homology in amino acid sequence to CRH, 63% to urotensin, and 35% to sauvagine. Additionally, UCN-II shows 34% homology to human/rat CRH (h/r CRH) and urotensin, 43% homology to human UCN (hUCN), 37-40% homology to UCN-III, and minimal homology to sauvagine (15%) (Dautzenberg F & Hauger R, 2002).

Both UCNs and CRH are synthesised as precursors and are subsequently processed to the mature bioactive peptides (Vale W *et al*., 1997). CRH derives from a 196-amino acid precursor highly conserved among mammalian species. The CRH gene contains only two exons separated by a short intron. The mature peptide sequence is entirely encoded by the second exon (Hillhouse EW & Grammatopoulos DK, 2006).

CRH and CRH-related peptides are differently distributed in the brain and periphery highlighting the importance of the peptides in different physiological processes such as stress adaptation, learning, memory, glucose metabolism and energy balance (Dautzenberg F & Hauger R, 2002; Hsu SY & Hsueh AJ, 2001).

1.1.2 The action of CRH and CRH-related peptides

1.1.2.1 The pituitary and extrapituitary action of CRH and CRH-related peptides

The core of the neuroendocrine system is represented by the hypothalamic-pituitary complex. CRH was isolated for the very first time from ovine hypothalamic extracts in 1981 by Vale (Vale W *et al.*, 1981). Produced in the hypothalamus CRH reaches the pituitary gland via the portal vessels, where it controls the secretion of peptides derived from pro-opiomelanocortin (POMC). POMC, a 241 amino acid precursor polypeptide, can be enzymatically cleaved into: ACTH and β-lipotropin (β-LPH) in the anterior pituitary gland; and corticotropin-like intermediate lobe peptide (CLIP), γ-LPH, α-MSH and β-endorphin in the intermediate lobe (Figure 1.1). Each of these peptides is packaged in large dense-core vesicles that are released from the cells by exocytosis in response to appropriate stimulus. ACTH, released in response to stimulation by CRH, induces the release of adrenal glucocorticoids; this represents the final stage in the activation of the hypothalamic-pituitary-adrenal axis (HPA), which mediates the endocrine response to stress.

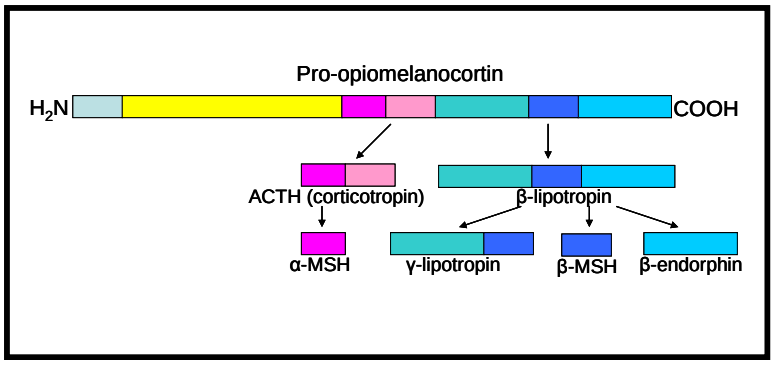

Figure 1.1. Schematic representation of POMC prohormone. (Adapted from Copper JR *et al.*, 1991)

However, the action of CRH does not stop here; CRH and related peptides play a fundamental role in the coordination of behavioural, endocrine, autonomic, cardiovascular and immune responses to stress. Independently from the stimulatory effects on glucocorticoid secretion, CRH also induces anxiogenic effects, increases cardiovascular activity, induces anorexia, and inhibits luteinising hormone-releasing hormone (LHRH) secretion (Ojeda SR, 2004). The extrapituitary action of UCN is in influencing feeding, anxiety, and auditory processing. Moreover, UCN is a more potent suppressor of feeding behaviour than CRH; additionally, it also has more potent effects on the cardiovascular system than CRH, suggesting that UCN might play a crucial role in the cardiovascular response to stress possibly through involvement of the CRH type 2 receptor (CRH-R2). Similarly to UCN, UCN-II decreases feeding behaviour, however it also appears to play a role in delaying gastric emptying (Ojeda SR 2004).

The CRH action on the immune response to stress is very complex. As mentioned above, CRH stimulates POMC production in the pituitary; the release ACTH and ACTH-induced cortisol have anti-inflammatory action on circulating immune cells. In contrast, when CRH is released into local tissue beds, from either peripheral nerve endings or immune cells, the action of CRH is pro-inflammatory; it stimulates the production of IL-1, TNF-α and other pro-inflammatory cytokines, promotes neutrophil influx, but also acting through β-endorphin can enhance natural killer cell activity and reduce pain. This distinctive CRH action in different tissues is called "context-dependent" action, relatively common phenomenon among cytokines and neurohormones (Munford RS, 2004).

1.1.2.2 CRH and CRH-related peptides action in pregnancy

CRH and related peptides play an important role in implantation and endocrinology of pregnancy. CRH, produced by the trophoblast cells, promotes blastocyst implantation and facilitates immune tolerance of the early pregnancy by eliminating activated maternal T cells (Carr, BR and Rehman, KS, 2004). Placentaly derived CRH increases in maternal serum throughout pregnancy and peaks during labour and delivery. Levels of CRH at term may be 50- to 100-fold higher than those in non pregnant women. There is also an increase in carrier protein, CRH-binding protein (CRH-BP), which binds CRH and may blunt the increase in CRH biological activity. Elevated levels of maternal plasma CRH have been found in women in preterm labour who are destined to deliver within 24-48 hours, compared with those who continued pregnancy despite threatened preterm labour (McLean, M *et al*, 1995). Although the biological role of CRH remains enigmatic, the presence of functional CRH receptors in the myometrium suggests that CRH might modulate myometrial contractility and hence parturition. CRH action is mediated via multiple receptor subtypes, these receptors are primarily coupled to the adenylyl cyclase second messenger system, which promotes uterine quiescence. CRH can exert further actions such as inhibition of prostaglandin production to prevent contractions. Grammatopoulos and Hillhouse have postulated a hypothesis that at term under the influence of oxytocin, there is a modification in the coupling mechanism that leads to a decrease in the biological activity of the CRH-R and in the generation of cAMP favours myometrial contractility. Additionally, CRH, via distinct receptor subtype, is then able to enhance the contractile response of the myometrium (Grammatopoulos DK & Hillhouse EW, 1999). Moreover, the findings that pregnant and non-pregnant myometrium have a

different CRH receptors profile supports this hypothesis (Sec. 1.3.1). Also, in favour of this hypothesis, there is evidence suggesting that UCN-II action via CRH-R2 promotes phosphorylation of myosin light chain (MLC) leading to increased contractility (Karteris E *et al*, 2004).

1.1.2.3 CRH and CRH-related peptide action in metabolism and energy homeostasis

Beside the well-known role of CRH and CRH-related peptides in controlling the HPA axis, the peptides have been implicated as important mediators of metabolism and energy homeostasis. Administration of CRH into the paraventricular nucleus (PVN), promotes a state of negative energy balance and weight loss (Schwartz MW *et al*., 1999), including suppression of food intake (Arase K *et al*., 1988), coupled with stimulation of sympathetic nervous system (SNS) outflow (Arase K *et al*., 1988; Egawa H *et al*., 1990), which increases lipolysis (Egawa H *et al*., 1990) and activates brown adipose tissue (BAT) lipolysis (Rothwell N, 1989). Additionally, chronic central CRH administration reduces food intake and body mass in normal rats (Arase K *et al*., 1988), genetically obese rats (Arase K *et al*., 1989), and primates (Glowa J & Gold P, 1991). Recently, Kotz and colleges have demonstrated that during food restriction, UCN in the PVN increases plasma leptin and uncoupling protein 1 (UCP-1) in brown adipose tissue and decreases UCP-3 gene expression in muscles, which might have important consequences for thermogenesis (Kotz CM *et al.*, 2002), suggesting that the CRH system could be a potential target for anti-obesity drugs. Additionally, it has been reported that CRH receptors are expressed in human adipose tissue (Seres J *et al.*,

2004), and that adipocytes synthesize UCN-II and UCN-III ("natural" ligands of CRH-R2). A recent report by Wellhoner and colleges (Wellhoner P *et* al., 2006) highlighted the *in vivo* effects of CRH on femoral adipose tissue metabolism. They have found that intravenous administration of CRH leads to increased levels of interstitial and plasma glycerol suggesting stimulated lipolysis. Additionally, the report describes the effect of CRH on glucose levels, of which plasma levels do not alter. However, the interstitial glucose levels increase biphasically; suggesting potential effects of CRH on glucose transport (Wellhoner P *et* al., 2006).

Moreover, the CRH system is present in the pancreas and could modulate insulin and glucagon secretion, thus controlling glucose blood levels. Also it has been demonstrated that UCN-II null mice display increased glucose uptake in skeletal muscle through the removal of UCN-II-mediated inhibition on insulin signalling (Chen, A. *et al*. 2006). Since UCNs have a higher affinity for CRH-R2 than CRH and from the fact that UCN-III does not bind to CRH-R1, it is likely that these metabolic and homeostatic actions could be mediated via actions of CRH-R2 (section 1.3.2)

1.2 CRH-Binding Protein (CRH-BP)

CRH-BP, a 37 kDa binding protein for CRH, was first purified from human plasma in the late 1980s (Orth DN & Mount CD, 1987; Behan DP *et al*., 1989). The human CRH-BP has been cloned and mapped to the distal region of chromosome 13 and locus 5q in the mouse and human genomes (Behan DP *et al*., 1993). The CRH-BP three-dimensional structure has not yet been identified. Photoaffinity labelling experiments indicated that, although the human CRH-BP had previously

been observed to dimerize after association with the ligand, the rCRH-BP was found to dimerize, in part, and be exclusively bound to the ligand as a monomer (Woods RJ *et al*., 1996). Additionally, the sequence of 23-36 amino acid residues of CRH-BP was found to be involved in the ligand-binding site of human/rat CRH (h/rCRH) (Woods RJ *et al*., 1996).

CRH-BP has the ability to modulate the bioactivity of CRH suggesting that this protein may be an important regulator of the HPA axis (Linton EA *et al*., 1990). A CRH-BP cleavage product, with molecular weight of 27 kDa, has been identified in the synovial fluid (Woods RJ *et al*., 1999), which binds with the same affinity as the intact CRH-BP to CRH. However, the role of this cleavage product has not yet been determined.

Urocortin is also bound to CRH-BP (Vaughan J *et al*., 1995). Interestingly, CRH-BP binds CRH and UCN-I with picomolar affinity, approximately 5-fold higher than the affinity of either peptide for the CRH-Rs (Huising MO *et al*., 2007). It has been reported that the two arginines Arg-23 and Arg-36 are the sites of photoincorporation of mono- and bifunctional probes, suggesting that these residues are involved in ligand binding (Jahn O *et al*., 2002). However, a recent report suggested that the mutation of Arg-23 and Arg-36 to alanine did not have an effect on CRH nor UCN-I binding to CRH-BP (Huising MO *et al*., 2007). In addition, it has reported that CRH-BP binding affinity for CRH and sauvagine (Svg) differs by two orders of magnitude and a single amino acid residue on both peptides was identified as being responsible for differing binding affinities (Eckart K *et al*., 2001). The authors demonstrated that Ala-22 of CRH is responsible for this peptide ‘s high affinity binding capacity, and that Glu-21 located on the equivalent position of Svg prevented high affinity binding to CRH-BP. Additionally, it has been

demonstrated that exchange of these two amino acids serves as a switch enhancing or preventing the binding of the h/rCRH and sauvagine, to the CRH-BP and the receptor (Eckart K *et al*., 2001).

1.3 The CRH receptor (CRH-R)

Signals from CRH and CRH-related peptides are transduced across the cell membrane via activation of the two types of CRH-receptors (CRH-R), termed R1 and R2, which are encoded by different genes (Hillhouse EW *et al.*, 2002). A third type of CRH receptor has been identified in fish (Arai M *et al*., 2001). The CRH-R1 gene is located on the long arm of chromosome 17 at 17q12-q22 (Vamvakopoulos NC & Sioutopoulou TO, 1994) whereas the CRH-R2 gene is located on the short arm of chromosome 7 at 7p21-p15 (Meyer AH *et al*., 1997). Structurally, CRH-R1 and R2 are approximately 70% identical at the amino acid level, but exhibit considerable divergence at the N-terminus, consistent with their distinct pharmacological properties. The CRH receptor sequence contains multiple potential phosphorylation sites for second messenger kinases and casein kinase II that are identical in both receptor types (Chen R *et al*., 1993). Modulation of CRH receptor function by G-protein coupled receptor kinase 3 (GRK3) has been recently demonstrated (Dautzenberg F, 2001).

The receptors belong to the class II (B) superfamily of G-protein coupled receptors (GPCR), which all contain seven transmembrane helical domains and share considerable sequence identity with one another especially in the transmembrane domains and intracellular loops. All class B receptors possess a large extracellular domain (ECD) with which they bind with high affinity to the C-

terminal regions of their peptide ligands. This interaction alone is not sufficient to stimulate coupling of the receptor to G-proteins, but, a second interaction between the juxtamembrane domain of the receptor and the first few residues within N-terminal portion of the ligand has to occur (Perry SJ *et al*., 2005). Upon agonist binding, GPCRs change their structural conformation and transduce signals across cells mainly through activation of heterotrimeric G-proteins, which regulate a diverse network of intracellular systems (Hillhouse EW and Grammatopoulos DK, 2006). Beside the CRH receptor, other members of the B superfamily include the calcitonin, parathyroid hormone (PTH), pituitary adenylyl-cyclase-activating peptide (PACAP), growth-hormone-releasing hormone (GHRH), glucagon, glucagone-like peptide (GLP), and secretin receptors.

CRH-R are widely distributed in the central nervous system and in a variety of peripheral tissues, including the immune, cardiovascular and reproductive systems, adrenals, lungs, liver, pancreas, small intestine, stomach, skin, and also in some types of human tumours such as melanomas and corticotrope tumours (Suda T *et al*. 1993; Hillhouse EW & Grammatopoulos DK, 2006) .

1.3.1 The CRH-R type 1 (CRH-R1)

The CRH receptor type 1α (CRH-R1α), cloned from human pituitary cell tumour, is a 415-amino acid protein (Chen, R. *et al.* 1993). On the basis of the cDNA sequence coding for the CRH-R1α, the receptor is predicted to have a molecular weight of approximately 44 kDa (Chen R *et al*., 1993). There appear to be five putative N-glycosylation sites (Asn-Xaa-Ser/Thr) in the N-terminus (Chen R *et al*., 1993). Differential post-translational glycosylation events might be

responsible for the differences shown between CRH-R molecular weight. The molecular weight of CRH-R1 in pituitary and human reproductive tissues was detected as 75 kDa (Hillhouse EW *et al*., 1993), fetoplacental receptor as 55 kDa (Karteris E *et al*., 1998), while human, monkey and rat cerebral cortex receptor as 58 kDa protein (Grigoriadis DE and DeSouza EB, 1989).

In most mammals, the fully active CRH-R1 protein arises from transcription of all 13 exons present within the CRH-R1 gene sequence. However, it is only in humans that the CRH-R1 gene contains 14 exons and the complete gene product is a 444-amino acid protein; this isoform is termed R1β. This insertion interferes with the signal transduction and reduces the coupling efficiency to adenylyl cyclase by 100-fold (Xiong Y *et al*., 1995). However, this receptor isoform is still able to internalize (Markovic D *et al*., 2006). Moreover, several other splice variants of the mRNA for this receptor have been identified, which might encode different isoforms, termed R1c-n (Grammatopoulos DK & Chrousos G, 2002) (Table 1.1 and Figure 1.2). The protein sequence of splice variants predicts receptors with amino acid inserts or various deletions in the N-terminus, C-terminus, intracellular loops, or transmembrane domains. Moreover, CRH-R1e1 and R1h are predicted to be soluble isoforms (Pisarchik A & Slominski A, 2002). These different isoforms would be expected to show different degrees in the efficiency of agonist-binding and varying signalling capability.

Regarding the receptor pharmacology, CRH-R1 binds CRH, UCN, urotensin I and sauvagine, with approximately equal affinity, but does not recognize UCN II or III.

CRH-R1 mRNA was found in high levels in the forebrain, cerebellum, septum, and amygdala, the anterior and intermediate lobe of the rat pituitary, and

with only low expression levels in thalamic and hypothalamic nuclei (Potter E *et al.*, 1994; Chalmers DT *et al.*, 1995). There is also evidence suggesting the presence of functional CRH receptors in the mouse spleen (Webster EL *et al*., 1989). CRH receptor binding sites were localised on resident splenic macrophages but not T or B lymphocytes (Webster EL & DeSouza EB, 1988). These findings suggest that CRH may play a physiologically significant role in regulating immune responses mediated by macrophages, such as chemotaxis, phagocytosis, and antigen presentation. Additionally, CRH-R1 expression was found in the mouse and human skin (Slominski A *et al*., 1995; Ermak G and Slominski, 1997), human leukemic mast cells, rat mammary carcinoma and melanocarcinoma cells, suggesting a possible explanation for the CRH proinflammatory effects (Tjuvajev J *et al*., 1998; Sato H *et al*., 2002). Furthermore, the CRH-R1α, R1d and splice variants- e, f, h, j, k, m, and n- were found to be differentially expressed in hamster pituitary, eye, spleen and heart, human and mouse skin, and four human melanoma cell lines (Pisarchik A & Slominski AT, 2001).

CRH-R1 subtype	Structural characteristics	References
R1α (415 aa)	Contains 13 exons	Chen R *et al*, 1993
R1β (444 aa)	Exon insertion after exon 5, CRH-R1 with extra 29 aa in the first IC loop	Chen R *et al*, 1993
R1c (375 aa)	Exon 3 deletion, CRH-R1 with 40 aa missing from the N-terminus	Ross PC *et al*, 1994
R1d (401 aa)	Exon 12 deletion, CRH-R1 with 14 aa missing from the seventh TMD	Grammatopoulos DK *et al*, 1999
R1e (194 aa and 240 aa)	Exon 3 and 4 deletion, frame shift, two potential reading frames	Pisarchik A *et al*, 2001
R1f (370 aa)	Exon 11 deletion, frame shift	Pisarchik A *et al*, 2001
R1g (341 aa)	Exon 10, 27bp of exon 9 and 28bp of exon 11 deletion	Pisarchik A *et al*, 2001
R1h (145 aa)	Cryptic exon insertion after exon 4, translation terminator	Pisarchik A *et al*, 2001

Table 1.1. Structural and splicing characteristics of CRH-R1 subtypes.

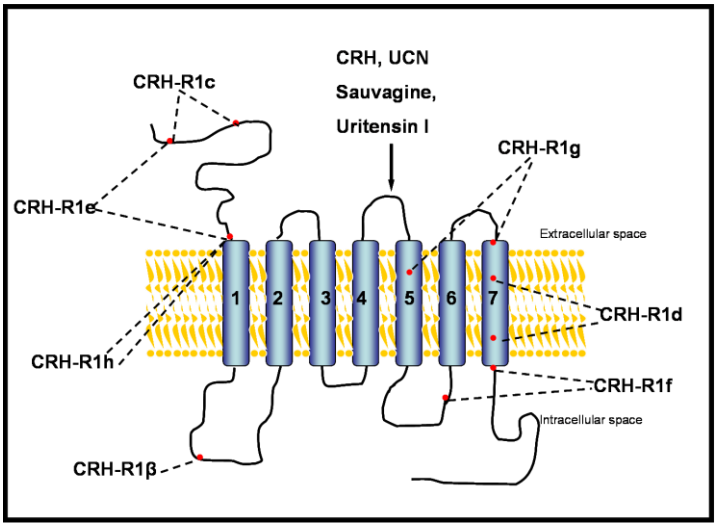

Figure 1.2 CRH-R1 isoforms. The presented receptor is CRH-R1α, and the other isoforms are compared to CRH-R1α (adapted from Grammatopoulos DK & Chrousos G, 2002).

Furthermore, CRH specific binding sites have also been demonstrated in the male reproductive system. In the female reproductive system, CRH receptor expression has been shown in a number of tissues, reinforcing the evidence for a significant CRH function during pregnancy and other reproductive events. In particular, it has been shown that CRH-R1 receptors are expressed in the human endometrial epithelial (Papadopoulou N *et al.*, 1998) and stromal cells (Di Blasio AM *et al.*, 1997), indicating a role for locally produced CRH in the physiological events of the endometrium. The CRH-R1 mRNA has also been found in the human ovary, located exclusively in the theca cells of mature follicles and moderately in small antral follicles, suggesting an autocrine and paracrine regulatory role for CRH in steroidogenesis and a possible implication in the aseptic inflammatory processes of ovulatory events (Asakura H *et al.*, 1997). The specific receptor subtype CRH-R1 mRNA and protein were detected in the human placenta and foetal membranes

(Karteris E *et al.*, 1998). Two CRH-R1 isoforms, R1α and the c splice variant, were identified in the syncytiotrophoblasts of the placenta and the amniotic epithelial cells of the foetal membranes. Additionally, the presence of CRH R1d splice variant expression has been found in foetal membranes (Grammatopoulos DK *et* al., 1999d). Furthermore, seven subtypes of the CRH receptors were found in the human pregnant myometrium at term before the onset of labor, R1α, R1β, R1c, R2α, R2β, and R2γ (Grammatopoulos DK *et al*., 1998a), and the splice variant R1d (Grammatopoulos DK *et* al., 1999d), whereas only three subtypes, R1α, R1β and R2β were found in the non-pregnant myometrium. This data demonstrates a differential expression pattern of the CRH receptor during pregnancy and suggests that CRH acting via different receptor subtypes might be able to exert distinct actions on the human myometrium in the pregnant, compared to the non-pregnant state (Grammatopoulos DK *et al*., 1998a).

1.3.2 The CRH-R type 2 (CRH-R2)

A distinct gene encodes the type 2 CRH receptor. There are very large regions of amino acid identity between the CRH-R1 and CRH-R2 particularly between the transmembrane domains (TMDs) five and six. This similarity underlies the conservation of second messenger function, since this 3rd intracellular loop region is presumed to play an important role in G protein coupling (Chalmers DT *et al*., 1996). However, the CRH-R2 gene exhibits a completely different splicing pattern compared to CRH-R1. This gene has three mRNA splice variants, termed R2α, R2β, and R2γ. All three variant mRNA are produced by the use of an alternative 5' exon 1 that splice onto a common set of downstream exons, resulting

in R2 variants, with identical transmembrane and C-terminus domains. Therefore, the variants differ only in their N-terminal extracellular domains; CRH-R2α has 34-amino acids at the N-terminus, which are replaced by 61-amino acids to form the CRH-R2β or 20-amino acids to form the CRH-R2γ (Hillhouse, EW & Grammatopoulos DK, 2006) (Figure 1.3). Both CRH-R2α and R2β have five potential glycosylation sites, which are analogous to those found in CRH-R1. The third splice variant, CRH-R2γ, has only four potential glycosylation sites (Kostich WA *et al*., 1998). In adenylyl cyclase activation assay, urocortin and sauvagine, appeared to be 10-fold more potent at the CRH-R2β than R2α or R2γ, suggesting that the N-terminus of the receptor is responsible for the ligand-receptor interaction (Kostich WA *et al*., 1998).

Interestingly, by contrast to CRH-R1, CRH-R2 binds UCN, UCN II, UCN III, sauvagine and urotensin I with significantly higher binding affinity than it does CRH, suggesting that these peptides might be its natural ligands (Perrin MH *et al*., 1999; Reyes TM *et al*., 2001; Lewis K *et al*., 2001). The CRH R2 was detected in the rat and mouse subcortical structures of the brain: in the lateral septal nucleus, ventromedial hypothalamic nucleus, olfactory bulb, amygdala and the choroid plexus (Sawchenko PE & Arias C 1995; Chalmers DT *et al.*, 1995). Additionally, CRH R2 mRNA was also identified in the PVN and supra-optic nucleus, as well as within the cerebral arterioles.

CRH R2α appeared to be the predominant CRH-R2 isoform, which is expressed on neuronal tissue, whereas CRH-R2β is localised to the non-neuronal elements such as the choroid plexus and cerebral arterioles (Chalmers DT *et al.*, 1995). CRH-R2 subtypes are highly expressed in the cardiac and skeletal muscle

(Perrin M *et al.*, 1995). In rodents, it appears that CRH-R2β is mainly a peripheral receptor produced in the heart and in blood vessels, whereas CRH-R2α has been found only in the central nervous system (CNS) (Lovenberg TW *et al.*, 1995a; Lovenberg TW *et al.*, 1995b; Turnbull AV & Rivier C, 1997). In contrast to rodents, both human CRH-R2α and CRH-R2β are co-expressed in peripheral organs and the CNS (Valdenaire O *et al.*, 1997; Ardati A *et al.*, 1999); however, CRH-R2γ, isolated only from human tissue, and it was found only in the brain (Kostich WA *et al.*, 1998). Additionally, CRH-R2α appears to be the predominant CRH receptor subtype present in the human heart (Hillhouse EW & Karteris E, 2002). Also, it has been shown that CRH-R2 mRNA was detected in human umbilical vein endothelial cells (HUVEC) (Simoncini T *et al.*, 1999) suggesting another action for placentally derived CRH during pregnancy. In pregnant myometrium CRH-R2β and R2γ mRNA was detected, while in non pregnant myometrium only CRH-R2β mRNA was present (Grammatopoulos DK *et al.*, 1998a).

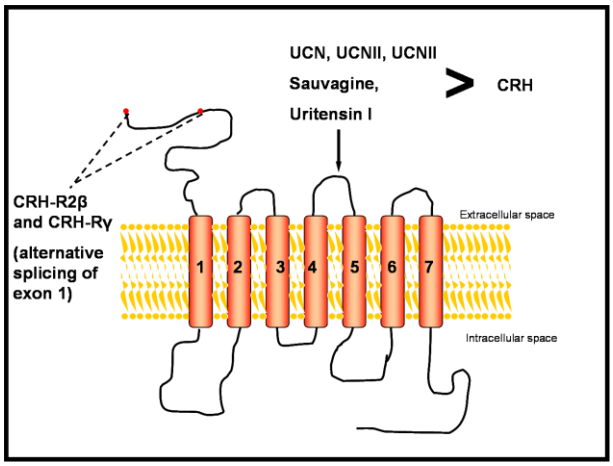

Figure 1.3 CRH-R2 isoforms. The presented receptor is CRH-R2α, and the other isoforms are compared to it (adapted from Grammatopoulos DK & Chrousos G, 2002).

1.4 Intracellular signalling of GPCRs

Binding of a ligand to GPCR causes conformational changes of the receptor, resulting in the positional changes of transmembrane domains and transduction of the signal from the extracellular environment to the inside of the cell. Initiation of signal transduction pathways mediated by guanine nucleotide binding proteins (G-proteins) lead to production of second messengers cAMP, inositol 1,4,5-triphosphate (IP_3), diacylglycerol (DAG), and calcium (Wettschureck N & Offermanns S, 2005).

G-proteins are dependent on the guanyl nucleotide guanosine triphosphate (GTP) for their regulatory actions. They are located in the cell membrane and are composed of three subunits: α (36-52 kDa), β (35-36 kDa), γ (8-10 kDa), each being encoded by distinct genes. The β- and γ- subunits are assembled into dimers that function as one unit and are only separable under strongly denaturing conditions. In an inactive state, the Gα-subunit is bound to GDP. GPCR's conformational change upon hormone binding stimulates GDP-GTP exchange on the Gα-subunit. The activated GTP bound α-subunit dissociates into α-GTP and βγ components. G-protein activation and subunit dissociation is accompanied by separation from the receptor, which reverts back to the low-affinity agonist binding state. Free α-GTP and βγ dimers then modulate activities associated with a range of effector enzymes or ion channels. The slow intrinsic GTPase activity of the Gα-subunit promotes reassociation of GDP-bound Gα-subunit with βγ, thus ending the interaction of α with its effector system and also terminating the βγ-mediated signalling (Cerione RA *et al*., 1984) (Figure 1.4).

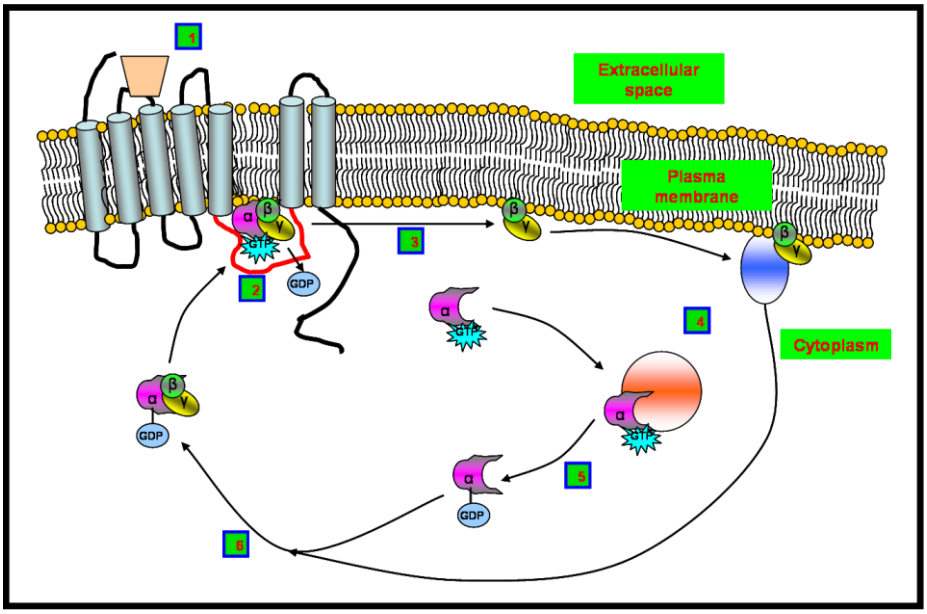

Figure 1.4 The G-protein cycle. When the ligand binds to its receptor (1), the receptor activates a G-protein by causing the Gα subunit to release GDP and bind GTP (2). The Gα and βγ subunits than dissociate (3), and initiate signal transduction events with a wide range of effectors (4). The Gα's intrinsic GTPase activity leads to hydrolysis of its bound GTP to GDP (5). The Gα-GDP subunit associates with βγ to form an inactive G-heterotrimer The events of dissociation, action and association of G-protein subunits occur at the plasma membrane (adapted from Cerione RA *et al*., 1984).

An individual G protein is primarily distinguished by the identity of the α subunits. More than 100 Gα subunits have been cloned from various species (Simon MI *et al*., 1991). According to their sequence homology and differential coupling to their effectors these proteins are classified in four distinct families: G_s, G_i, $G_{q/11}$, and $G_{12/13}$.

1.4.1 CRH-R coupling to G-proteins, second messengers and downstream signals

In many tissues endogenously expressing CRH-R (i.e. brain, heart, and myometrium) stimulation of the receptor by CRH or CRH-related peptides leads to the activation of adenylyl cyclase (AC) and increases cAMP levels

(Grammatopoulos D. *et al.* 1994). However, in some tissues such as that of the testes and placenta, CRH is unable to activate the AC pathway, but it stimulates hydrolysis of phosphoinositols. Such distinct responses of CRH-R activation has been attributed to differential and multiple G-protein activation. Several studies investigating CRH-R in native tissue and overexpressed in cellular systems have demonstrated multiple G-protein activation, with an order of potency $G_s \geq G_o > G_{q/11} > G_{i1/2} > G_z$. Interestingly, in native tissues, the pattern of G-protein activation by endogenous CRH-Rs appears to be unique for each tissue (Grammatopoulos D *et al.* 1999, Grammatopoulos D *et al.* 2001). Additionally, studies utilizing yeast cells (*Sz. Pombe*) containing Gα-transplants that enable exogenous CRH-Rs to couple to the yeast signalling pathways demonstrated that CRH-Rs couple to various G-proteins in agonist specific manner (Ladds G *et al*., 2003). The authors reported that CRH-activated CRH-R1α coupled to Gs, Gi_2, Gi_3 and G_{16}, while UCN activated receptor coupled to Gq and G_{16} (Ladds G *et al*., 2003). Moreover, CRH activated CRH-R2β coupled only to Gs and Gi_2; however, UCN-activated receptor interacted with Gi_2, Gi_3 and G_{16}, but not with Gs. While UCN-II and UCN-III stimulation of cells expressing CRH-R1α did not lead to any coupling of the receptor to G-proteins; these two agonists induced CRH-R2β interaction with Gs, Gi_2, Gi_3 and G_{16}, and with Gs, Gi_3, and Gq, respectively (Ladds G *et al*., 2003).

Due to its promiscuous coupling to diverse G-proteins, CRH-Rs can activate a plethora of intracellular protein kinases, such as PKA, PKC, PKB /Akt, and the p42/p44 and p38 MAPKs, by generating a number of second messengers (cAMP, NO/cGMP, Ca^{2+}, DAG, IP_3). Moreover, in a tissue-specific manner, signalling through CRH-R can activate other important molecules, such as steroidogenic

enzymes and Fas ligand (Grammatopoulos DK and Chrousos G, 2002). In immune cells, the local effects of CRH are complex since CRH can potentially inhibit and stimulate production of the proinflammatory cytokines (IL-1 and IL-6) by peripheral blood mononuclear cells. In reproductive tissues, CRH-R activation leads to prostaglandin production in human foetal membranes and placenta, and induces vasodilatation in the human foetal-placental circulation via a NO/cGMP-mediated pathway (Karteris E *et al.* 2000; Karteris E *et al.* 2005). The complexity and tissue specific diversity of CRH-R signalling in different types of cells is best illustrated by reports describing CRH as an inhibitor and stimulator of NF-κB pathway in human HaCaT keratinocytes and epidermal keratinocytes, respectively (Zbytek B *et al.* 2003; Zbytek B *et al.* 2004).

In the majority of cells, activation of CRH-Rs with CRH or UCNs leads to coupling of the receptors to the Gαs proteins and subsequent activation of adenylyl cyclase, resulting in cAMP production and PKA activation (Hillhouse EW & Grammatopoulos DK, 2006). The initiation of this signalling cascade modulates many cytoplasmic as well as nuclear target proteins. In a tissue-specific manner, the physiological results of activation of this cascade result in the vasodilatation of aorta and renal arteries (Sanz E *et al*., 2003; Maki I *et al*., 2004), possible glycerol release from adipose depose (Wellhoner P *et al*., 2007), upregulation of genes having the CREB transcription site (cAMP responsive element-binding protein) such as c-*fos* (Boutillier AL *et al*., 1991) and *Mif* (macrophage mitogen-inhibitory factor gene) in pituitary cells (Waeber G *et al*., 2004), and activation of the inflammatory responses in synovial tissue (McEvoy AN *et al*., 2002).

1.5 Termination of GPCRs signalling

After ligands bind GPCRs and trigger signal transduction cascades, there are many steps that occur over a period of seconds, minutes and hours that work to terminate the activation. An obvious termination mechanism is the dissociation of the ligand from the receptor, but this is dependent upon the affinity of the interaction. However, the waning of GPCR signalling in the continued presence of the agonist is accomplished by a co-ordinated series of events:

- Receptor desensitization
- Internalization
- Down-regulation
- Resensitization

These mechanisms include the uncoupling of the receptor from heterotrimeric G proteins in response to receptor phosphorylation by both second messenger-dependent kinases and GPCR kinases (GRKs), binding of β-arrestins to the receptor, the internalization of cell surface receptors to intracellular membranous compartments, and the down-regulation of the total cellular complement of receptors due to reduced receptor mRNA and protein synthesis, as well as both the lysosomal and plasma membrane degradation of pre-existing receptors (Ferguson SS, 2001).

1.5.1 Receptor desensitization

The exposure of GPCRs to agonists often results in a rapid attenuation of receptor responsiveness. This process, termed desensitization, begins within seconds of agonist exposure. Desensitization is initiated by phosphorylation of the

receptor on serine and threonine residues within the intracellular loops and C-terminal tail of many GPCRs (Luttrell LM & Lefkowitz RJ, 2002). There are two types of desensitization: heterologous and homologous. During heterologous desensitization the agonist occupancy of the target GPCR in not required; the receptor can be phosphorylated and desensitized by the activation of second messenger dependent protein kinases such as PKA and PKC. On the other hand, homologous desensitization is a consequence of conformational changes of the receptor upon ligand binding, and further phosphorylation of the receptor by GRKs and subsequent binding of β-arrestin. These events lead to the uncoupling of receptors from their respective heterotrimeric G-proteins.

1.5.1.1 G-protein coupled receptor kinases

The GRK family of serine/threonine (Ser/Thr) kinases is comprised of seven family members that phosphorylate agonist-occupied or activated GPCRs as their primary targets. GRKs identified up to date include: GRK1 (also known as rhodopsin kinase) (Lorenz W *et al*., 1991), GRK2 (β-adrenergic receptor kinase-1) (Benovic JL *et al*., 1989), GRK3 (β-adrenergic receptor kinase-2) (Benovic JL *et al*., 1991), GRK4 (IT-11) (Ambrose *et al*., 1992), GRK5 (Kunapuil P & Benovic JL, 1993, Premont RT *et al*., 1994), GRK6 (Benovic JL and Gomez J, 1993), and GRK7 (Hisatomi O *et al*., 1998).

In unstimulated cells, GRK1-3 are localized in the cytosol; upon the agonist activation of their GPCR targets GRK1-3 translocate to the plasma membrane. Since membrane targeting of all of the GRKs is crucial to their function, the mechanisms of this translocation has been the topic of many studies. Examining the structure of GRKs revealed that the NH_2-terminal domain contains a conserved

RGS domain responsible for binding to GPCRs, whilst distinct covalent modifications of the C-terminus are essential for membrane targeting (Stoffel RH *et al*., 1997). GRK1 and GRK7 are farnesylated at CAAX motifs (Inglese J *et al*., 1992), while GRK2 and GRK3 contain a βγ-subunit binding domain within their C-tails (Pitcher JA *et al*., 1992; Touhara K *et al*., 1994). The GRK5 C-terminus contains a stretch of 46 basic amino acids that mediate plasma membrane phospholipid interactions (Kunapuil P *et al*., 1994b; Premont RT *et al*., 1994). GRK4 and GRK6 are palmitoylated at cystein residues which restricts them to the plasma membrane even in unstimulated cells (Stoffel RH *et al*., 1994; Stoffel RH *et al*., 1998).

GRKs phosphorylate GPCRs on Ser and Thr residues in their third intracellular loop and C-terminal domains; this phosphorylation increases affinity of the receptor for arrestins. However, GRKs phosphorylation of GPCRs alone has little effect on receptor and G-protein coupling in the absence of arrestins (Lohse MJ, 1993). It is the binding of arrestin to receptor domains involved in G-protein coupling, rather than GRK phosphorylation, that leads to homologous desensitization of the receptor (Luttrell LM & Lefkowitz RJ, 2002).

1.5.1.2 The arrestin family

The arrestins constitute a small gene family with four members, all of which interact with activated and GRKs phosphorylated GPCRs. Aresstin1 and arrestin4 are found exclusively in retinal rods and cones, respectively, where they regulate rhodopsin and colour opsins (Shinohara T *et al*., 1987; Murakami A *et al*., 1993). By contrast, arestin2 and arrestin3 (Lohse MJ *et al*., 1990), commonly known as β-

arrestin1 and β-arrestin2, are expressed in all tissues where they regulate most GPCRs. There are reports suggesting the existence of two more arrestins, D-arrestin and E-arrestin (Craft CM *et al*., 1994). However, although partial cDNA clones for these two arrestins have been found in a broad range of tissues, it still remains uncertain as to whether full length D- and E-arrestin proteins exist.

The crystal structure of visual arrestin indicates that the protein contains two major domains, an N-domain (residues 8-180) and a C-domain (residues 188-362), each of which is composed of a seven stranded β-sheet (Figure 1.5) (Granzin J *et al*., 1998). Based upon mutagenesis studies, the β-arrestins are composed of two major functional domains an N-terminal (A) domain which is important in the recognition of activated receptor, and C-terminal (B) domain which is responsible for secondary receptor recognition. These two domains are separated by a phosphate sensor domain (P-domain). N (R1)- and C (R2)-terminal regulatory domains reside at either end of the protein. The R2 domain contains the primary site of β-arrestin phosphorylation (S412) as well as the LIEF binding motif for clathrin and the RXR binding domain for β2-adaptin (AP2). The recognition domain for inositol phospholipids as well as JNK3 and possibly other MAP kinases recognition sequence reside within the B domain (Luttrell LM & Lefkowitz RJ, 2002).

Beside their role in the specific uncoupling of agonist-bound GPCR from their cognate G proteins, numerous studies suggested that β-arrestins have an important role as adaptors and scaffolding proteins that link the receptors to the clathrin-coated pit endocytosis machinery (Goodman OB *et al*., 1996; Laporte SA *et al*., 1999) as well as to a variety of signaling systems such as ERK1/2 (Tohgo A *et al*., 2002), JNK3 (McDonald PH *et al*., 2000) and p38 (Sun Y *et al*., 2002).

Moreover, a mechanism by which β-arrestins attend to the degradation of cAMP has been suggested whereby they act as adaptors for the translocation of phosphodiesterase (PDE4) to activated β2-adrenergic receptors to sites of localized PKA activity at the plasma membrane (Perry SJ *et al*., 2002). As such, β-arrestins coordinate both receptor desensitization and the quenching of PKA activity.

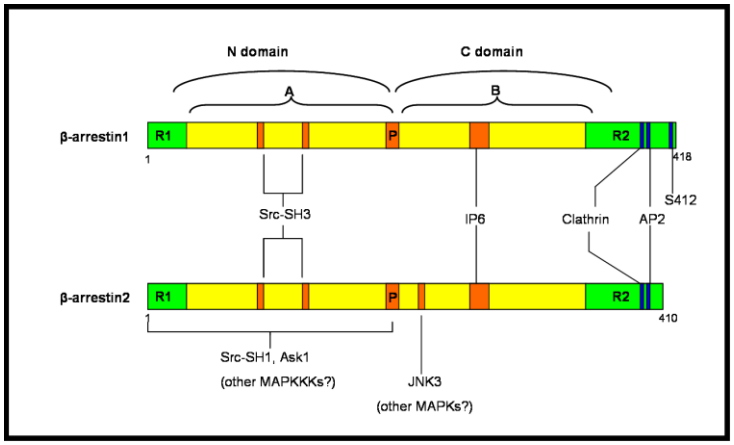

Figure 1.5 Structural and functional domains of β-arrestin1 and β-arrestin2 (adapted from Luttrell LM & Lefkowitz RJ, 2002).

1.5.2 Receptor internalization

Internalization of GPCRs, also known as receptor sequestration or endocytosis, occurs more slowly than desensitization, happening over a period of several minutes after agonist exposure (Ferguson SS, 2001). GRK-mediated GPCR phosphorylation and binding of β-arrestin to the receptor facilitates the agonist-promoted endocytosis of many GPCRs. The extent of β-arrestin involvement appears to vary depending on the receptor, agonist and cell type. As mentioned earlier, β-arrestins contain two motifs that allow them to function as adapter proteins that link the GPCRs to components of the clathrin-dependent endocytic machinery. β-arrestins have a high affinity for clathrin in vivo (Goodman OR *et al*., 1996). In addition, β-arrestins bind directly to AP-2 (Laporte SA *et al*., 1999). The

AP-2 complex links many receptors to the clathrin endocytic machinery by binding clathrin, dynamin and EPS-15, and is involved in the initiation of clathrin-coated pit formation (Kirchhausen T, 1999).

The phosphorylation state of β-arrestin1 is crucial in its endocytic function. Cytoplasmic β-arrestin1 is phosphorylated on S412 (Lin FT *et al*., 1997) by ERK1 and ERK2 (Lin FT *et al*., 1999). However, upon translocation to the membrane, β-arrestin1 is rapidly dephosphorylated. On the other hand, β-arrestin2 is not phosphorylated at its C-terminus, but its endocytic function is regulated by post-translational modification after binding to the receptor. Shenoy has demonstrated that β-arrestin2 and β2 adrenergic receptors undergo rapid, β-arrestin-dependent ubiquitination in response to agonist binding (Shenoy SK *et al*., 2001). β-arrestin ubiquitination is required for receptor internalization, whereas the receptor ubiquitination is involved in degradation of the receptor but not its internalization (Luttrell LM & Lefkowitz RJ, 2002).

Based on the β-arrestin involvement in the internalization process, GPCRs are grouped into two distinct classes (Oakley RH *et al*., 2000). Class A receptors bind to β-arrestin2 with higher affinity than β-arrestin1 and do not bind visual arrestin. Their interaction with β-arrestin is transient. β-arrestin is recruited to the receptor and translocates to clathrin-coated pits; but the receptor-β-arrestin complex dissociates upon internalization of the receptor, and the receptor proceeds into an endosomal pool, while β-arrestin translocates back to the plasma membrane (Zhang J *et al*., 1999). The members of this class include β2 and α1B adrenergic, μ opioid, endothelin A, and dopamine D1A receptors. Class B receptors, such as neurotensin 1, vasopressin 2, and angiotensin AT1a receptors, bind to β-arrestin1 and β-arrestin2 with equal affinity and also interact with visual arrestin. The receptor-β-

arrestin complex is stable and it internalizes as a unit that is targeted to endosomes (Luttrell LM & Lefkowitz RJ, 2002). The stability of receptor-β-arrestin complex is dictated by the specific clusters of Ser and Thr residues in the C-terminal tail of the receptor as well as the C-terminus of β-arrestin (Oakley RH *et al*., 2001).

The precise mechanism by which all GPCRs internalize is still a topic surrounded by much controversy. It is now thought that not all GPCRs internalize in a β-arrestin and clathrin-dependent manner (Ferguson SS, 2001). An example of this case is that both angiotensin II type 1A receptor and m2 muscarinic acetylcholine receptor seem to internalize normally in the presence of dominant-negative β-arrestin and dynamin mutants, however the internalization of both these GPCR subtypes seems to be dependent on receptor phosphorylation (Smith RD *et al*., 1998; Lee KB *et al*., 1998).

1.5.3 Receptor down-regulation

Down-regulation of GPCRs is defined as the persistent loss of cell surface receptors that occurs over a period of hours to days. Control of cell surface receptor density occurs at least partially at the transcriptional level, but the removal of agonist-occupied receptor from the surface and their sorting for either degradation or recycling is important, at least in the early stages of down-regulation (Luttrell LM & Lefkowitz, RJ, 2002). As mentioned earlier, the complexes between receptor and β-arrestin have varying stability. In fact, the stability of these complexes might dictate the fate of the internalized receptor. Class A receptors are rapidly dephosphorylated and recycled back to the plasma membrane; whereas the stable complex of class B receptors and β-arrestin retards resensitization and might favour the receptor for degradation.

1.5.4 Receptor resensitization

In order for an internalized GPCR to become resensitized, it is not only β-arrestin-dependent targeting of receptors to clathrin-coated pits and their subsequent endocytosis to endosomes that is required, the receptors also have to release β-arrestin, become dephosphorylated, sorted and recycled back to the cell surface. It was found that involvement of small RabGTPases is essential for these processes (Ferguson SS, 2001). Rab5 (GTPase Rab5) is involved in formation of receptor-bearing vesicles at the cell surface (Seachrist JL *et al*., 2000), their trafficking and fusion with early endosomes. The dephosphorylation of the receptor occurs during the receptor transition between Rab5- and Rab4-positive endosomal compartments (Seachrist JL *et al*., 2000). The low pH in endosomes could contribute to ligand dissociation as well as conformational changes in the receptor. It has been reported that protein phosphatases (PP2A) are capable of dephosphorylating GPCRs in acidic conditions (Sibley DR *et al*., 1986; Pitcher JA *et al*., 1995) Rab4 also regulates the recycling of the receptor back to the plasma membrane. These events all contribute to receptor resensitization.

1.5.5 CRH-R desensitization and internalization

In most tissues, CRH actions are dependent on the adequate expression of CRH-R in the plasma membrane. The exposure of CRH-R to CRH and other agonists results in rapid attenuation of CRH-R responses, through a mechanism of receptor desensitization. In recent years, CRH-R1 desensitization and internalization have been extensively studied (Teli T *et al.* 2005; Rasmussen TN *et al.* 2004; Perry SJ *et al*., 2005, Holmes KD *et al*., 2006, Markovic D *et al*., 2006).

Teli *et al* (2005) has demonstrated that half-maximal desensitization of CRH-R1α occurred after approximately 40 min of pre-treatment and full recovery of the receptor's functional response was established within 2h of removal of CRH pre-treatment. In HEK293 cells, desensitization of CRH-R1α was associated with receptor phosphorylation and subsequent endocytosis (Teli T *et al*., 2005). Moreover, it has been shown that the mechanism leading to the desensitization of CRH-R1α involves GRK3 and GRK6 as the main isoforms that interact with the receptor, and that recruitment of GRK3 requires Gβγ-subunits as well as β-arrestin. Site-directed mutagenesis of Ser and The clusters within the C-tail of CRH-R1α, pointed toward Thr399 as an important residue for GRK-induced receptor phosphorylation and desensitization (Teli T *et al*., 2005).

Further internalization studies demonstrated that β-arrestin was recruited toward the plasma membrane of HEK293 over-expressing CRH-R1α, upon stimulation with CRH (Rasmussen TN *et al*., 2004; Perry SJ *et al*., 2005; Holmes KD *et al*., 2006). Perry and Holmes pin-pointed β-arrestin2 as a major isoform involved in CRH-R1α sequestration, but further fate of the receptor is still controversial. Holmes (2006) defines CRH-R1α as a class A receptor regarding the lack of β-arrestin2 co-localisation with the receptor in the endosome structure in HEK293, whereas Perry (2004) has demonstrated co-localisation of the two in the cytoplasm. However, Holmes (2006) has demonstrated that CRH-R1α does indeed co-localise with β-arrestin2 in the cytoplasm of primary cortical neurons. Moreover, it has been shown that following endocytosis, the receptor transited from Rab5-positive early endosome to Rab4-positive recycling endosome, and that the receptor was not targeted for degradation in lysosomes in HEK293 overexpresing CRH-R1α and in primary cortical neurons (Holmes KD *et al*., 2006). In contrast, CHO-K1

stably expressing CRH-R1 challenged with CRH for 1h had 83% of the receptor remain, but after 24h treatment only 38% the total CRH-R1 proteins were detected, clearly demonstrating the receptor down-regulation (Perry SJ *et al*., 2005). Taken together these findings suggest that different cellular systems might have distinct patterns of CRH-R1 endocytosis.

1.6 GTPase Rho and Rho-dependent response

Currently around 100 members of the small GTPase superfamily ranging from 20-30 kDa have been identified. These are broadly divided into five subfamilies: Ras, Rho/Rac/cdc42, Rab, Sar1/Arf and Ran. The functions of many small G-proteins are still unknown. In general, the Ras family of GTPases regulates cell signalling events that lead to alterations in gene transcription; Rho family GTPases function as regulators of the actin cytoskeleton and can also influence gene transcription (one of possible mechanisms is through activation of the NF-κB pathway (Perona R *et al*. 1997)); Rab and Arf family GTPases control the formation, fusion and movement of vesicular traffic between different membrane compartments of the cell; and Ran GTPase regulates both microtubule organisation and nucleo-cytoplasamic protein transport (Bhattacharya M *et al.*, 2004).

The small GTPase Rho have been reported to regulate many cellular functions such as cell adhesion, cell contraction, cell migration and tumour cell invasion, growth control and survival responses, phospholipid metabolism, MAP kinase activation and gene transcription, endocytosis, exocytosis, glucose transport and ion channel function (Wettschureck N & Offermanns S, 2002). RhoA is the best characterized member of the Rho family. All members of the Rho family of

proteins, like any other small GTPases, function as molecular switches, cycling between an inactive GDP-bound state and an active GTP-bound state (Somlyo AP & Somlyo AV, 2003). In the resting state, RhoA-GDP exists in the cytosol tightly associated with its partner, GDP dissociation inhibitor (RhoGDI). Activation of receptors coupled to certain trimeric G proteins such as $G\alpha_q$, $G\alpha_{12,13}$, and receptor tyrosine kinases lead, through activity of guanine nucleotide exchange factors (GEFs), to the exchange of GDP for GTP on RhoA. This causes RhoGDI dissociation and "free" RhoA-GTP translocation to the membrane where it interacts with Rho-kinase (ROCK) to initiate a number of signalling events. The GTP-bound form of RhoA is converted in the GDP-bound form due to its intrinsic GTPase activity, which is stimulated by GTPase-activating proteins (Rho-GAPs) (Figure 1.6).

It is well documented that GPCR signalling through heterotrimeric G-proteins can lead to the activation of Ras and Rho-GTPases. Most GPCRs can couple to multiple G proteins, making it difficult to pin point which specific G protein is involved in the activation of RhoA. It has been shown that the stimulation of heterologously expressed α_2-adrenergic receptor in preadipocytes leading to Rho-mediated changes in cell morphology is pertussis toxin sensitive (Betuing S *et al.*, 1998). Paradoxically, βγ subunits isolated from $G_{i/o}$ were shown to bind to Rho and inhibit Rho-GTPγS binding, suggesting a possible additional inhibitory effect of $G_{i/o}$ proteins on Rho (Harhammer R *et al.*, 1996).

Most of the GPCRs shown to activate Rho are coupled to $G_{q/11}$. In spite of this, accumulating evidence suggest that $G_{q/11}$ proteins might be insufficient activators of Rho-mediated responses, but that an additional interaction with other proteins such as β-arrestins is required for the activation. Recently, it has been

demonstrated in the case of angiotensin II type 1A receptor ($AT_{1A}R$) that neither β-arrestin1 nor $G\alpha_{q/11}$ activation alone are sufficient to robustly activate RhoA, but that the concurrent recruitment of β-arrestin1 and activation of $G\alpha_{q/11}$ leads to full activation of RhoA and to the subsequent formation of stress fibres (Barnes WG *et al.*, 2005).

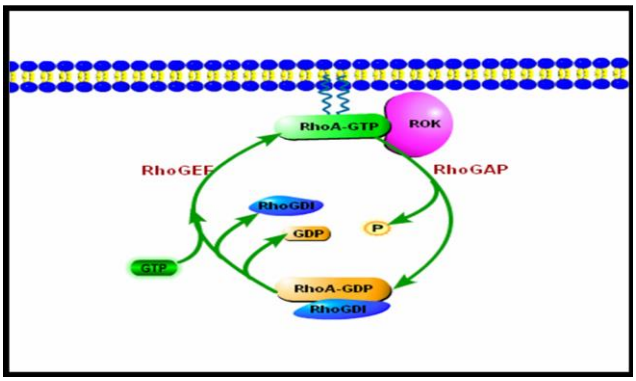

Figure 1.6 RhoA activation cycle. Upon stimulation, cytoplasmic RhoA-GDP is activated by GEF. RhoA-GTP translocates to the plasma membrane where it interacts with ROCK. RhoA-GTP is inactivated by GAP which hydrolyses GTP to GDP. Inactive RhoA is reunited with its cytoplasmic partner (GDI). (Adapted from Somlyo AP & Somlyo AV, 2003).

There is increasing evidence showing that in some cellular systems activation of Rho is primarily mediated via G proteins of the $G_{12/13}$ family. $G_{12/13}$ can bind to and activate Rho-specific GEFs (p115RhoGEF, LARG, PDZ-RhoGEF) (Kozasa T *et al.*, 1998) providing a possible mechanism by which GPCRs could activate Rho and its downstream responses. However, it has been demonstrated that these two G-proteins activate Rho via distinct mechanisms (Gohla A *et al.*, 1998; Diviani D *et al.*, 2001). Although most of current evidence suggest that $G\alpha_{12/13}$ can interact directly with RhoGEFs, it is likely that second messenger pathways and kinase cascades also regulate Rho activity. Phosphorylation of Rho or its regulators (GAPs, GDIs and GEFs) by MAP kinase, PKC, PKG, and PKA (Murthy KS *et al.*,

2003), is likely to provide additional mechanisms by which GPCRs can modulate Rho signalling pathways.

Once activated, Rho can bind to a large number of proteins. The best characterized Rho effectors are the Ser/Thr-directed Rho kinases (Rho kinase/ ROKα/ROCK II and p160ROCK/ROCKβ, generically known as Rho kinase). The development of a selective inhibitor, Y27632 (Uehata M *et al.*,1997), has made it possible to monitor the involvement of Rho kinase in cellular responses. Much less is known about the specific function of other groups of Rho effectors, which are PKC-related Ser/Thr kinases (PKN/PRK1 and PRK2), citron kinase, p140mDia, rhophilin and rhotekin.

1.7 Nuclear factor kappa B (NF-κB)

NF-κB was first discovered as a constitutive protein in the nuclei of mature murine B-lymphocytes that bound to a ten-base pair DNA motif (GGGACTTTCC) in the κ immunoglobulin light chain enhancer (Sen R & Baltimore D, 1986). NF-κB is now known to be an inducible transcription factor widely distributed in eukaryotic cells (Lenardo MJ & Baltimore D, 1989; Sen R & Baltimore D, 1986). This ubiquitous transcription factor modulates many gene products involved in inflammation and acute phase responses (Baeuerle PA & Henkel T, 1994;). NF-κB also plays an important role in immune responses, thymus development, apoptosis, embryonic development, growth control, malignant transformation and viral gene expression (Beg AA *et al.*, 1995; Kopp EB & Ghosh S, 1995). Over 150 stimuli are known to activate NF-κB (Pahl, 1999). These include multiple bacterial and viral infections, as well as bacterial and viral products. Because of this NF-κB has often

been termed “the central mediator in the immune system”. In addition, NF-κB is also activated by numerous other stimuli that are not derived from bacterial and viral infections, including various cellular and environmental stresses such as irradiation, osmotic shock, oxidative stress, hyperglycaemia, the ER overload response, and haemorrhage (Pahl HL, 1999).

Upon activation, NF-κB promotes transcription of over 150 genes many of which are involved in the host immune/inflammatory responses. These include cytokines, chemokines, immunoreceptors, adhesion molecules, stress response genes, apoptotic regulators, growth factors, transcription factors, and inflammatory enzymes known to be active in inflammatory diseases (Barnes PJ & Karin M, 1997; Pahl HL, 1999).

NF-κB is a homo- or heterodimeric protein composed of different combinations of members of the Rel family of transcriptional factors. This family shares an N-terminal domain of approximately 300-amino acid, known as the Rel homology domain (RHD). The N-terminal part of the RHD contains the DNA-binding domain, whereas the dimerization domain is located in the C-terminal region of the RHD. Close to the C-terminal end of the RHD is the nuclear localization signal (NLS), which is essential for the transport of active NF-κB complex into the nucleus. Also RHD is responsible for binding to the inhibitor of Kappa B (IκB) (Chen FE & Ghosh G, 1999).

Five mammalian NF-κB family members have been characterised; these are p65 (RelA), RelB, c-Rel, NF-κB1 (p50 and its precursor p105) and NF-κB2 (p52 and its precursor p100) (Bonizzi G & Karin M, 2004). The NF-κB proteins are divided into two groups based on the C-terminal sequence on the RHD. Members of the first group (p105, p100, and *Drosophila* Relish) have long C-terminal domains

that contain multiple copies of ankyrin repeats, which act to inhibit these molecules. These proteins become active by either limited proteolyisis or arrested translation (p105 to p50, and p100 to p52) (Gilmore TD, 1999). As such, members of this group are generally not activators of transcription, except when they form dimers with the members of the second group. The second group includes p65 (RelA), RelB and c-Rel as well as Dorsal and Dif. These proteins are not synthesised as precursors and they possess one or more C-terminal transactivation domains (TD), in addition to the RHD (Gilmore TD, 1999). RelB, c-Rel and p65 do not bind DNA efficiently, but are effective transactivators. However, p50 and p52 are the main DNA-binding subunits with poor transactivation abilities unless in a dimer with RelB, c-Rel or p65 (Siebenlist U *et al.,* 1994). The most abundant of the complexes is NF-κB which consists of p65/p50 heterodimers.

There are currently eight known members of the IκB family including IκBα, IκBβ, IκBγ, IκBε IκBζ, Bcl-3, p105, p100 and the *Drosophila* protein cactus (Ghosh S *et al.*, 1998; Yamazaki S *et al.*, 2001). The proteins p105 and p100 are the pre-cursors of (p50) and (p52) respectively. All IκBs contain 6 or 7 ankyrin repeats which bind the RHD of NF-κB (Karin & Ben-Neriah, 2000). Little is known about the functional significance of the different IκBs. However, IκBα, IκBβ and IκBε are the only IκBs to possess the N-terminus regulatory regions required for stimulus induced NF-κB activation (Karin M & Ben-Neriah Y, 2000). In the majority of cells, the p65/p50 heterodimer form of NF-κB is found complexed with IκBα, which is targeted by IKK-dependent phosphorylation of serines 32 and 36 (Hayden and Ghosh, 2004; Karin and Ben-Neriah, 2000). The phosphorylated IκBα proteins are recognised by ubiquitin ligases, which polyubiquitinate IκBα at lysines 21 and

22 leading to the degradation of IκBα by the 26S proteosome (Hayden MS & Ghosh S, 2004; Karin M & Ben-Neriah Y, 2000).

The IκB kinase was first identified by biochemical methods as a 700 kDa complex with IκB kinase activity (Chen ZJ *et al.,* 1996). To date three proteins have been confirmed as components of the IKK complex (Chen ZJ *et al.*, 1996), IKKα, IKKβ and NF-κB essential modulator (NEMO) or IKKγ (Karin M and Ben-Neriah Y, 2000). Recent reports have shown that the IKK complex might contain two additional proteins, Hsp90 and Cdc37 (Chen F *et al.*, 2002; Krappmann D *et al.*, 2000). According to these reports, the IKK complex contains a heterodimer of IKKα and IKKβ, a homodimer of Hsp90 and two or three molecules of IKKγ and Cdc37 giving an approximate molecular weight of 800 kDa (Chen F *et al.*, 2002; Krappmann D *et al.,* 2000). The IKK complex is the convergence point of the numerous pathways that lead to IκB-degradation dependent NF-κB activation.

1.7.1 NF-κB activation

There are two NF-κB activation pathways: classical and alternative. In the classical pathway, the activated IκB kinase (IKK) complex, predominantly acting through IKKβ in an IKKγ-dependent manner, catalyzes the phosphorylation of IκBs (at the sites equivalent to Ser32 and Ser36 of IκBα), polyubiquitination (at the sites equivalent to Lys21 and Lys22 of IκBα) and subsequent degradation by the 26S proteosome. The released NF-κB dimers (most commonly p65/p50) translocate to the nucleus, bind DNA and activate gene transcription, including IκBα (Ghosh S and Karin M, 2002). After re-synthesis, IκBα enters the nucleus through its nuclear localisation signal (NLS) and removes NF-κB from the κB binding sites. IκBα is able to do this because NF-κB has a greater affinity for IκBα binding than it does

for DNA binding (Arenzana-Seisdedos F *et al.*, 1997). Once bound the IκBα/NF-κB complex is exported back into the cytoplasm through the IκBα nuclear export signal (NES). Thus, the resynthesis of IκBα acts as a negative feedback loop and limits the duration of NF-κB activity (Arenzana-Seisdedos F *et al.*, 1997). The alternative pathway is independent of IKKβ and IKKγ. The target for IKKα homodimers in this pathway is NF-κB/p100, which is phosphorylated at two C-terminal sites, leading to processing of p100 to p52 (Xiao G *et al.*, 2001).

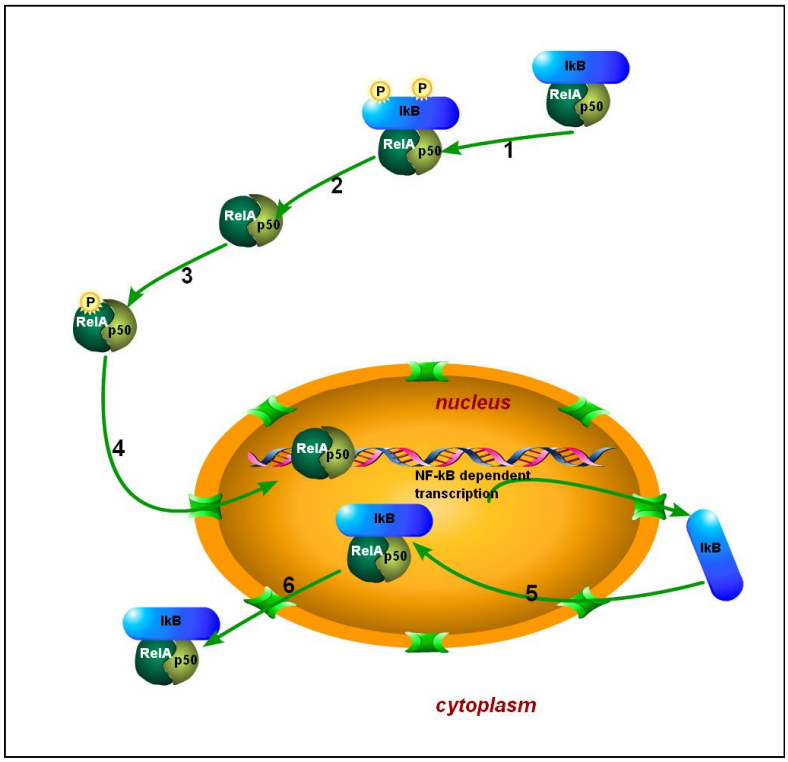

Figure 1.7 NF-κB activation pathway. Activation of various receptors leads to phosphorylation of IκB (1), and subsequent ubiqutination and degradation (2). RelA is than phosphorylated (3) which enhances its translocation to the nucleus (4), where it binds to the DNA leading to NF-κB dependent transcription. One of the transcribed genes is IκBα. Newly synthesised IκBα enters the nucleus (5), where it binds to RelA/p50. The complex then leaves the nucleus (6). (Adapted from Bonizzi G & Karin M, 2004)

A number of kinases, including NF-κB inducing kinase (NIK), MEKK-3, NF-κB activating kinase (NAK) (also known as TANK binding kinase (TBK) or

T2K), MAPK and Akt have been implicated in NF-κB activation via the IKK complex (Pomerantz JL & Baltimore D, 1999; Romashkova JA and Makarov SS, 1999; Bonnard M *et al*., 2000). Nevertheless, it has proved difficult to unambiguously confirm that any of these kinases activate the IKKs and it is likely that activation of the IKKs is a complex process involving multiple kinases and adapter proteins.

1.8 Brown adipose tissue

Mammalian adipose tissue is characterised into white adipose tissue (WAT) and brown adipose tissue (BAT), according to their colour and distinct function. The presence, amount and distribution of each varies depending on the species (Albright AL & Stern JS, 1998). Until recently it was believed that the function of WAT was heat isolation, mechanical cushioning and energy storage. Moreover, WAT is an endocrine organ able to produce many adipocytokines or adipokines such as leptin, adiponektin, resistin, plasminogen activator inhibitor-1 (PAI-1), tumor necrosis factor α (TNF-α), visfatin, and retinol binding protein 4 (RBP4). The role of these peptides involved in modifying appetite, insulin resistance and artheriosclerosis is under vigorous investigation. Morphologically, BAT differs from WAT by its rich vascularisation and numerous unmyelinated nerves which provide sympathetic stimulation to the adipocytes (Nnodim JO & Lever JD, 1988) Additionally, in contrast to white adipocytes which contain a single, large lipid droplet, brown adipocytes contain numerous smaller lipid droplets and an extraordinary number of mitochondria (Weber WA, 2004). The function of BAT is

to transfer energy from stored energy into heat. A mitochondrial protein, uncoupling protein 1 (UCP-1) is responsible for this unique function of BAT. UCP-1 gives the mitochondria the ability to uncouple oxidative phosphorylation and utilize substrates to generate heat rather than ATP. The development of BAT and UCP-1 was probably determinative for the evolutionary success of mammals, as thermogenesis enhances the survival chances of hibernating animals and also that of neonates, and also facilitates active life in cold conditions (Cannon B & Nedergaard J, 2004). BAT is most predominant in newborn animals. In human babies it comprises up to 5% of total body weight and it is present in the neck and interscapular area.

1.8.1 Lipolysis and proteins involved in lipolysis

The information on body temperature, energy reserves and feeding status are coordinated in the ventromedial hypothalamic nucleus (VMN) of the brain. When there is a need to increase the rate of heat production, a signal (norepinephrine) is transmitted via the sympathetic nervous system to the individual brown adipocytes (Cannon B & Nedergaard J, 2004). The released norepinephrine binds to its receptor (β3-adrenergic receptor) on the plasma membrane of the brown adipocyte. Activation of β3-adrenergic receptors leads to increased cAMP production, which is followed by activation of PKA and subsequent phosphorylation of hormone sensitive lipase (HSL) and perilipin, resulting in triglyceride and diglyceride breakdown to free fatty acids (FFA) and glycerol (Egan JJ *et al*., 1992) (Figure 1.8).

It was thought that the rate limiting step of lipolysis is controlled by the actions of HSL, however recent studies on HSL null mice have changed this

perception, indicating adipose triacylglycerol lipase (ATGL) as the major triacylglycerol lipase (Jaworski K *et al*., 2007), There are three isoforms of the enzyme ranging from 84 to 130 kDa. (Carmen GY & Victor SM, 2006). Beside acylglycerols, HSL can hydrolyse cholesteryl esters, retinyl esters, steroid esters and *p*-nitrophenyl esters (Holm C *et al*., 2000). This enzyme has three domains, a catalytic domain, a regularory domain with several phosphorylation sites and an N-terminal domain involved in protein-protein and protein-lipid interactions (Yeaman SJ, 2004). It has been demonstrated that upon lipolytic stimulation of fat cells and 3T3-L1 adipocytes, HSL translocates from cytoplasmic compartments to the lipid droplets, the site of its action (Egan JJ *et* al., 1992; Londos C *et al*., 1995).

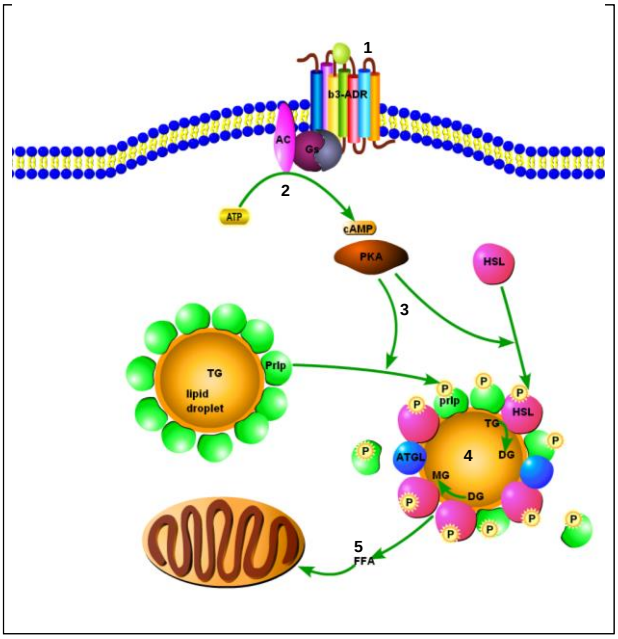

Figure 1.8. PKA-stimulated lipolysis in adipocytes. Activation of β3-adrenergic receptor (1) leads to activation of adenylyl cyclase (AC) and subsequent elevation of cAMP levels and activation of PKA (2). PKA phosphorylates perilipin (prlp) and HSL; perilipin undergoes conformational changes in order to make space on the droplet surface for activated HSL (3). Once on the droplet surface, ATGL and HSL mediate hydrolysis of triacylglycerol (TG) to diacylglycerol (DG), and HSL catalyses hydrolysis of DG to MG (monoacylglycerol). Released FFAs (free fatty acids) than enter mitochondria. (Adapted from Tansey J *et al*., 2004)

PKA phosphorylates HSL at Ser-563, Ser-659 and Ser-660 stimulating the activity of the lipase (Degerman E *et al*., 1990; Anthonsen MW *et al*., 1998). On the other hand, AMP-dependent protein kinase (AMPK) phosphorylates HSL at Ser-565 and the phosphorylation of this site prevents the phosphorylation of Ser-563, thus decreasing the lipase activity (Garton AJ & Yeaman SJ, 1990). Recently, It has been demonstrated that phosphorylation at Ser-600 ERK enhances the enzymatic activity of HSL (Greenberg AS *et al*., 2001).

The perilipins are hydrophobic lipid droplet-associated phosphoproteins that can be phosphorylated by PKA in multiple residues. It has been proposed that in nonstimulated cells perilipin may deter HSL interaction with the droplet by forming a barrier around it (Clifford GM *et al*., 2000). However, upon HSL translocation to the lipid droplet, perilipin is phosphorylated by PKA and lose their blocking capability, possibly through translocation from the droplets (Carmen GY & Victor SM, 2006).

Adipocyte lipid binding proteins (ALBP) are cytosolic proteins that interact with HSL, favouring the translocation from the cytosol to lipid droplets (Shen WJ *et al*., 1999). ALBP form 1:1 complex with fatty acids and other hydrophobic ligands, sequestering fatty acids inside the cytosol to protect the cell from its harmful effect (Bernlohr DA *et al*., 1997).

1.8.2 Thermogenesis in BAT

FFAs, the product of lipolysis, are activated to acyl-CoAs (CoenzymeA) by acyl-CoA synthetase and are transferred to acyl-carnitine by carnitine palmitoyltransferase I (CPT-I). The acyl-carnitine probably enters the mitochondria

through the carnitine transporter and it is probably reconverted to acyl-CoA by CPT-II. The ensuing β-oxidation of the acyl-CoA and the activity of the citric acid cycle lead to formation of the reduced electron carrier FADH and NADH, which are then oxidized by the electron transport chain (respiratory chain), ultimately though oxygen consumption. This results in a pumping out of protons from the mitochondria and the formation of a proton-motive force. In cells other than brown adipocytes, protons re-enter mitochondria via ATP synthesis. If ADP is unavailable, protons are unable to re-enter mitochondria, increasing the proton gradient and limiting further electron transfer and fuel oxidation (Lowel BB & Flier JS, 1997). However, mitochondria of brown adipocytes have UCP-1 present in the inner membrane, which dissipates the proton gradient by driving protons back into the mitochondrial matrix, thereby uncoupling fuel oxidation from the availability of ADP. Thus, the physiological consequence of UCP-1 activity is unrestrained oxidation of fuels with the generation of heat (Cannon B & Nedergaard J, 2004) (Figure 1.9).

The proton transport mediated by UCP-1 is highly regulated. Fatty acids are the main physiologically relevant intracellular regulator of UCP-1 activity (Locke RM *et al*., 1982). Studies utilising isolated brown adipocyte mitochondria have demonstrated that proton transport is significantly stimulated by increasing concentration of fatty acids (Cannon B & Nedergaard J, 2004). It has been suggested that UCP-1 is a FFA anion transporter and not a proton transporter (Jezek P *et al*., 1994; Jezek P *et al*., 1996). Membrane impermeable FFA anions are transported out of the mitochondria by UCP-1. These FFA anions become protonated and, in this permeable state, re-enter the mitochondria, with the net

result being transport of protons onto the mitochondria (Lowel BB & Flier JS, 1997).

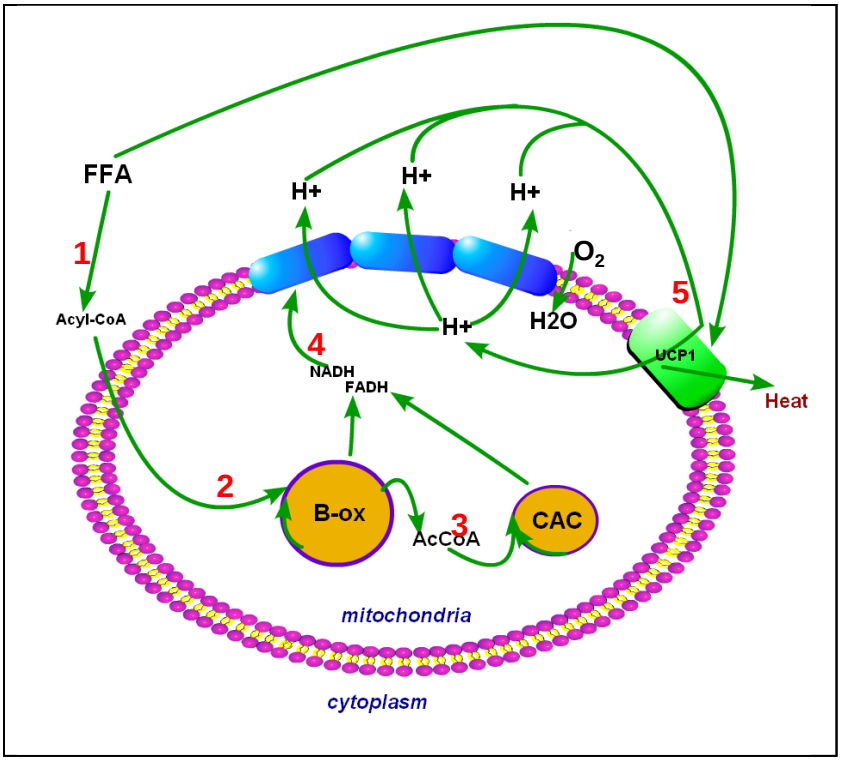

Figure 1.9.Thermogenesis in brown adipocytes. Lipolysis generated FFAs are activated to acyl-CoAs and as such they are transported into mitochondria (1) where the fatty acids enter β-oxidation (β-ox) (2) followed by the citric acid cycle (3). Products of these processes are the reduced FADH and NADH, which are oxidized by the respiratory chain (blue boxes) (4). This leads to pumping protons out of mitochondria and the formation of proton gradient which drives protons back to mitochondrial matrix through UCN-1 (5). The energy stored in this proton-motive force is released as heat. (Adapted from Cannon B & Nedergaard J, 2004).

1.8.3 BAT and regulation of total body fat

Beside to its thermoregulatory role, BAT plays an important role in regulating total body fat, at least in rodents. Transgenic mice with decreased BAT show glucose intolerance and insulin resistance as well as enhanced susceptibility to

diet-induced obesity and diabetes (Hamann A *et al*., 1993; Hamann A *et al*., 1995). This suggests that BAT protects against obesity caused by a high calorie diet.

As newborns, we have relatively large deposits of BAT. The heat produced in BAT can be imaged using a thermal-infrared camera. If such pictures are taken of an unwrapped infant sleeping at room temperature, "hot spots" can be seen in the skin overlying BAT deposits in the neck and interscapular area (Austgen L 2002). It is believed that with age, but probably more with size, our relative functionality of BAT decreases and disappears. Recently, it has been reported that within WAT depots in adult humans, islets of BAT may be found; additionally UCP-1 mRNA is detectable in WAT and its levels can be increased in vitro by norepinephrine (Cannon B & Nedergaard J, 2004). However, the evidence for adaptive adrenergic nonshivering thermogenesis in humans is limited. There are two positive reports, suggesting the recruitment of an adaptive adrenergic nonshivering thermogenesis in adult humans, but only to the levels of 15% above basal body temperature (Cannon B & Nedergaard J, 2004). In adults with pheochromocytomas (catecholamine secreting tumors) abundant BAT depots were detected, indicating that BAT in human adults has a marked capacity for expansion (Ricquier D *et al*., 1982). However, due to the diffuse distribution of BAT in adults, the analysis of BAT function in lean versus obese people is hard to perform. Moreover, it has been suggested that because of its capacity for expansion, BAT is a reasonable target for anti-obesity drugs (Lowel BB & Flier JS, 1997).

1.9 Aim of the study

Due to the fact that the CRH system is expressed in various tissues where it can mediate diverse cellular functions, this research project was designed to investigate a broad spectrum of CRH-Rs properties in overexpression as well as in endogenous cellular systems. In particular, the project was set up:

- to investigate expression and internalization properties of CRH-R1 splice variants
- to study structural and functional characteristics of CRH-R1d, a splice variant with impaired signalling characteristics
- to characterise signalling and internalization characteristics of CRH-R2β
- to investigate the regulation of CRH-R1 gene expression and signalling characteristics of endogenous CRH-Rs in human pregnant myometrial smooth muscle cells
- to characterise CRH-R signalling in brown adipocytes

2 MATERIALS AND METHODS

2.1 LIST OF BUFFERS AND CHEMICALS

- **Buffer A**

1mM EDTA, 1mM $MgCl_2$, 1mM PMFA (phenylmethylsulfonylfluoride), 0.1% BSA, 0.1% bacitricin in Dulbbeco's PBS (without $MgCl_2$ and $CaCl_2$), pH 7.2

- **Buffer B**

1mM EDTA, 1mM $MgCl_2$, 1mM PMFA (phenylmethylsulfonylfluoride), 0.1% BSA, 0.1% bacitricin in 10mM Tris-HCl pH 7.2

- **Buffer D**

10mM Tris-HCl pH 7.4, 1% Triton X-100, 1% Na-deoxycholate, 0.5% SDS, 150mM NaCl, 1mM DTT, 1mM EDTA, 0.2mM PMSF, 10µg/ml aprotinin.

- **DNA loading buffer**

1mM Tris-HCl pH 7.5, 40% glycerol (v/v), 0.1% bromphenol blue (w/v)

- **Dulbecco's PBS**

0.132 g $CaCl_2$ x $2H_2O$, 0.2 g KCl, KH_2PO_4, 0.1 g $MgCl_2$ x $6H_2O$, 8.0 g NaCl, 1.15 g Na_2PO_4, up to 1000 ml in distilled water.

- **HBSS**

0.294 g $CaCl_2$ x $2H_2O$, 0.4 g KCl, 0.06g KH_2PO_4, 0.1 g $MgCl_2$ x $6H_2O$, 0.1 g $MgSO_2$ x $7H_2O$, 8 g NaCl, 0.35 g $NaHCO_3$, 0.048 g Na_2HPO_4 in 1000 ml of distilled water.

- **HBSS with 2mM $CaCl_2$ and 30mM HEPES (HBSS with calcium)**

0.294 g $CaCl_2$ x $2H_2O$, 0.4 g KCl, 0.06g KH_2PO_4, 0.1 g $MgCl_2$ x $6H_2O$, 0.1 g $MgSO_2$ x $7H_2O$, 8 g NaCl, 0.35 g $NaHCO_3$, 0.048 g Na_2HPO_4, 1 g D-glucose, 7.149 g HEPES up to 1000ml in distilled water.

- **HBSS without $CaCl_2$ and 30mM HEPES (HBSS without calcium)**

0.4 g KCl, 0.06g KH_2PO_4, 0.1 g $MgCl_2$ x $6H_2O$, 0.1 g $MgSO_2$ x $7H_2O$, 8 g NaCl, 0.35 g $NaHCO_3$, 0.048 g Na_2HPO_4, 1 g D-glucose, 7.149 g HEPES up to 1000ml in distilled water.

- **G-PBS**

30mM glycerin in PBS

- **L-agar plates**

5 g Tryptone, 2.5 g yeast extract, 5 g NaCl, 1.5% agar (w/v) in 500ml distilled water, autoclaved, when warm ampicillin was added to final concentration of 100μg/ml. The mix was poured in plates.

- **L-agar plates (low salt)**

5 g Tryptone, 2.5 g yeast extract, 2.5 g NaCl, 1.5% agar (w/v) in 500ml distilled water, autoclaved, when warm Zeocin was added to final concentration of 50μg/ml. The mixture was poured in plates. The plates were kept in dark at 4^oC for a week.

- **L-Broth (LB)**

5 g Tryptone, 2.5 g yeast extract, 5 g NaCl in 500ml distilled water, autoclaved

- **L-Broth low salt (LB low salt)**

5 g Tryptone, 2.5 g yeast extract, 2.5 g NaCl in 500ml distilled water, autoclaved

- **MTT (thioazolyl blue)** (thioazolyl blue, 3-[4,5-dimetylthiazol-2yl]-2,5 diphenyl tetrazolium bromide)

1 mg/ml in HBSS

- **pen/strep**

100 u/ml penicillin and 100µg/ml streptomycin in PBS

- **Protease inhibitor cocktail**

1.6 mg/ml benzamidine HCL, 1 mg/ml phenanthroline, 1 mg/ml aprotinin, 1 mg/ml pepstatin A, 1 mg/ml leupeptin in absolute ethanol.

- **RIPA buffer**

50 mM Tris-HCl (pH 7.4), 150 nM NaCl, 1mM PMSF, 1 mM EDTA, 5µg/ml aprotinin, 5 µg/ml leucopeptin, 1% Triton X-100, 1% sodium deoxycholate, 0.1% SDS

- **Stimulation buffer for cAMP assay**

0.1 mg/ml 3-isobutyl-1-methylxanthine (IBMX), 10 mM $MgCl_2$ in DMEM

- **Trypsin-EDTA in HBSS without Ca^{2+} and Mg^{2+} (trypsin-EDTA)**

0.4 g KCl, 0.06g KH_2PO_4, 8 g NaCl, 0.35 g $NaHCO_3$, 0.048 g Na_2HPO_4, 1 g D-glucose, 10 ml phenol red 0.1 %, 2.5 g trypsin (1:250), 0.38g EDTA up to 1000ml in distilled water.

SDS-PAGE & Western Blot:

- **Resolving gel (10%)**

4ml Acrylamide(30% 37.5:1), 3ml 1.5M Tris-HCl pH 8.8, 120µl 10% SDS, 4.84ml distilled water, 40µl 10% ammonium persulphate, 10µl TEMED

- **Stacking gel (4.5%)**

1.5ml Acrylamide(30% 37.5:1), 2.5ml 0.5M Tris-HCl pH 6.8, 100µl 10% SDS, 5.8ml distilled water, 100µl 10% ammonium persulphate, 10µl TEMED

- **2X SDS Loading buffer (stock) (2X SDS-Sample buffer)**

6% SDS, 20% glycerol in 0.12M Tris-HCl pH 6.8

- **SDS Loading buffer (working solution)- SDS sample buffer**

900µl 2X SDS-PAGE loading buffer, 100µl β-mercapto-ethanol, 50µl 0.08% bromphenol blue

- **10X Electrode Buffer**

30g Tris-HCl, 144g glycine, 10g SDS and distilled water to 1000ml

- **Transfer Buffer**

7.575g Tris-HCl, 36g glycine, 500ml methanol, distilled water to 2500ml

- **10X TBS**

24.2 g Tris-base, 80 g NaCl, up to 1000ml distilled water, pH 7.6

- **Wash Buffer TBS/T (500 ml)**

50ml 10X TBS in 450 ml distilled water, add 0.5 ml Tween-20.

- **Blocking Buffer**

1X TBS, 0.1% Tween-20 with 5% w/v nonfat dry milk or BSA

- **De-staining solution**

40% (v/v) methanol, 7% (v/v) acetic acid in distilled water

- **Ponceau-S staining solution**

0.5% (w/v) Ponceau-S, 1% (v/v) acetic acid in distilled water

- **Stripping buffer (ECL detection)**

6 ml of 10% SDS, 1.875 ml of 1M Tris-HCl (pH 6.8), 233 µl β-mercapto-ethanol, distilled water up to 30 ml

- **Stripping buffer (Odyssey Infrared Imaging System)**

25 mM glycine pH 2, 2% (w/v) SDS

- **10% Ammonium persulphate (APS)**

0.1 g ammonium persulphate in 1 ml distilled water, made up prior to use and stored at 4^{o}C for a week

- **Coomassie blue staining solution**

0.1% (w/v) Coomassie blue G-250, 40% (v/v) methanol, 7% (v/v) acetic acid in distilled water

Glycerol-PAGE

- **10X Running buffer**

7.575g Tris-HCl, 36g glycine (20mM Tris-glycine)

- **Urea sample buffer**

4.8g urea (8M), 1ml 10X transfer buffer (20mM Tris-glycine pH 8.6), 0.5ml glycerol (5%), 10µl DTT stock (10mM),water to 10ml

- **Resolving gel**

1ml Tris-glycine (20mM Tris-glycine pH8.6), 4ml glycerol (40% final) ,3ml 30% acrylamide/bis 19:1 (10% final), 10µl TEMED, 40µl (10%) APS, 2ml distilled water

- **Stacking gel**

1ml Tris-glycine (20mM Tris-glycine pH8.6), 4ml glycerol (40% final), 1.16ml 30% acrylamide/bis 19:1 (3.5% final), 10µl TEMED, 40µl (10%) APS, 3.84ml distilled water

2.1.1 Chemicals

CRH and related peptides were purchased from Bachem (Weil am Rhein, Germany). IL-1β, forskolin and all inhibitors used during the project were from Merck Biosciences (Nottingham, UK). Antibodies (CRH-R, p65, IκBα, PGHS-2, myc, MLC, HSL, RhoA) were from Santa Cruz Biotechnology (Santa Cruse, California, USA), GAPDH antibody was from BioGenesis (Bournemouth, UK). The following antibodies were purchased from Abcam (Cambridge, UK): pan-arrestin, β-arrestin-1, pan-cadherin, CRH-R2 (N-terminal), clathrin heavy chain, V5 and perilipin. Total and phospho ERH1/2 MAPK, total and phospho p38 MAPK, phosho-β-arrestin-1 antibody were purchased from New England Biolabs (Hitchin, UK). Secondary horse-radish peroxidase (HRP)-conjugated immunoglobulins were from DAKO (Eye, UK); while secondary antibodies conjugated to Alexa-Flour®680, Alexa-Flour®594, Alexa-Flour®488 and Alexa-Flour®405, Alexa-Fluoro®488-phalloidin and *Slowfade*® gold antifade reagent with DAPI (Molecular probes, Paisley, UK). VectaShield® Hard Set™ mounting medium for fluorescence was from Vector Laboratories, Inc. (Burlingame, CA). Cell culture media and restriction enzymes were from Gibco/Invitrogen (Paisley, UK). Ligation reagents, *Pfu* polymerase, RNasin, AMV, random hexamers and ologo-dTTP were from Promega (Madison, USA), while dNTPs, Taq polymerase and DNA ladder were purchased from Bioline Ltd (London, UK). SYBER®Green I and PCR reaction mixture for quantitative PCR was from BioGene (Kimbolton, UK). TaqMan Gene Expression Assay was performed with chemicals from Chemicals were from Applied Biosystems (Warrington, UK) Primers were purchased from TANG

(Gateshead, UK). All other chemicals were purchased from Sigma Aldrich Company Ltd (Gillingham, UK).

2.2 PATIENTS

For CRH-R mRNA analysis of the pregnant myometrial tissue, the biopsies were obtained from women undergoing elective caesarean section pre-term (30-35 weeks of gestation, n=12) or at term (>37 weeks of gestation, n=12) before (n=6) or after (n=6) the onset of labour for non-maternal problems at the Women's Hospital, Walsgrave Hospital, Coventry. The biopsy site was standardized to the upper margin of the lower segment of the uterus in the midline. This provides the closest approximation to the upper segment of the uterus. The biopsies were immediately snap-frozen in liquid nitrogen and subsequently stored at -70^0 C until use, or processed immediately for myocyte cell culture as previously described (Grammatopoulos DK & Hillhouse EW, 1999 b). The age range was 25-35 years old for both groups. Ethical approval was obtained from the local ethical committee and informed consent to the study was obtained from all patients.

Pregnant myometrial biopsies obtained from women undergoing elective caesarean section at term (39/40 weeks) before the onset of labour for nonmaternal problems and collected in ice-cold Hank's balanced salt solution (HBSS) containing pen/strep) were used for cell culture.

2.3 TISSUE CULTURE METHODS

2.3.1 Primary myometrial cell cultures

All cell culture techniques presented in this project were carried out under a flow cabinet (sterile conditions) assigned for handling animal tissues or human material, and using sterile dissecting tools to avoid any kind of contamination.

2.3.1.1 **Digestion and primary culture**

Each biopsy (100-300 mg) was washed several times in HBSS without calcium in order to remove any excess blood. The tissue was placed in the shallow lid of a petridish and chopped into 2 mm^3 pieces with a sterile round edged scalpel. The tissue was transferred in 10mL HBSS to be washed (repeat if necessary to eliminate of excess blood cells). Finally the tissue pieces were placed in a 50 ml Falcon tube containing 10ml of enzyme solution (pen/strep, 1mg/ml collagenase IAS, 1mg/ml collagenase XI, 0.5% BSA (fatty acid free) in HBSS without calcium). The tissue was incubated in the enzyme solution for 30-40 minutes at 37^{o}C. Meanwhile, the cells were dissociated by pipetting through sterile plastic pipette (more than 100 times).1-2 ml of supernatant (containing dissociated cells) was removed and put through a cell sieve (Falcon, 70 μm), and collected in the normal growth media (DMEM containing 10% FCS, 1% glutamine, pen/strep). Gradually all digest was put through the sieve. The cells were centrifuged at 650 x g for 15 min. The supernatant was removed, the cells were washed 1-2 times, and resuspended in the normal growth media, and transferred into a 25cm^2 tissue culture flask. The cells were incubated at 37^{o}C in an atmosphere of 95% : 5% (air : CO_2). After 1-2 hours, unattached cells (smooth muscle cells) were removed and the

myometrial smooth muscle cells were left to grow in the fresh culture medium. The medium was changed ever day over a period of one week.

.

2.3.1.2 **Subculture of the human myometrial smooth muscle cells (HMSM cells)**

When cells were 85-95 % confluent, the medium was removed by aspiration and monolayers were washed twice with PBS, pre-warmed at 37^{o}C, to remove any debris and traces of FCS which would inhibit the action of trypsin. 3mls of 0.25% trypsin containing 0.02% EDTA in HBSS (without calcium) solution per 75 cm^2 flask was added and cells were incubated for 5min at 37^{o}C. Detachment of cells was monitored using light microscopy. The action of trypsin was stopped by addition of 15 ml the normal growth media medium, pre-warmed at 37^{o}C. Cells were centrifuged at 650 x g for 5min, and resuspended in the normal growth media. The total volume of culture medium added was enough to distribute cells in 3 75cm^2 flasks, or 9 six-well plates. In the majority of experiments cells of passage 4 were used.

2.3.1.3 **Stimulation of HMSM cells**

18 h prior to treatments the cells were kept in DMEM without L-glutamine, FCS and antibiotics. Cells were treated with IL-1β (1 ng/ml) for various time intervals (2-18 h). In some experiments cells were pretreated with or without specific inhibitors, as follows: 10 μM U0126 (2 h) (U0126 inhibits MEK1/2), 10 μM SB203580 (1 h) (SB203580 is a selective inhibitor of p38MAP kinase, which acts by competitively inhibiting ATP binding) (Karteris E *et al*., 2004), 25 μM IKK inhibitor II, Wedelolactone (4h) (IKK inhibitor II is a selective and irreversible

inhibitor of IKKα and β kinase activity; it inhibits NF-κB-induced gene transcription by blocking the phosphorylation and degradation of IκBα). Proteins and RNA were harvested as described later. For confocal microscopy experiments, serum deprived cells were stimulated with 1 ng/ml IL-1β for 30 and 60min. The purity of myometrial muscle cells was assessed by immunocytochemical staining for α-actin (smooth muscle cells marker) and vimentin (fibroblast marker) (Figure 2.1).

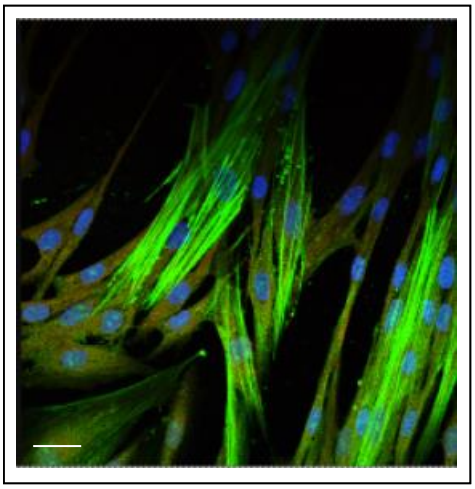

Figure 2.1. Confocal micrograph of HMSM cells shows α-actin and vimentin distribution. The specific primary antibodiy for smooth muscle α-actin and vimentin (fibroblast marker) with Alexa-Fluor®488 (green) and Alexa-Fluor®594 secondary antibody (red), respectively, were used. Cell nuclei were stained with the DNA specific dye DAPI (blue). Scale bar is 20 μm.

2.3.2 Culture of HEK 293 cell line

Human Embryonic Kidney (HEK) 293 cells were obtained from the European Collection of Animal Cell Cultures (ECACC). HEK 293 cells were routinely maintained in DMEM with Glutamax containing 10% FCS, 100 U/ml pen and 100 μg/ml strep. The media was replaced every 2-3 days. Confluent cell cultures grown in vented flasks were washed with PBS and subcultured using trypsin-ETDA. 3mls of trypsin-EDTA solution per 75 cm^2 flask were added and

cells were incubated for 1-2 min at 37ºC. Detachment of cells was monitored using light microscopy. The action of trypsin was stopped by addition of 15 ml of the normal growth media medium, pre-warmed at 37ºC. Cells were centrifuged at 650 x g for 5min. The pellet was diluted in culture medium to the total volume required and distributed among several flasks. To freeze stocks of cells for future use, cells were trypsinized as described above. The pellet from one medium flask was resuspended in 4.5mls freezing medium containing 90% FCS and 10% DMSO. 1.0 ml of cell suspension was place in a cryovial, and stored at –70ºC for not longer than 24 hours, and then transferred and stored in liquid nitrogen.

To revive frozen cells, a cryovial was taken from liquid nitrogen, quickly warmed at 37ºC (by dipping the vial in a water bath) and the content was transferred in a 25 cm^2 vented flask containing 5-7 ml pre-warmed normal growth media. The cells were incubated at 37ºC in an atmosphere of 95% : 5% (air : CO_2). After 18 h the medium was replaced.

2.3.3 Transient transfection in HEK293 cells and HMSM cells

The Lipofectamin2000 was used for transfection in HEK293 cells and HMSM cells. Transient transfection was carried out in 50-70% confluent cells seeded in 25cm^2 or 75cm^2 vented flasks. 5µg or 10µg DNA (CRH-R1α, CRH-R1β, CRH-R1d and CRH-R1β/d in pcDNA3.1 (-), CRH-R2β and dominant negative β-arrestin (DN β-arrestin) in pcDNA3.1(+)) was transfected in 25cm^2 or 75cm^2 vented flask, with 5µl or 10µl Lipofectamin2000 reagent, respectively, in 5 ml or 10ml of OptiMEM+GlutaMax and was left overnight according to the manufacturer's instructions. After 18 h the transfection mixture was replaced with normal growth

media. After 8 h cells were transferred onto poly-D-lysine coated plates (6, 12 or 24-well plates) or on coated glass cover slips (for confocal microscopy studies). The experiments were carried out 48-96h after transfection. Expression was verified by immunoblotting or confocal microscopy analysis.

In some experiments HEK293 stably expressing CRH-R1α and CRH-R1d were used. These cells were generated by Dr. Teli (Teli T *et al*., 2005).

2.3.4 Transient transfection of HEK293 with the pBudCE.4.1 mammalian expression plasmid

Co-expression of CRH-R1 and CRH-R2 was carried out using pBudCE4.1 expression vector. This vector contains CMV and EF-1 promoter sites that enable expression of two genes from a single plasmid in mammalian cells (Section 2.8). The Lipofectamin2000 reagent was used for transfection in HEK293. Transient transfection was carried out in 50-70% confluent cells seeded in 25cm^2 vented flasks. 5μg DNA and 5μl Lipofectamin2000 reagent, in 5 ml of OptiMEM+GlutaMax were used for overnight transfection according to the manufacturer's instructions. The transfection efficiency was significantly reduced compared to HEK293 cells transfected with the identical receptor constructs using pcDNA3.1(+) expression vector (Figure 2.2). Only 17±11% of cells transfected with CRH-R2β subcloned in pBudCE4.1 expressed the receptor, compared with 87±8% of cells transfected with CRH-R2β subcloned in pcDNA3.1.

After 18 h the transfection mixture was replaced with normal growth media (DMEM with 10% FBS).After 8 h cells were transferred on poly-D-lysine (Sigma) coated glass cover slips (for confocal microscopy studies) or to 12-well plates for

signalling studies (cAMP production and MAPK activation). The experiments were carried out 48h after transfection. Expression was verified by confocal microscopy analysis.

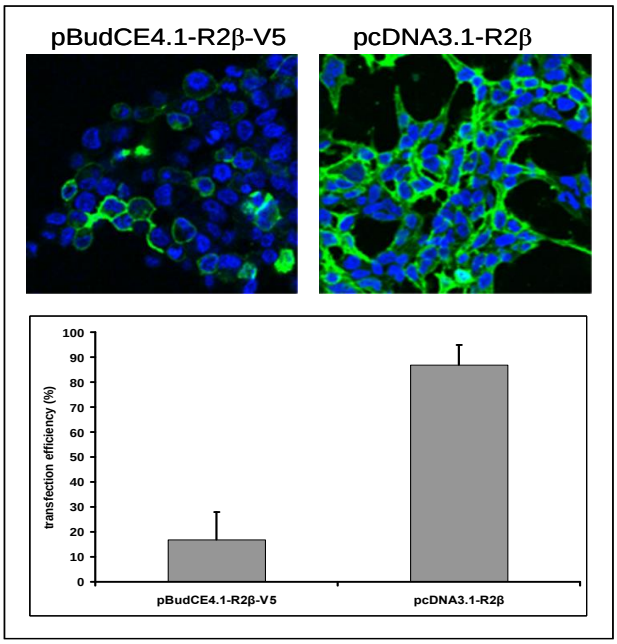

Figure 2.2. Transfection efficiency. HEK293 cells were transiently transfected with CRH-R2β subcloned into pBudCE4.1 or pcDNA3.1. 24-48 h following the transfection, the receptor expression was visualized by indirect confocal microscopy using CRH-R antibody and Alexa-Flour®488 (green). Cells from five random fields of vision were counted and classified as cells that over-express CRH-R2β or not. Transfection efficiency was expressed as a percentage of transfected cells in the total population of cells. The results are expressed as mean ± SEM from three independent transfections.

2.3.5 Stable transfection in HEK293 cells (st293 R2β)

For stable transfection 10μg pcDNA3.1(+) CRH-R2β plasmid was transfected into HEK293 cells grown in 75cm^2 vented flasks using Lipofectamine2000. After 3 days of non-selective growth in normal growth media (DMEM with Glutamax and 10% FCS), followed by 15 days of growth in the same media with 500μg/ml gentamicin (G418, Gibco), clones were selected by serial

dilution of surviving foci and maintained in 250µg/ml gentamicin. The optimal concentration of gentimcin and the length of cell growth before cloning out was determined by growing non-transfected HEK293 cells in media containing different concentrations of the antibiotic (50-1000µg/ml) for 13 days and performing a cell viability MTT assay (Figure 2.3) as described in 2.3.5.1

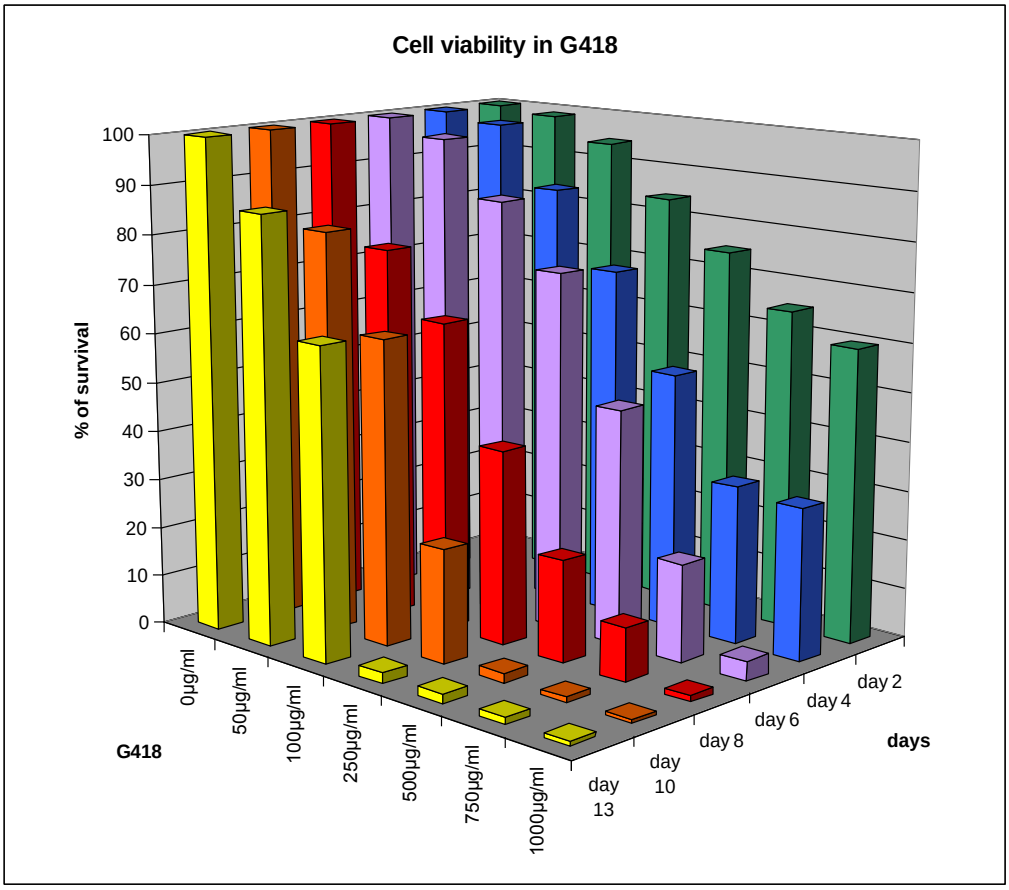

Figure 2. 3. Cell viability in the presence of G418. HEK293 cells were grown in normal growth media containing 0-1000 µg/ml G418 for 2 weeks. The cell viability was determined by a MTT assay. The assay was performed in quadruplets.

After 2 months the expression of CRH-R2β was verified by confocal microscopy analysis. The clones that expressed the receptor uniformly on plasma membrane were subjected to a further verification of the receptor expression by PCR and immunoblotting. Those clones were also tested for cAMP production and

ERK1/2 activation following 10-100 nM UCN-II treatment to assess the functionality of the clones. A clone that had shown the most desirable properties (dose-dependent cAMP production, dose-dependent ERK1/2 activation, and uniform expression of the receptor on the plasma membrane) was used in further studies. The stables (st.293-R2β) were maintained in DMEM with Glutamax containing 10% FCS, pen/sterp and 250 μg/ml gentamicin, until reaching passage 18, when a fresh frozen stock of the same clone was revived.

2.3.5.1 **MTT assay**

Cells were seeded in 24-well plates. After the treatments, the media was removed, and 200μl of 1mg/ml MTT in HBSS was added in each well. The cells were incubated at 37ºC for 20-30min or until the cells showed a purple tinge. The MTT solution was aspirated off. 200μl of DMSO was added, samples were collected and transferred into a 96-well plate and the absorbance was measured at 550nm.

2.3.6 Clathrin siRNA transfection to st.293-R2β

Three sets of clathrin heavy chain Stealth™ RNAi (3216-3241 oligo 1; 3543-3528 oligo 2; 3928-3953 oligo 3) were obtained from Invitrogen Ltd (Paisley, UK). One day before transfection st.293-R2β were plated in 6 well plates in normal growth media without any antibiotics. Lipofectamine 2000 was used for the delivery of 0.5 and 1nmol siRNA into cells according to manufacturer's instructions. Subsequent experiments were performed 72-96h after transfections.

2.3.7 Culture of T37i cells

The T37i cells were a generous gift from Dr. Lombes (Institut National de la Santé et de la Recherche Médicale, Faculté de Médecine Xavier Bichat, Paris, France). The T37i cell line is derived from a hibernoma (malignant brown adipose tumor) of the transgenic mouse founder 37 carrying a hybrid gene composed of the human MR proximal promoter linked to the SV40 large T antigen. T37i cells were cultured in DMEM-Ham's F12 medium supplemented with 10% FCS, 2mM glutamine, 100 U/ml pen and 100 μg/ml strep, and 20mM HEPES (containing 1g/l glucose) and were grown in at 37^{o}C in a humidified atmosphere with 5%CO_2. Differentiation into adipocytes was achieved under standard conditions by incubating subconfluent undifferentiated T37i cells with 2nM triiodothyronine (T3) and 20nM insulin for 10-13 days. The differentiation process was monitored by examining cells for lipid droplet formation under light microscope, and staining cells with oil-O-red.

2.3.7.1 **Oil Red O staining**

The T37i cells grown on cover slips and differentiated for 0, 5 and 10 days, were fixed in 4 % PFA in PBS for 10 min. The cells were washed with 60 % isopropanol and allowed to dry. Oil Red O was added on cover slips for 10 min. The solution was removed and slides were washed with distilled water. The slides were mounted and examined under a light microscope.

2.3.7.2 **Stimulation of T37i cells**

For MAPK phosphorylation assays, cells were grown in 12-well plates. 18 h prior to treatment, adipocytes were washed and kept in DMEM/F12 medium supplemented with 0.5% fatty acids free BSA, 2 mM glutamine, 100 U/ml

penicillin, 100 μg /ml streptomycin and 15 mM HEPES. Two hours prior to treatments, cells were washed and incubated in DMEM/F12 only. Cells were stimulated with various concentrations of UCN-II and CRH (1-100 nM) for various time periods (0-60 minutes). When inhibitors were used, cells were pretreated with 10 μM U0126 for 40min, 1μM PKAi, 10μM Ht31 peptide or 50μM LY294002 for 30min prior to agonist stimulation. At the end of the stimulation period, cells were washed with ice-cold PBS and lysed in 2x SDS-PAGE sample buffer.

2.3.7.3 **Cell proliferation assay**

The cell proliferation assay was performed on non-differentiated T37i cells grown in a 96-well plate until 50% confluent. The cells were treated with 1-100nM UCNII and CRH for 24 and 48h. Promega's CellTiter 96® AQueous One Solution Cell Proliferation Assay was used according to manufacturer's instruction. The assay is a colorimetric method for determining the number of viable cells in proliferation or cytotoxicity assays. The assay contains a tetrazolium compound [3-(4,5-dimethylthiazol-2-yl)-5-(3-carboxymethoxyphenyl)-2-(4-sulphenyl)-2H-tetrazoliun, inert salt, MTS] and an electron coupling reagent (phenazine ethosulfate, PES). The MTS tetrazolium compound is bioreduced by cells into a coloured formazan product that is soluble in tissue culture medium. This conversion is accomplished by NADPH or NADH produced by dehydrogenase enzymes in metabolically active cells. Assays are performed by adding 20μl of the supplied reagent directly to culture wells, incubating for 1-4 hours and reading the absorbance at 490nm. One row of a 96-well plate contained only media, and the absorbance value recorded was used as a background absorbance.

2.3.7.4 **Glycerol release assay**

Differentiated T37i cells grown in 24-well plates were kept in DMEM/F12 containing 2% charcoal stripped FBS for 18 h. Cells were equilibrated in DMEM/F12 without phenol red for 2 h and then pretreated with or without 1 μM PKAi (30min) or 10μM U0126 (40min). This was followed by stimulation for 1 or 2 h with 400 μl of 1-100 nM UCNII and CRH or 1 μM isoproterenol (positive control). At the end of the stimulation period, supernatants were collected and stored at –20^{o}C until assayed. The resulting cells were lysed in RIPA buffer and protein concentration was determined using a BCA^{TM} Protein Assay Kit (Pierce, Rockford, IL, USA), in order to standardize glycerol release. The released glycerol was measured in 30 μl of supernatant using a Randox glycerol kit (Randox. Laboratories, Co Antrim, UK), according to the manufacturer's instructions.

2.4 SECOND MESSENGER STUDIES: cAMP PRODUCTION

2.4.1 Stimulation of cells

The assay was performed on myometrial smooth muscle cells, transiently and stably transfected HEK293 cells, and T37i cells. The cells were plated in 12 well plates. When 70-80% confluent the media was aspirated from the cells and the cells were washed with plain DMEM. The stimulation buffer (with 10mM $MgCl_2$ and 0.1mg/ml IBMX) was placed on the cells for 20 min at 37^{o}C. The buffer was removed, cells washed with plain DMEM, and stimulated with 1-100nM UCNII, CRH and UCN for 15min, as a positive control 10μM forskolin was used. The reaction was stopped by adding 10μl of concentrated HCl. After 15-20 min most of the cells had burst. The cells were scraped and then transferred into a 1.5ml tube.

After a brief centrifugation step (1000 x g for 30 secs), the cells and media were stored at -20^{o}C.

In some instances, myometrial smooth muscle cells were incubated with IL-1β (1ng/ml) for 2h and 18h before the stimulation buffer was placed on the cells.

2.4.2 Receptor desensitization/ cAMP production

The media was aspirated from 80% confluent st293-R2β (in 12-well plates) and the cells were washed with plain DMEM. The stimulation buffer was placed on the cells for 20 min at 37^{o}C. The buffer was removed, cells washed with plain DMEM, and pre-treated for various time intervals (0-30min) at 37^{o}C with 100nM UCN-II or CRH, following a brief wash the cells were stimulated with 100nM UCN-II for 15min. The reaction was stopped with addition of 10µl concentrated HCl, as described above.

2.4.3 cAMP measurement

The cAMP levels were determined by commercially available ELISA Direct Cyclic AMP Enzyme Immunoassay Kit (Assay Designs Ins., Ann Arbor, MI, USA) or cAMP low pH ELISA kit (R&D systems, Minneapolis, MN, USA). The supernatant of HEK293 cells transiently or stably expressing CRH-R was diluted twice (except the basal, which was not diluted); however supernatant of myometrial smooth muscle cells and T37i were used neat. All of the treatments were done in duplicates or triplicates, and all experiments were repeated at least three times. The assay was performed according to the manufacturer's instructions.

2.5 MAPK ACTIVATION STUDIES

2.5.1 Stimulation of cells

MAPK activation assay: 18 hours prior to stimulation 60-70% confluent HEK293 cells (transiently or stably transfected), or 80-90% confluent HMSM cells were FCS deprived. If inhibitors were used then they were added as follows: concanavalin A 0.25 mg/ml for 40 min, U0126 10 μM for 1 h, 1 μM PKAi for 30 min, 10 μM st-Ht-31 for 30 min, 50 μM LY -294002 for 30 min (Karteris E *et.al*., 2004; Papadopoulou N *et al*., 2004; Teli T *et al*., 2005; Punn A *et.al.,* 2006) followed by stimulation of cells with different concentrations (1-100 nM) of UCN, UCN-II or CRH for various time periods (2 min-60 min). The MAPK phosphorylation was analysed by western blotting.

2.6 MOLECULAR BIOLOGY TECHNIQUES

2.6.1 Gel electrophoresis of DNA and RNA

Vertical gel electrophoresis was routinely used to analyze DNA and RNA. The agarose concentration was 1.5-2% in TBE, depending on the fragment to be analyzed. DNA and RNA were visualized by ethidium bromide (0.25μg/ml) present in gels. Samples were loaded in a volume of 10-20μl with 1/5 volume of DNA loading buffer. Electrophoresis was carried out in 1X TBE, at 80-120V for 1-2 hours. The nucleic acids were visualized under UV light.

2.6.2 Gel purification of DNA fragments

Agarose gels were exposed to UV light and the DNA fragments were cut out with a clean razor blade. The DNA was purified from the agarose slice using a Qiagen gel purification kit, according to the manufacturer's guidelines.

2.6.3 RNA isolation

70-80% confluent cells from a well of 6 well plates were used for RNA extraction. After a treatment cells were washed with ice cold PBS, and left in a lysis buffer (from Sigma GenElute Mammalian Total RNA Kit) for 10 min or until the solution became viscose. The extraction was done by using Sigma GenElute Mammalian Total RNA Kit, according to the manufacturer's guidelines.

2.6.3.1 **RNA extraction from BAT**

Primary adipocytes were isolated from interscapular BAT depots using the method of Rodbell (Rodbell M, 1964). Briefly, adipose tissue samples, 0.5-1.0 g, were chopped finely and adipocytes isolated by collagenase digest (HBSS, containing 3 mg ml^{-1} collagenase [type II] and 1.5 % BSA) in a shaking water bath at 37^{o}C for up to 60 min. Mature adipocytes were separated from the stromal vascular cells through an inert oil, Bis [3,5,5 trimethylhexyl] phthalate (Fluka Chemicals, Gillingham, UK) according to the method of Gliemann (Glienmann J *et al*., 1972). Total RNA was extracted using the Qiagen RNeasy™ Lipid Tissue Mini Kit and reverse-transcribed into cDNA using 1 µg RNA and oligo(dT)B_{15B}/random hexamers in equal concentrations as primers. The isolated RNA from tissue was kindly provided by Dr Janet Digby (The Warwick Medical School, University of Warwick).

2.6.4 Determination of DNA and RNA concentration

DNA and RNA concentration was determined on a UV-Vis Spectrophotometer (NanoDrop Technologies, Wilmington, USA). 1.5µl of sample was loaded in a chamber.

2.6.5 RT-PCR (reverse transcription polymerase chain reaction)

0.2-1µg RNA (1-3µl), 1.5µl random hexamers and up to 16.5µl of molecular biology grade water, were mixed in a sterile eppendorf tube, and heated at 70ºC for 5min, and then cooled slowly to the room temperature. Once at room temperature the RNA was centrifuged down and the following mixture was added: 3µl dNTP (10mM), 6µl of 5 x buffer (provided with AMV), 1.5µl RNasin (RNase inhibitor), 0.5µl AMV (reverse transcriptase) (25u/µl), and 2.5µl water. The mixture was centrifuged at 650 x g for 30 secs and set to the following cycle: 37ºC for 60 mins (reverse transcription), 95ºC for 5 mins (inactivates AMV and separates the 2 cDNA strands), ice for 5 mins. cDNA was stored at -20ºC.

2.6.6 Primers design

cDNA sequence was found using the National Centre for Biotechnology Information (NCBI) database. The sequence was loaded in Primer3 Input (primer3_www.cgi v 0.2). The product size was chosen to be 250-350bp, Tm (melting temperature) was set 57-63 ºC, and the primer size 18-24bp. The resulting primers were checked for specificity by nucleotide-nucleotide BLAST Nucleic Acid Database Searches.

2.6.7 Polymerase chain reaction (PCR)

The PCR mixture was prepared as in table 2.1:

$MgCl_2$ (50mM)	**0.6µl**
NH^+_4 buffer (x10)	**2.0µl**
dNTP(10mM each)	**0.4µl**
PrimerA(0.1µg/µl)	**1.0µl**
PrimerB(0.1µg/µl)	**1.0µl**
Taq	**0.2µl**
cDNA	**4.0µl (can vary)**
water	**up to 20µl**

Table 2.1: PCR reaction components used for majority of PCR reaction. The NH^+_4 buffer is provided with *Taq* polymerase.

After a centrifugation step (650 x g, for 30 sec), the PCR reactions were set up.

The PCR conditions for amplification of human CRH-R1 mRNA were as follows: 95ºC for 15 secs, 64ºC for 15 secs and 72ºC for 30 secs, in a total of 35 cycles with a final extension step at 72ºC for 7 min. Primers sequence were: forward, 5'-CAAACAATGGCTACCGGGAG-3', and

reverse 5'ACACCCCAGCCAATGCAGA-3'.

These primers amplified a 475bp DNA fragment present in all CRH-R1 mRNA variants except CRH-R1α and a 538bp DNA fragment specific for CRH-R1β.

The PCR conditions for amplification of human CRH-R2 mRNA were as follows: 96ºC for 15 secs, 58ºC for 15 secs and 72ºC for 30 secs, in a total of 35 cycles with a final extension step at 72ºC for 7 min. Primers sequences were: forward, 5'- CTCCTGGGCATCACCTACAT -3', and

reverse 5'- GTCTGCTTGATGCTGTGGAA -3'.

These primers amplified a 278 bp DNA fragment present in all CRH-R2 mRNA.

PCR assays to detect mouse CRH-R1 and CRH-R2 mRNA were performed as previously described (Brar BK *et al*., 2004).The following specific mouse CRH-R1 primers were used in the PCRs:

forward 5'-GGTGTGCCTTTCCCCATCATT-3' and

reverse 5'-CAACATGTAGGTGATGCCCAG-3'

The predicted size of the band is 279 bp.

The primer sequences for mouse CRH-R2 were:

forward 5'-GGCAAGGAAGCTGGTGATTTG-3', and

reverse 5'-GGCGTGGTGGTCCTGCCAGCG-3'.

The predicted size of the band was 378 bp.

The products were stored at -20^{o}C until run on an agarose gel (as described in 2.4.1).

2.6.8 Real time PCR performed on a Light Cycler system

Quantitative (real time) PCR of PGHS-2 was performed on a Roche Light Cycler^{TM} system (Roche Molecular Biochemicals, Germany). The PCR reaction was carried out in a 10 µl reaction mixture containing 5µl of PCR 2x Mastermix with 2 mM $MgCl_2$, 0.5 µl of Light Cycler DNA Master SYBER®Green I, 1 µl of each primer (2 ng/µl), and 1 µl of cDNA. The PCR protocol consisted of a denaturation step at 95^{o}C for 15 secs, followed by 40 cycles of amplification at 95^{o}C for 5 secs, 58^{o}C for 10 secs, and 72^{o}C for 15 secs, and finally by a melting curve analysis step at 95^{o}C for 0 secs, 56^{o}C for 15 secs and 99^{o}C for 0 secs. For analysis, quantitative amounts of gene of interest were standardized against the house-keeping gene β-actin. The sequences of PGHS-2 mRNA primers used were:

forward, 5'-TTCAAATGAGATTGTGGGAAAATTGCT-3', and

reverse, 5'-AGATCATCTCTGCCTG AGTATCTT-3'.

The β-actin primers were:

forward, 5'-AAGAGAGGCATCCTCACCCT-3', and

reverse, 5'-TACATGGCTGGGGTGTTGAA-5'.

As negative controls, preparations lacking RNA or reverse transcriptase were used. RNA expression was tested in four independent experiments. The mRNA levels were expressed as a ratio, using the "Delta-delta method" for comparing relative expression between treatments. The PCR products were sequenced in an automated DNA sequencer (Dept of Biological Sciences, The University of Warwick, UK) and the sequence data was analyzed using Blast Nucleic Acid Database Searches from the National Centre for Biotechnology Information (NCBI).

PCR for mouse UCP-1 and β-actin was performed by using a Roche Light Cycler™ system. The UCP-1 forward primer sequence was: 5'-GGCCTCTACGACTCAGTCCA, and reverse sequence was: 5'- TAAGCCGGC TGAGATCTTGT, with an amplified DNA fragment of 87 bp. The β-actin forward primer sequence was: 5'- TGCGTGACATCAAAGAGAAG, and reverse was: 5'-GATGC CACAGGATTCCAT, with an amplified DNA fragment of 197 bp.

2.6.9 Semi-quantitative RT-PCR analysis

The conditions for the semi-quantitative RT-PCR of PGHS-2 mRNA were as follows: 95ºC for 15 secs, 64ºC for 15 secs and 72ºC for 30 secs, in a total of 35 cycles with a final extension step at 72ºC for 7 min. The primer sequence was same as described in 2.6.8. As an internal standard a commercially available 18S set of primers and competamers was used as described in manufacturer's instruction

(Ambion Inc, Warrington, UK). Briefly, both sets of primers (PGHS-2 and 18S) were amplified in the same PCR reaction. 20 μl of the reaction mixture were subsequently electrophoresed on a 1.2% agarose gel and visualized by ethidium bromide, using a 1-kb DNA ladder (Life Technologies, Inc.). The amount of DNA was determined by measuring intensity of bands using the GeneDoc System. As a negative control for all of the reactions, distilled water was used in place of the cDNA.

2.6.10 Real time PCR performed on a TaqMan System

Quantitative PCR on a TaqMan Gene Expression Assay (Applied Biosystems, UK), was also employed to determine expression levels of various CRH-R1 mRNA variants in human gestational myometrium and human primary myometrial cells. This analysis was performed by Dr. Mei Gu (Warwick Medical School). Briefly, four sets of oligonucleotide primers and four TaqMan probes specific for various human CRH-R1 mRNAs were designed from the GenBank database by *mySciences* software (Applied Biosystems, UK). The 1st primer/probe combination used amplified a sequence overlapping exons 8-9, which is present in all known CRH-R1 variants detected in the human myometrium, R1α, R1β, R1c and R1d (Grammatopoulos DK *et al*., 1998). Therefore the PCR product reflected total CRH-R1 mRNA expression and was designated as CRH-R1$_T$. In addition, primers and fluorescent probes specific for exon 6 (found in R1β mRNA variant only) were designed and the PCR amplification product was designated as CRH-R1β. Similarly, primers and probes overlapping exons 2-4 and 12-14 were designed in order to amplify sequences specific for CRH-R1c and CRH-R1d (Figure 2.4). Real-time RT-PCRs were performed using the ABI PRISM 7000 Sequence Detection System

(Applied Biosystems) in a total volume of 30 µl reaction mixture following the manufacturer's protocol, using the Universal 2x PCR Master Mix (Applied Biosystems) and 0.1 µM of each primer using the dissociation protocol for the amplification of CRH-R1 mRNA variants. Negative controls containing water instead of first-strand cDNA were also used. Each sample was normalized on the basis of its 18S ribosomal RNA (rRNA) content. The 18S quantification was performed with a TaqMan ribosomal RNA reagent kit using the manufacturer's protocol. All samples were run in triplicate and results were calculated with reference to the amplification of 18S rRNA using the comparative Ct method for relative quantification (ABI Prism 7000 SDS v1.1 software). A previous report by Sehringer and colleagues investigated the quantifying strategy on accuracy in detecting and quantifying the CRH, CRH-BP, and CRH-Rs mRNA levels in human gestational tissues (Sehringer B *et al*., 2005). The authors used the TaqMan Gene Expression Assay, and compared the standard curve method and the comparative Ct method (ΔΔCt or ΔCt' method) to assess their findings. They reported that both the methods give consistent results, concluding that the simpler comparative Ct method is adequate for analysis of the mRNA levels of CRH-Rs in tissues (Sehringer B *et al*., 2005).

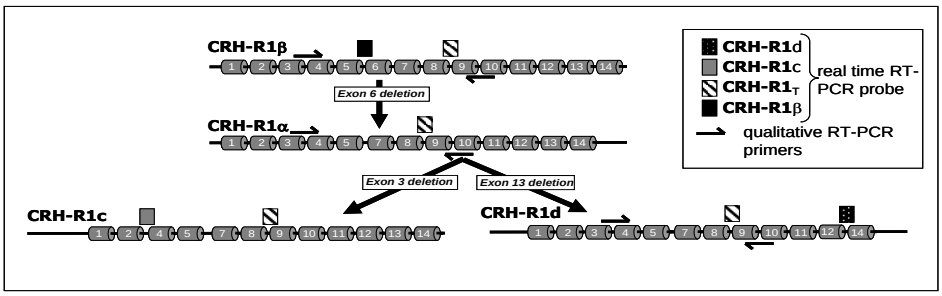

Figure 2.4. Schematic diagram of CRH-R1 gene splicing pattern and the annealing position of PCR primers and probes relative to the structure of CRH-R1 alternative spliced variants. Arrows indicate position of primers (Markovic D *et al*., 2007).

2.7 MUTAGENESIS AND CLONING TECHNIQUES

2.7.1 PCR mutagenesis of 14 amino acids within the 7th transmembrane domain (TMD) of CRH-R1

The CRH-R1d isoform lacks 14 amino acids encoded by the 13th exon. In order to see which amino acids are required for CRH-R1 to be expressed in the plasma membrane, the series of CRH-R1α and CRH-R1d mutants were created via deletion or insertion of 3 amino acids. Primers that have mismatched sequences to the template DNA were used to introduce a mutation through the process of PCR amplification as described by Higuchi in 1988 (Higuchi R *et al*., 1988). Overlap extension PCR (OE-PCR) utilizes four primers in two sequential PCR reactions to introduce an internal mutation into the target sequence (Figure 2.5). Two separate PCR reactions are run, using primers F (forward primer containing a sequence for *HindIII* restriction site adjacent to the 5'-of the receptor sequence 5'-CCCAAGCTTGGGATGGGAGGGCACCCGCAGCTCCGTCT-3') and RM (reverse primer that contains a mutation), and primers R (reverse primer containing 3'-end of the receptor sequence and a sequence for *XbaII* restriction site 5'-TGCTCTAGAGCATCAGACTGCTGTGGACTGCTTGATGC-3') and FM (forward primer that contain a mutation) to amplify separate, overlapping sequences of the template DNA. Primers RM and FM have overlapping homologous regions containing the required mutation (reverse complement sequences). The fragments were run on a 2% agarose gel, purified and combined, denatured, reannealed and amplified by a third PCR reaction using primers F and R; the outer, conserved primers. The PCR conditions were empirically established. The reaction was performed on a Hybaid Thermal Reactor. The reaction mixtures were run on 2% agarose gel and visualized by ethidium bromide staining. The bands were cut and

purified from a gel as described above. In order to estimate the band size a 1Kb DNA ladder was used. A representative agarose gel with PCR products from reaction 1, 2 and 3 is shown on Figure 2.6.

The PCR components are shown in the Table 2.2, the PCR program is shown in the Table 2.3, and the nucleotide sequences of primers used to create mutant CRH-R1α and CRH-R1d receptors are given in the Table 2.4.

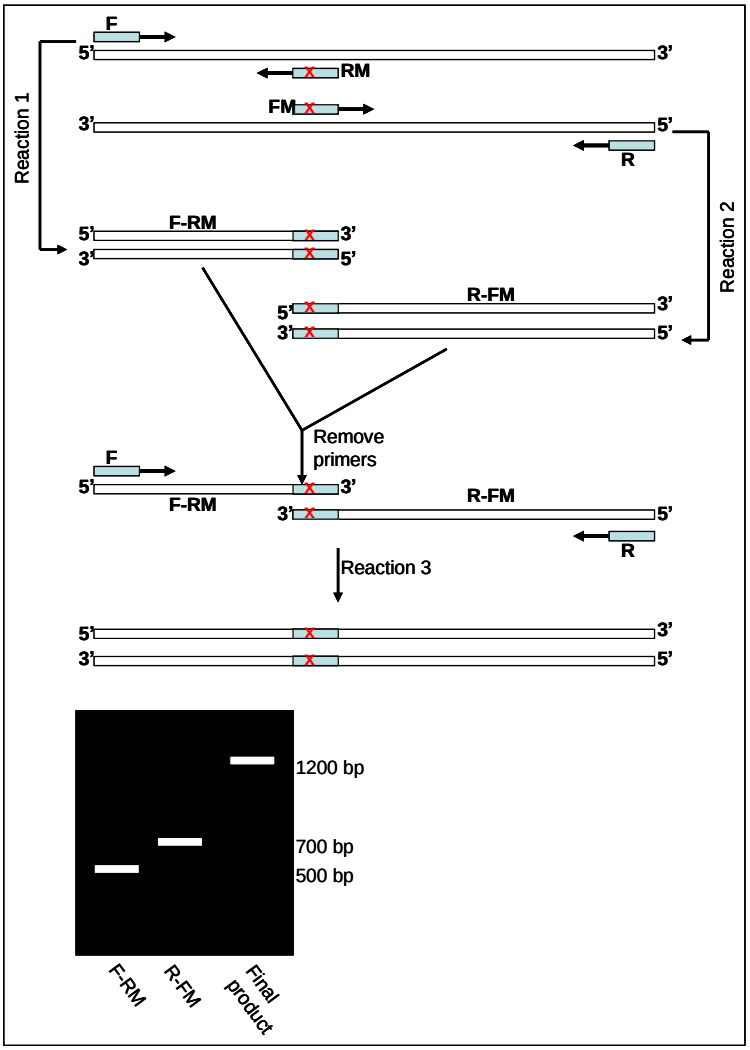

Figure 2.5. Schematic representation of OE-PCR. Desired mutations (deletion or insertion) were introduced with three separate PCR reactions. RM-reverse mutation containing primer and conserved forward, F, primer were used in reaction 1. In reaction 2, FM-forward mutation containing primer and conserved reversed, R, primer were used. The PCR products were separated on 2% agarose gel and purified. The resulting products were used as templates for the PCR reaction 3 with F and R primers.

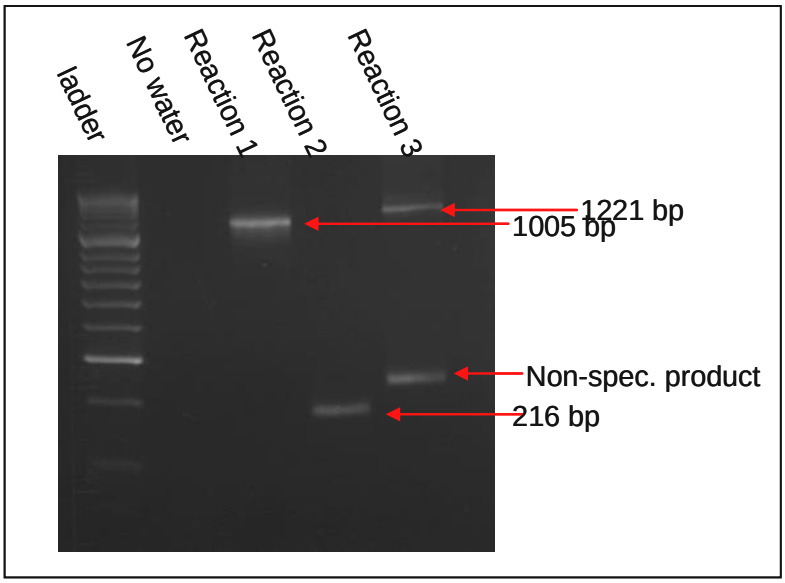

Figure 2.6. Products of PCR reactions. A representative agarose gel with PCR products from reaction 1, 2 and 3.

PCR reaction buffer	**2 µl**
***Pfu* polymerase (1.5u/µl)**	**0.5 µl**
Each primer(0.1µg/µl)	**1.0µl**
DNA template	**5ng**
dNTP (10µM each)	**0.4µl**
water	**up to 20µl**

Table 2.2: PCR reaction components used to generate CRH-R1α and CRH-R1d mutants. PCR reaction buffer was provided with *Pfu* polymerase (proof-reading DNA polymerase)

	Temp (ºC)	**Time (min)**	**Number of cycles**
Initial denaturation	95	5	1
Denaturation	95	0.45	35
Annealing	48	0.45	35
Extension	72	1.5	35
Final extension	72	7	1

Table 2.3: PCR conditions used for the two first rounds of the overlap extension PCR and for the overlapping PCR.

CRH-R1α Δ(356-358)	FM: 5'GGAATCCTTCCAGGTGTCTGTGTTCTACTGTTTCC
	RM:5'GGAAACAGTAGAACACAGACACCTGGAAGGATTCC
CRH-R1α Δ(359-361)	FM:5'GGAATCCTTCCAGGTCTACTGTTTCCTCAATAGTGAGG
	RM:5'CCTCACTATTGAGGAAACAGTAGACCTGGAAGGATTCC
CRH-R1d +(356-358)	FM:5'GGAATCCTTCCAGGGCTTCTTTGTCCGTTCTGCCATCC
	RM:5'GGATGGCAGAACGGACAAAGAAGCCCTGGAAGGATTCC
CRH-R1d +(356-361)	FM:5' CCTTCCAGGGCTTCTTTGTGTCTGTGTTCCGTTCTGCC
	RM:5'GGCAGAACGGAACACAGACACAAAGAAGCCCTGGAAGG
CRH-R1d +(356-364)	FM:5'CCAGGGCTTCTTTGTGTCTGTGTTCTACTGTTTCCGTTCTGCC
	RM:5'GGCAGAACGGAAACAGTAGAACACAGACACAAAGAAGCCCTGG

Table 2.4: Nucleotide sequences of primers used to created CRH-R1α and CRH-R1d mutants.

2.7.2 Digestion and ligation of CRH-R1α and CRH-R1d mutant inserts into pcDNA.3.1(+)

The purified fragments were digested with *HindIII* and *XbaII* at 37^{o}C overnight (in the presence of Tango buffer which was provided with the restriction enzymes). The following mix was prepared:

HindIII	1µl
XbaI	1µl
Tango buffer	2µl
DNA	4µl (can vary)
Water	up to 20µl

The digested inserts were run on 2% agarose gel, cut and purified. The ligation was performed with FastLiga System. The open vector (pcDNA3.1) and the insert DNA were mixed in a 3:1 molar ratio of insert to vector in 10µl containing 1µl T4 ligase and 5µl of accompanying buffer and incubated at room temperature for 5minutes.

The amount of insert was determined using the following formula:

Insert (ng)= (100ng (vector) x A Kb (insert) x 3)/ B Kb (vector)

After transformation into *E.coli* DH-α and purification of plasmid (described later), the resulting plasmids were digested with *HindIII* and *XbaII* at 37°C for 2h to determine the presence of inserts. The plasmids containing the inserts were sequenced (Molecular Biology Service of the Biology Department, University of Warwick).

2.7.3 PCR mutagenesis of 4 amino acids in the C-terminus of CRH-R2β

The amino acid homology of CRH-R2β and CRH-R1α is ~70%. The C-terminus of CRH-R2β has the following sequence: Thr-Ala-Ala-Val (TAAV), and CRH-R1α has this sequence Ser-Thr-Ala-Val (STAV). Site-directed mutagenesis was used to create CRH-R2β receptors, in which the cassette TAAV at the end of C-tail was replaced by AAAA, STAV, or deleted (DEL) [CRH-R2β(STAV), CRH-R2β(4A), and CRH-R2β(Del)]. Human CRH-R2β cDNA was subcloned into the mammalian cell expression vector pcDNA3.1(+) and was used as a template for mutagenesis using a DNA polymerase with proofreading ability, *Pfu* polymerase. The PCR mixture (20μl) contained 5ng of cDNA, 5ng/μl of each primer, 1unit of *Pfu* polymerase and 20 nM of each dNTP. cDNAs were amplified at 48°C in a total of 35 cycles. The forward primer contained a sequence for EcoRI restriction site adjacent to the 5'-end of the receptor sequence 5'-ATTCCGATGAGGG GTCCCTCAGGGCCCCCAGG-3'; while the reverse primer was specific for each mutant and contained the sequence for XhoI restriction site (Table 2.5).

CRH-R2β(STAV)	5'-CCGCTCGAGCGGGTCACACAGCGGTCGACTG CTTGATGCTGTGGAAGCT-3'
CRH-R2β(4A)	5'-CCGCTCGAGCGGGTCACGCAGCGGCCGCCT GCTTGATGCTGTGGAGCT-3',
CRH-R2β(Del)	5'-TCGAGCGGGTCACTGCTTGATGCTGTGGAA GCT-3'

Table 2.5. Nucleotide sequences of primers used to create CRH-R2β mutant receptors.

The resulting PCR products were run on 1.2% agarose gel, purified using a QIAquick gel extraction kit, digested with *EcoRI* and *XhoI*, purified again and ligated into pcDNA3.1(+) using the FastLiga System, according to manufacturer's instructions. E.coli DH-5α were transformed with the resulting plasmids, and after selective overnight growth on LB plates containing 100μg/ml ampicillin, five colonies were selected for further analysis. The entire regions amplified by PCR were sequenced to ensure the fidelity of the mutant cDNAs and confirm the presence of the mutations. DNA sequence analysis was performed by the Core Facility of the Department of Biological Sciences, University of Warwick.

2.8 DUAL EXPRESSION VECTOR

The pBudCE4.1 expression vector contains two promoter sites (CMV and EF-1α). The expression of CRH-R1α or CRH-R1d (with or without stop codons) was driven from CMV promoter. These receptors were ligated into the vector on *HindIII* and *XbaI* sites. The receptors that lacked a stop codon had C-tagged myc. The expression of CRH-R2β was driven from the EF-1α promoter. The insert was ligated into the vector on *KpnI* and *BglII* sites. CRH-R2β was V5 tagged at the C-terminus (Figure 2.7).

The receptor's cDNA was cut from constructs already available in the lab. The restriction sites at the 5' and 3' end of the cDNA were introduced with sets of primers (Table 2.6).

R2β-rev	5'GAAGATCTTCTCACACAGCGGCCGTCTGCTTGATG3'
R2β-rev(no stop codon)	5'GAAGATCTTCCACAGCGGCCGTCTGCTTGATG3'
R2β-for	5'CGGGGTACCCCGATGAGGGGTCCCTCAGGGCCCCCAGG3
R1α/d-rev	5'TGCTCTAGAGCATCAGACTGCTGCTGTGGACTGCTTGATGC3'
R1α/d-rev(no stop codon)	5'TGCTCTAGAGCAGACTGCTGCTGTGGACTGCTTGATGC3'
R1α/d-for	5'CCCAAGCTTGGGATGGGAGGGCACCCGCAGCTCCGTCT3'

Table 2.6. Primer sequences used to insert CRH-Rs cDNA into pBudCE4.1.

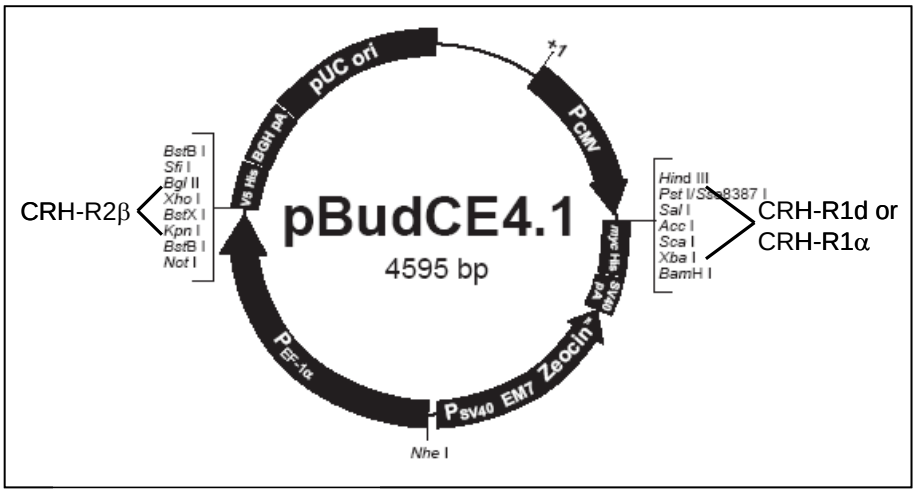

Figure 2.7. Map of pBudCE4.1. CRH-R2β cDNA was inserted between *KpnI* and *BglII* restriction sites. CRH-R1α or R1d cDNA was inserted between *HindIII* and *XbaI* restriction sites (adapted from www.invitrogen.com).

2.9 BACTERIAL METHODS

2.9.1 Transformation of *E.coli* DH5-α with pcDNA based plasmids

100µl of competent cells (*E. coli* DH5-α, Invitrogen), were transferred into a pre-cooled 15ml Falcon tube. Then 1-10ng of plasmid DNA was added to the cells, by moving the pipette through the cells while dispensing. After the incubation for 30 min on ice, the cells were heat-shocked at 42^{o}C for 45 sec. The tube was placed on ice for 2 min, then 0.9 ml of LB was added and the cells were incubated at 37^{o}C for 1h with shaking. After 1h, the cells were diluted 1:100 with LB, and 100µl (or 200µl) was spread on an LB100amp plate (LB agar containing 100µg/ml ampicilin). The plate was incubated at 37^{o}C overnight.

2.9.2 Transformation of *E.coli* DH5-α with pBudCE4.1 based plasmids

100µl of competent cells (*E. coli* DH5-α, Invitrogen), were transferred into a pre-cooled 15ml Falcon tube. Then 1-10ng of plasmid DNA was added to the cells, by moving the pipette through the cells while dispensing. After the incubation of 30 min on ice, the cells were heat-shocked at 42^{o}C for 45 sec. The tube was placed on ice for 2 min, then 0.9 ml of LB low salt was added and the cells were incubated at 37^{o}C for 1h with shaking. After 1h, the cells were diluted 1:100 with LB low salt, and 100µl (or 200µl) was spread on a LB low salt containing 100µg/ml Zeocine. The plate was incubated at 37^{o}C overnight.

2.9.3 Mini-prep of plasmid DNA

Single colony was picked up and grown in 4-5ml of LB with 100µg/ml ampicillin (if insert in pcDNA3.1) or in LB low salt with 100µl/mg Zeocine (if inserts in pBudCE4.1). The cells were incubated at 37^{o}C overnight with shaking. The following morning, the cells were harvested at 2500 x g for 5min. The Qiagen miniprep kit was used for the DNA preparation following the manufacturer's instructions.

2.9.4 Midi-prep of plasmid DNA

Single colony from a plate was used to inoculate 100mls of LB with the selective antibiotic (100µg/ml ampicillin if insert in pcDNA3.1 or in low salt LB 100µl/ml Zeocine if inserts in pBudCE4.1), and was cultured at 37^{o}C overnight with shaking. The cells were harvested by centrifugation and the DNA was prepared with the Qiagen HiSpeed Plasmid midiprep kit according to the manufacturer's instructions.

2.10 BIOCHEMICAL TECHNIQUES

2.10.1 Preparation of membrane fraction from cultured cells

Membrane and membrane associated proteins were extracted with ProteoExtract® native Membrane Protein Extraction Kit (M-PEK) from Calbiochem. The proteins were extracted in the mild and non-denaturating conditions, making it suitable for a variety of assays (co-immunoprecipitation, kinase assays, non-denaturating gel electrophoresis; also for SDS-PAGE). The extraction is based on a robust yet mild differential extraction procedure. In contrast to the two phase partitioning techniques, where detergents are used to separate

membrane proteins based on their hydrophobicity, the kit uses a differential extraction procedure that selectively extracts integral and membrane-associated proteins based on their actual association with cellular membranes.

Cells (st-293-R2β) were grown in poly-D-lysine coated 60mm cell culture dishes. When 60-70% confluent, cells were deprived of FCS for 1h, and treated with 100nM UCNII and CRH for 2, 10 and 15min. Media was removed, dishes placed on ice, and cells were washed twice with 2ml wash buffer (supplied in the kit). 10µl of protease inhibitors (supplied in the kit) was added on the well of the dish and 2ml of extraction buffer-I (supplied in the kit) was added in the dish. The dish was gently swirled allowing the buffer and protease inhibitors to mix, and the dish was placed on an agitation rotor in the cold room for 15min. The extraction buffer-I was removed and collected since it contained soluble proteins. 5µl of protease inhibitors was added on the well of the dish and 1ml of extraction buffer-II (supplied in the kit) was added in the dish. The dish was gently swirled so that the buffer and protease inhibitors could mix, the cells were scraped and transferred in a 2ml eppendorf tube. The tube was placed in a rotary shaker in the cold room for 15min. The proteins were spun down at 16,000 x g at 4^{o}C for 15min. The supernatant containing membrane proteins was collected, aliqoted and stored at -20^{o}C. The protein concentration was determined as described later. 5µg of proteins was used for SDS-PAGE.

In a number of experiments, plasma membranes were made by homogenizing cells in the extraction buffer A. The homogenization was done by passing cells 20-30 times though a 16g syringe. Unbroken cells and nuclei were removed by centrifugation at 600 x g for 30 min at 4^{o}C. The supernatant was collected and centrifuged at 40,000 x g for 60 min at 4^{o}C. The pellet was washed

twice with the buffer B. After the final spin (40,000 x g, for 60 min at 4^{o}C), the pellet was resuspended in buffer D. The proteins were aliqoted and store at -80^{o}C.

2.10.2 Preparation of total cellular proteins from cultured cells

60-70% confluent cells were serum starved for 18 h. The fresh media was placed on cells for 1h before the treatments were added. After the treatments, the media was removed, cells were briefly washed with ice-cold PBS, and 75-200µl of 2X Sample buffer (SDS-PAGE loading buffer) was added on the cells. The cells were kept on ice and total proteins were collected by scraping the cells with a blue tip and placing the proteins in 1.5 ml eppendorf tubes. The proteins were sonicated for 20sec, boiled for 5min, briefly centrifuged down, and stored at -20^{o}C until used. Alternatively, instead of lysing cells in 2X Sample buffer, the cells were lysed in 75-200µl of RIPA buffer containing protease and phosphatase inhibitors. The cells were scraped in RIPA buffer, transferred into 1.5 ml eppendorf tubes and left on ice for 15 min, then the suspension was sonicated for 10 secs, and left on ice for 30 min. The resulting lysates were centrifuged for 10 min at 4^{o}C at 10,000g. The supernatant was collected, protein concentration was determined, and the proteins were stored at -20^{o}C.

2.10.3 Determination of protein concentration

To determine the protein concentration from the cell lysate the bicinchoninic acid (BCA) protein assay (Pierce, Cramlington, UK) was used. The principle of this method is based on the reduction of Cu^{2+} to Cu^{+} by protein in an alkaline medium (the biuter reaction) and the highly sensitive and selective colorimetric detection of the cuprous cation using BCA containing reagent. The purple-coloured reaction

product of this assay is formed by the chelation of two molecules of BCA with one cuprous ion. This complex has a strong absorbance at 562 nm which is nearly linear with increasing protein concentration over a broad concentration range (20-2000µg/ml). The advantage of this assay is a detergent-compatibility. The assay was performed according to the manufacturer's instructions. The unknown protein concentration was determined by using two different dilutions (1:5 and 1:10) of proteins from cell lysates. All vials were vortexed and incubated at 37°C for 30 minutes. The absorbance of each sample at 562 nm was then determined against a blank containing distilled water. Sample protein concentrations were calculated from the standard curve and corrected after the subtraction of the standard BSA concentration (1mg/ml) in the protein extraction buffer (sample medium).

2.10.4 Sodium-dodecyl-sulphate polyacrylamide gel electrophoresis (SDS-PAGE)

The glass plates of the SDS-PAGE minigel (Mini-Protean III Electrophoresis Cell) were assembled according to the manufacturer's instruction (Bio-Rad, Hemel Hempstead, UK). The resolving polyacrylamide solution was poured between clean glass plates, overlaid with water. The polymerisation usually takes 30-45 mins. After the gel had polymerised, the overlay was washed off with distilled water and the top of the gel was dried by a filter paper. Immediately after the stacking gel was poured on the top of the resolving gel, the 10-well comb was inserted. The stacking gel was allowed to polymerise for 10-15min at room temperature. When set, the comb was removed and the wells washed with distilled water. The gels were set up in the tank following the manufacturer's instruction. The tank was filled up with 1X SDS-PAGE running buffer. The samples and the

BioRad protein marker were loaded onto the stacking gel wells. The electrophoresis was run at 200V, until the dye front had migrated to the bottom of the gel.

Solution components	**10% resolving** Gel (ml)	**4.5% stacking** Gel (ml)
Distilled H_2O	4.84	5.80
30% acrylamide mix (37.5:1)	4.00	1.50
1.5 M Tris (pH 8.8)	3.00	-
0.5 M Tris (pH 6.8)	-	2.50
10% SDS	0.120	0.100
10% ammonium persulphate	0.04	0.100
TEMED	0.01	0.01

2.10.5 Electrophoretic transfer to PVDF membrane

Western transfer of proteins was performed using a wet electroblotter (BioRad) onto a PVDF membrane. Just before the gel has finished running 6x10cm pieces of PVDF membrane were cut and the membranes were activated by soaking in 100% methanol for 2-5 secs. The membranes were washed in distilled water for 2mins, and equilibrated in transfer buffer for 10-15min. Also the chromatography paper was cut (6 sheets/gel), and equilibrated in the transfer buffer, together with the fibre pads, for 10-15min. Once when the gel has finished running the stacking gel was removed, and the running gel (with the proteins) was equilibrated in the transfer buffer for 10-15 min. Then the "transfer sandwich" was assembled on the black side of the cassette as follows: fibre pad, three filter papers, gel, membrane, three filter papers, fibre pad. Each layer was wetted with 1-3mls of transfer buffer, and extra care had to be taken not to trap any air bubbles between the gel and the

membrane. The shut cassette was placed in the tank and ice-cold transfer buffer was added. The transfer was run at 100V for 1h, with an ideal current of 150-200mA, (much higher or lower current means that the transfer buffer is probably not correct).

2.10.6 Immunodetection of transferred proteins using enhanced chemiluminescence (ECL)

Following electroblotting the membranes were blocked in TBS-T (TBS containing 0.1% (v:v) Tween-20) containing 5% (w:v) BSA or 5% (w:v) milk for 1h at room temperature with constant shaking. After a brief wash with TBS-T, the membranes were incubated with primary antibodies as described in the Table 2.7. Next, the membranes were washed three times, 15 minutes each, with TBS-T at room temperature. The membranes were then incubated with secondary horse-radish peroxidase (HRP)-conjugated immunoglobulin (DAKO) (1:2000) diluted in 5% BSA TBS-T for 1h at room temperature. After the washes, the antibody complex was detected by ECL as described by the Amersham detection kit.

2.10.7 Stripping membranes following ECL detection

30ml of water based buffer containing 6ml of 10% SDS, 1.875 ml of 1M Tris-HCl pH6.8, and 233µl of β-mercapto-ethanol was used per membrane. The procedure was carried out in a fume hood. The buffer was heated to 55^{o}C and poured over a membrane. The temperature was kept constant for 30min (the membrane was placed in a carrier in a water bath). Then the membrane was washed 4-5 times with TBS-T, and immunodetection was carried as described above.

2.10.8 Immunodetection of transferred proteins using Odyssey Infrared Imaging System detection

After completion of transfer, the PVDF membrane was incubated with 8-10ml LI-COR blocking buffer (LI-COR Biosciences, Cambridge, UK) for 1h at room temperature with gentle agitation. This step minimises non-specific binding of antibody to the membrane. After the membrane was briefly washed with TBS-T, it was incubated with primary antibody at 1:1000 dilution in 10 ml of LI-COR blocking buffer with gentle agitation overnight at 4^{o}C. These conditions were used for the majority of antibodies (Table 2.7). However, the phospho-p44/42 MAPK (Thr202/Tyr204) antibody which detects p42 and p44 MAPK only when catalytically activated by phosphorylation Thr202 and Tyr204 and the p42 MAPK antibody which is phosphorylation-state independent antiserum and detects total p42 MAPK levels were used at the same time in the dilutions of 1:1500 and 1:2000, respectively, in LI-COR blocking buffer for overnight incubation at room temperature with gentle agitation. The next day the antiserum was removed and the membrane was washed 3 times for 10 minutes each with 15 ml of TBS-T. It was then incubated with secondary antibody conjugated to a fluorescent entity at 1:6000 in 10 ml of blocking buffer with gentle agitation for 1 hour at room temperature. Finally, the blot was washed twice more each with 15 ml of TBS-T, and once with TBS only. The membrane was dried between sheets of fine tissue, visualized and analysed on the Odyssey Infrared Imaging System (LI-COR Biosciences, Cambridge,UK).

Antibody	Blocking reagent	Primary antibody	Secondary antibody	Detection method
CRH-R1/2 (c-20)	5% BSA in TBS-T, 1h at RT	1:500 in TBS-T, 18h at 4°C	1:2000 in 5% BSA in TBS-T, 1h at RT	ECL
Pan-arrestin	5% BSA in TBS-T, 1h at RT	1:500 in 1% BSA in TBS-T, 18h at 4°C	1:2000 in 1% BSA in TBS-T, 1h at RT	ECL
RhoA	5% BSA in TBS-T, 1h at RT	1:1000 in 1% BSA in TBS-T, 18h at 4°C	1:2000 in 1% BSA in TBS-T, 1h at RT	ECL
PGHS-2	5% BSA in TBS-T, 1h at RT	1:1000 1% BSA in TBS-T, 18h at 4°C	1:2000 in 1% BSA in TBS-T, 1h at RT	ECL
MLC	5% BSA in TBS-T, 1h at RT	1:1000 1% BSA in TBS-T, 18h at 4°C	1:2000 in 1% BSA in TBS-T, 1h at RT	ECL
GAPDH	Non	1:60,000 in TBS-T, 1h at RT	1:2000 in TBS-T, 1h at RT	ECL
IκBα	5% BSA in TBS-T, 1h at RT	1:500 in 1% BSA in TBS-T, 18h at 4°C	1:2000 in 1% BSA in TBS-T, 1h at RT	ECL
p38 MAPK total	LI-COR blocking reagent, 1h at RT	1:500 in LI-COR blocking reagent, 18h at 4°C	1:6000 in LI-COR blocking reagent, 1h RT	Odyssey Imaging system
phospho-p38 MAPK	LI-COR blocking reagent, 1h at RT	1:1000 in LI-COR blocking reagent, 18h at 4°C	1:6000 in LI-COR blocking reagent, 1h RT	Odyssey Imaging system
GAPDH	Non	1:60000 in TBS-T, 1h RT	1:6000 in LI-COR blocking reagent, 1h RT	Odyssey Imaging system
IκBα	LI-COR blocking reagent, 1h at RT	1:500 in LI-COR blocking reagent, 18h at 4°C	1:6000 in LI-COR blocking reagent, 1h RT	Odyssey Imaging system
β-arrestin -1	LI-COR blocking reagent, 1h at RT	1:1000 in LI-COR blocking reagent, 18h at 4°C	1:6000 in LI-COR blocking reagent, 1h RT	Odyssey Imaging system
phospho-β-arrestin-1 (Ser412)	LI-COR blocking reagent, 1h at RT	1:500 in LI-COR blocking reagent, 18h at 4°C	1:6000 in LI-COR blocking reagent, 1h RT	Odyssey Imaging system

Table 2. 7. The antibody and conditions used for immunodetection of proteins by western blotting.

2.10.9 Stripping membranes following Odyssey Infrared Imaging System detection

Membranes were placed in a stripping buffer (25mM glycine buffer pH 2 and 2% SDS) for 15 min at room temperature. Then the membranes were placed in fresh stripping buffer for another 15 min. Following two TBS washes (15 min each) the membranes were placed in LI-COR Blocking buffer for 1h, and re-probed with appropriate antibody.

2.10.10 Commassie blue staining of SDS-PAGE gels

The gels were stained in Commassie blue stained for 10min, the solution was replaced with de-stain solution. Once the protein bands become visible the gel was transferred in distilled water and scanned using the Odyssey Infrared Imaging System.

.

2.10.11 Glycerol-polyacrylamide gel electrophoresis

The plates were assembled and gels poured as described for SDS-PAGE. The gel was pre-run for 30-45min at 200V. After the samples were loaded the gel was run at 200-300V for at least 2-3h, or until the blue dye was completely gone. The proteins were transferred as described above.

2.10.12 RhoA activation assay

To detect RhoA translocation/activation the commercially available kit was used, Rho activation assay (Cytoskeleton, Denver, USA). Briefly, the principle of the assay is to detect Rho-GTP (active form). The Rho Binding Domain (RBD) of Rhotekin has been shown to bind specifically to Rho-GTP. This allows one to "pull-

down" Rhotekin-RBD/Rho-GTP complex with glutathione-agarose beads. 18 h before the treatments, the cells were deprived of FCS (since RhoA activation and translocation are FCS sensitive). The assay was performed according to the manufacturer's instruction. The Rhotekin-RBD/Rho-GTP complex with glutathione-agarose beads were dissolved in 2x SDS loading sample buffer, boiled for 5min, centrifuged at 650g for 5min and 10µl of supernatant was loaded on a 10% SDS-PAGE gel. A separate gel was loaded with 10µl of total cell lysate to demonstrate equal amount of RhoA protein in all samples. Following protein transfer to a PVDF membrane, the membrane was probed with RhoA-antibody as described in the Table 2.9.

2.10.13 On-cell western

st293-R2β cells were cultured on poly-D-lysine coated 24-well plates. When 80% confluent, cells were treated with 100nM UCN-II or CRH for 15-45 min. Cells were fixed with 4% PFA for 20min, and after three brief washes with PBS, non-specific binding was blocked with LI-COR blocking buffer. A rabbit antibody raised against the N-terminus of CRH-R2 was used in dilution of 1:2000 (Abcam, Cambridge, UK) in LI-COR blocking buffer at 4^{o}C overnight. After 3 washes with PBS, cells were incubated with the secondary anti-rabbit antibody conjugated to a fluorescent IRDye™800 dye (dilution) 1:800 for 1h at room temperature. The signal was detected and analyzed using the Odyssey Infrared Imaging System.

2.11 IMMUNOCYTOCHEMISTRY AND CONFOCAL MYCROSCOPY

2.11.1 Preparation of cover slips

Round glass cover slips were placed in a beaker and treated with concentrated acetic acid for at least 30min, then with 70% ethanol for 30min, and with the mixture of 10ml acetone containing 200µl 3-(aminopropyl)triethoxy saline (APES). After each treatment, the cover slips were washed with approximately 1liter of distilled water. The cover slips were dried on air, and place in 6 well plates. Prior to use, the plates were sterilized by UV radiation for 30 min.

2.11.2 Plating cells on the cover slips

The cover slips were coated with 100µg/ml poly-D-lysine in PBS (if HEK293 cells were seeded). 200µl of poly-D-lysine was placed on a cover slip, and after 10min poly-D-lysine was removed, cover slips were washed with filter sterilised PBS (F/S PBS). Confluent cells were trypsinized as described earlier, and resuspended in 15mls of media. 100-150µl of cells were left on a cover slip for 20min, and then 4ml of media was added. When the cells reached 70-80% confluency, they were treated and fixed.

2.11.3 Stimulation of cells

For the data described in the Chapter 3, one hour prior to stimulation transiently transfected cells were FBS deprived. The cells were treated for various times (0-60minutes) with 0.1-100nM CRH, or 200nM PMA (phorbol 12-myristate 13-acetate). At the end of the treatment cell were placed on ice and washed with ice cold PBS.

Internalisation assay: one hour prior to stimulation transiently transfected HEK293 were serum deprived. The cells were stimulated for 0-60min with 100nM UCNII, or CRH.

To monitor NF-κB(p65) and IκB translocation, serum deprived HMCM cells were treated with 1 ng/ml IL-1β for 30-60min.

2.11.4 Fixing the cells

Media was removed from the wells, and cells were briefly washed with F/S PBS. 0.5ml of 4% PFA in PBS was added and left for 30min. The cells were washed with F/S PBS, and either stored in sodium azide (to prevent growth of microorganisms) at 4^{o}C, or immunostained.

2.11.5 Immunostaining

The fixed cells were washed with F/S PBS. Non-specific binding was blocked with 3% BSA PBS-Triton X-100 (0.01%). Triton X-100 was used to permeabilize the cells. After one hour and three 5min washes with F/S PBS, the cells were incubated with primary antibody (1:50-1:100) overnight at 4^{o}C as shown in the Table 2.8. After 18 h, cells were washed, and incubated with secondary antibody (donkey anti-goat/mouse/rabbit Alexa-Flour®594, Alexa-Flour®488, Alexa-Flour®405) for 1h at room temperature (from this point on the cells were protected from the light). Cover slips were washed with F/S PBS and mounted on microscope slides with VectaShield® Hard Set™ mounting medium for fluorescence or *Slowfade*® gold antifade reagent with DAPI. The slides were kept in darkness at 4^{o}C until the microscopy was done.

Antibody	Primary antibody	Secondary antibody
α-actin	1:100 in 1%BSA in PBS-T, 18h at 4°C	1:400 Alexa-Fluor®488 in PBS-T, 1h at RT
Clathrin heavy chain	1:100 in 1%BSA in PBS-T, 18h at 4°C	1:400 Alexa-Fluor®405 in PBS-T, 1h at RT
CRH-R1/2 (c-20)	1:100 in 1%BSA in PBS-T, 18h at 4°C	1:400 Alexa-Fluor®488 or 594 in PBS-T, 1h at RT
HSL	1:150 in 1%BSA in PBS-T, 30 min at 37°C	1:400 Alexa-Fluor®594 in PBS-T, 30 min at 37°C
IκBα	1:100 in 1%BSA in PBS-T, 18h at 4°C	1:400 Alexa-Fluor®488 in PBS-T, 1h at RT
myc-Texas Red conjugated	1:100 in 1%BSA in PBS-T, 18h at 4°C	
p65	1:100 in 1%BSA in PBS-T, 18h at 4°C	1:400 Alexa-Fluor®594 in PBS-T, 1h at RT
Pan-arrestin	1:100 in 1%BSA in PBS-T, 18h at 4°C	1:400 Alexa-Fluor®488 in PBS-T, 1h at RT
PGHS-2	1:100 in 1%BSA in PBS-T, 18h at 4°C	1:400 Alexa-Fluor®594 in PBS-T, 1h at RT
phospho-ERK1/2	1:100 in 1%BSA in PBS-T, 18h at 4°C	1:400 Alexa-Fluor®488 or 594 in PBS-T, 1h at RT
phospho-p38 MAPK	1:100 in 1%BSA in PBS-T, 18h at 4°C	1:400 Alexa-Fluor®488 in PBS-T, 1h at RT
perilipin	1:100 in 1%BSA in PBS-T, 18h at 4°C	1:400 Alexa-Fluor®488 in PBS-T, 1h at RT
perilipin A/B	1:100 in 1%BSA in PBS-T, 30 min at 37°C	1:400 Alexa-Fluor®594 in PBS-T, 30 min at 37°C
V5	1:100 in 1%BSA in PBS-T, 18h at 4°C	1:400 Alexa-Fluor®488 in PBS-T, 1h at RT
vimentin	1:100 in 1%BSA in PBS-T, 18h at 4°C	1:400 Alexa-Fluor®594 in PBS-T, 1h at RT

Table 2. 8. The antibody and conditions used for immunodetection of proteins by confocal microscopy.

The specificity of antibody employed was demonstrated in the presence of blocking peptide (Figure 2.8). The blocking peptide for CRH-R (c-20) antibody was a peptide identical to the CRH-R's C-terminus (Santa Cruz, USA) that the antibody was raised against. The blocking peptide for pan-arrestin antibody was a peptide (CD(384)DIVFEDFARLRLK(397)) that the antibody was raised against (Abcam, Cambridge, UK). The antibody was pre-incubated with 10 fold molar excess of the blocking peptide overnight at 4°C, before being placed on a slide. The concentration

of antibody and blocking peptides were known and expressed in μg/ml. The amount (in moles) of antibody and blocking peptide was determined using ***n=m/Mw***, where *n* was the amount of compound in moles, *m* was the amount of compound in grams, and *Mw* was the molecular weight of compounds. The laser settings were not changed during an experiment, with the exception of the 405 laser that was used to detect DAPI staining.

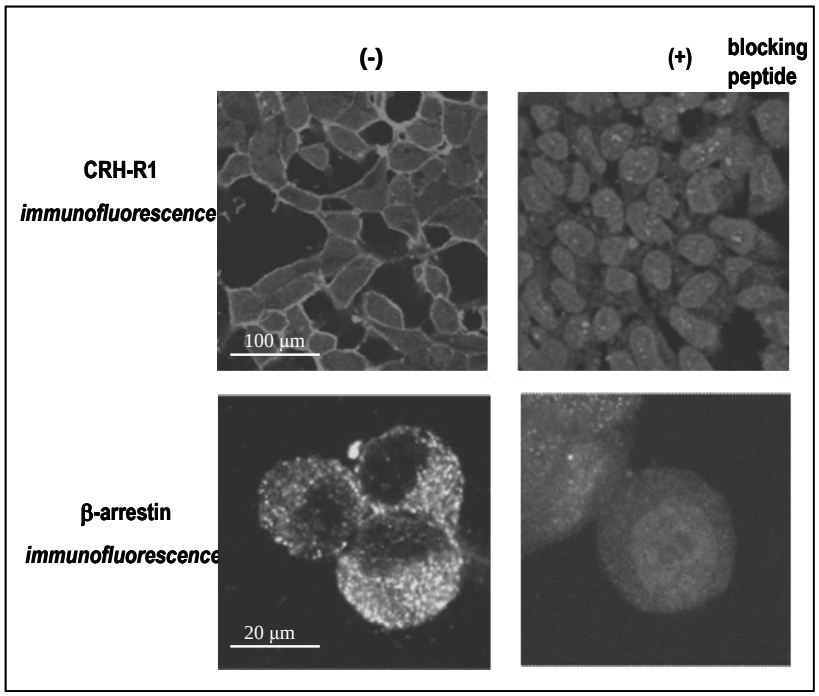

Figure 2.9. Characterisation of CRH-R1 and β-arrestin antibody specificity. st-293-R1α cells were grown on cover slips. The CRH-R1 and β-arrestin signals were monitored by indirect immunofluorescence using specific primary antibodies in the presence and absence of corresponding blocking peptides (10-fold molar excess) and Alexa-Fluor®594 secondary antibody for CRH-R1 and Alexa-Fluor®488 secondary antibody for β-arrestin visualisation. Cell nuclei were stained using the DNA-specific dye, DAPI.

2.11.6 Fixing and immunostaining for RhoA translocation

Cells were fixed with 10% ice cold TCA in PBS for 15 min at 4ºC. After three 5min washes with G-PBS , the cells were permeabilized with 0.2% Triton-

x100 in G-PBS for 15min. The cells were washes three times with G-PBS, and non-specific binding was blocked with 1% BSA in G-PBS for 1h at room temperature. After a brief wash the cells were incubated overnight with RhoA antibody (1:100) at 4^{o}C. The following morning, the cells were washed and incubated with donkey anti-mouse Alexa-Flour®595.

2.11.7 Confocal microscopy

Cells were examined under an oil immersion objective (x63) using a Leica model DMRE laser scanning confocal microscope (Leica Microsystems, Milton Keynes, UK) with TCS SP2 scan head. Laser 543 nm at 50% of power and emission filter set at 555-620nm were used to examine Alexa-Flour®594 staining, and Laser 488 nm at 30% of power and emission filter set at 500-535nm was used to examine Alexa-Flour®488 staining. DAPI and Alexa-Fluor®405 staining was examined with Laser 405 at 10% of power and emission filter set at 410-450 nm. The scan speed was 400 Hz, and the format was 1024x1024 pixels. Increasing pixel number increases the quality of picture, but it bleaches dye. Optical sections (0.5 μm) were taken, and representative sections corresponding to the middle of the cells were presented. After indirect immunofluorescent staining, no specific fluorescence was observed in cells treated only with a secondary antibody. The images were manipulated with Leica (5x zoom) and ImageJ software developed at the National Institutes of Health (NIH) (http://rsb.info.nih.gov/ij/)

For every experiment HEK293 cells that have not been transfected with CRH-R, were immuno-stained for the receptor expression and analysed using confocal microscopy, under the same exposure conditions as transfected HEK293 cells. During confocal microscopy analysis, the microscope and laser settings were

kept constant, with an exception of the 405 nm laser when used to detect DAPI staining.

2.11.8 Quantitative analysis of protein localization

For each treatment, between 20-25 individual cells in five random fields of view were selected and examined. Fluorescence intensity profiles were generated along a line drawn through the middle of a cell, analysed and quantified using Image J software. The line depth was 0.1mm (set as a default). Relative quantification of intracellular CRH-R1 was carried out by measuring the amount of total fluorescence along the longitudal axis corresponding to the intracellular space (average 4-18μm). The activated β-arrestin that was translocated to the plasma membrane was quantified by measuring fluorescence along the area corresponding to the cell membrane (1-3μm and 19-21μm). The data are expressed as total fluorescence (intracellular or membrane) compared to basal as a fold increase from basal, when basal was set to be 1.

2.12 STATISTICS

cAMP production: the data obtained as pmol/well was normalised with forskolin-induced cAMP production, and expressed as a fold increase above basal using the following formula ***"(treated – basal)/ basal"***. The results obtained from at least three independent experiments performed in duplicates or triplicates were presented as the mean ± SEM. Single-factor one-way ANOVA was performed for each treatment, and significance was assumed when $P<0.05$.

Protein phosphorylation: all experiments were performed in duplicates and repeated at least three times. Phosphorylated and total levels of proteins were

quantified using the Odyssey Infrared Imaging System or TotalLab software (when X-ray films were analysed). Background was automatically corrected using default settings. The raw data were obtained as the first derivatives of the band intensities. All results were normalized as ***"Phospho/Total***" and expressed as a fold increase above basal, using the following formula ***"(treated – basal)/ basal***". In some instances the results were expressed as "% of basal". The results were presented as the mean ± SEM of at least three independent experiments performed in duplicates. Single-factor one-way ANOVA was performed for each treatment, and significance was assumed when $P<0.05$.

CRH-R1 mRNA expression: The results were expressed as mean ± SEM. Relative gene expression of target mRNA was normalized to a calibrator that was chosen to be the basal condition (untreated sample). Results were calculated with the ΔΔCt method; they were expressed as the *n*-fold differences in gene expression relative to 18S rRNA and calibrator and were determined as follows: $n\text{-fold} = 2^{-(\Delta Ct\ sample\ -\ \Delta Ct\ calibrator)}$, where the parameter Ct (threshold cycle) is defined as the fractional cycle number at which the PCR reporter signal passes a fixed threshold. ΔCt values of the sample and calibrator were determined by subtracting the average Ct value of the transcript under investigation from the average Ct value of the 18S rRNA gene for each sample.

3 EXPRESSION AND INTERNALIZATION PROPERTIES OF CRH-R1 SPLICE VARIANTS IN TRANSIENTLY TRANSFECTED HEK293 CELLS

3.1 INTRODUCTION

The type 1 CRH receptor (CRH-R1) is widely expressed in the central nervous system as well as in peripheral tissues (Hillhouse EW & Grammatopoulos DK, 2006). Several splice variants of the receptor have been described, at least at the mRNA level. However a lack of variant-specific antibody makes it impossible to demonstrate protein expression of variants. In most mammals, the fully active CRH-R1 is transcribed from all 13 exons present within the CRH-R1 gene. However, in humans the CRH-R1 gene contains 14 exons encoding a "pro-CRH-R1" receptor isoform (Grammatopoulos DK & Hillhouse EW, 2007) which is a 444-amino acid protein known as CRH-R1β (Chen R *et al*., 1993). Compared to the fully active CRH-R1α (which is a 415-amino acid protein), the CRH-R1β variant contains exon 6 which encodes a 29-amino acid insert within the first intracellular loop, resulting in a receptor protein with impaired agonist binding (Kd= 1.4 ±0.4 nM for CRH-R1α, and Kd=4.7±0.6 nM for CRH-R1β) and signalling properties (EC_{50}=3±2 nM for CRH-R1α, and EC_{50}=19±5 nM for CRH-R1β) (Markovic D *et al*., 2006). mRNA studies have demonstrated that CRH-R1β is expressed in the pituitary gland (Chen R *et al*., 1993), myometrium (Grammatopoulos DK *et al*., 1998), mast cells (Cao J *et al*., 2005), and endometrium (Karteris E *et al*., 2004), but the physiological function of this variant is unknown. Another CRH-R1 variant

investigated in this study was CRH-R1d. This variant has exon 13 deleted leading to the loss of 14-amino acids from the C-terminal end of the putative seventh transmembrane domain. Overexpression studies of recombinant CRH-R1d have demonstrated that this variant has impaired G protein coupling and signalling properties (EC_{50}=3±1 nM for CRH-R1α, and EC_{50}=18±5 nM for CRH-R1d), but it was able to bind agonists with intact affinity (Kd= 1.4 ±0.4 nM for CRH-R1α, and Kd=1.7±0.3 nM for CRH-R1d) (Grammatopoulos DK *et al*., 1999). CRH-R1d mRNA was found in the myometrium of pregnant women (Grammatopoulos DK *et al*., 1999) and skin (Pisarchick A & Slominski AT, 2001). In addition to the expression of CRH-R1α, R1β and R1d, the myometrial tissue from pregnant women expresses another variant of the receptor identified in our laboratory and termed CRH-R1β/d (unpublished data). This variant is a "cross" between CRH-R1β and R1d, since it contains exon 6 and lacks exon 13. The precise splicing mechanisms controlling the expression of CRH-R1 variants are still unknown. Studies in keratinocytes suggest that environmental stimuli (UV irradiation) as well as an intracellular messenger (cAMP) and phorbol esters could induce CRH-R1 splicing (Pisarchick A & Slominski AT, 2001).

CRH actions are dependent on the adequate expression of CRH-R in the plasma membrane. The exposure of CRH-R to CRH and other agonists results in rapid attenuation of CRH-R responses, through receptor desensitization. Current evidence suggests that this process is initiated by phosphorylation of the receptor on serine and threonine residues within the intracellular loops and C-terminal tail of many GPCRs (Luttrell LM & Lefkowitz RJ, 2002), including the CRH-R1 receptor (Teli T *et al*., 2005; Oakley RH *et al*., 2007). There are two types of desensitization: heterologous and homologous. During heterologous desensitization agonist

occupancy of the target GPCR is not required; the receptor can be phosphorylated and desensitized by the activation of second messenger dependent protein kinases such as cAMP-dependent kinase (PKA) and protein kinase C (PKC). On the other hand, homologous desensitization is a consequence of conformational changes of the receptor upon ligand binding, and further phosphorylation of the receptor by G-protein coupled receptor kinases (GRKs) and subsequent binding of β-arrestin. These events lead to the uncoupling of receptors from their heterotrimeric G-proteins and agonist-promoted endocytosis of many GPCRs. The extent of β-arrestin involvement appears to vary depending on the receptor, agonist and cell type. GPCRs are grouped into two distinct classes according to β-arrestin involvement in receptor internalization (Oakley RH *et al*., 2000). Activated receptors of the class A, bind β-arrestin transiently and with low affinity. β-arrestin is released after targeting the receptor to clathrin-coated pits; the receptor proceeds into an endosomal pool, while β-arrestin translocates back to the plasma membrane (Zhang *et al*., 1999). Class A receptors typically undergo rapid recycling to the plasma membrane. The members of this class include β2 and α1B adrenergic, μ opioid, endothelin A, and dopamine D1A receptors. Class B receptors, such as neurotensin 1, vasopressin 2, and angiotensin AT1a receptors, show a much stronger and more prolonged binding to β-arrestin. The receptor-β-arrestin complex is stable and it internalizes as a unit that is targeted to endosomes (Luttrell LM and Lefkowitz RJ, 2002). The stability of receptor-β-arrestin complex is dictated by the specific clusters of serine and threonine residues in the C-terminal tail of the receptor as well as the C-terminus of β-arrestin (Oakley RH *et al*., 2001).

In recent years, CRH-R1α desensitization and internalization have been a topic of several studies (Rasmussen TN *et al.* 2004; Perry SJ *et al*., 2005; Teli T *et*

al. 2005; Holmes KD *et al*., 2006; Markovic D *et al*., 2006; Oakley RH *et al*., 2007). However, the internalization characteristics of CRH-R1 variants have not been studied. Since tissue sensitivity to agonists is determined by the availability of receptor in the plasma membrane and how fast the signal is terminated, the aims of my studies were to investigate the cellular expression of CRH-R1 variants (α, β, d and β/d), and internalization characteristics of the receptors. HEK293 cells over-expressing different variants (293-R1α, 293-R1β, 293-R1d, 293-R1β/d) were chosen as a model system, because the system has been well characterised and validated and used successfully to investigate various aspects of CRH signalling (Papadopoulou N *et al*., 2004; Teli T *et al*., 2005)

3.2 RESULTS

3.2.1 The cellular expression of CRH-R1 variants

HEK293 transiently transfected with recombinant CRH-R1 variants were examined by a confocal microscope. The expression of CRH-R1α was found to be predominantly on the plasma membrane of the cell. The same pattern of expression was observed for the CRH-R1β variant, suggesting that the insertion of 29 amino acids within the first intracellular loop does not effect receptor expression in the plasma membrane. Interestingly, CRH-R1d and R1β/d immunoreactivity was distributed primarily in the cytosol although cell membrane expression was also evident (Figure 3.1 A). The specificity of the staining is shown on figure 3.1B. Since the experiment was performed on transiently transfected cells, a percentage of the cells failed to uptake the required DNA and therefore did not over-express CRH-R1, and consequently showed the absence of immunoreactive staining on the

membrane or cytoplasm (Figure 3.1 B). The confocal microscope and laser settings were not altered during the course of an experiment.

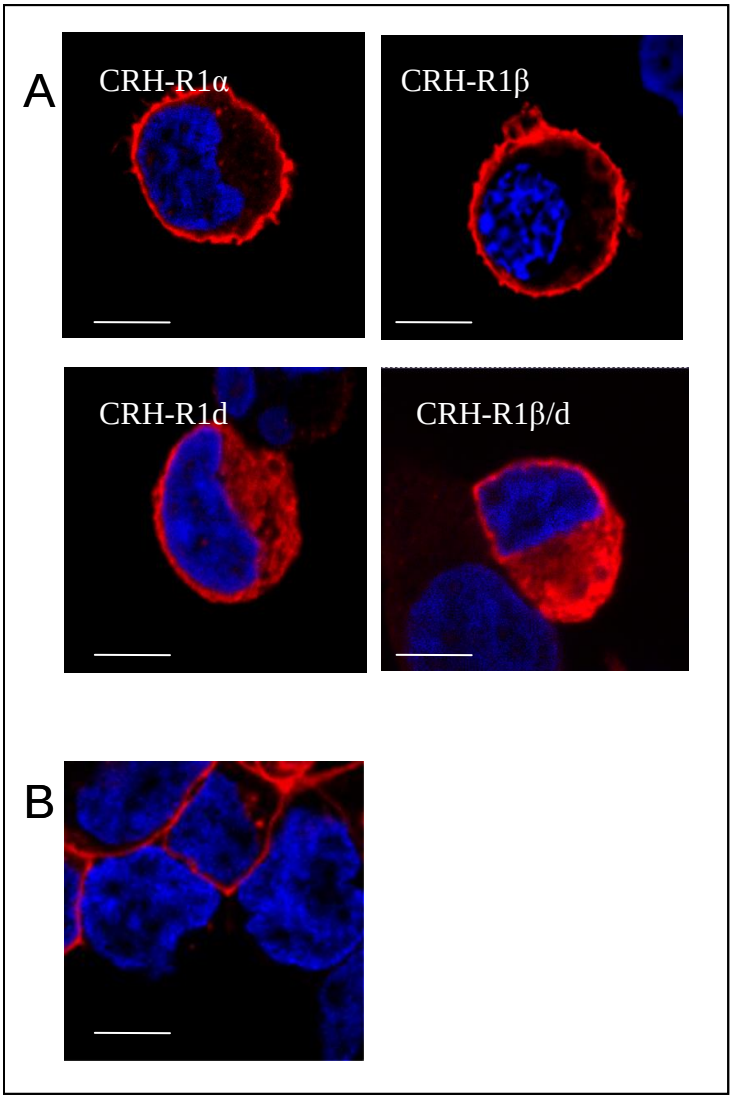

Figure 3.1. The cellular expression of CRH-R1 variants visualised by confocal microscopy. A. HEK293 were transiently transfected with CRH-R1α, CRH-R1β, CRH-R1d and CRH-R1β/d. CRH-R1α and R1β are expressed only on the plasma membrane of the cell; on the other hand the immunoreactivity of CRH-R1d and R1β/d was observed in cytoplasm as well as cell membrane. B. HEK293 cells that did not uptake CRH-R1α cDNA did not show staining on the plasma membrane. The immunofluorescence was monitored using CRH-R1-specific antiserum and Alexa-Fluor®594 secondary antibody. The cell nuclei are visualised using DNA-specific dye-DAPI. Identical results were obtained in five independent experiments. Scale bar is 10μm.

3.2.2 Internalization characteristics of CRH-R1α

In order to investigate homologous internalization, st-293-R1α were stimulated with 0.1-100nM CRH for 0-60minutes. The internalization of CRH-R1α showed to be an agonist-dose dependent as well as time-dependent process. In the absence of CRH, the receptor was located exclusively on the plasma membrane. Treatment of cells with 0.1 nM CRH for 45 minutes did not cause redistribution of the receptor; CRH-R1α staining was still very clearly on the plasma membrane. However 1nM CRH treatment for 45 minutes led to a partial reduction of the receptor staining from the cell surface. Treatment of cells with concentrations of CRH greater than 10 nM for 45 minutes led to redistribution of cellular imunoreactivity; the majority of cells had strong punctuate staining in the cytoplasm, indicative of receptor endocytosis (Figure 3.2). Since 100 nM CRH treatment led to the strongest redistribution of the receptor, this concentration was chosen to investigate further the time-dependent internalization characteristics. Lower concentrations (0.1-10 nM) of CRH were also used in these experiments for comparison (data not shown). 0.1 nM CRH treatment did not lead to visible redistribution of the receptor even after 60 minutes. Cells treated with 1nM CRH showed some redistribution of CRH-R1α from the membrane, which was observed as intracellular staining. 10 nM CRH treatment induced internalization was similar to 100 nM CRH induced internalization, though there was a delay of 10-15 minutes. When st-293-R1α were treated only with vehicle (acetic acid), the receptor was exclusively expressed on the plasma membrane. Treatment with 100 nM CRH for 15 minutes led to the appearance of punctuate staining in the near proximity of the plasma membrane, possibly indicative of early endocytosis. After 30 minutes of exposure to 100 nM agonist, significant immunoreactivity was observed in the

cytoplasm. Similar results were seen after 45 minutes. The most dramatic change in the receptor localisation was after 60min of treatment (Figure 3.3). Quantitative analysis of the images confirmed these observations (Figure 3.3). To demonstrate that the internalization of CRH-R1α was CRH specific, st-293-R1α cells were treated with 100nM UCN-II (CRH-R2 receptor specific agonist) for 60 min. The plasma membrane distribution of CRH-R1α was not affected by UCN-II (Teli T *et al*., 2005).

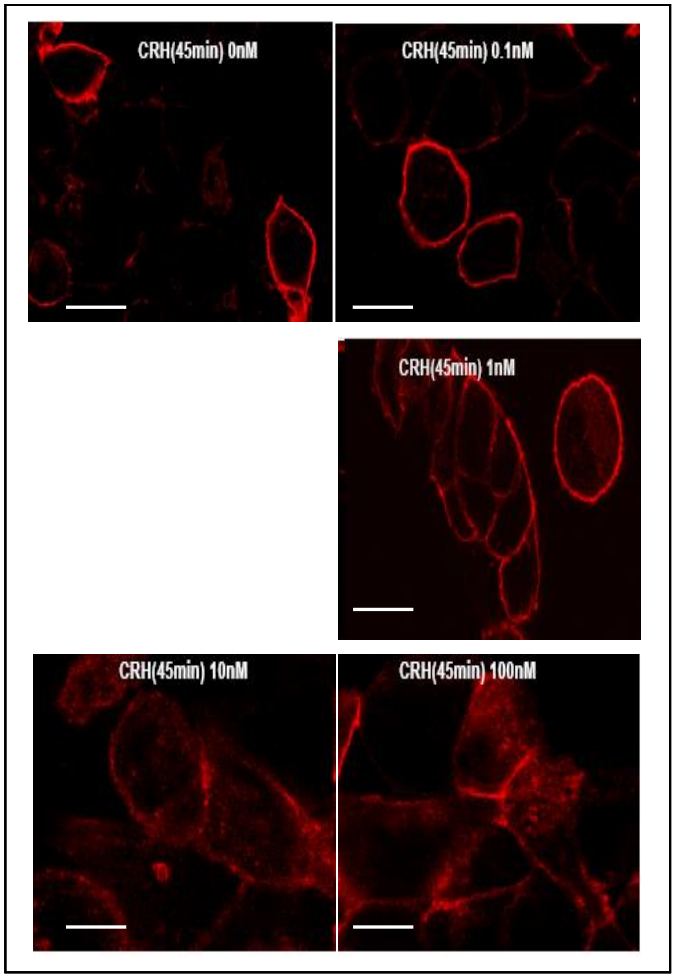

Figure 3.2. Internalization of CRH-R1α in st-293-R1α- agonist-dose dependency. st.293-R1α cells were grown on cover slips and after exposure to CRH (0.1–100 nM) for 45 minutes, CRH-R1 distribution was monitored by indirect immunofluorescence using CRH-R1-specific antiserum and Alexa-Fluor®594 secondary antibody. Identical results were obtained from four independent experiments. Scale bar is 20μm. Magnification x 63. (Teli T *et al*., 2005)

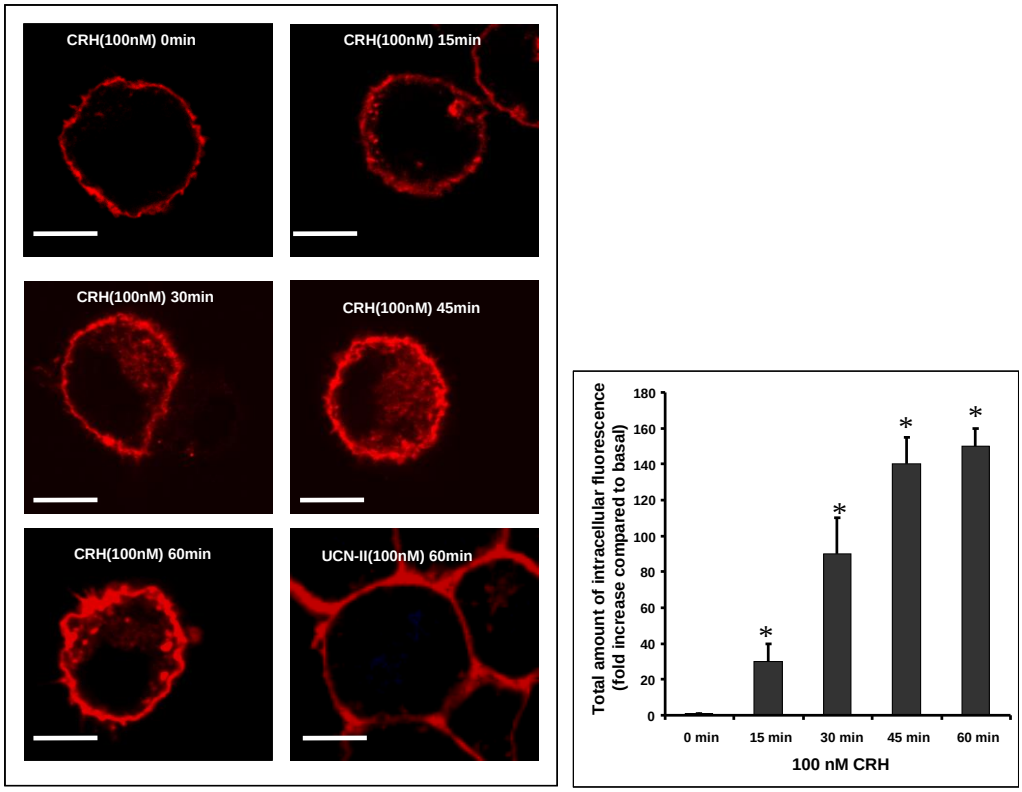

Figure 3.3. Internalization of CRH-R1α in st-293-R1α- time course. st.293-R1α cells were grown on cover slips and exposed to 100nM CRH for various time points (0-60min); no apparent internalization was observed when the cells were challenged with 100nM UCN-II (CRH-R2 specific agonist) for 60min. CRH-R1 distribution was monitored by indirect immunofluorescence using CRH-R1-specific antiserum and Alexa-Fluor®594 secondary antibody. Scale bar is 10 μm. Identical results were obtained from four independent experiments. Magnification x 63, and optical zoom x 5. (Teli T *et al*., 2005). The graph represents quantification of CRH-R1α intracellular distribution following 100 nM CRH stimulation (as described in the Materials and Methods) for various time points (0-60 min). The results are presented as the mean ± SEM of 20-25 individual cell estimations from four independent experiments. *, $P<0.05$ compared with cells without CRH treatment.

3.2.3 Internalization of CRH-R1α leads to β-arrestin recruitment to the plasma membrane

The internalization of most GPCR requires recruitment of β-arrestin to the plasma membrane (DeWire SM *et al*., 2007). In the absence of CRH the endogenous β-arrestin (green) was uniformly distributed throughout the cytoplasm, whereas the receptor was exclusively located on the plasma membrane (Figure 3.4 top row). Two minutes treatment with 100nM CRH elicited a significant and rapid translocation of β-arrestin to the plasma membrane, as demonstrated by a significant increase (more than 60 fold increase above basal) in cell surface immunostaining for β-arrestin signal (Figure 3.4 graph). To measure these changes, fluorescence was quantified along chosen axis (as shown on Figures 3.4, 3.6. and 3.9.) with effective thickness of 0.1 mm. Quantification of fluorescence showed an increased green fluorescence at the point where the line demarcated the cell membrane (1-3 and 19-21μm). 2 minutes treatment with CRH did not affect cellular distribution of the receptor, which still remained restricted to the plasma membrane (red). Following 30 minutes treatment with 100 nM CRH, a significant pool of the receptor was internalized. A fraction of internalized CRH-R1α was potentially co-localized with β-arrestin in endosomes (yellow dots), however some vesicles of the receptor (red) were not associated with β-arrestin in the same intracellular compartments; potentially suggesting more than one pathway of receptor internalization. This was also evident in the analysis of fluorescent spectra where some (but not all) intensity peaks of green and red fluorescence could be observed at the same position (Markovic D *et al*., 2006).

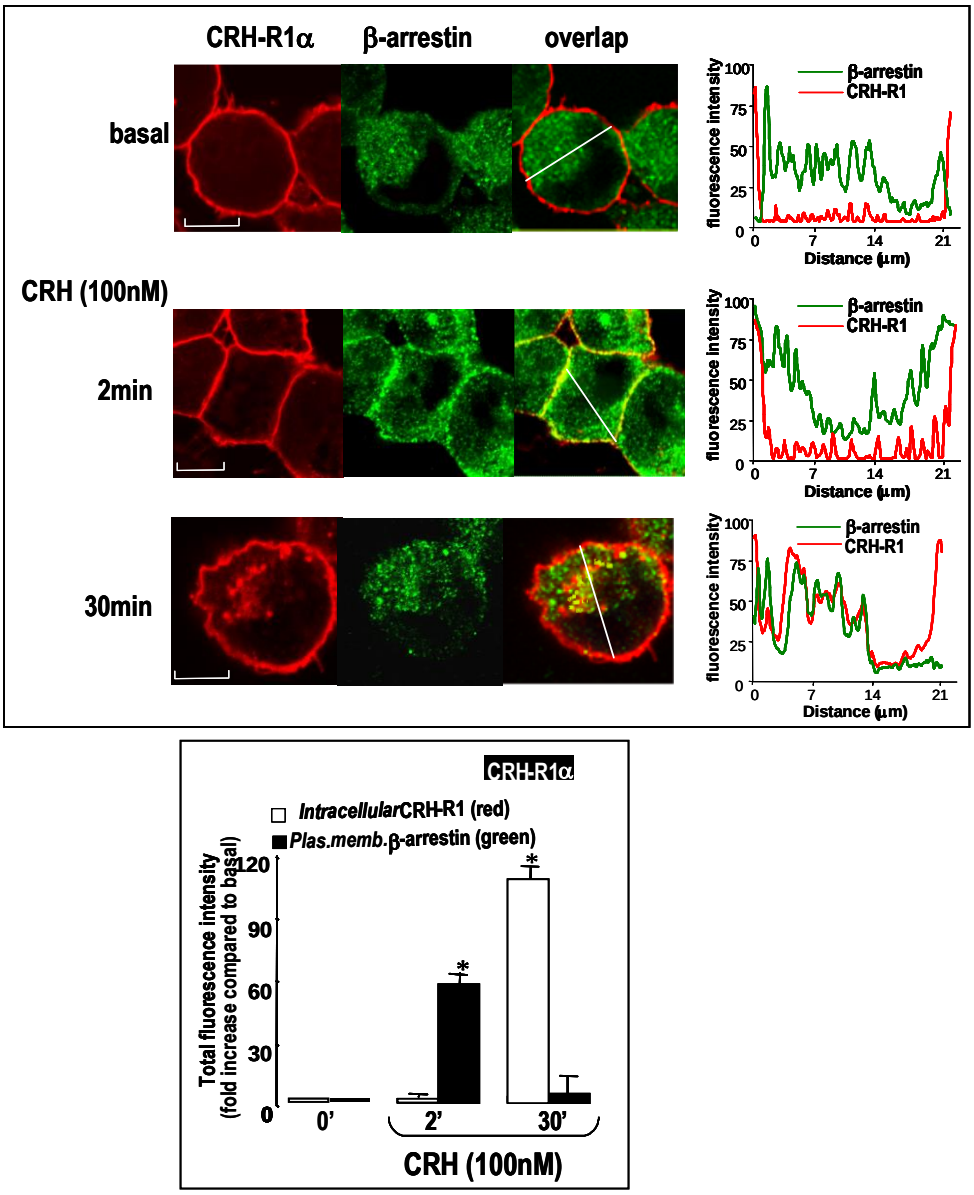

Figure 3.4. Cellular distribution of CRH-R1α and β-arrestin following CRH stimulation of st.293-R1α cells. st.293-R1α cells were grown on cover slips and exposed to 100nM CRH for 2 and 30min. CRH-R1 distribution was monitored by indirect immunofluorescence using CRH-R1-specific antiserum and Alexa-Fluor®594 secondary antibody (red). β-arrestin distribution was monitored by indirect immunofluorescence using pan-arrestin antiserum and Alexa-Fluor®488 secondary antibody (green). Scale bar is 10 μm. Identical results were obtained from four independent experiments. Magnification x 63, and optical zoom x 5. For quantification of cytoplasmic CRH-R1α and plasma membrane β-arrestin distribution, 20-25 individual cells in five random fields of view were examined, and the sum of fluorescence intensity is presented as described in 2.11.8. Results are expressed as the mean ± SEM from four independent experiments (Markovic D *et al.*, 2006). *, P<0.05 compared to basal (time=0).

3.2.4 Internalization characteristics of CRH-R1β

In order to determine whether the insertion of 29 amino acids within the first intracellular loop has an effect on internalization characteristics of CRH-R1β, tr-293-R1β were stimulated with 0.1-100nM CRH for 0-60minutes. Internalization of CRH-R1β was shown to be an agonist-dose dependent as well as time-dependent process. The pattern of internalization was similar to the internalization pattern of CRH-R1α (Figure 3.5).

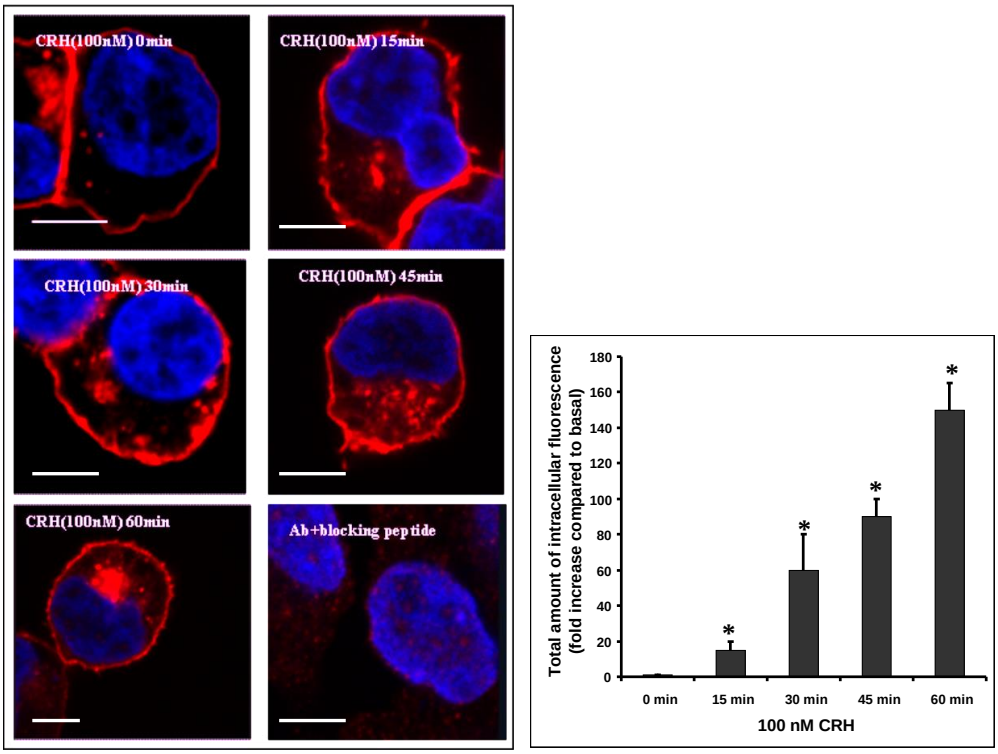

Figure 3.5. Internalization of CRH-R1β in tr-293-R1β- time course. tr.293-R1β cells were grown on cover slips, treated and analysed as described in the legend of the Figure 3.3. The specificity of CRH-R1 antibody was demonstrated by lack of staining when antibody was incubated with the corresponding blocking peptide prior to addition on the slides. Cell nuclei (blue) were stained using the DNA-specific dye DAPI. Scale bar is 10 μm. Identical results were obtained from four independent experiments. Magnification x 63, and optical zoom x 5. The graph represents quantification of CRH-R1β intracellular distribution. The results are presented as the mean ± SEM of 20-25 individual cell estimations from four independent experiments. *, $P<0.05$ compared with cells without CRH treatment.

3.2.5 Internalization of CRH-R1α leads to β-arrestin recruitment to the plasma membrane

To determine whether β-arrestin was recruited to the plasma membrane prior to the internalization of CRH-R1β, the same experimental approach was employed as described in 3.2.3.

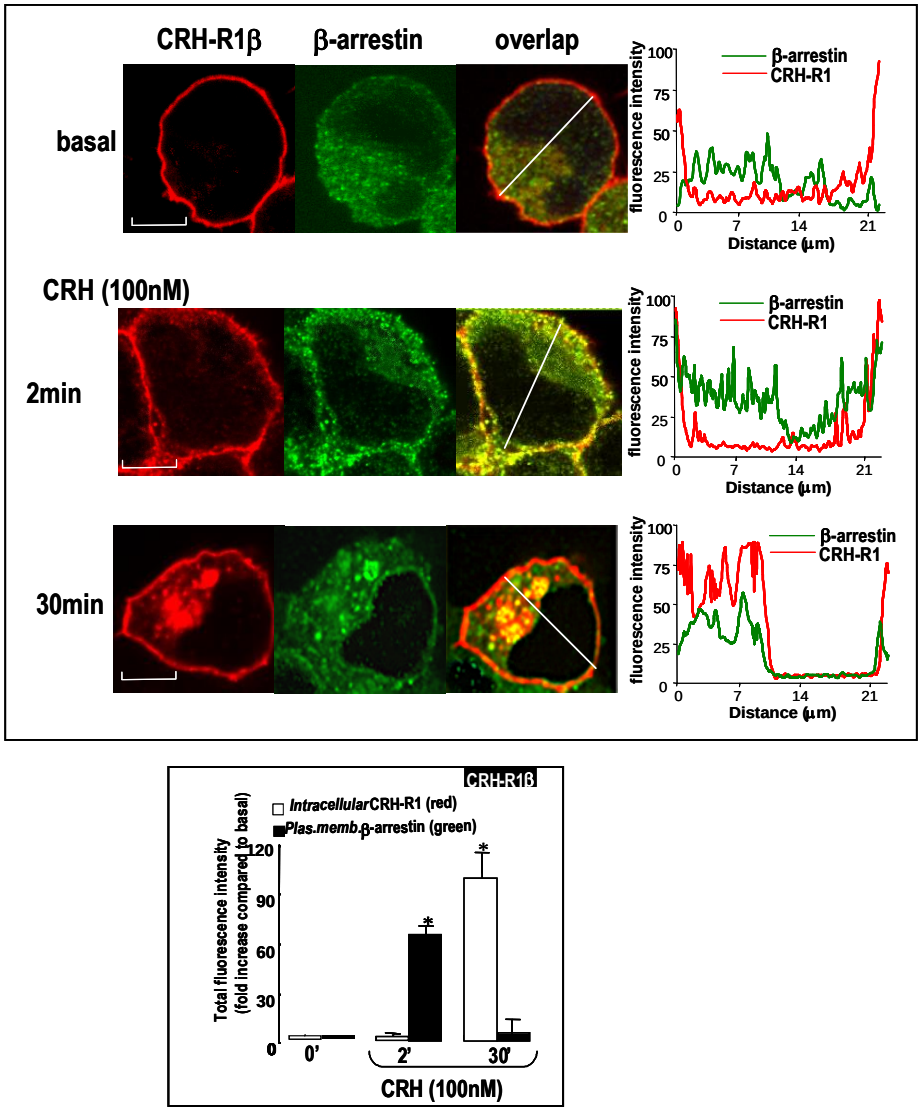

Figure 3.6. Cellular distribution of CRH-R1β and β-arrestin following CRH stimulation of tr.293-R1β cells tr.293-R1β cells were grown, stimulated and analysed as described for in the legend of Figure 3.4. Scale bar is 10 μm. The graph represents CRH-R1β and β-arrestin cellular redistribution. Results are expressed as the mean ± SEM from four independent experiments (Markovic D *et al.*, 2006). *, P<0.05 compared with cells without CRH treatment.

In the absence of the agonist treatment the β-arrestin staining (green) was uniformly distributed through the cytoplasm, whereas the receptor was exclusively expressed on the plasma membrane (Figure 3.6 top row). 2 minute treatment with 100nM CRH caused a significant and rapid translocation of β-arrestin to the plasma membrane, which resulted in 70 fold increase of green fluorescence on the plasma membrane. 30 minutes exposure to 100nM CRH led to significant accumulation of CRH-R1β in the cytoplasm, a fraction of the internalized receptor was potentially co-localised with the endogenous β-arrestin (Figure 3.6). These results demonstrated for the first time that CRH-R1β, a signalling impaired receptor (reduced cAMP production compared to CRH-R1α), retains some characteristics of a functionally active receptor (Markovic D *et al*., 2006).

3.2.6 Internalization characteristics of CRH-R1d

As shown on the figure 3.1 CRH-R1d is predominantly expressed in the cytoplasm or cellular compartments such as endoplasmatic reticulum of tr-293-R1d. However there is also a small portion of the receptor that is present on the cell plasma membrane, as shown by western blot analysis (Figure 3.7). The plasma membrane proteins were prepared as previously described (Karteris E *et al*., 2004)

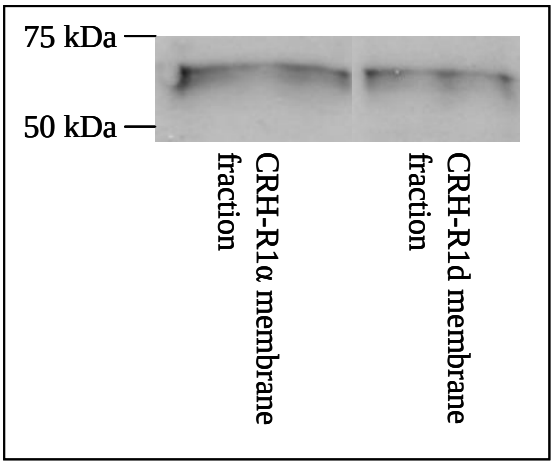

Figure 3.7. Western blot analysis of plasma membrane fraction of HEK293 transiently expressing CRH-R1α and CRH-R1d. Cytoplasmic and membrane fraction were separated as described in the Methods. 10μg of proteins were loaded and separated on a 10% SDS-PAGE. Following transfer on a PVDF membrane, the CRH-R band was identified using an antibody that recognises both CRH-Rs. Identical results were obtained in three independent experiments.

In this part of the study, the potential internalization of membrane-expressed CRH-R1d was investigated. In the absence of CRH, the imunoreactivity of the receptor was uniformly distributed through the cytoplasm and plasma membrane. An addition of 100nM CRH for 15 minutes caused redistribution of the receptor, evident as an appearance of punctuated distribution of the receptor immuno-signal in the cytoplasm. The redistribution of the receptor was more evident after 60min treatment with 100nM CRH. At this time point there was little or no immunoreactivity of the receptor on the plasma membrane, however the majority of intracellular immunoreactivity showed a punctuated pattern possibly indicative of the receptor in endocytotic vesicles. The specificity of staining was demonstrated by lack of staining when CRH-R1 antibody was pre-absorbed with the synthetic blocking peptide (10 fold molar excess) prior to addition on the slides (Figure 3.8).

Next, the involvement of β-arrestin in the internalization of CRH-R1d was investigated. In the absence of agonist stimulation, the endogenous β-arrestin was

distributed in the cytoplasm. Similarly to the experiments with CRH-R1α and R1β, 100nM CRH treatment for 2min of tr-293-R1d led to recruitment of β-arrestin to the plasma membrane; however after 30min there was no significant co-localisation between the receptor and β-arrestin (Figure 3.9). This was confirmed with an analysis of fluorescent spectra, where the majority of intensity peaks of green and red fluorescence could not be observed at the same position.

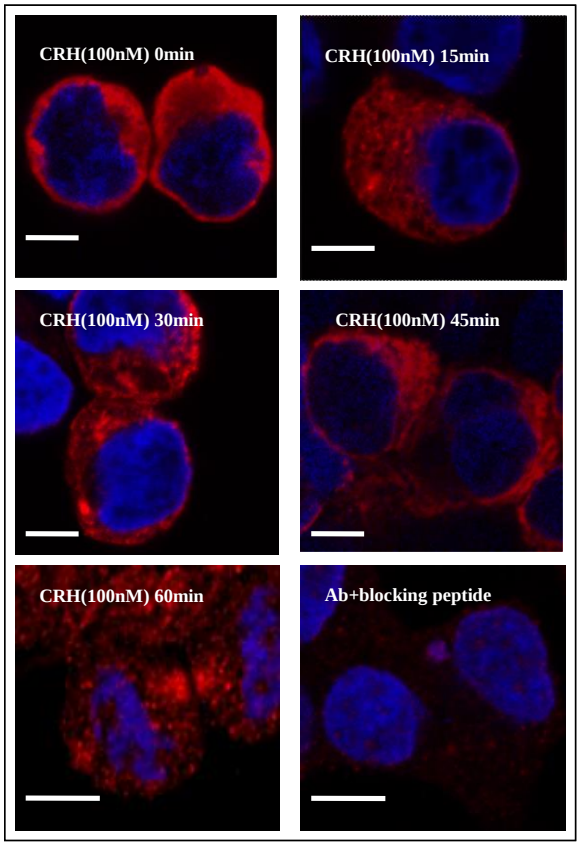

Figure 3.8. Cellular distribution of CRH-R1d in tr-293-R1d- time course. tr.293-R1d cells were grown, stimulated and visualized as described in the legend of the Figure 3.3. The specificity of CRH-R1 antibody was demonstrated by lack of staining when antibody was incubated with the corresponding blocking peptide prior to addition on the slides. Cell nuclei (blue) were stained using the DNA-specific dye DAPI. Scale bar is 10 μm. Identical results were obtained in four independent experiments. Magnification x 63, and optical zoom x 5.

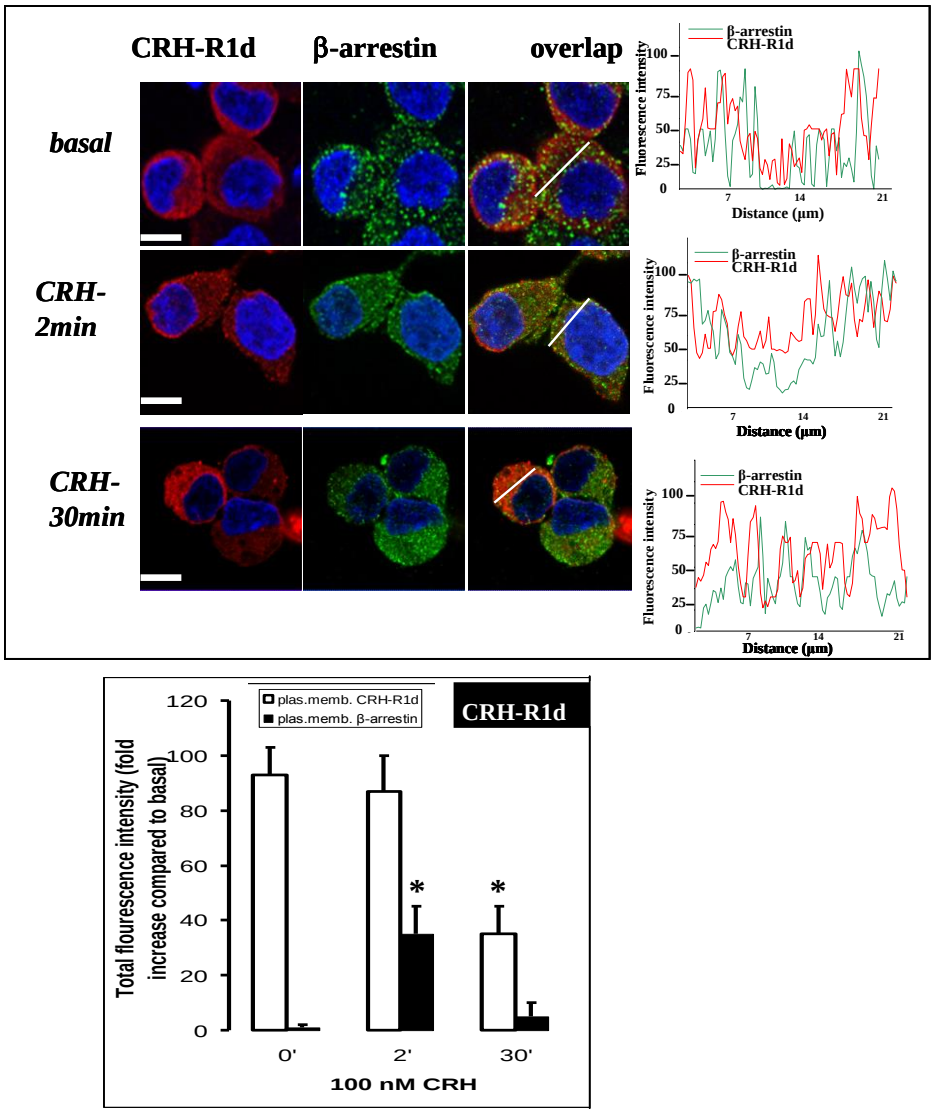

Figure 3.9. The involvement of β-arrestin in CRH-R1d internalization. tr.293-R1d cells were grown, stimulated and visualized as described above for the Figure 3.4. Scale bar is 10 μm. For quantification of plasma membrane CRH-R1d and β-arrestin distribution, 20-25 individual cells in five random field of view were examined, and the sum of fluorescence intensity of plasma membrane (plas.memb.) (1-3 and 19-21μm) fluorescence was measured as described in 3.1.5. Results are expressed as the mean ± SEM from three independent experiments. *, P<0.05 compared with cells without CRH treatment.

3.2.7 Heterologous internalization of CRH-R1α and CRH-R1β

In tissues such as myometrium that express multiple CRH receptor subtypes, heterologous activation of protein kinase C (PKC) by oxytocin leads to a

differential CRH binding to the CRH receptor and to the attenuation of CRH induced cAMP production (Grammatopoulos DK and Hillhouse EW, 1999). Since the CRH receptors contain multiple putative PKC phosphorylation sites within the first and second intracellular loops and at the C-terminus, it is possible that the heterologous phosphorylation of these sites could lead to conformational changes of the receptor resulting in impaired functionality. Further investigation of the PKC effects on various subtypes of CRH-R, demonstrated that CRH-R1α and CRH-R1β exhibited differential functional responses to PKC-induced phosphorylation, with only CRH-R1β susceptible to cAMP signalling desensitisation (Markovic D *et al*., 2006). Interestingly, internalization studies revealed that a challenge with 200nM PMA for 30min led to differential cellular redistribution of CRH-R1α and CRH-R1β. Treatment of tr-293-R1α with 200nM PMA for 30min did not have any effect on cellular distribution of the receptor. In contrast, PMA induced CRH-R1β internalization demonstrated by a significant redistribution of cellular immunostaining (Figure 3.10). This observation was confirmed by quantification of intracellular fluorescence spectra of 15-20 individual cells treated with 100nM CRH for 45min and 200nM PMA for 30min (Figure 3.11).

Next, the involvement of β-arrestin in PMA induced internalization of CRH-R1β was investigated. PMA treatment for 2 and 30 min did not affect β-arrestin cellular distribution in either cellular system, tr-293-R1α nor tr-293-R1β (Figure 3.12).

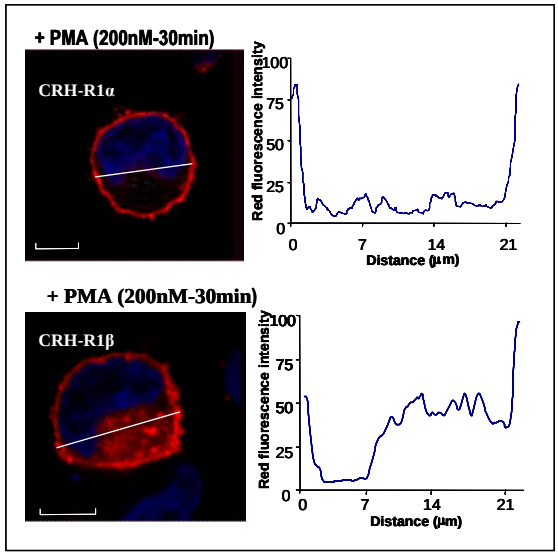

Figure 3.10. Effect of PMA on cellular redistribution of CRH-R1α and CRH-R1β in transiently transfected HEK293. Cells were grown on cover slips and exposed to 200nM PMA for 30min. CRH-R1 distribution was monitored as described above. Cell nuclei (blue) were stained using the DNA-specific dye DAPI. Identical results were obtained from four independent experiments. Scale bar is 10μm. Representative profile of fluorescent intensities is also shown. Magnification x 63, and optical zoom x 5. (Markovic D *et al*., 2006)

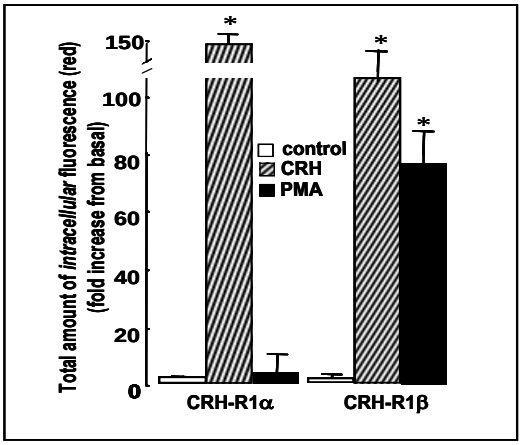

Figure 3.11. Relative quantification of intracellular CRH-R1α and CRH-R1β following CRH and PMA treatment. Following a treatment, cells were examined using confocal microscopy and intracellular CRH-R1 fluorescence intensity measurements were generated by summing the spectral measurement from 20 individual cells from (distance 4-18μm) from four independent. The results are presented as the mean ± SEM. *, P<0.05 compared with untreated (control) values (Markovic D *et al*., 2006).

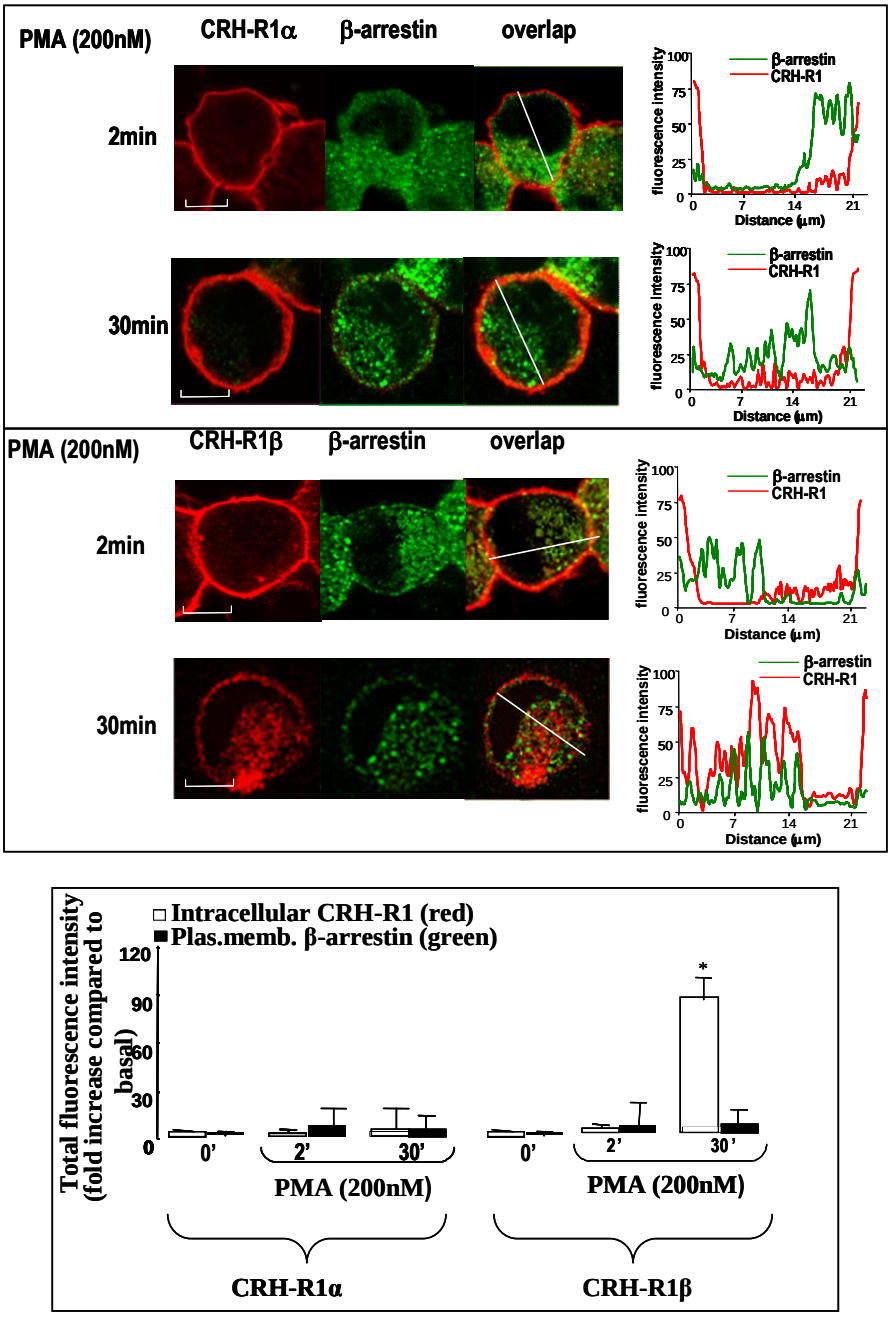

Figure 3.12. The effect of PMA treatment on β-arrestin distribution. tr.293-R1α and tr-293-R1β cells were grown on cover slips, and treated with 200nM PMA 2 and 30min. CRH-R1 and β-arrestin distribution was as described on the Figure 3.4. Scale bar is 10 μm. Identical results were obtained from four independent experiments. Magnification x 63, and optical zoom x 5. The graph represents CRH-R1β and β-arrestin cellular redistribution. Results are expressed as the mean ± SEM from four independent experiments. *, P<0.05 compared with untreated values (Markovic D *et al*., 2006).

3.3 DISCUSSION

The exposure of CRH-R to CRH and other agonists results in rapid attenuation of CRH-R responses, through a mechanism of receptor desensitization and internalization. In recent years, CRH-R1 desensitization and internalization have been extensively studied by various groups (Rasmussen TN *et al.* 2004; Teli *et al.* 2005; Perry SJ *et al*., 2005, Holmes KD *et al*., 2006; Markovic D *et al*., 2006). In HEK293 cells over-expressing CRH-R1α, desensitization of the receptor was associated with its phosphorylation and subsequent endocytosis (Teli *et al*., 2005). Further internalization studies demonstrated that β-arrestin was recruited toward the plasma membrane of HEK293 over-expressing CRH-R1α, upon the stimulation with CRH (Rasmussen TN *et al*., 2004; Perry SJ *et al*., 2005; Holmes KD *et al*., 2006; Markovic D *et al*., 2006). Perry and Holmes pin-pointed β-arrestin2 as a major isoform involved in CRH-R1α sequestration, but the subsequent fate of the receptor still remains controversial. Holmes et al (2006) defined CRH-R1α as a class A receptor regarding the lack of β-arrestin2 co-localisation with the receptor in the endosome structure in HEK293, whereas Perry (2004) has demonstrated co-localisation of the two in the cytoplasm. These discrepant results could be possibly due to different experimental approaches that the two groups employed. Although, both groups used CRH-R1-tagged receptors, Holmes et al monitored the colocalisation of the receptor with β-arrestin in live cells, while Perry et al (2005) carried out the experiments in fixed cells. However, Holmes et al (2006) has demonstrated that CRH-R1α indeed co-localise with β-arrestin2 in the cytoplasm of primary cortical neurons, but in a small proportion to the total amount of β-arrestin2-GFP. Moreover, it has been shown that following the endocytosis, the

receptor transited from Rab5-positive early endosome to Rab4-positive recycling endosome, and that the receptor was not targeted for degradation in lysosomes in HEK293 over-expressing CRH-R1α and in primary cortical neurons (Holmes KD *et al*., 2006). In contrast, CHO-K1 stably expressing CRH-R1 challenged with CRH for 1h had 83% of the receptor remaining in the cell, while after 24h treatment only 38% of the total CRH-R1 proteins were detected, clearly showing receptor down-regulation (Perry SJ *et al*., 2005). Taken together these findings suggest that different cellular systems might have distinct patterns of CRH-R1 endocytosis, possibly depending on availability of accessory proteins involved in the internalisation process and mechanisms regulating the sensitivity of the target tissue to active CRH.

The evidence shown in this chapter highlights the complexity of CRH-R1 sequestration. CRH-R1 internalizes in a time and agonist concentration dependent manner, and β-arrestin is recruited to the plasma membrane as early as 2min following CRH stimulation, suggesting that the process of CRH-R1 internalization is β-arrestin dependent. Following 60min treatment with CRH, CRH-R1α is redistributed from the plasma membrane to intracellular compartments as a consequence of receptor endocytosis. A fraction of the internalized receptor might be co-localised with β-arrestin in the endosome, however another portion of the receptor is not, defining the receptor as a member of the both classes of receptors, A and B, regarding interaction with β-arrestin during internalization. This could suggest the existence of distinct pathways (β-arrestin dependent and independent) involved in CRH-R1 trafficking. However, further biochemical analysis (such is co-immunoprecipitation) of potential CRH-R1 and β-arrestin physical interactions would provide concrete evidence that these two proteins interact. Nevertheless, one

has to keep in mind, that the internalization is studied in a cellular system that over-expressed the receptor, and that the promiscuous behaviour of the CRH-R1α receptor could be because of an unbalanced ratio of the receptor and β-arrestin. This limitation could have been overcome using controlled over-expression of the receptor and β-arrestin by viral vectors in a cellular system that has low expression of endogenous CRH-R1 and β-arrestin, such as CHO cells.

In addition, the investigation of CRH-R1α internalization in primary myometrial smooth muscle cells overexpressing the receptor demonstrated that in this system too, β-arrestin is recruited to the plasma membrane following CRH stimulation. Moreover, a more prolonged exposure to CRH (30 minutes) induced CRH-R1α endocytosis and a partial co-localization with β-arrestin was detected (data not shown).

The human specific CRH-R1β variant is identical to the fully functional, wild type receptor, CRH-R1α, except for a 29-amino acid insert within the first intracellular loop of the R1β. It has been demonstrated that CRH-R1β has impaired agonist binding and G protein coupling (Chen R *et al*., 1993). Internalization properties of this variant had not been investigated prior to our report (Markovic D *et al*., 2006) in which it was demonstrated that despite signalling impairment, the CRH-R1β receptor retained the same internalization properties as the functional CRH-R1α receptor. Agonist-activation of both CRH-R1 variants was associated with the initial recruitment of β-arrestin to the plasma membrane; this provides indirect evidence that the intracellular mechanisms inducing β-arrestin translocation to the membrane are independent of CRH-R1 signalling potency (EC_{50}=3±2 nM for CRH-R1α, and EC_{50}=19±5 nM for CRH-R1β) (Markovic D *et al*., 2006).

Interestingly, a substantial difference between CRH-R1α and R1β was observed in response to heterologous desensitisation mediated via PKC. It was demonstrated that activation of PKC led to phosphorylation of both CRH-R1 isoforms (α and β), but only the CRH-R1β variant was susceptible to PKC-induced desensitization (Markovic D *et al.,* 2006). The reduction in the functional response of CRH-R1β following PKC activation, could potentially be explained by the reduction of cell surface expression of CRH-R1β due to internalisation, but not CRH-R1α following activation of PKC. These data complement previous observation showing that PKC can potentiate CRH action in the pituitary where only CRH-R1α is expressed, while inhibiting CRH actions in the myometrium at term, which expresses several CRH-R1 variants, including CRH-R1β (Grammatopulos DK and Hillhouse EW, 1999a).

Additionally, this project provided evidence that PMA-induced internalization of CRH-R1β was not associated with recruitment of β-arrestin to the cell surface, suggesting an alternative β-arrestin-independent pathway that is activated in response to PKC phosphorylation of the CRH-R1 (Markovic D *et al*., 2006). It has been demonstrated that internalization of some GPCRs in the basal-unstimulated state can be triggered by direct activation of PKC. PKC-mediated phosphorylation of CXCR4 induces receptor internalization through a dynamin-dependent mechanism that is distinct from ligand induced endocytosis (Wolfe BL & Trejo J, 2007). It is quite likely that such a mechanism drives PKC-induced internalization of CRH-R1β. This mechanism might be physiologically relevant since it suggests that the response of CRH-R1 to PKC and the tissue sensitivity to CRH depends upon the splicing pattern of the CRH-R1.

Previous mRNA studies carried out on myometrial tissue from pregnant women identified a splice variant of CRH-R1 receptor that lacks 14-amino acids within the seventh transmembrane domain, termed CRH-R1d (Grammatopoulos DK *et* al., 1999). Recent quantitative RT-PCR studies have shown that CRH-R1d mRNA levels increase as the uterus switches from a quiescent to labouring state (Markovic D *et al*., 2007) suggesting a physiologically important role of this variant at the end of pregnancy and the onset of labour. CRH-R1d has impaired signalling properties and G protein coupling, but it is able to bind agonists with high affinity (Grammatopoulos DK *et* al., 1999). In this study it was demonstrated that CRH-R1d is predominately expressed intracellularly, possibly in the endoplasmatic reticulum (ER), with a small portion of receptor on the plasma membrane. It is possible that the deletion of 14 amino acids from the 7th TMD leads to inability of the newly synthesised receptor to leave the ER and integrate into the plasma membrane. If this is the case, it would imply the intact 7th TMD is crucial for the receptor trafficking to the plasma membrane. The cell surface portion of the receptor was susceptible to CRH induced internalization in a time dependent manner. Additionally, the initial recruitment of β-arrestin following receptor activation was observed, but in contrast to the CRH-R1α and R1β receptors, there was no evidence of co-localisation between CRH-R1d and β-arrestin in the cytoplasm. It is tempting to speculate that the deletion of 14-amino acids from the 7th TMD could lead to misfolding of the C-terminus orienting it towards extracellular space, which makes the C-terminus inaccessible to β-arrestin (data from Chapter 4 suggests that this might be the case).

The C-terminus of many GPCRs contains serine/threonine clusters that can be phosphorylated by GRKs and regulate β-arrestin translocation and binding to the receptor (Reiter E & Lefkowitz RJ, 2006; Kohout TA & Lefkowitz RJ, 2003). A

recent study investigating internalization characteristics of CRH-R1 has revealed that when the last 30 amino acids of the C-terminus were removed, phosphorylation of the activated receptor and β-arrestin2 recruitment were markedly reduced. Although the truncation of the last four amino acids (STAV) from the C-terminus resulted in reduced receptor phosphorylation, it did not have an effect on β-arrestin2 recruitment to the activated receptor (Oakley RH *et al*., 2007). Also this report suggests that CRH-R1 contains an arrestin binding domain in one or more of the intracellular loops which is dependent on receptor activation but independent of GRK phosphorylation (Oakley RH *et al*., 2007). The identical arrestin binding domain has been identified in several GPCRs including vasopressin V2, luteinizing hormone, parathyroid hormone, substance P and neurotensin receptors and rhodopsin family GPCRs (Oakley RH *et al*., 2007). The biochemical study investigating potential CRH-R1d/β-arrestin physical interaction would be of great importance to further understand the nature of this CRH-R1 splice variant. Also, it would be interesting to determine if CRH induces, and if so in which extent, phosphorylation of CRH-R1d. In addition, it would be extremely beneficial to determine if the second intracellular loop that contains a few features of arrestin binding motif (His^{214}, Ala^{216}, Ile^{217}, Val^{218}, Leu^{219}- as identified in Oakley RH *et al*., 2007) is involved in agonist induced CRH-R1d internalisation.

4 STRUCTURAL AND FUNCTIONAL CHARACTERISTICS OF CRH-R1d

4.1 INTRODUCTION

In humans, the CRH-R1 gene spans over 50.3 kb, and contains 14 exons; one exon more than in other mammalian species. The CRH-R1 gene contains introns within its transmembrane domain/cytoplasmic region, highly conserved cysteins in its extracellular domains, and the first intacellular loop, which is characteristics of the glucagon/PTH receptor gene family (Hillhouse EW & Grammatopoulos DK, 2006). The omission of exon 13 (exon 12 in a case of other species but human) from the CRH-R1 transcript, results in expression of receptor protein termed CRH-R1d. This protein lacks 14 amino acids within the 7th transmembrane domain and exhibits impaired G-protein binding abilities and signalling properties, but it retains agonist binding characteristics of the wild type receptor (Grammatopoulos DK *et al*., 1999). Since the some of post-translational modifications of GPCRs as well as docking sites for signalling proteins are found in the C-terminus of receptors, it is possible that the deletion of the 14 amino acids from the 7th TDM of CRH-R1d leads to retraction and distortion of the C-tail, altering its signalling properties, and hence its function. CRH-R1d is not a unique example of a GPCR splice variant. The exon encoding the C-terminal 14 amino acids of the 7th TMD is highly conserved in most class B GPCR genes. The calcitonin receptor family, members of the class B GPCRs, has also numerous splice variants, and the splicing profile is identical to

that of CRH-R1. Both receptors have splice variants that contain inserts in the first intracellular loop (16 and 29 amino acids in the calcitonin and CRH-R1, respectively) and exon deletion in the 7th TMD (Grammatopoulos DK *et al*., 1999). Additionally, cloning of the rabbit calcitonin receptor identified a variant, identical to CRH-R1d, with a deletion of exon 13, termed CTRΔe13, which encodes the C-terminal part of the 7th TMD (Shyu *et al*., 1996). Activated by calcitonin, this variant demonstrates significantly impaired production of inositol phosphate and cAMP, also it fails to induce ERK phosphorylation; some of these findings are caused by the fact that the Δe13 variant is poorly expressed on the plasma membrane (Seck T *et al*., 2003). Moreover, splice variants identical to CRH-R1d have been reported for the vasoactive intestinal peptide receptor (Grinninger C *et al*., 2003) and PTH/PTHrP receptor (Ding C *et al*., 1995).

On the other hand the CRH-R2 gene exhibits a very different splicing pattern compared with CRH-R1. Mammals express only three known CRH-R2 variants: R2α, R2β and R2γ, which differ only in their N-terminus. The different N-termini do not significantly alter agonist binding and signalling properties, although the CRH-R2β is about 10-fold more potent in second messenger activation than R2α and R2γ (Hillhouse EW and Grammatopoulos DK, 2006).

The peripheral expression of CRH-R1 and –R2 exhibits a species dependent pattern with R2 receptor as the main functional receptor in animal peripheral tissues (Bale TL *et al*., 2003; Brar BK *et al*., 2004). In contrast, most peripheral human tissues express both types of CRH receptors, indicating higher levels of complexity and more subtle roles for CRH and UCNs in human physiology (Hillhouse EW and Grammatopoulos DK, 2006). Current knowledge suggests that the expression of both CRH-R1 and R2 in human peripheral tissues allows CRH and its related

peptides to exert diverse and contrasting effects (Hillhouse EW and Grammatopoulos DK, 2006). Although recent reports have demonstrated homodimerisation of CRH-R1 (Kraetke O *et al*., 2005) and heterodimerisation between vasopressin V1b and CRH-R1 receptors (Young SF *et al*., 2007), there are no reports investigating the interactions, possible cross-talk and dimerisation, between two types of the CRH receptors, R1 and R2.

In this part of the project the structural and functional characteristics of the CRH-R1d receptor were investigated. Since co-expression studies between the CRH-R1d and CRH-R1α demonstrated that the R1d receptor does not play a role of dominant negative receptor for CRH (Grammatopoulos DK *et al*., 1999), CRH-R1d and CRH-R2β were co-expressed in HEK293 cells in order to investigate potential effect of this variant on signalling and functional characteristics of CRH-R2β. The generated conditions could be used as a simpler model to investigate the potential interactions between the two receptors, which actually might occur in human peripheral tissues which express both types of CRH receptors, such as the uterus.

4.2 RESULTS

4.2.1 Expression of CRH-R1d in over-expressing systems

It was showed in the previous chapter that the CRH-R1d variant shows intracellular expression and poor expression on the cell surface. To confirm that cellular distribution of over-expressed CRH-R1d is not due to transcriptional conditions present in HEK293 cells, primary myometrial smooth muscle cells were

transfected with the recombinant CRH-R1d. Parallel transfection of CRH-R1α in the same model systems were used as a control to confirm that the intracellular staining was a specific characteristic of the CRH-R1d receptor. The results shown in figure 4.1 confirm that the CRH-R1d receptor is expressed predominantly in the cytoplasm of both the model systems, primary myometrial smooth muscle cells and HEK293, whilst the CRH-R1α receptor was exclusively expressed in the plasma membrane.

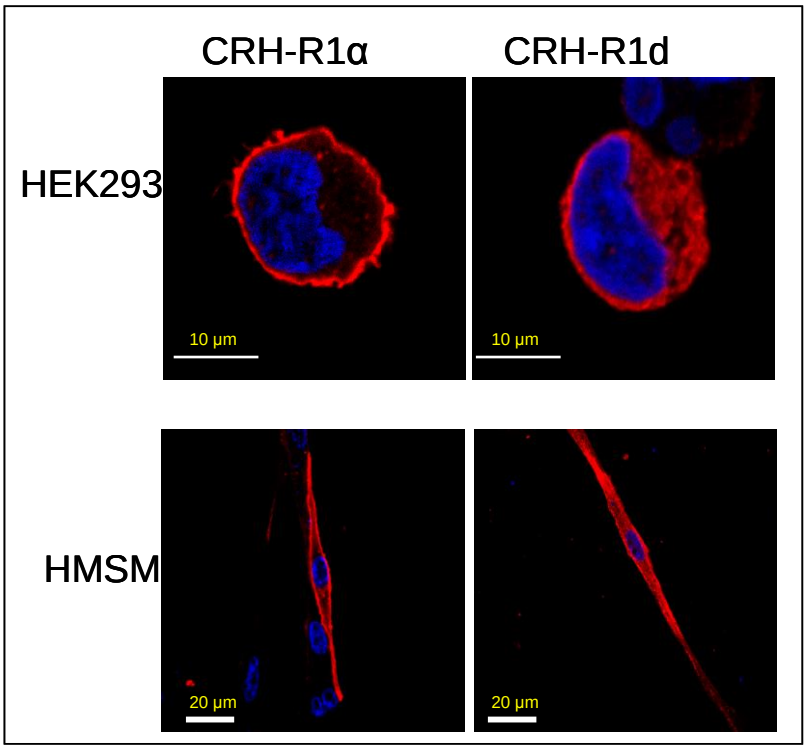

Figure 4.1. Visualization of over-expressed CRH-R1α and CRH-R1d distribution in HEK293 and HMSM cells by indirect immunofluorescent confocal microscopy. Indirect immunofluorescent confocal microscopy and specific primary antibody for CRH-R and Alexa-Fluor®594 (red) were used. The cell nuclei were stained with a DNA specific dye-DAPI. Identical results were obtained in three independent experiments.

4.2.2 Prediction of transmembrane domains and loops using the transmembrane helix prediction (TMHMM) algorithm

Since the deletion of the 14 amino acids from the 7th TMD leads to significant changes in the receptor cellular distribution, the possible effects of the deletion on the receptor folding within the plasma membrane were investigated and also whether misfolding leads to expression of the intracellular form of the receptor. The algorithms available at http://workbench.sdsc.edu were used for this analysis. Protein sequences of CRH-R1α and CRH-R1d were loaded and compared using the TMHMM software. TMHMM is a method used for prediction of transmembrane helices based on a hidden Markov model. It scores probability from 0 to 1 (0 meaning that there is no probability that an event would happen, 1 meaning that there is a strong possibility that the event actually occurs). The results obtained from this analysis are presented in figure 4.2.

As shown at the top part in the Figure 4.2, CRH-R1α is a classical example of seven TMD protein. However, there is an equal probability (50:50) for CRH-R1d to be a six or seven TMD protein; and if the receptor is a 6 TMD protein then it is likely that the C-terminus is actually present in the extracellular space.

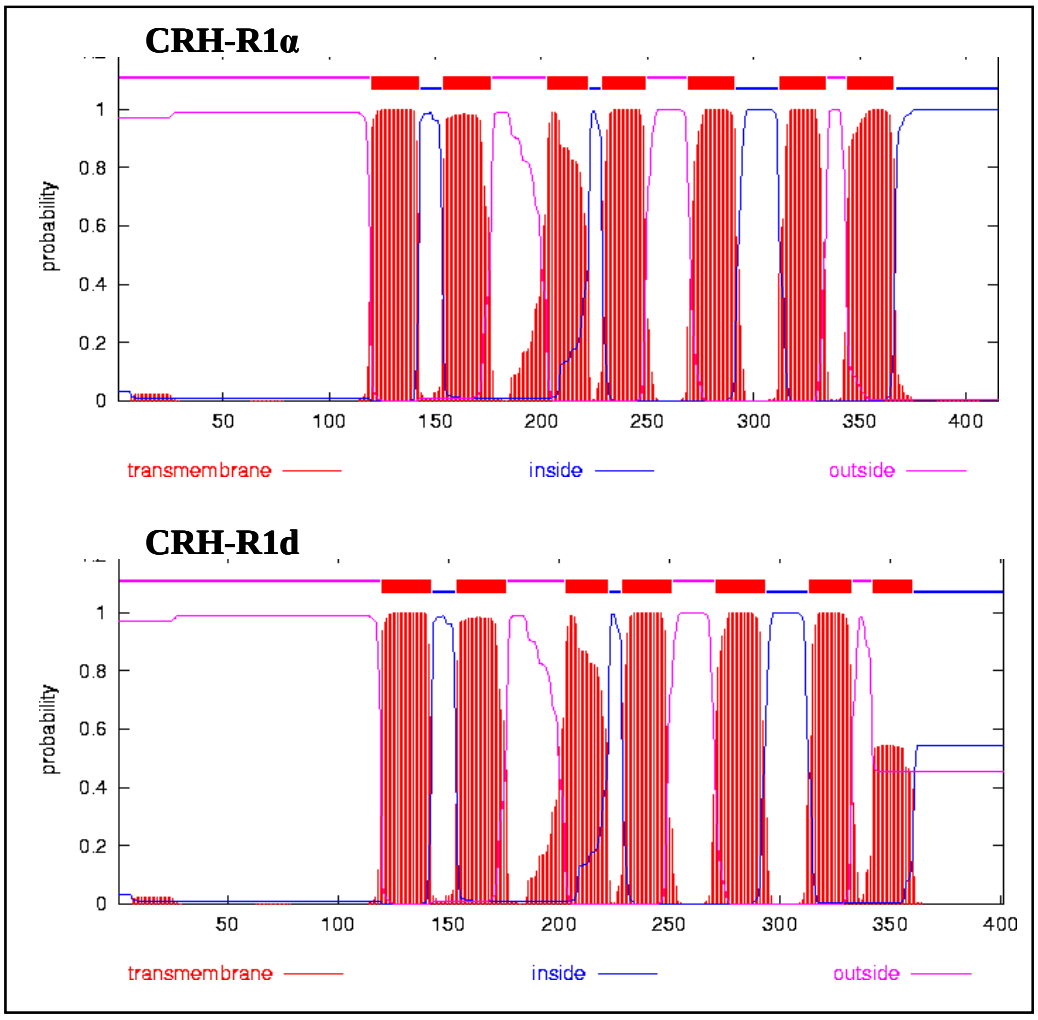

Figure 4.2. TMHMM prediction of TMD and loops (http://workbench.sdsc.edu). The protein sequences of CRH-R1α and CRH-R1d were analysed and compared. The red colour represents TMD, the intacellular loops are presented in blue and the extracellular in pink.

4.2.3 The C-terminus of CRH-R1d is in the extracellular space

The majority of GPCRs have seven TMDs, the N-terminus facing the extracellular space and the C-terminus in the intacellular area. However, there is an exception; the adiponectin receptor has the N-terminus facing inside of the cell and the C-terminus in the extracellular side of the cell (Deckert CM *et al*., 2006). Also a

splice variant of the calcitonin receptor, termed CTR eΔ13, is a 6 TMD protein (Seck T *et al*., 2005). Interestingly, this splice variant is encoded without exon 13 of the calcitonin receptor gene, identical to the R1d variant of CRH-R1.

To investigate CRH-R1d C-tail localisation, indirect confocal microscopy and a CRH-R specific antibody raised against the C-terminus of the receptor were used. Immunoreactivity would be detected in non-permeabilesed cells only if the C-tail is on the extracellular side of a cell; if the C-tail is in the intracellular space, it is inaccessible to the antibody in non-permeabilised cells, and thus no imunoreactivity would be detected. HEK-293 cells stably expressing CRH-R1α or CRH-R1d were grown on glass cover slips, fixed and stained as described in the Materials and Methods section. In Triton x-100 treated CRH-R1α expressing cells the receptor was localised on the membrane and in the CRH-R1d expressing cells the receptor was also located in the intracellular space. CRH-R1α over-expressing cells without treatment with Triton x-100 had no detectable fluorescence. The lack of signal suggests the C-tail was not accessible to the antibody because of its intracellular localisation. Interestingly, in the CRH-R1d over-expressing HEK293 cells substantial fluorescence was detected even without treatment with Triton x-100. This suggests that the C-terminus of CRH-R1d was accessible to the antibody, possible due to the C-terminus localization in the extracellular space (Figure 4.3)

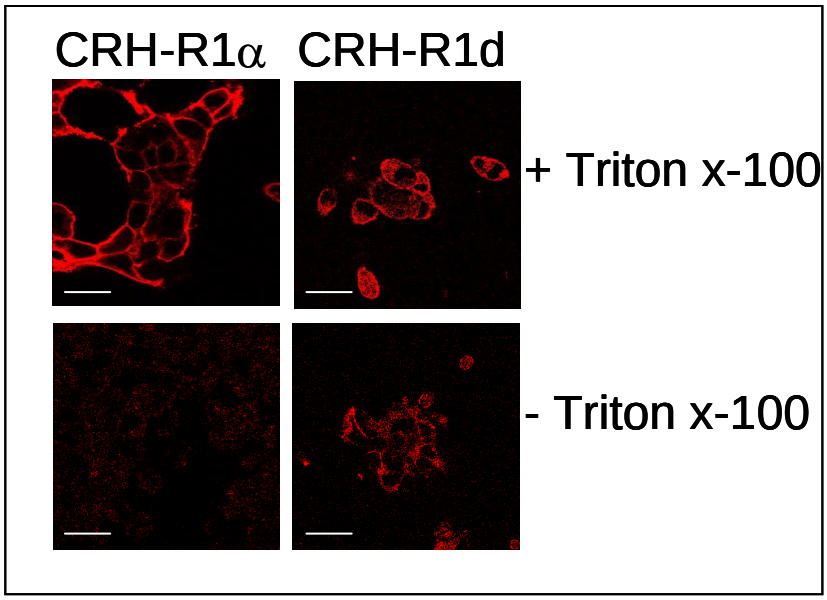

Figure 4.3. Orientation of the C-terminus of CRH-R1. Visualization of over-expressed CRH-R1α and CRH-R1d distribution in permeabilised (top row) and non-permeabilised (bottom row) HEK293 by indirect immunofluorescent confocal microscopy using the specific primary antibody for the C-terminus of CRH-R and Alexa-Fluor®594 (red) as described in above. Scale bar 40 μm. Identical results were obtained in three independent experiments.

4.2.4 Identification of amino acids encoded from the exon 13 that are necessary for the membrane expression of the receptor

The particular characteristics of CRH-R1d cellular localisation and the high probability to form a 6TMD receptor, most likely results from the deletion of 14 amino acids from the 7th TMD of CRH-R1 that as a consequence affects the expression of a missfolded six TMD receptor, with the C-terminus in the extracellular space that is unstable in the plasma membrane and shuttles between membrane and cytoplasm. To identify which amino acids are necessary for the membrane expression, a series of CRH-R1α and CRH-R1d mutant receptors were made. Two CRH-R1α mutant and three CRH-R1d mutant receptors were generated

with subsequent deletion and insertion, respectively, of a cassette of three amino acids each starting from the N-terminus encoded by the exon 13 (table 4.1). The mutants were generated as described in the Materials and Methods.

Amino acid sequence	Name of the receptor
GFFVSVFYCFINSE	CRH-R1α
VSVFYCFINSE	CRH-R1α Δ(356-358)
GFFFYCFINSE	CRH-R1α Δ(359-361)
	CRH-R1d
GFF	CRH-R1d +(356-358)
GFFVSV	CRH-R1d +(356-361)
GFFVSVFYC	CRH-R1d +(356-364)

Table 4.1.CRH-R1α and CRH-R1d mutant receptors.

These mutants were expressed in HEK-293 cells and the cellular localisation of the resulting receptors was visualized using indirect confocal microscopy (Figure 4.4 and 4.5). Deletion of the GFF (Gly356-Phe357-Phe-358) cassette from the 7th TMD of CRH-R1α in the mutant CRH-R1α Δ(356-358) resulted in transcription of an intracellular receptor or constitutively internalized receptor. This was confirmed by quantitative analysis of CRH-R1 intracellular fluorescence intensity (Figure 4.6) using ImageJ software as described in the Materials and Methods. However, deletion of the VSV cassette (Val359-Ser360-Val361) from the 7th TMD of CRH-R1α in the mutant CRH-R1α Δ(359-361) had no effect on membrane expression of the receptor (Figure 4.4). These results suggest that the GFF cassette is necessary for the stability of CRH-R1 in the plasma membrane. Next, it was investigated whether the insertion of the GFF cassette in CRH-R1d would be sufficient for the

plasma membrane expression of the receptor. As shown in figure 4.5, the insertion of GFF had no effect on intracellular localisation of CRH-R1d, even the insertion of GFF-VSV did not result in a transcription of membrane receptor. Only when 9 amino acids (GFFVSVFYC) were inserted was the mutant receptor expressed primarily in the plasma membrane. Further quantitative analysis of the CRH-R1 intracellular fluorescence intensity confirmed these observations (Figure 4.6.).

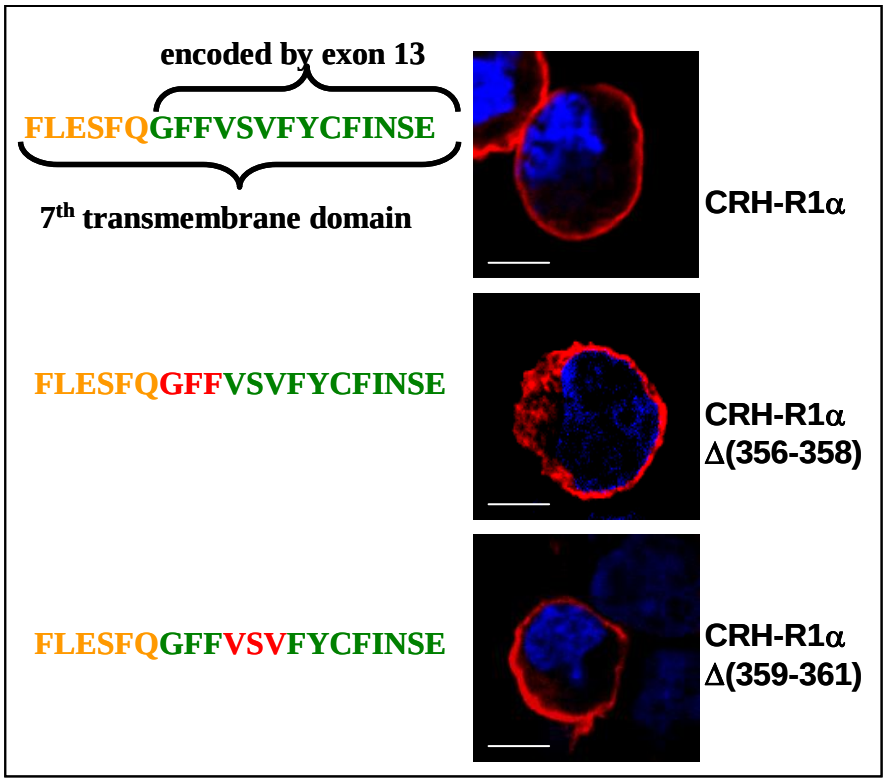

Figure 4.4. The cellular localisation of CRH-R1α wild type and mutant constructs. HEK-293 cells were transiently transfected with CRH-R1α constructs (amino acids highlighted in red were deleted from the sequence). The receptor was visualized by indirect confocal microscopy using CRH-R antibody and Alexa-Fluor®594 (red). The cell nuclei were stained with the DNA specific dye-DAPI. Scale bar is 10 μm. Identical results were obtained in three independent experiments

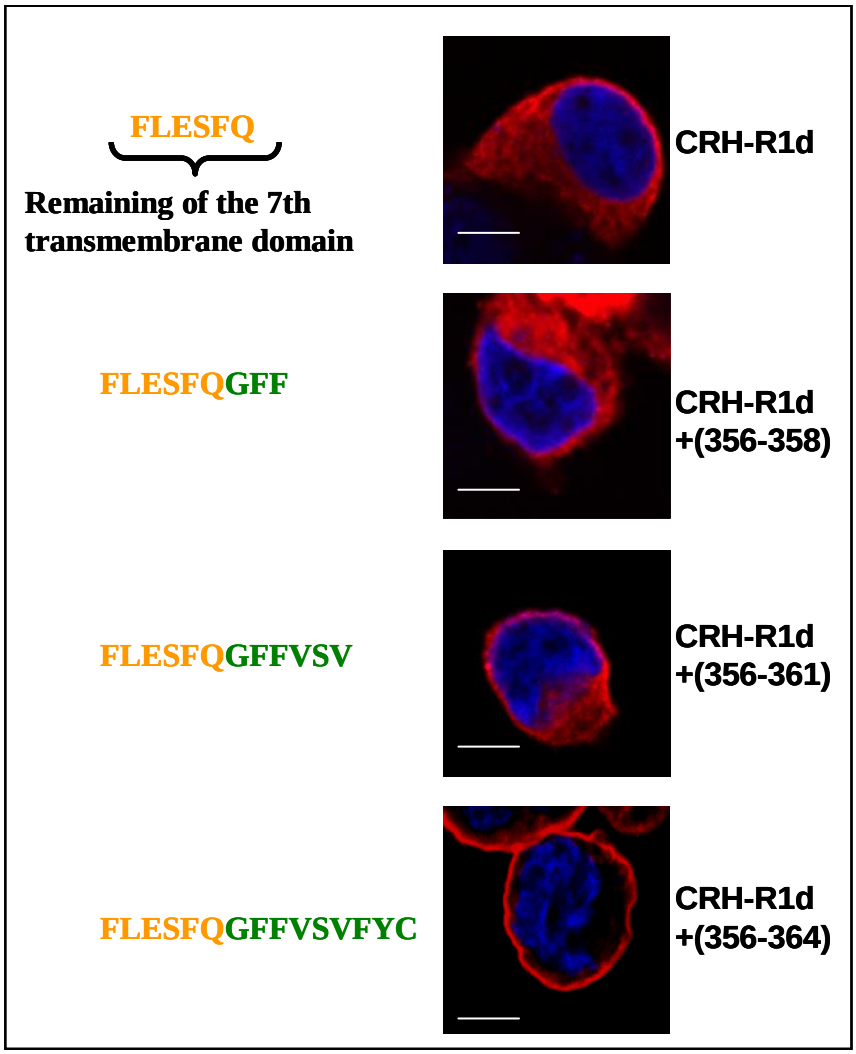

Figure 4.5. The cellular localisation of CRH-R1d wild type and mutant constructs. HEK-293 were transiently transfected with CRH-R1d constructs. The receptor was visualized by indirect confocal microscopy using CRH-R antibody and Alexa-Fluor®594 (red). The cell nuclei were stained with the DNA specific dye-DAPI. Scale bar is 10 μm. Identical results were obtained in three independent experiments

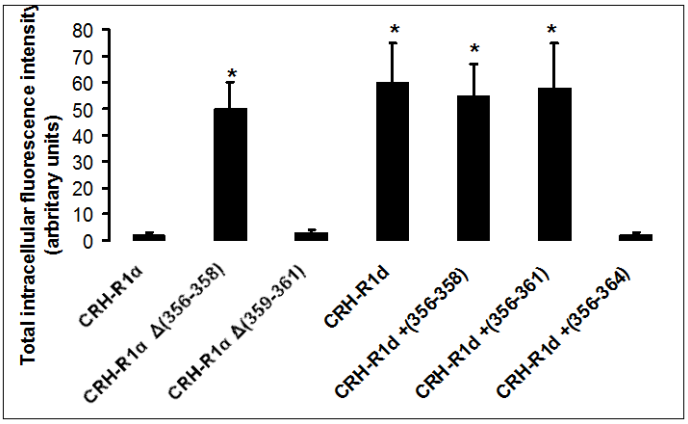

Figure 4.6. Quantitative analysis of CRH-R1 intracellular fluorescent intensity in HEK293 cells over-expressing different CRH-R1 constructs. The analysis was performed by measuring fluorescence spectra as described in the Materials and Methods. See the Table 4.1 for description of the constructs. The results are expressed as the mean ± SEM of 20-25 cells in an experiment that was representative of three independent experiments. *, $P<0.05$ compared with cells expressing CRH-R1α.

4.2.5 Co-expression of CRH-R1d and CRH-R2β in HEK293 cells

Previously it has been demonstrated that although signalling function was impaired, CRH-R1d does not act as a "decoy" receptor for CRH-R1α (Grammatopoulos DK *et al*., 1999). In order to investigate the effect of CRH-R1d on functional characteristics of CRH-R2β, both receptors were co-expressed in HEK293 cells as described in the Materials and Methods. The cellular localisation and internalization properties of CRH-R2β in the presence of CRH-R1d, as well as CRH-R2β mediated MAP kinase activation and cAMP production were investigated.

4.2.5.1 Characterisation of cellular localisation of CRH-R2β-V5, CRH-R1α-myc, and CRH-R1d-myc

In order to monitor cellular localization and internalization of two types of CRH-R in one cell, a tag to the C-terminus of the receptors was introduced. Firstly,

the effect of the receptor tagging on the cellular localisation of the receptor was examined. CRH-R1α was tagged with a V5-tag or a myc-tag, CRH-R1d was tagged with a myc-tag and CRH-R2β with a V5-tag, as controls the receptors without tags were used. HEK293 cells were transfected with different constructs and the resulting receptors were visualized by indirect confocal microscopy (Figure 4.7).

Localisation of the CRH-R1α-myc receptor (red) and CRH-R1α-V5 (green) was primarily on the plasma membrane (Figure 4.7 A and C), while CRH-R1d-myc was distributed both in the cytoplasm and plasma membrane (Figure 4.7 E). CRH-R2β-V5 (green) was expressed exclusively on the plasma membrane (Figure 4.7 G). The cellular localization of the receptors without V5 or myc tag was detected with CRH-R1/2 specific antibody (Figure 4.7 B, D, F, and H). CRH-R1α and CRH-R2β were expressed exclusively on the plasma membrane, while CRH-R1d was distributed in the cytoplasm compartments as well. This data demonstrates that the introduction of a myc-tag to the C-terminus of CRH-R1α or CRH-R1d, or a V5-tag to the C-terminus of CRH-R1α or CRH-R2β, have no effect on the cellular localisation of the receptors when expressed in HEK293 cells.

The plasmids containing CRH-R1α-V5 and CRH-R1d-myc, CRH-R2β-V5 and CRH-R1α-myc, CRH-R2β-V5 and CRH-R1d-myc, as well the same combinations of the wild type receptors (without tags) were expressed in HEK293 cells and the cellular localisation of the receptors was visualized using indirect confocal microscopy. CRH-R1α-V5 (green) and CRH-R1d-myc (red) were distinctively distributed; R1α receptor was expressed predominantly on the plasma membrane, while R1d was present only in intracellular compartments, no apparent co-localisation between the two receptors on the plasma membrane was detected (Figure 4.8 A). Immunofluorescent detection of the wild type receptors using CRH-

R1/2 antibody and Alexa-Fluor®594 revealed strong plasma membrane staining (possibly from CRH-R1α) as well as intracellular smeary and punctuate staining (possibly from CRH-R1d) (Figure 4.8 B). Co-expression of CRH-R2β-V5 (green) and CRH-R1α-myc (red) resulted in a detection of cells with yellow membrane staining indicative of potential co-localisation of the two receptors on the plasma membrane (Figure 4.8 C). The membrane expression of the two receptors was detected also in the cells co-expressing CRH-R1α and CRH-R2β wild type (without the C-terminus tag) (Figure 4.8 D).

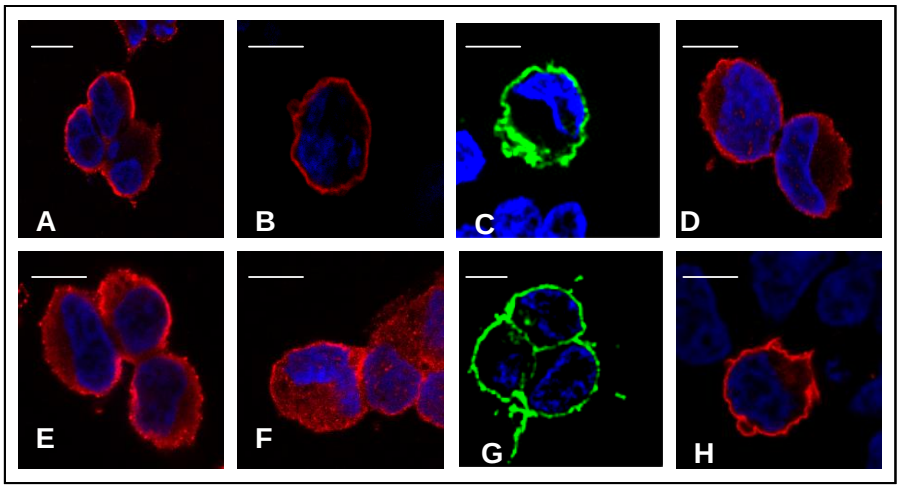

Figure 4.7. Expression of CRH-R1α-myc, CRH-R1α-V5, CRH-R1d-myc, CRH-R2β-V5 in HEK293 cells. HEK293 cells were transiently transfected with a mammalian expression vector pBudCE4.1 containing CRH-R1α-myc (A), CRH-R1α-V5 (C), CRH-R1d-myc (E), CRH-R2β-V5 (G), CRH-R1α-stop (B, D), CRH-R1d-stop (F) and CRH-R2β-stop (H). V5-tag was detected using mouse monoclonal antibody and secondary anti-mouse Alexa-Fluor®488 (green), myc-tag was detected with mouse monoclonal myc-antibody conjugated with Texas Red (red) entity. The receptors without a tag (labelled as stop) were visualized using CRH-R1/2 antibody and Alexa-Fluor®594 (red). The cell nuclei were stained with the DNA specific dye-DAPI (blue).The cells were examined using indirect confocal microscopy. Scale bar is 10 μm. Identical results were obtained from two independent transfections.

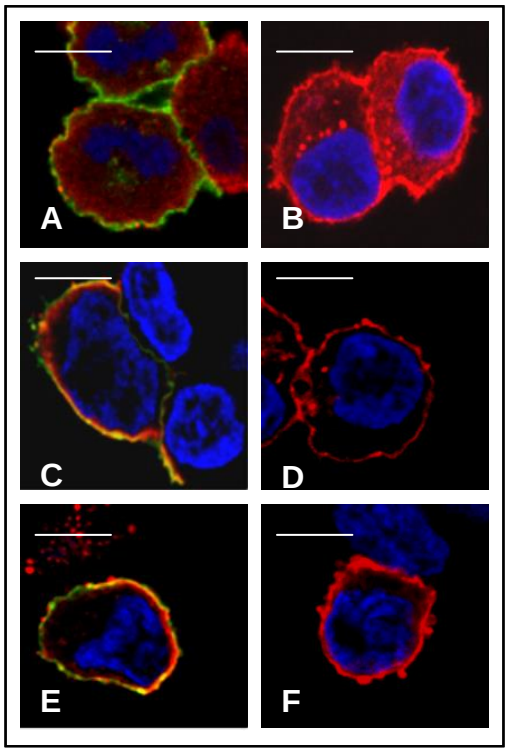

Figure 4.8. Co-expression of two types of CRH-Rs in HEK293 cells. The cells were transiently transfected with a mammalian expression vector pBudCE4.1 containing CRH-R1α-V5 and CRH-R1d-myc (A), CRH-R2β-V5 and CRH-R1α-myc (C), CRH-R2β-V5 and CRH-R1d-myc (E), CRH-R1α and CRH-R1d (B), CRH-R2β and CRH-R1α (D), CRH-R2β and CRH-R1d (F). The immunoreactivity of the receptors was detected as described in the legend of the Figure 4.7. The cells were examined using indirect confocal microscopy. Scale bar is 10 μm. Identical results were obtained from two independent transfections.

An interesting result was obtained from cells co-expressing CRH-R2β-V5 (green) and CRH-R1d-myc (red) (Figure 4.8 E). CRH-R2β-V5 was expressed on the plasma membrane; however the majority of red signal from CRH-R1d-myc came not from the cytoplasm but from the plasma membrane. A possibility that the introduction of the myc-tag to the C-tail of CRH-R1d could lead to the membrane expression of the receptor was eliminated by over-expressing CRH-R1d-myc on its own (Figure 4.7 E). However, it is possible that co-expression of the two receptors in the same cell could stabilise CRH-R1d in the plasma membrane, possibly due to

a receptor dimerisation. When CRH-R2β and CRH-R1d (wild types) were co-expressed and detected with CRH-R1/2 antibody and Alexa-Fluor®594, only membrane staining was observed (Figure 4.8 F); eliminating the possibility that the introduction of C-tail tags could affect R2β and R1d conformation leading to dimerisation of the receptors.

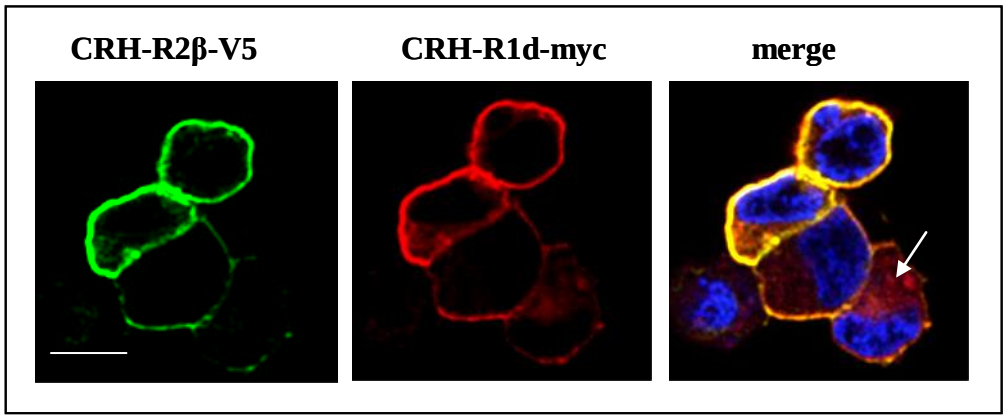

Figure 4.9. The cellular localisation pattern of CRH-R1d is dependent on the expression levels of CRH-R2β and CRH-R1d. The cells were transiently transfected with a mammalian expression vector pBudCE4.1 containing CRH-R2β-V5 and CRH-R1d-myc. V5-tag was detected using mouse monoclonal antibody and secondary anti-mouse Alexa-Fluor®488 (green), myc-tag was detected with mouse monoclonal myc-antibody conjugated with Texas Red (red) entity. A white arrow points out a cell that has a strong red intracellular signal (R1d) and weak green membrane signal (R2β). The cell nuclei were stained with a DNA specific dye-DAPI (blue). Scale bar is 10 μm. Identical images were obtained from two transfections.

Another interesting observation was that the cellular localisation of CRH-R1d-myc in a cell co-expressing CRH-R2β-V5 was dependent on levels of over-expressed receptors (Figure 4.9). A cell at the bottom of figure 4.9 (pointed by a white arrow) expresses a smaller amount of the R2β receptors than the other cells on the same image, this particular cell has a strong red (R1d) intracellular signal and weaker green (R2β) membrane signal, while the rest of the cells have both the signals on the plasma membrane.

4.2.5.2 The effect of CRH-R1d on the CRH-R2β receptor internalization properties

The internalization characteristics of CRH-R1α, CRH-R1d and CRH-R2β are investigated in detail and described in chapters 3 and 5. In this section it was determined whether over-expression of CRH-R1d has an effect on UCN-II induced internalization of CRH-R2β. In the previous chapter, it was demonstrated that CRH-R1α does not internalize when challenged with UCN-II (Figure 3.4), additionally it has been demonstrated that UCN-II does not bind to CRH-R1 (Zorrilla EP *et al*., 2004). Based on these observations it was expected that UCN-II induced effects in the R2β/R1d co-expression system would be mediated exclusively via the CRH-R2β receptor. In Figure 4.10, a time course of CRH-R2β internalization is shown. As previously demonstrated CRH-R2β-V5 was expressed in the plasma membrane; 5 minutes treatment with 100nM UCN-II did not cause any significant internalization. However, after 15 minutes of UCN-II or CRH treatment, punctuate staining was detected in the cytoplasm as an indication of significant receptor internalization. The amount of internalized receptor following CRH challenge was significantly less than following UCN-II treatment. 30 minutes after UCN-II treatment, the majority of CRH-R2β was located in the cytoplasm, and only partial staining was detected in the plasma membrane (Figure 4.10).

A short, 5 minutes, treatment with 100nM UCN-II did not induce internalization of CRH-R2β-V5 (Figure 4.10); however, introduction of CRH-R1d accelerated UCN-II induced CRH-R2β internalization (Figure 4.11). Interestingly, both receptors were internalized after 5min of UCN-II treatment, as shown by the punctuate pattern of green and red fluorescence in the cytoplasm. Additionally,

substantial levels of co-localisation between CRH-R2β and CRH-R1d were detected in the cytoplasm following UCN-II and CRH treatments (Figure 4.11).

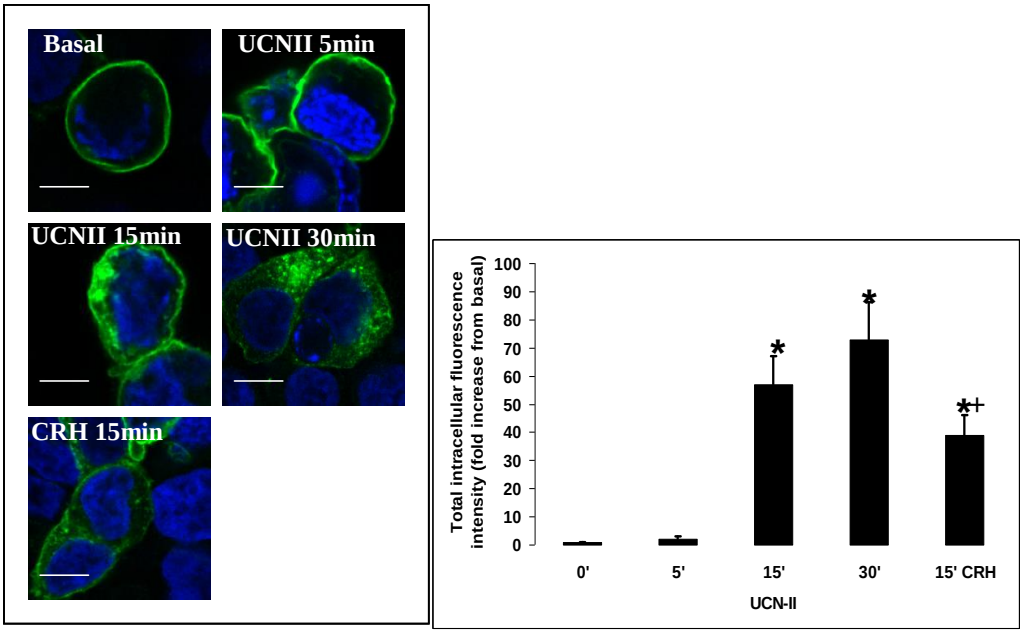

Figure 4.10. Cellular distribution of CRH-R2β-V5 in HEK293 cells: agonist time course. HEK293 cells were transiently transfected with a mammalian expression vector pBudCE4.1 containing CRH-R2β-V5 alone. The cells were treated with 100nM UCN-II for various times (0-30min) and with 100nM CRH for 15min. V5-tag was detected using mouse monoclonal antibody and secondary anti-mouse Alexa-Fluor®488 (green), The cell nuclei were stained with a DNA specific dye-DAPI (blue). Scale bar is 10 μm. Identical images were obtained from three independent transfection experiments. The quantitative analysis was performed as described in the Materials and Methods. The results are presented as the mean ± SEM of the CRH-R2 intracellular fluorescent intensities of 20-25 cells in an experiment that was representative of three independent experiments. *, $P<0.05$ compared with not treated cells; +, $P<0.05$ compared with cells treated with UCN-II for 15 min.

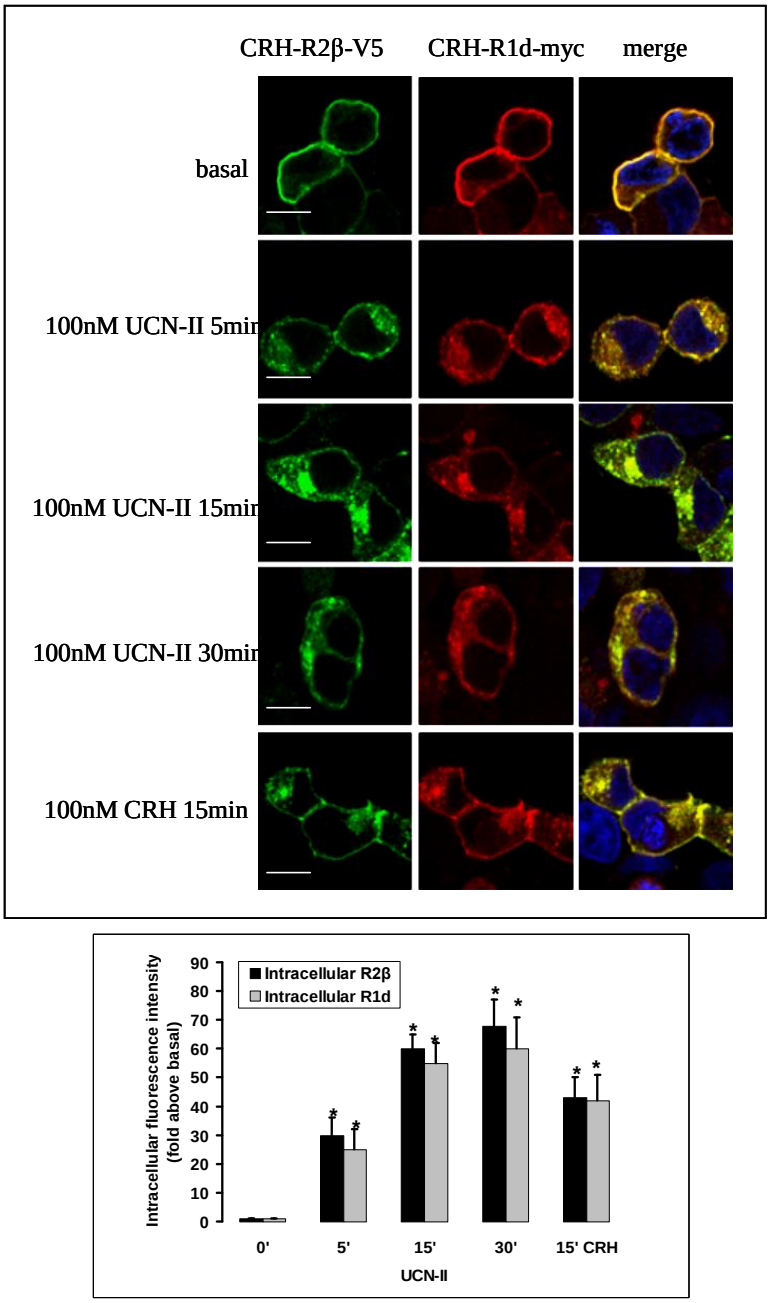

Figure 4.11. Internalization characteristics of CRH-R2β-V5 co-expressed with CRH-R1d-myc in HEK293 cells: time course. HEK293 cells were transiently transfected with a mammalian expression vector pBudCE4.1 containing CRH-R2β-V5 and CRH-R1d-myc. The cells were treated with agonists as described in Figure 4.10, and the receptors were visualized as described in Figure 4.9. Identical results were obtained from three independent transfection experiments. Quantitative analysis was performed as described in the Materials and Methods. The results are expressed as the mean ± SEM of the CRH-R intracellular fluorescence intensities of 20-25 cells in an experiment that was representative of three independent experiments. *, $P<0.05$ compared with non-treated cells.

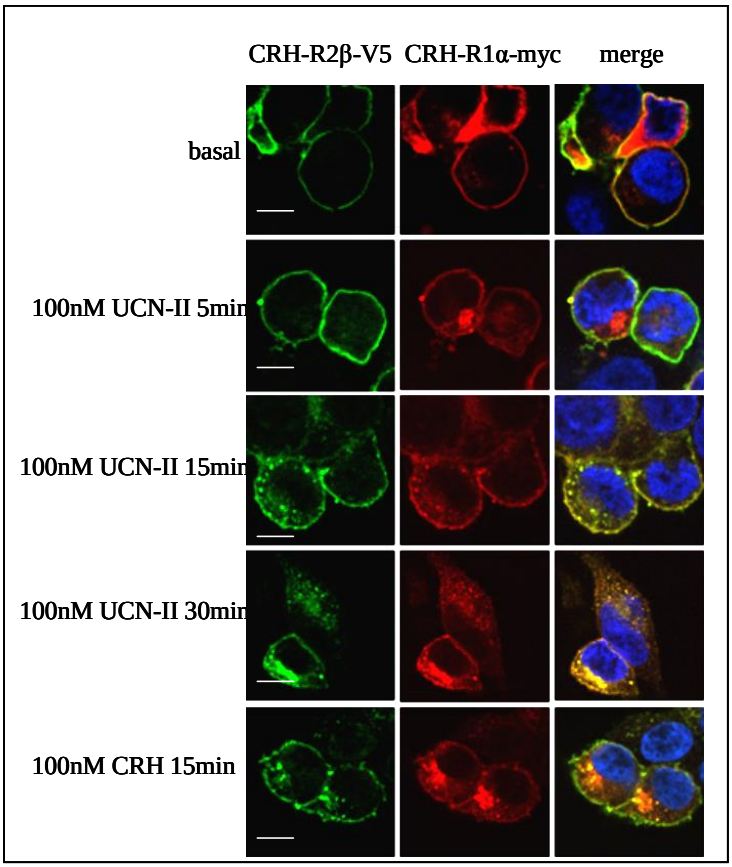

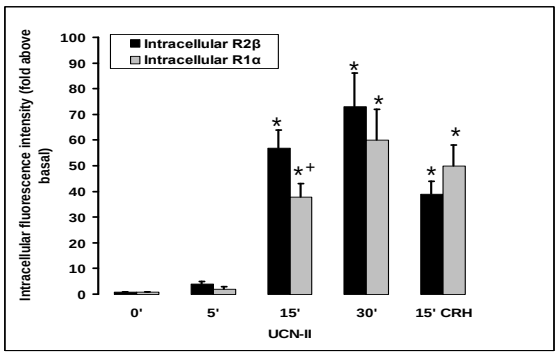

Figure 4.12. Internalization characteristics of CRH-R2β-V5 co-expressed with CRH-R1α-myc in HEK293 cells: time course. HEK293 cells were transiently transfected with a mammalian expression vector pBudCE4.1 containing CRH-R2β-V5 and CRH-R1α-myc. The cells were treated with agonists as described in Figure 4.10, and the receptors were visualized as described in Figure 4.9. Identical results were obtained from three independent transfection experiments. Quantitative analysis was performed as described in the Materials and Methods. The results are expressed as the mean ± SEM of the CRH-R intracellular fluorescence intensities of 20-25 cells in an experiment that was representative of three independent experiments. *, $P<0.05$ compared with non-treated cells; +, $P<0.05$ compared to CRH-R2β after the same treatment.

To demonstrate that the enhanced rate of CRH-R2β internalization, in the presence of CRH-R1d, was not due to non-specific events such as an increased number of receptors on the membrane or non-specific interaction between receptors, CRH-R2β-V5 was co-expressed with CRH-R1α-myc. The same internalization experiment was performed and the results shown on figure 4.12 demonstrate that 5 minutes UCN-II treatment dose not lead to redistribution of CRH-R2β-V5 immunoreactivity from the plasma membrane to cytosol, suggesting that accelerated internalization rate of CRH-R2β in the presence of CRH-R1d is likely to be due to the potential interactions between the two receptors.

4.2.5.3 The effect of CRH-R1d on CRH-R2β-mediated cAMP production

The functional characteristics of the CRH-R2β receptor such as cAMP production and MAP kinase activation were investigated in detail in the following chapter, where it was demonstrated that the treatment of HEK293 stably expressing CRH-R2β with various concentrations of CRH, UCN-I or UCN-II (1-100nM) for 15 minutes results in a dose-dependent increase of intracellular cAMP production. In this part of the study, HEK293 cells were transiently transfected with a mammalian expression vector pBudCE4.1 containing CRH-R2β and CRH-R1d or CRH-R2β and CRH-R1α, and each of the receptor cDNA separately. The cells were stimulated with 100nM UCN-II for 15minutes and cAMP levels were determined using a commercially available ELISA.

The cells over-expressing CRH-R1α or CRH-R1d did not show any significant production of cAMP following UCN-II treatment. The cells over-

expressing CRH-R2β showed a 3.42±0.44 fold increase in cAMP levels compared to non-stimulated cells. The cells co-expressing CRH-R2β and CRH-R1α produced 3.11±0.25 fold more cAMP than non-stimulated cells; suggesting that CRH-R1α has no effect on CRH-R2β mediated cAMP production. Interestingly, cells co-expressing CRH-R2β and CRH-R1d had only 2.03±0.05 times more cAMP than non-stimulated cells; which is 40% less than in cells expressing CRH-R2β only or co-expressing CRH-R2β and CRH-R1α (Figure 4.13).

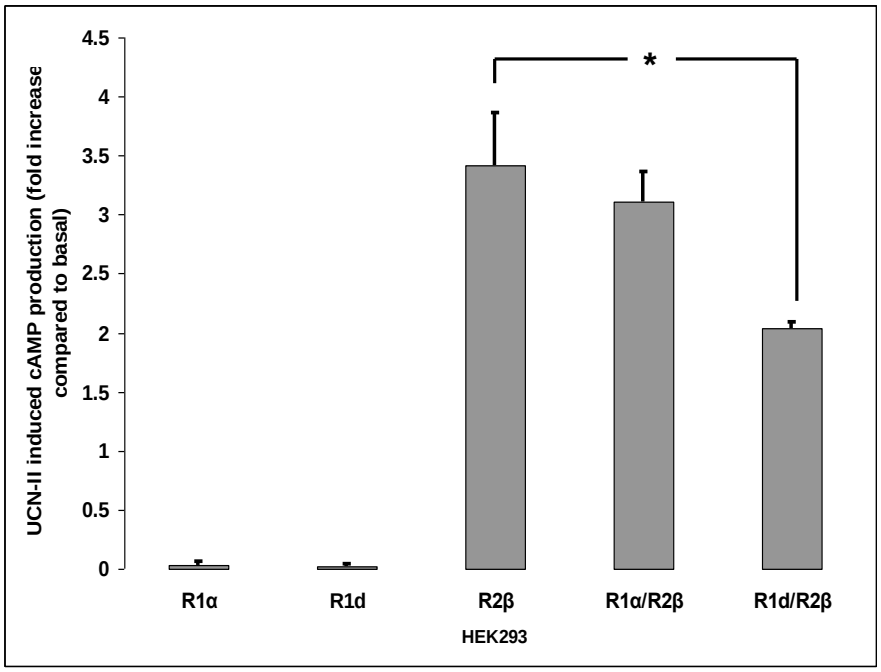

Figure 4.13. CRH-R2β mediated cAMP production. HEK293 cells transiently transfected with CRH-Rs, were stimulated with 100nM UCN-II for 15min and cAMP production was measured as described in the Materials and Methods. The results are normalised for forskolin-induced cAMP production and expressed as a fold increase above basal (not treated), when basal was set to be 1. The results are presented as the mean ± SEM of 3 replicates from two independent experiments. *, $P<0.05$ compared with cAMP production in cell over-expressing only CRH-R2β.

4.2.5.4 The effect of CRH-R1d on CRH-R2β-mediate MAP kinase activation

HEK293 cells were transiently transfected with a mammalian expression vector pBudCE4.1 containing CRH-R2β and CRH-R1d or CRH-R2β and CRH-R1α, and each of receptor cDNA separately. The cells were stimulated with 100nM UCN-II for 5minutes and total cellular proteins were collected. ERK1/2 and p38 MAPK phosphorylation was determined using western blot analysis. The cells over-expressing CRH-R1α or CRH-R1d did not show significant ERK1/2 nor p38 MAPK activation following UCN-II treatment. The cells over-expressing CRH-R2β showed 2.5 and 1.5 fold increase in ERK1/2 and p38 MAPK phosphorylation, respectively, compared to non-stimulated cells. The identical MAPK phosphorylation levels were detected in cells co-expressing CRH-R2β and CRH-R1α; suggesting that CRH-R1α does not have an effect on CRH-R2β mediated MAPK activation. Interestingly, ERK1/2 phosphorylation was only 1.5 fold above basal in UCN-II stimulated cells co-expressing CRH-R2β and CRH-R1d, while p38 MAPK phosphorylation was completely eliminated (Figure 4.14).

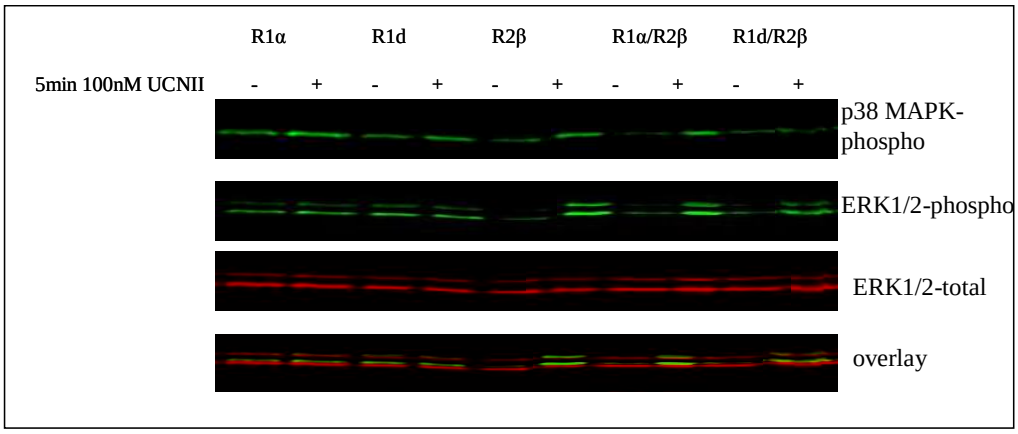

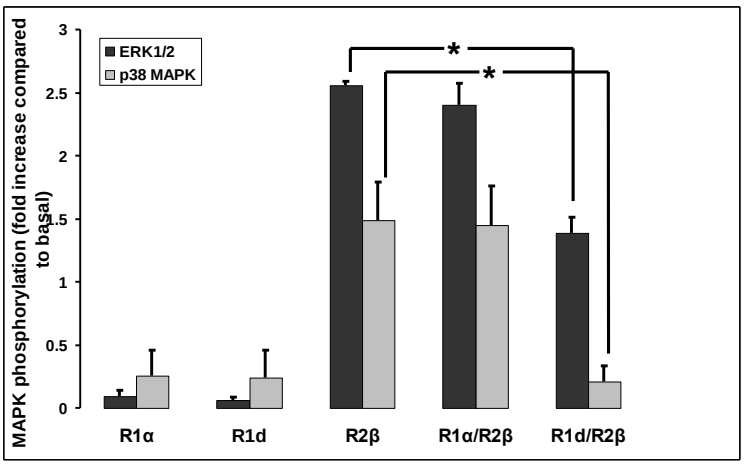

Figure 4.14. The effect of CRH-R1d on CRH-R2β mediated MAPK activation. HEK293 cells transiently transfected with CRH-Rs, were stimulated with 100nM UCN-II for 5min and total cellular proteins were assayed for ERK1/2 and p38 MAPK phosphorylation. The stimulations were performed in duplicates and the identical results were obtained from two independent transfections. All the results were normalised with total ERK1/2 and expressed as a fold increase above basal (not treated cells). The results are presented as the mean ± SEM. *, $P<0.05$ compared with the MAP kinase phosphorylation in cell over-expressing only CRH-R2β.

4.3 DISCUSSION

CRH actions are dependent on the adequate expression of CRH-R in the plasma membrane. The existence of multiple splice variants of CRH-R1 with impaired signalling characteristics raises a question as to whether the resulting

proteins demonstrate plasma membrane expression or not. It was demonstrated, in Chapter 3, that CRH-R1β is expressed in the plasma membrane, while CRH-R1d is predominantly expressed in intracellular compartments, with a small portion of receptor present on the cell surface, suggesting that the deletion of 14 amino acids from the C-terminus of the 7th TMD leads to reduced ability of the protein to integrate into the plasma membrane lipid phase. Another possibility, as mentioned in the previous chapter, is that CRH-R1d does not leave the ER following protein synthesis and maturation, suggesting that the intact C-terminus could be essential for the receptor trafficking to the plasma membrane.

The exon encoding the C-terminal 14 amino acids of the 7th TMD is highly conserved in Class B GPCR genes. The splice variants with the deletion of this exon, beside the CRH-R1d receptor (Grammatopoulos DK *et al*., 1999) were described for the calcitonin receptor (Shyu J-F *et al*., 1996), the PTH/PTHrP receptor (Ding C *et al*., 1995) and the vasoactive intestinal peptide receptor (Grinninger C *et al*., 2004). The Kyte-Dolittle hydrophobicity analysis of CRH-R1α and CRH-R1d amino acid sequence has demonstrated that the deletion of 14 amino acids from the distal part of the 7th TMD reduces the hydrophobicity of the residual sequence that follows the third extracellular loop (Grammatopoulos DK *et al*., 1999). As a consequence, this might reduce ability of the 7th TMD to anchor in the lipid bilayer of the plasma membrane, leading to a 6-TMD receptor with an extracellular C-terminus, as has been reported for the calcitonin splice variant CTRΔe13 (Seck T *et al*., 2005). The likelihood that CRH-R1d has the same structural characteristics as CTRΔe13 receptor was assessed by indirect confocal microscopy using CRH-R specific antibody raised against the C-tail of the receptor. The experimental approach employed was based on the hypothesis that if the C-

terminus of CRH-R1d is in the extracellular space, even in non-permeabilised over-expressing cells, the antibody would bind to the receptor resulting in detectable immunoreactivity on the cell surface. Seck *et al* (Seck T *et al*., 2005) used different experimental techniques to investigate the orientation of Δe13 C-terminus. Using an NMR analysis they demonstrated that the absence of the sequence encoding exon 13 leads to the loss of a functional 7th TMD and therefore an extracellular C-terminus of the CTRΔe13 variant. The extracellular orientation of the C-terminus was confirmed using FACS (fluorescence-activated cell sorter) analysis.

After establishing that the fraction of plasma membrane CRH-R1d has the extracellular orientation of the C-terminus, these studies focused on identifying the sets of amino acids encoded by exon 13 that were essential for the plasma membrane expression of the receptor. A series of CRH-R1α and CRH-R1d mutant constructs were generated and the cellular localisation of the receptors was investigated by using indirect confocal microscopy (Table 4.1). The mutagenesis study revealed that the GFF cassette (Gly356-Phe357-Phe-358) within the 7th TMD of CRH-R1α was required for a stable receptor expression in the plasma membrane. The protein structure prediction algorithms (PELE) available at http://workbench.sdsc.edu were used to investigate whether the GFF cassette is involved in the start of certain secondary protein structures such as the α-helix, β-sheets or turns (Figure 4.15). Most algorithms predict that the GFF cassette or at least one of amino acids in the cassette could be the start of the β-sheet following either α-helix or coil structure. It is tempting to speculate that the deletion of the GFF cassette as in the CRH-R1α Δ(356-358) mutant receptor, prevents the formation of the β-sheet, leading to the misfolding of the rest of the receptor. However, the cell surface expression of CRH-R1d is not rescued by the insertion of

the same cassette into the CRH-R1d protein sequence. Addition of 9 amino acids (GFFVSVFYC) to the CRH-R1d protein sequence resulted in the expression of the receptor within the plasma membrane. In future studies, it would be advisable to perform an NMR analysis of the mutant CRH-R1α and CRH-R1d receptors, and determine the effects of deletion and insertion on topological orientation of receptor domains. Since a detailed structural analysis was not a topic of this project, the attention was focused on the functional interactions between CRH-R1d and CRH-R2β.

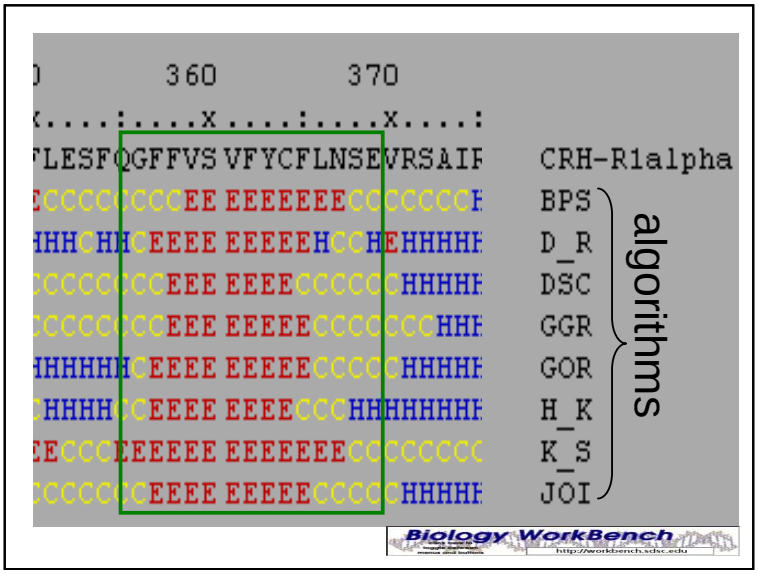

Figure 4.15. Secondary structure prediction. The algorithms available at the Biology Workbench web site were used to analyse amino acid sequence of CRH-R1α for the formation of secondary structures. Amino acid sequence encoded by exon 13 is highlighted by the green rectangle; C-random coil, H-α helix, E-β sheet.

Previous studies on the CRH-R1d variant have indicated that an intact 7th TMD is not required for efficient receptor-ligand interaction, but it is crucial for adequate signal transduction (Grammatopoulos DK *et al.*, 1999). In comparison to CRH-R1α, the activated CRH-R1d was less efficient in mediating cAMP production, and failed to induce IP_3 production, these were attributed to reduced coupling to G-proteins of the latter (Grammatopoulos DK *et al.*,1999). The

calcitonin Δe13 receptor demonstrated similar signalling impairment (Shyu J-F *et al*., 1996). However, while CTRΔe13 exhibited a dominant negative effect on receptor surface expression and signalling (Seck T *et al*., 2005), the CRH-R1d variant did not act as a dominant negative receptor when co-expressed with CRH-R1α (Grammatopoulos DK *et al.,* 1999). However, a possible link between two distinct types of the CRH receptors has not been investigated until now. The experiments presented in this chapter have provided novel evidence that CRH-R1d can heterologously modulate CRH-R2 functional characteristics; when co-expressed with CRH-R1d, CRH-R2β's signalling abilities are impaired.

The CRH-R2β receptor is primarily a Gs-protein coupled receptor, of which activation leads to cAMP production and activation of PKA; additionally, various studies have demonstrated that this receptor couples to multiple G-proteins (Gq, Gi and Go) activating diverse kinases (PI3-K, MAPK kinase 1, Raf-1 kinase) (Grammatopoulos DK *et al.*,2000; Brar BK *et al*., 2004). In view of recent studies implicating peripheral CRH-R2 in the control of energy balance and homeostasis (Li C *et* al., 2003; Chen A *et al*., 2006), it is of pivotal importance to establish a potential link between the two types of CRH receptors. There is only one study investigating the effects of co-expression on the signalling characteristics of CRH-R1 and R2 (Maya-Nunez G *et al*., 2005). This study reports that co-expression of CRH-R1α and CRH-R2α leads to reduced CRH induced cAMP production. Additionally, the study finds that the co-expression of the two receptors does not affect ligand binding nor internalization properties of the receptors. In my study, co-expression of CRH-R1α and CRH-R2β did not lead to impaired UCN-II induced cAMP production, MAPK activation nor internalization kinetics. The different results regarding cAMP production between these two studies can be attributed to

different agonists. In my study, UCN-II was purposely used because it only binds and activates CRH-R2, so any effect on signal transduction that might have been detected when co-expressing the two receptors was not due to activation of the type 1 receptor, but solely due to activation of CRH-R2 and possible physical interaction between the two receptors. Another reason for the discrepant result could be that co-transfection was performed differently, although the same cellular system, HEK293 cells, in my study, the pBudCE4.1 plasmid which was designed for the independent but equal expression of two genes within the same mammalian cell was used. However, Maya-Nunez *et al* used two pcDNA3.1 plasmids for the co-transfection. These experimental conditions do not guarantee that each transfected cell would up take both plasmids. It is very likely that the use of pcDNA3.1 for this kind of transfection would lead to the creation of a mixed population of cells in which some of the cells express only one type of receptor.

Given that in this study it was found that co-expression of CRH-R1α and CRH-R2β has no effect on UCN-II induced cAMP production, MAPK activation nor internalization of CRH-R2β, this co-expression system was used as a control to study the potential effects of CRH-R1d on CRH-R2β functional characteristics.

Co-expression of CRH-R1d did not affect CRH-R2β membrane expression. However, an interesting phenomenon was observed: when the two receptors were expressed in a high number of copies in the same cell, a significant portion of CRH-R1d was present in the plasma membrane; but in cells with lower levels of receptor expression, CRH-R2β was expressed only in the plasma membrane and CRH-R1d was detected primarily in the cytoplasm. It is possible that CRH-R1d and R2β form a physical contact through dimerisation, which leads to the stabilisation of CRH-R1d in the plasma membrane. To draw a concrete conclusion about these data

detailed biochemical experiments (co-immunoprecipitation and fluorescence resonance energy transfer analysis) on cells stably expressing the two types of receptors would be required. These experiments could be a topic of a future study.

The internalization studies revealed that the presence of CRH-R1d enhances UCN-II induced CRH-R2β internalization, and that both types of receptors are co-localised in the cytoplasm. It is tempting to speculate that formation of dimers is responsible for this effect. Increasing evidence suggests that GPCRs are more common as dimmers than monomers, and that heterodimerization can modify receptor trafficking and signalling compared to the individual homodimers (Gomes JI *et* al., 2001). Along these lines is evidence that the CTRΔe13 receptor forms a heterodimer with the wild type calcitonin receptor, leading to the retention of the wild type receptor in intracellular compartments (Seck T *et al*., 2003). Up to date, there are only two reports describing dimerization of CRH-R1 (Kraetke O *et al*., 2005; Young *et al*., 2007). Functional cooperativity between the effects of CRH and AVP in the pituitary suggests that CRH-R1 and vasopressin V1b receptor (V1b-R) form a physical interaction (Young *et al*., 2007). Using BRET and co-immunoprecipitation techniques, Young et al (2007) reported that V1b-R and CRH-R1formed homo- and heterodimers and this interaction did not affect the binding abilities of the receptors.

Second messenger studies and MAPK activation assays have shown that the co-expression of CRH-R1d and CRH-R2β attenuated UCN-II induced cAMP as well as ERK1/2 and p38 MAPK phosphorylation. The impaired signal transduction could be due to the rapid endocytosis rate of CRH-R2β in the co-expression system. Detailed time course studies should be able to provide more conclusive evidence for this speculation.

This part of the project has provided evidence that the co-expression of CRH-R1d does have an effect on UCN-II induced CRH-R2β activation. This is of potential importance in understanding how the action of urocortins via activation of CRH-R2 are controlled in peripheral tissues, such as skin, muscle and adipose tissue, that express both types of receptors.

5 SIGNALLING AND INTERNALIZATION CHARACTERISTICS OF CRH-R2β RECEPTOR

5.1 INTRODUCTION

Corticotropin-releasing hormone (CRH), urocortin–I (UCN-I), urocortin–II (UCN-II and urocortin-III (UCN-III) are members of the CRH-like family of peptides that play various roles in mammalian development and physiology, especially in the adaptation to stressful stimuli (Bale TL & Vale WW, 2004). Two classes of CRH receptors, termed R1 and R2, mediate the diverse actions of CRH and UCNs in the brain, pituitary and peripheral tissues (Hillhouse EW & Grammatopoulos DK, 2006).

Mammals express three known CRH-R2 variants: R2α and R2β expressed both centrally and peripherally and R2γ which has so far been found only in the limbic regions of the human CNS (Hillhouse EW & Grammatopoulos DK, 2006). These variants have identical transmembrane and C-terminal domains and only differ in their N-terminal extracellular domains. Pharmacological characterization of the CRH-R2 has shown that this seven TMD G-protein coupled receptor (GPCR) preferentially binds UCNs rather than CRH (Lewis K *et al*., 2001). CRH-R2 activation is important in mediating UCNs' diverse physiological actions including anxiolytic and feeding reduction effects in the brain as well as cardioprotection,

tissue angiogenesis and gastrointestinal regulatory effects at the periphery (Bale TL *et al*., 2000; Bale TL *et al*., 2002; Carlin KM *et al*., 2006; Lawrence KM & Latchman DS, 2006). Recent findings showing involvement of UCNs in the control of glucose utilization and insulin sensitivity in skeletal muscle as well as stimulation of insulin and glucagon secretion in pancreatic β-cells, implicate CRH-R2 in the control of energy balance and homeostasis (Li C *et al*., 2003; Chen A *et al*., 2006).

The CRH-R2, similar to the CRH-R1 receptor, is primarily a Gsα/adenylyl cyclase/cAMP-coupled GPCR (Hoare SR *et al*., 2005). In addition, two members of the family of mitogen-activated protein kinases (MAPK), extracellular signal regulated kinase (ERK1/2) and p38 MAPK, have also been implicated as key signalling proteins downstream of CRH-R2 activation (Dermitzaki E *et al*., 2002; Sananbenesi F *et al*., 2003; Brar BK *et al*., 2004; Karteris E *et al*., 2004). Various studies (Grammatopoulos D *et al*., 2000; Brar BK *et al*., 2004) demonstrated the involvement of multiple G-proteins (Gq-, Gi- and Go-) and a number of signalling molecules including PI3-K, MAPK kinase 1, phospholipase C and Raf-1 kinase in the CRH-R2-ERK1/2 interaction.

At present, there is little information about the intracellular mechanisms regulating CRH-R2 signalling efficiency. A characteristic feature of most GPCRs function is their ability to adjust their biological activity in response to prolonged agonist stimulation. This is achieved through a series of fine tuned signalling events involving receptor phosphorylation by protein kinases, β-arrestin recruitment to the plasma membrane and association with the receptor that leads to GPCR signalling desensitization and uncoupling from G-proteins; this is followed by receptor endocytosis, sometimes via a clathrin/dynamin-mediated process (Claing A *et al*., 2002). Interestingly, for many GPCRs this mechanism also appears to be essential

for activation of the ERK1/2 signalling pathway in a G-protein independent manner (Lefkowitz RJ & Shenoy SK, 2005).

Previous studies addressing CRH-R1 signalling properties (Perry JS *et al*., 2005; Teli T *et al*., 2005; Markovic D *et al*., 2006) demonstrated that the CRH-R1 is sensitive to β-arrestin-dependent signalling desensitization and internalization. Receptor internalization is also one of the mechanisms employed by CRH-R1 to induce ERK1/2 and p38 MAPK phosphorylation and activation (Punn A *et al*., 2006).

In this part of my project, the aim was to determine the signalling and internalization characteristics of CRH-R2β and explore the possible link between the CRH-R2 internalization and MAPK activation. Also, some of the spatio-temporal characteristics of MAPK activation were analysed, and potential receptor structural domains that are involved in this process were investigated. The model system was recombinant human CRH-R2β stably expressed in HEK293 cells.

5.2 RESULTS

5.2.1 Characterisation of st.293-R2β cells

Following two months of selective growth in media containing 500μg/ml G418, 49 clones survived. The clones were tested for receptor expression and functional activity. Firstly, the clones were screened for receptor expression at the plasma membrane using CRH-R specific antibody and indirect confocal microscopy (Figure 5.1). Weak immunoreactivity was detected in HEK293 cells; some clones such as 1 and 4 had an even receptor distribution on the plasma membrane; on the other hand not all of the cells originated from clones 15 and 46 over-expressed

CRH-R2β. Clones 9, 10, 17, 19, 25, 36, and 45 expressed the receptor on the plasma membrane. However, it was noted that the proliferation of clone 10 was faster whilst clone 36 was proliferated more slowly than the other clones.

Further analysis of mRNA and protein levels of CRH-R2β by RT-PCR (Figure 5.2) and western blot (Figure 5.3), demonstrated that clone 10 had a weaker mRNA and protein expression than the other clones. Additionally, clone 36 did not express significant levels of CRH-R2β mRNA and proteins. Clones 9, 17, 19, 25 and 45 expressed substantial mRNA and protein levels of CRH-R2β.

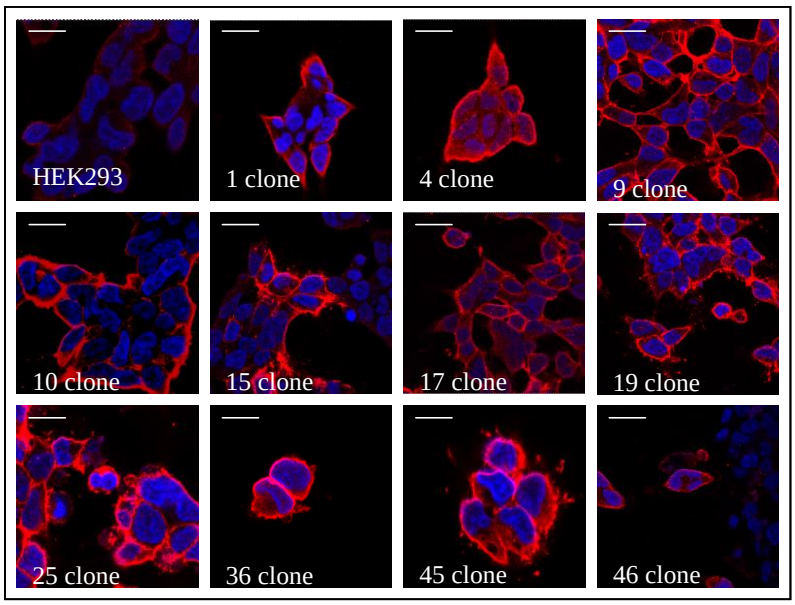

Figure 5.1. Characterisation of CRH-R2β cellular expression in HEK293 stably expressing the receptor by indirect confocal microscopy. The clones that survived in selective media containing 500 μg/ml G418, were grown on cover slips and the expression of CRH-R2β was monitored by indirect confocal microscopy using CRH-R1/2 specific antibody and Alexa-Fluor®594 secondary antibody. Cell nuclei were visualized using the DNA specific dye-DAPI. Scale bar is 20 μm.

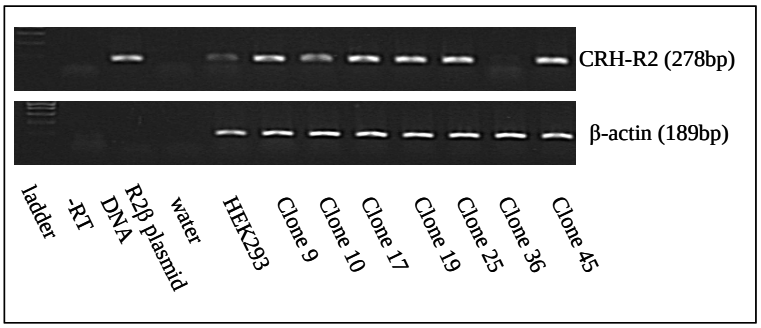

Figure 5.2. Characterisation of mRNA CRH-R2β expression in HEK293 stably expressing the receptor by RT-PCR. RNA and cDNA was made from the seven clones having membrane expression of the receptor. PCR using CRH-R2β specific primers was performed, β-actin was used as an internal control demonstrating the good quality of cDNA. Two negative controls were used: to confirm that there was no contamination with genomic DNA in the RNA prep, in the –RT control, reverse transcriptase was omitted when RNA was converted to the cDNA; to confirm that the PCR chemicals are "clean" of contaminants, water was placed instead of cDNA in the PCR reaction in the water control. Identical results were obtained in two independent experiments

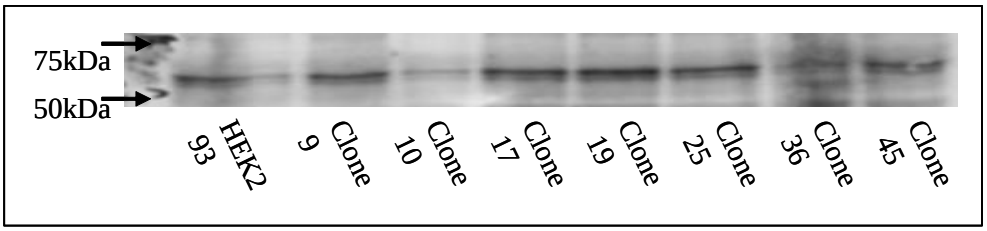

Figure 5.3. Characterisation of protein CRH-R2β expression in HEK293 stably expressing the receptor by western blot analysis. Total cellular proteins from the seven clones were made and subjected to separation by SDS-PAGE and electrotransfer. The protein expression of the receptor was detected by CRH-R specific antibody. A representative blot from three independent experiments is shown.

The functionality of the over-expressed receptor in the six clones was assessed by investigating cAMP production and ERK1/2 MAP activation. The clone 25 was lost due to a fungal infection.

In order to demonstrate that the over-expression of CRH-R2β does not affect the adenylyl cyclase activity, the plasma membrane components were by-passed by use of forskolin, an adenylyl cyclase activator. The forskolin induced cAMP production among all of the clones and wild type HEK293 was comparable, 58-65 fold above basal (Figure 5.4 A). This demonstrated that the clones retained the functional adenylyl cyclase system.

Since CRH-R2 is primarily coupled to the Gsα/adenylyl cyclase/cAMP system, it was of pivotal importance to demonstrate that the generated clones were indeed able to produce cAMP following UCN-II treatments. Treatment of the cells with 1-100 nM UCN-II (Figure 5.4B) showed that the endogenous levels of CRH-R2 in HEK293 were not sufficient to induce a marked cAMP production. In addition, clones 10 and 35 failed to produce cAMP following UCN-II treatments; which is not surprising since the PCR and western blot analysis fail to detect substantial levels of mRNA and protein expression of CRH-R2β in those clones. Clone 17, although able to produce high levels of cAMP following UCN-II stimulation, failed to demonstrate the agonist dose dependent cAMP production. It is possible that because of a high number of the receptor molecules in the plasma membrane, the plateau of cAMP production was reached. To investigate if this was the case, binding studies determining the number of receptors on the membrane were needed. However, since that would side track the project, this clone was eliminated from the study. Moreover, other clones such as 9, 19 and 45 showed UCN-II dose dependent cAMP production. Clone 45 had a 30% reduced ability of UCN-II induced cAMP production than the other two clones (9 and 19).

Another major pathway activated by UCN-II, downstream of CRH-R2β, is the mitogen activated protein kinase (MAPK) signalling cascade. To assess the ability of the selected clone in an activation of this cascade, the cells were treated with 10 and 100 nM UCN-II for 5 min, total cellular proteins were made and ERK1/2 phosphorylation was determined as described in the methods (Figure 5.5).

Stimulation of clone 36 and the wild type HEK293 cells with UCN-II did not led to significant ERK1/2 activation; UCN-II induced ERK1/2 activation in clone 10 was not dose dependent as well as in clone 45. Clone 17 demonstrated the highest ERK1/2 activation following the UCN-II stimulation, however because of lack of a dose-dependent cAMP production pattern this clone was eliminated from the further studies. Clones 9 and 19 were equally potent in mediating UCN-II induced ERK1/2 phosphorylation.

As clones possessing the best qualities regarding the plasma membrane receptor expression and functional characteristics, cAMP production and ERK1/2 phosphorylation, clones 9 and 19 were chosen to be used in further studies. The majority of experiments were performed using clone 9 (st.293-R2β).

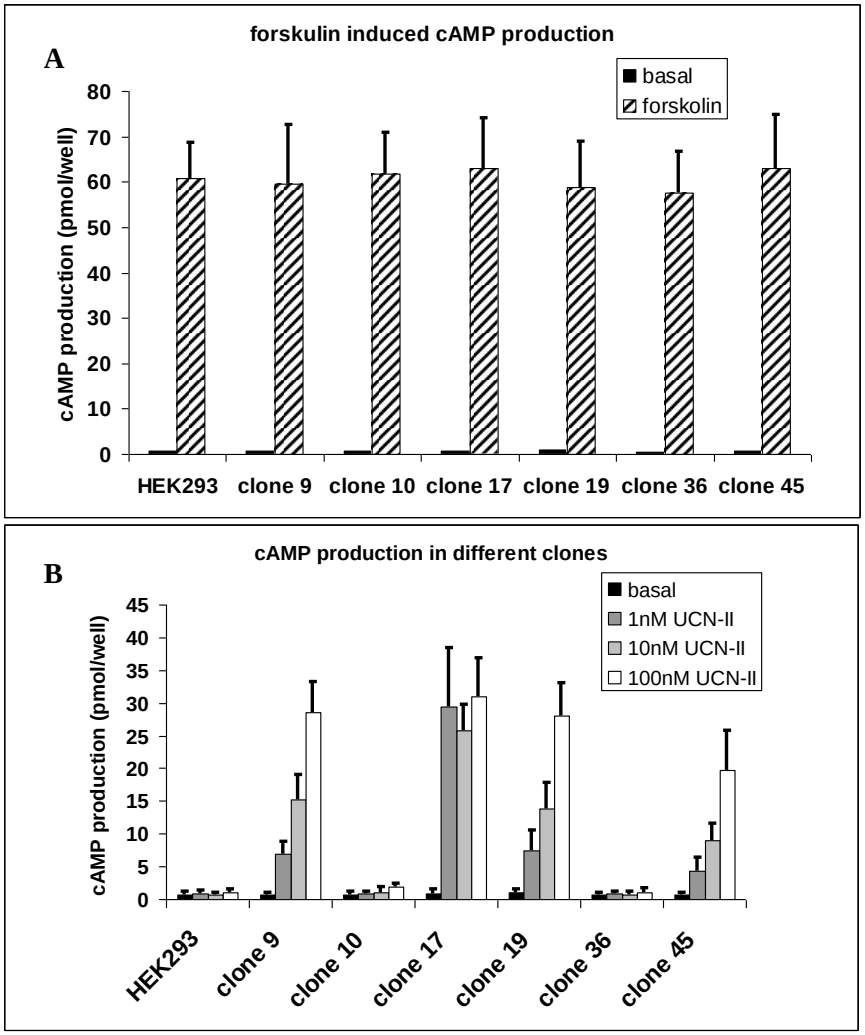

Figure 5.4. cAMP production in HEK293 and CRH-R2β clones. (A).1μM forskolin for 15 min was used to assess the intactness of the adenylyl cyclase system in the cells. (B) the cells were treated for 15 min with 1-100 nM UCN-II. cAMP levels were determined as described in the Materials and Methods. The results are presented as pmol of cAMP per well and represent the means ± SEM of two independent experiments.

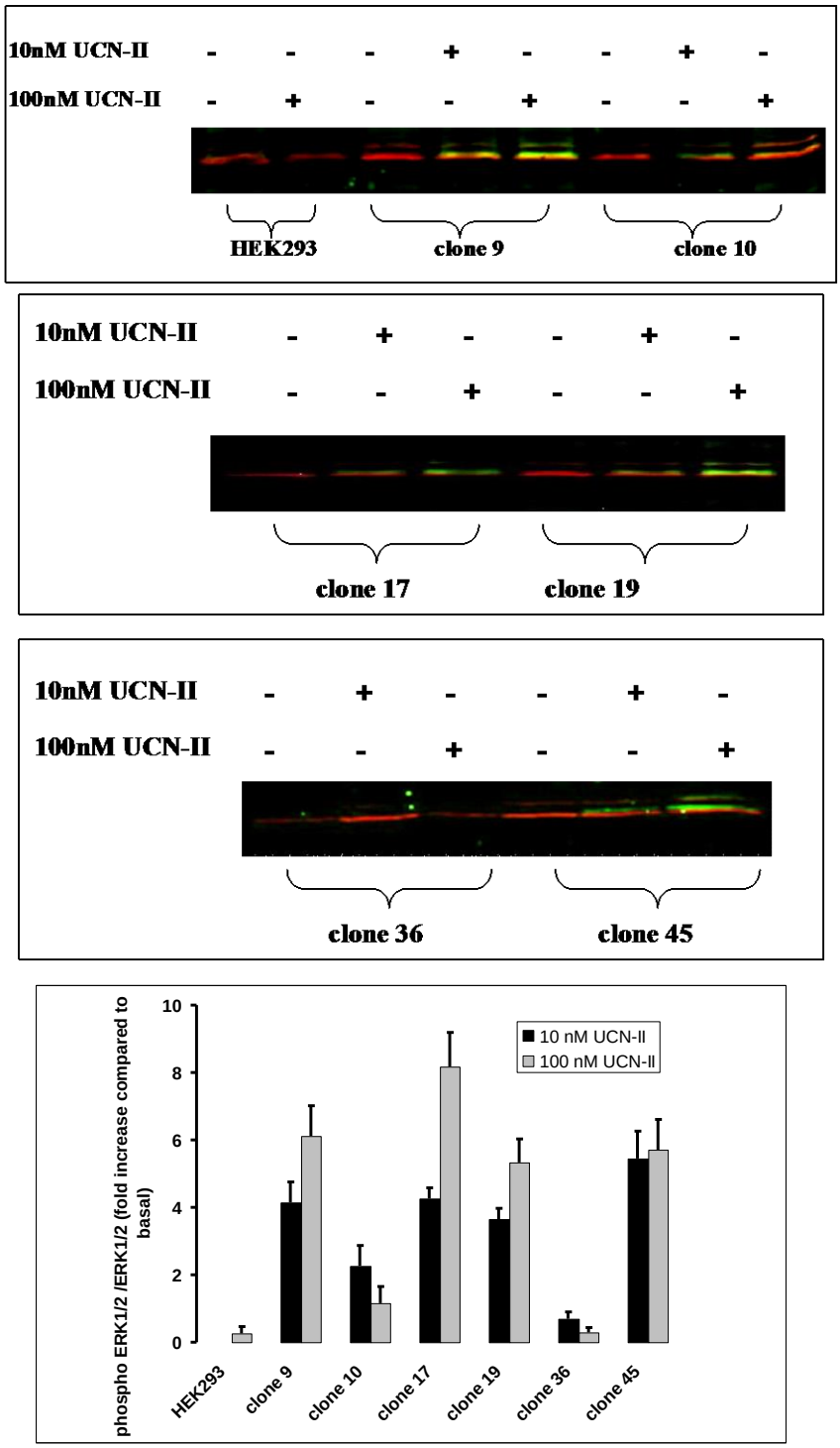

Figure 5.5. ERK1/2 phosphorylation in HEK293 and CRH-R2β clones. The cells were treated for 5 min with 10-100 nM UCN-II and assayed for ERK1/2 activation and analysed as described in the Materials and Methods. The results represent the mean ± SEM of two independent experiments.

5.2.2 Agonist induced cAMP production in st.293-R2β

The functional coupling of CRH-R2 to the Gsα/adenylyl cyclase/cAMP pathway in response to different agonists was assessed in st.293-R2β cells. Treatment of cells with various concentrations of CRH, UCN-I or UCN-II (1-100 nM) for 15 min resulted in a dose-dependent increase of intracellular cAMP accumulation (Figure 5.6.). In agreement with previous studies (Lewis K *et al*., 2001), both UCN-II and UCN-I were equally efficient in inducing adenylyl cyclase activation and were 40% more effective than CRH.

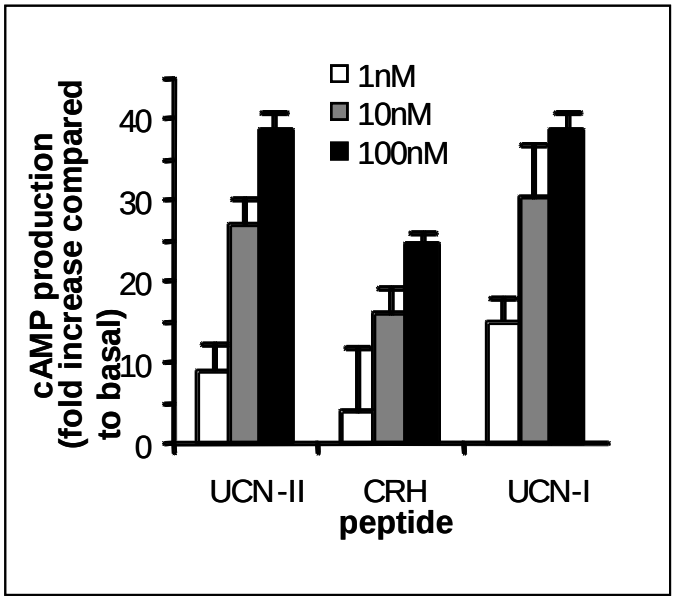

Figure 5.6. Agonist-induced cAMP production in st.293-R2β cells. Cells were treated with various concentrations of UCN-II, CRH and UCN-I for 15 min. cAMP production was determined and analysed as described in the Materials and Methods. Results were normalised with forskolin-induced cAMP production and expressed as the mean ± SEM of three independent experiments.

5.2.3 CRH-R2β desensitization is dependent on the agonist potency

CRH-R1α is susceptible to agonist-induced desensitization, however little is known about the desensitization characteristics of CRH-R2. In order to determine whether CRH-R2β functional coupling to the cAMP signalling pathway is susceptible to agonist-induced (homologous) desensitization, UCN-II was used because of its specificity for CRH-R2 binding and activation. For that purpose, st.293-R2β cells were pretreated with 100 nM of UCN-II for various time intervals (0-30 min) and the maximal UCN-II-induced cAMP stimulation was determined.

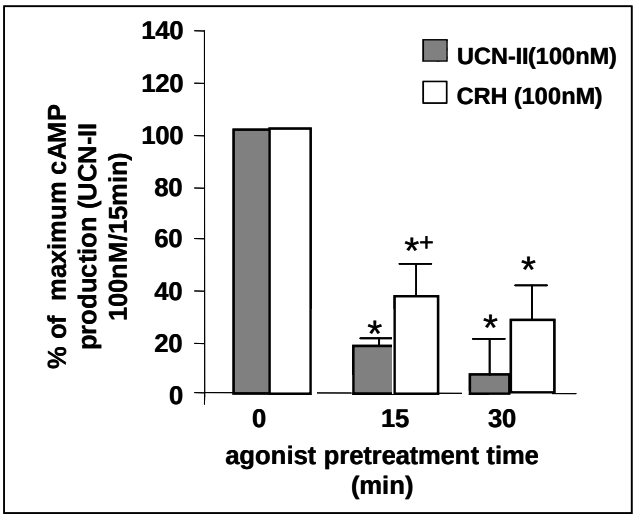

Figure 5.7. CRH-R2β desensitization characteristics in st.293-R2β cells. Cells were pretreated with CRH or UCN-II (100 nM) for various time intervals to induce desensitization. After extensive washing, cAMP response to a second UCN-II stimulus (100 nM for 15 min) was determined. Data represent the mean±SEM from three independent experiments. *, P <0.05 compared with cells without pretreatment. +, P <0.05 compared to each other with agonist pretreatment.

Results showed (Figure 5.7) that agonist pre-treatment for only 15 min was sufficient to induce a 80% decrease in CRH-R2β responsiveness, and a 30 min pre-exposure to 100 nM UCN-II almost completely abolished the subsequent UCN-II (100 nM)-induced cAMP response. Interestingly, when CRH (100 nM) was used to induce receptor desensitization we observed a weaker effect on CRH-R2β

responsiveness; CRH pre-treatment for 15 min caused only a 60% decrease in subsequent UCN-II (100 nM)-induced cAMP response whereas a 30 min pre-exposure to 100 nM CRH reduced UCN-II effect on cAMP stimulation by 80%.

5.2.4 The effect of different growth conditions on UCN-II induced ERK1/2 and p38 MAPK phosphorylation in st.293-R2β

Several studies have implicated ERK1/2 and p38 MAPK as key signalling intermediates downstream of CRH-R2 activation (Dermitzaki E *et al*., 2002; Sananbenesi F *et al*., 2003; Brar BK *et al*., 2004; Karteris E *et al*., 2004). In order to further characterise these signalling cascades, firstly it was tested how different growth conditions effect the activation of ERK1/2 and p38 MAPK.

18 hours prior to stimulation cells were deprived from FCS. Two hours prior to stimulation the cells were given fresh DMEM or HBSS. The cells were stimulated with 1-100 nM UCN-II for 5 min, and the MAPK activation was assayed as described in the Material and Methods. Agonist induced ERK1/2 activation was significantly higher when DMEM was used. The effect was more evident at a lower concentration of agonist (1-10 nM) than when 100 nM UCN-II was used. 1nM UCN-II induced a 2.5 fold increase in ERK1/2 phosphorylation in the cells kept in DMEM and a 1.3 fold increase in the cells kept in HBSS. Treatment with 10 nM UCN-II led to a 6.5 and 4 fold increase in ERK1/2 activation in cells kept in DMEM and HBSS, respectively; whilst 100 nM UCN-II induced ERK1/2 activation was 10 and 9.5 fold increased than in non treated cells kept in DMEM and HBSS, respectively (Figure 5.8).

On the other hand, in contrast to the cells kept in DMEM, the cells kept in HBSS failed to show agonist dose dependent p38 MAPK phosphorylation (Figure 5.9). All the further experiments were performed on the cells kept in DMEM only.

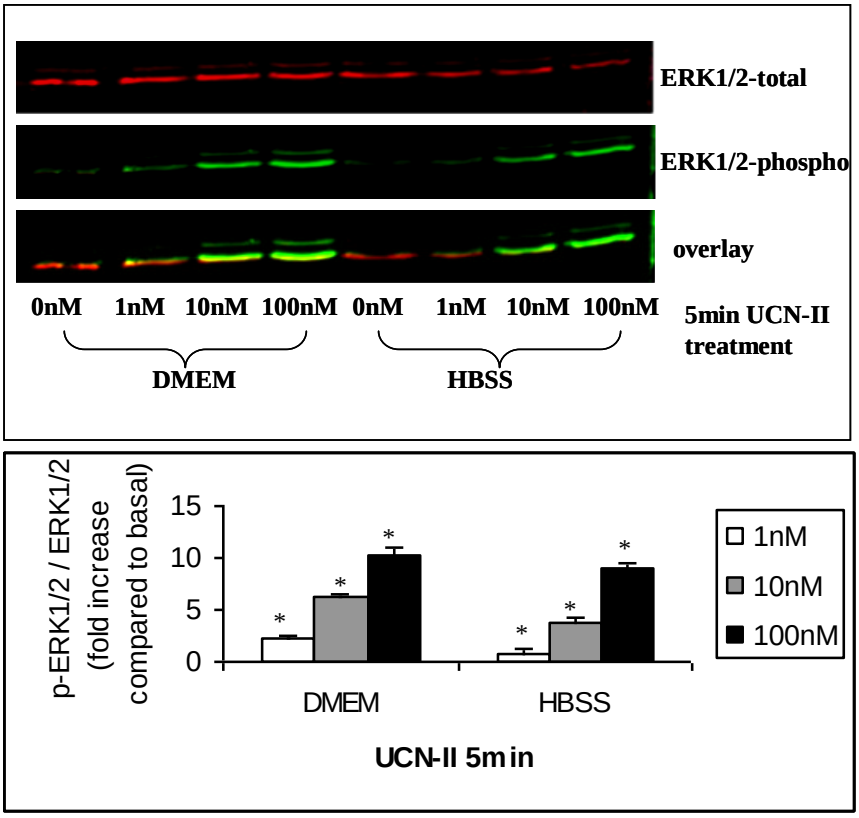

Figure 5.8. The effect of media on UCNII-induced ERK1/2 phosphorylation. 2 h prior to stimulation with 1-100 nM UCN-II, st.293-R2β were transferred in DMEM or HBSS. Following treatment the total cellular proteins were harvested and the ERK1/2 phosphorylation was assessed as described in the Materials and Methods. Results are expressed as the means ± SEM of three independent experiments. *, $P<0.05$ compared to basal.

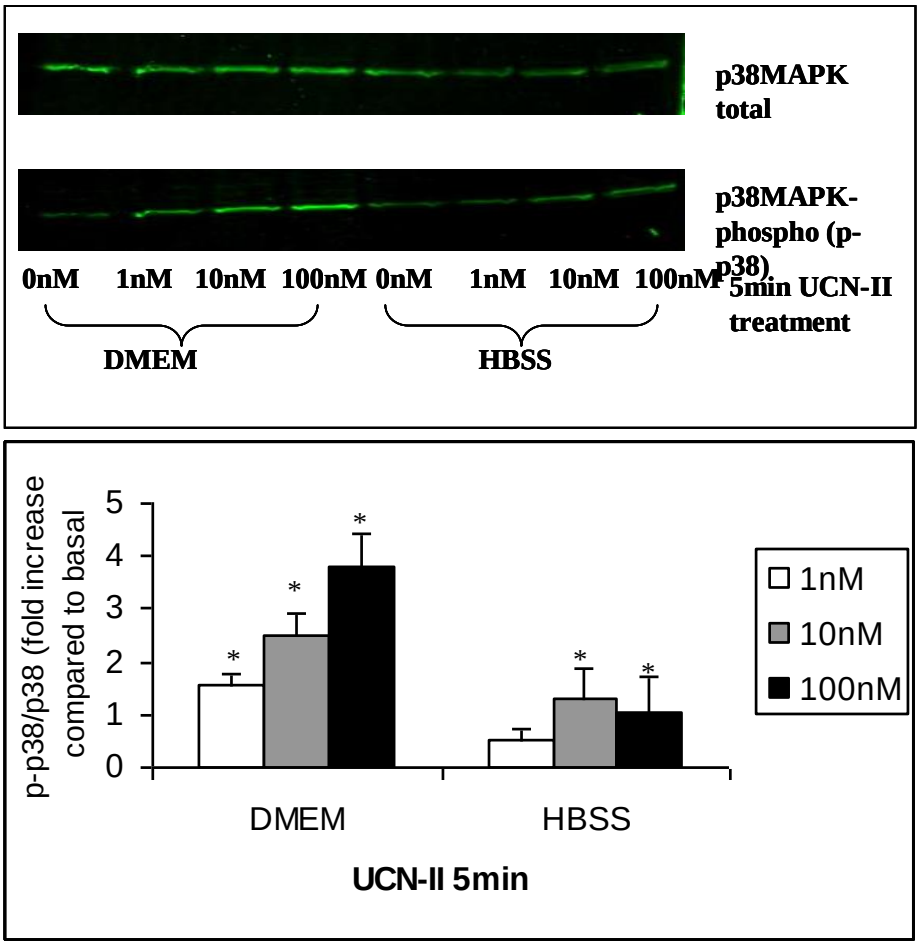

Figure 5.9. The effect of media on UCNII-induced p38 MAPK phosphorylation. 2 h prior to stimulation with 1-100 nM UCN-II, st.293-R2β were transferred in DMEM or HBSS. Following treatment the total cellular proteins were harvested and the p38 MAPK phosphorylation was assessed as described in the methods. Results are expressed as the means±SEM of three independent experiments.*, P<0.05 compared to basal.

5.2.5 The ERK1/2 and p38 MAPK activation depends on type and dose of the agonists

The effects of UCN-II and UCN-I on both ERK1/2 and p38MAPK activation were significant at concentrations greater than 1nM and maximal at 100

nM; maximal ERK1/2 activation was 10 fold increased compared to the basal levels (Figure 5.10), whereas maximal p38 MAPK activation was found to be 4 fold above basal (Figure 5.11). On the other hand, CRH was less efficient and led to maximal ERK1/2 activation of 6 fold above basal, while maximal p38 MAPK activation was 2.5 fold above basal.

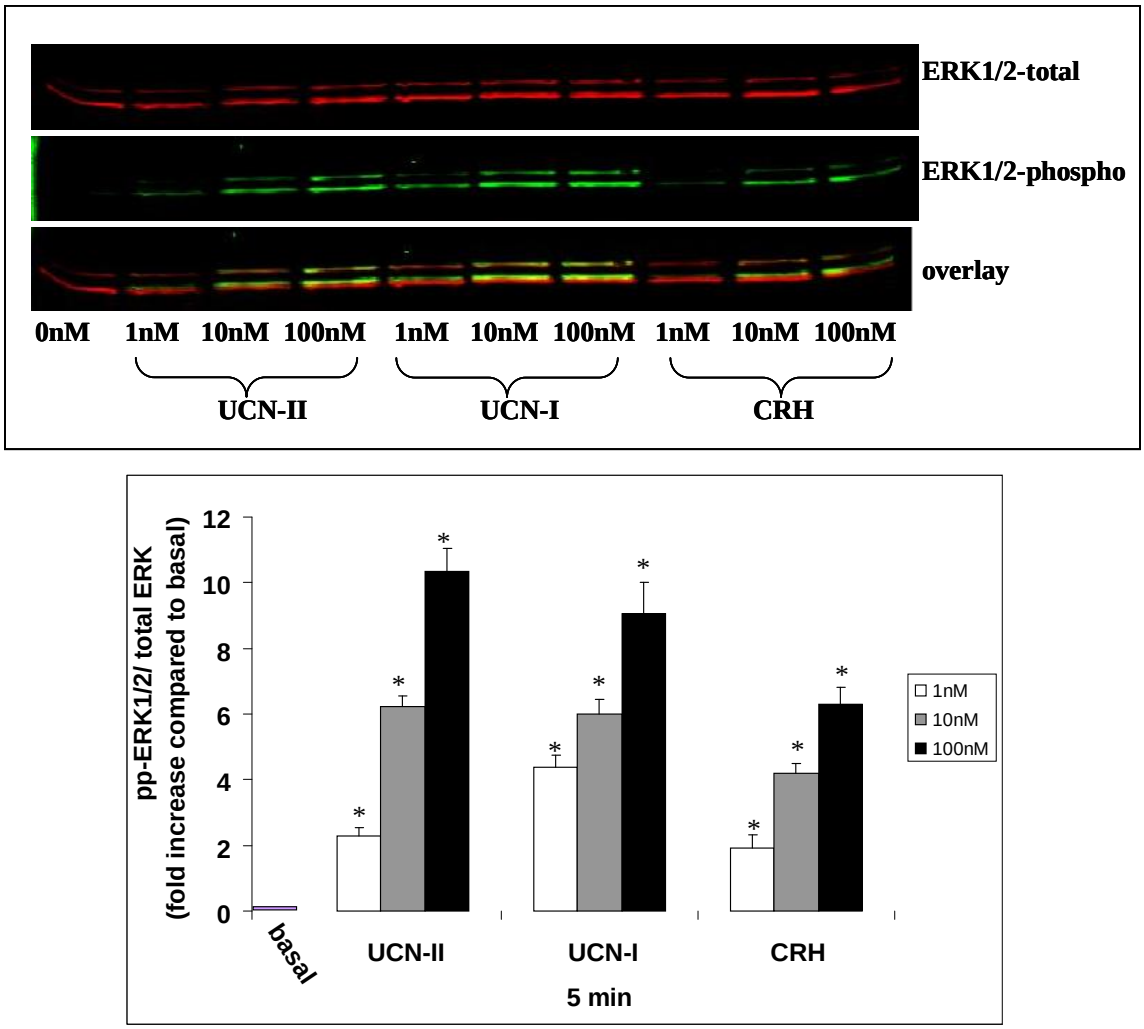

Figure 5.10. Agonist-induced and dose-dependent ERK1/2 phosphorylation in st.293-R2β. The cells were stimulated with 1-100 nM UCN-II, UCN-I and CRH for 5 min. ERK1/2 phosphorylation was detected and analysed as described in the Materials and Methods. Data represent the mean ±SEM from three independent experiments. *, P<0.05 compared to basal.

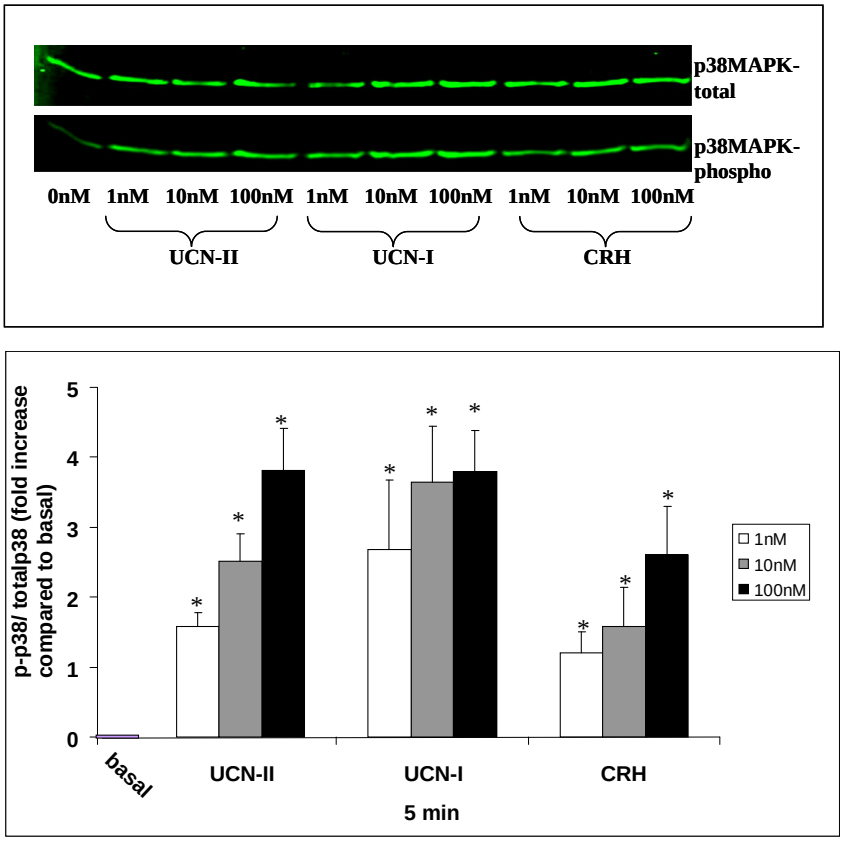

Figure 5.11. Agonist-induced and dose-dependent p38 MAPK phosphorylation in st.293-R2β. The cells were stimulated with 1-100 nM UCN-II, UCN-I and CRH for 5 min. p38 MAPK phosphorylation was detected and analysed as described in the Materials and Methods. Data represent the mean ±SEM from three independent experiments. *, $P<0.05$ compared to basal.

5.2.6 Agonist-induced ERK1/2 and p38 MAPK phosphorylation is transient

UCN-II induced ERK1/2 activation was transient and maximal stimulation was observed after 5 min of treatment and returned to basal levels after 30 min of treatment (Figure 5.12). UCN-II effect on p38MAPK phosphorylation showed a similar response with maximal stimulation after 5-10 min of treatment and returned to basal levels after 30 min of treatment (Figure 5.13). A similar pattern was observed when UCN-I and CRH were used for the simulation (data not shown).

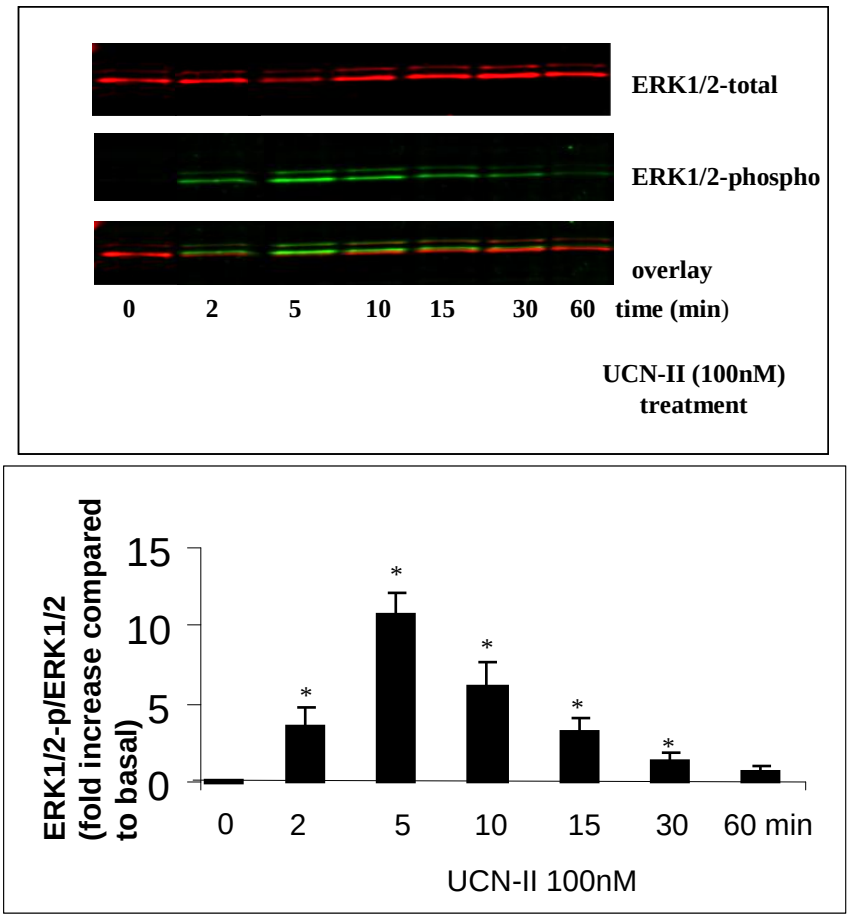

Figure 5.12. Time-dependent ERK1/2 activation by UCN-II in 293-R2β cells. Top panels are representative Western blots of cells stimulated with UCN-II (100 nM) for various time points (2-60 min). ERK1/2 phosphorylation was detected and analysed as described in the Materials and Methods. Data represent the mean ±SEM from three independent experiments. *, P<0.05 compared to basal.

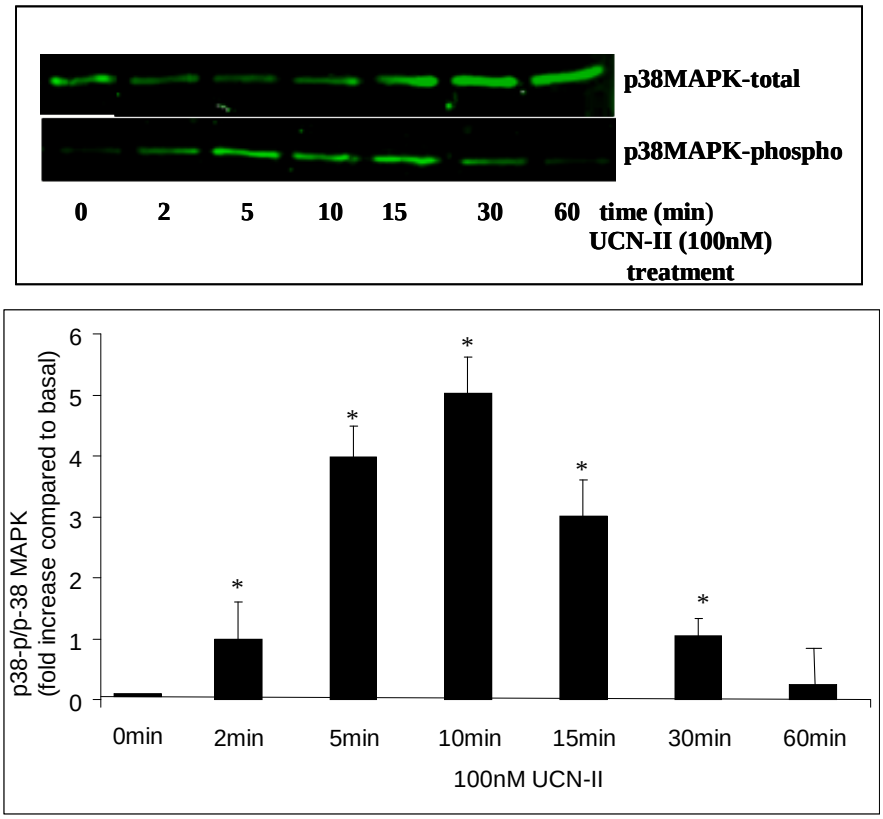

Figure 5.13. Time-dependent p38 MAPK activation by UCN-II in 293-R2β cells. Top panels are representative Western blots of cells stimulated with UCN-II (100 nM) for various time points (2-60 min). p38 MAPK phosphorylation was detected and analysed as described in the Materials and Methods. Data represent the mean ±SEM from three independent experiments. *, P<0.05 compared to basal.

5.2.7 The spatio-temporal characteristics of MAPK activation following UCN-II stimulation

Beside the phosphorylation of a plethora of cytoplasmic targets, the MAPK are important in direct activation of various transcription factors, such as Elk, c-Fos, c-Myc (Roux PP & Blenis J, 2004) and indirect activation of NF-κB (Markovic D *et*

al., 2007). In addition, it has been reported that ERK1/2 can translocate to the nucleus in order to activate downstream targets (Ebner HL *et al*., 2007)

To examine the spatio-temporal characteristics of MAPK activation in st.293-R2β, indirect immunofluorescence confocal microscopy was employed with phospho-specific MAPK antibodies, to monitor the relative subcellular distribution of activated MAPK and CRH-R2β after agonist stimulation (Figure 5.14). In unstimulated st.293-R2β cells, low levels of activated (phosphorylated) ERK1/2 and p38MAPK were found. As expected, CRH-R2β was primarily localized in the plasma membrane. UCN-II treatment for 5-10 min led to a rapid increase in the amount of fluorescent signal for both phospho-ERK1/2 and p38MAPK indicating increased activity. The phospho-ERK1/2 immunoreactive signal was widespread throughout the intracellular space suggesting cytoplasmic as well as nuclear localization of activated ERK1/2. In contrast, phospho-p38MAPK immunoreactivity was present only in the cytoplasm and no phospho-p38 MAPK immunoreactivity was detected in the nucleus. In agreement with the immunoblotting experiments suggesting transient MAPK activation, prolonged treatment (15-20 min) with UCN-II (100 nM), caused only a small increase in the amount of phospho-ERK1/2 and p38MAPK immunofluorescent signal, reflecting deactivation of the signalling pathway. Interestingly, in contrast to CRH-R1α (Punn A *et al*., 2006) no co-localization between internalized CRH-R2β and phospho-ERK1/2 or p38MAPK was found to be present (Figure 5.14).

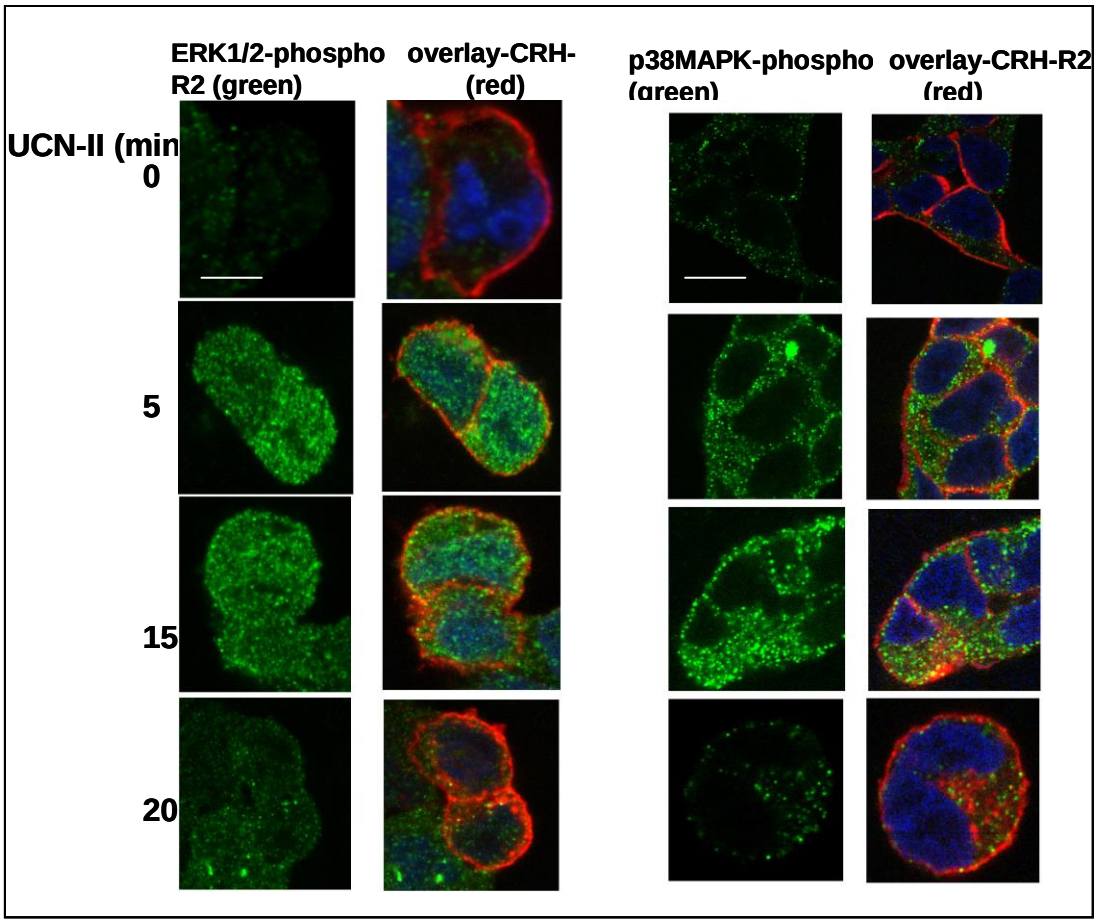

Figure 5.14. CRH-R2β and phospho-ERK1/2 or phospho-p38 MAPK subcellular distribution induced by UCN-II in st.293-R2β cells: visualization by confocal microscopy. st.293-R2β cells were stimulated with or without UCN-II (100 nM) for various time intervals (5–20 min). CRH-R2β and phospho-ERK1/2 or phospho-p38 MAPK distribution was monitored over the ensuing time period as described in the Materials and Methods. Identical results were obtained from four independent experiments. Scale bar is 10 μm.

5.2.8 UCN-II induced ERK1/2 phosphorylation, but not p38 MAPK phosphorylation, is protein kinase A (PKA) dependent

The cAMP and ERK1/2 pathways play crucial roles in controlling a wide range of diverse cellular responses in different cell types. Accumulating evidence suggest that there is a cross-talk between these two pathways. It has been

documented that in st.293-R1α, UCN-I induced ERK1/2 phosphorylation was negatively regulated by PKA (Papadopoulou N *et al*., 2004). However, in a different over-expressing system, CHO cells, the inhibition of PKA led to partial inhibition of UCN-I induced ERK1/2 phosphorylation (Brar BK *et al*., 2004). Additionally, the latter report provided evidence that CRH-R2β mediated ERK1/2 activation was also partially dependent on PKA.

In order to determine whether PKA activation was important for the ERK1/2 and p38 MAPK phosphorylation in st.293-R2β cells, PKA inhibitor peptide (14-22) that had been myristilated at the N-terminus in order to enhance its cell permeability, was used. The advantage of inhibitor peptides over chemical inhibitors such as H-89 is in the specificity and toxicity. While chemical inhibitors if used in excess could potentially inhibit activity of other enzymes and be toxic to the cell, the inhibitor peptides compete with the endogenous substrate for the active site of the enzyme, or prevent binding of different subunits to form an active complex. The other inhibitor used in this project was St-Ht31 inhibitor peptide (St-Ht-31). This peptide is derived from AKAPs (**A** **K**inase **A**nchoring **P**roteins), it has an amphipatic helical structure that has been shown to interrupt PKA binding to AKAPs (Colledge M & Scott JD, 1999) and as such prevents further transduction of the signal from PKA.

UCN-II induced ERK1/2 phosphorylation was reduced by 40% in st.293-R2β cells pretreated with PKAi or st-Ht-31, at the same time p38 MAPK phosphorylation was not affected with the pretreatments (Figure 5.15).

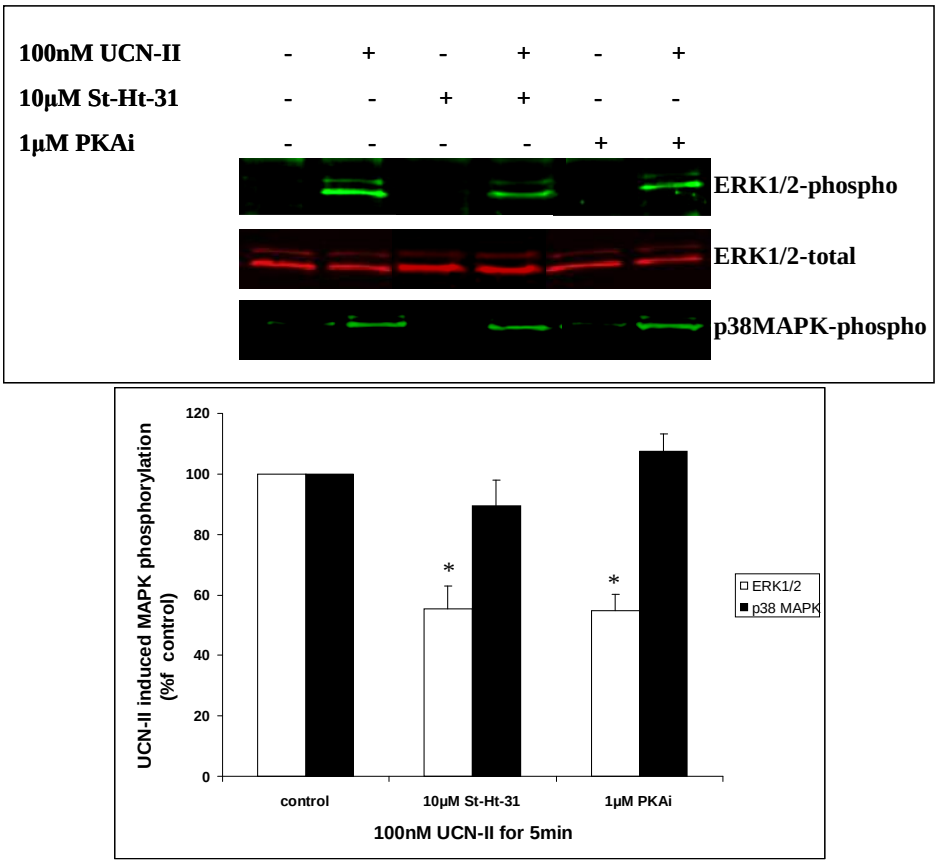

Figure 5.15. The effect of PKA inhibition on UCN-II induced ERK1/2 and p38 MAPK activation in st.293-R2β cells. Top panels are representative Western blots of cells stimulated with inhibitors and 100 nM UCN-II for 5 min. Following treatment the total cellular proteins were harvested and the ERK1/2 and p38 MAPK phosphorylation were assessed as described in the Materials and Methods. Results are expressed as the means ± SEM of three independent experiments. *, $P<0.05$ compared to control (no inhibitors pre treatment).

However, that the interaction between cAMP/PKA and ERK MAPK pathways is not a straight forward cross-talk was demonstrated in a time course experiment in the presence of the PKA inhibitor. As shown in figure 5.16, the inhibition of PKA activity stimulated a 60% increase in ERK1/2 phosphorylation with UCN-II for 2 min. However, a more prolonged exposure of the cells to UCN-II for 5 and 10 min in the presence of the PKA inhibitor resulted in attenuation of ERK1/2 phosphorylation (Figure 5.16).

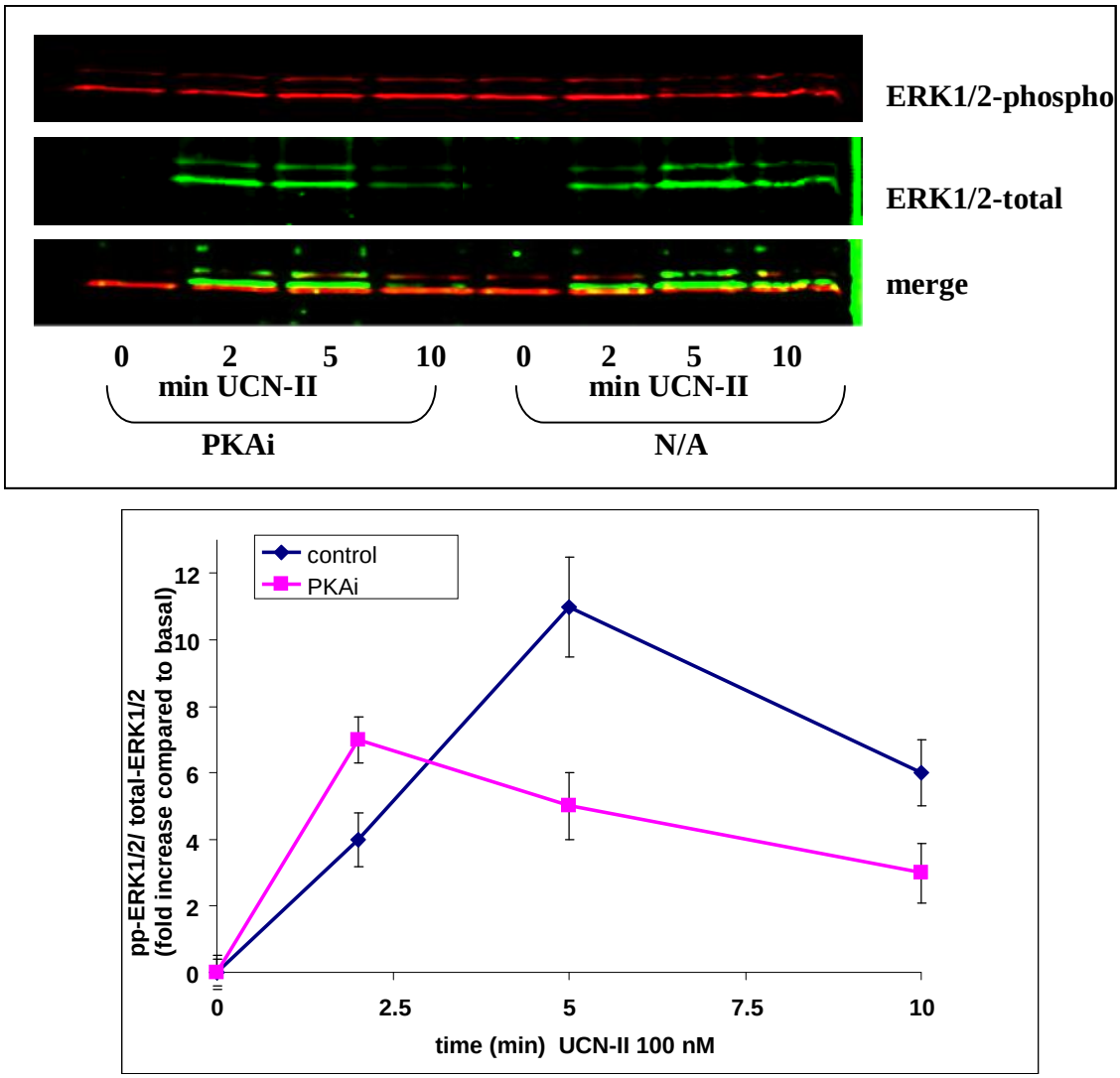

Figure 5.16. Time course: the effect of PKA inhibition on UCN-II induced ERK1/2 in st.293-R2β cells. Top panels are representative western blots of cells stimulated with and without PKA inhibitor and 100 nM UCN-II for 2, 5 and 10 min. Following treatment the total cellular proteins were harvested and the ERK1/2 MAPK phosphorylation was assessed as described in the Materials and Methods. Results at the lower panel are expressed as the means ± SEM of three independent experiments.

5.2.9 UCN-II induced ERK1/2 phosphorylation, but not p38 MAPK phosphorylation, is PI(3) kinase dependent

Another kinase implicated in UCN-I induced ERK1/2 activation in st.293-R1α (Punn A *et al*., 2006) and CHO cells overexpressing CRH-R1α and R2β (Brar BK *et al*., 2004) is PI(3)-kinase. However, UCN-I induced p38 MAPK activation in st.293-R1α was PI(3)-kinase independent (Punn A *et al*., 2006). Inhibition of PI(3)-kinase by LY-294002, revealed that UCNII-induced ERK1/2 phosphorylation in st.293-R2β reduced by 90±5% compared to control cells, while p38 MAPK phosphorylation was insensitive to the kinase inhibition (Figure 5.17).

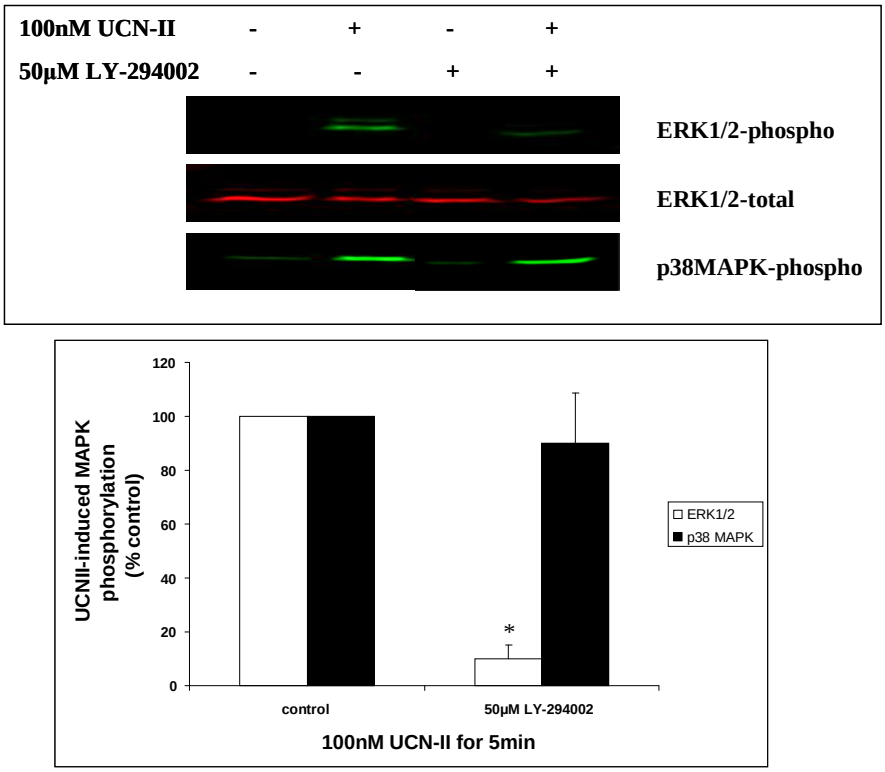

Figure 5.17. The effect of PI(3)-kinase inhibition on UCN-II induced ERK1/2 and p38 MAPK activation in st.293-R2β cells. Top panels are representative western blots of cells stimulated with inhibitors and 100 nM UCN-II for 5 min. Following treatment the total cellular proteins were harvested and the ERK1/2 and p38 MAPK phosphorylation were assessed as described in the Materials and Methods. Results are expressed as the means±SEM of three independent experiments. *,P<0.05, compared to control (no inhibitor).

5.2.10 Internalisation characteristics of CRH-R2β

In order to investigate homologous internalization, st-293-R2β cells were stimulated with 0.1-100 nM UCNII, UCN-I and CRH for 0-60 minutes. The internalization of CRH-R2β proved to be a dose-dependent (due to lack of space, data not shown) as well as time-dependent process. In the absence of UCN-II or CRH, the receptor was located exclusively on the plasma membrane. Since 100 nM UCN-II and CRH treatment led to strongest redistribution of the receptor, this concentration was chosen to investigate the time-dependent internalization characteristics. When st-293-R2β were treated only with vehicle (acetic acid), the receptor was exclusively expressed on the plasma membrane. Treatment with 100 nM UCN-II for 15 min led to the appearance of punctuate staining in the cytoplasm, possibly indicative of endocytosis (Figure 5.18). After 30 minutes of exposure to 100 nM agonist, strong immunoreactivity was observed in the cytoplasm. Similar results were seen after 45 and 60 minutes (data not shown for the latter) (Figure 5.18). CRH was less efficient in inducing early endocytosis, after 15 min of the exposure to 100 nM CRH no visible receptor redistribution was detected (Figure 5.18). After 30 min and especially 45 min significant cytoplasmic immunoreactivity was detected, as an indication of CRH-R2β internalization (Figure 5.18).

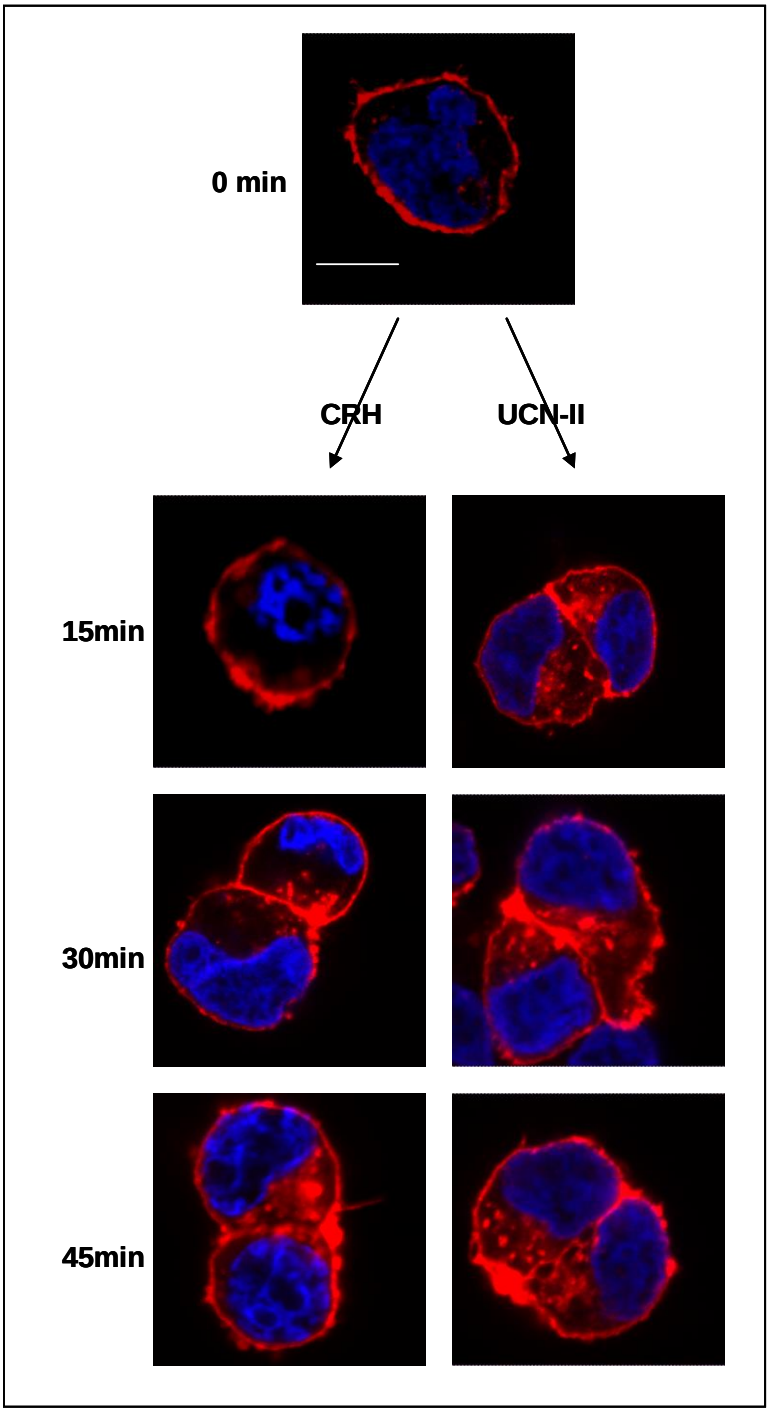

Figure 5.18. Internalization of CRH-R2β in st293-R2β is dependent on agonist efficiency. st.293-R2β cells were grown on cover slips and exposed to 100 nM UCN-II or CRH for various time points (0-45 min). CRH-R2 distribution was monitored by indirect immunofluorescence using CRH-R1/2-specific antiserum and Alexa-Fluor®594 secondary antibody. Identical results were obtained from four independent experiments. Magnification x 63, and optical zoom x 5. Scale bar is 10 μm.

The efficiency of different agonists in inducing CRH-R2β internalization was quantitatively determined using On-cell western assay with near IR dyes in non-permeabilized cells. For that purpose antibodies targeted against the CRH-R2β N-terminus and the Odyssey infrared (IR) imaging system were employed, as previously described (Miller JW, 2004). In preliminary experiments the IR signal characteristics were established; signal intensity was typically 80% higher than the signal obtained when secondary anti-mouse IRDye 800-conjugated IgG was used alone (Table 5.1). The calculated % specific signal of the antibodies used in this assay was determined to be between 45-55% of total signal. Results showed that UCN-II (100 nM) treatment for 30 min induced a 58-67% decline in CRH-R2β immunoreactivity from the cell surface of 293-R2β cells compared to basal, whereas an equimolar concentration of CRH reduced CRH-R2β immunoreactivity by only 43-52% (Figure 5.19).

	Signal Intensity levels (average)
Total binding (1st+2nd Ab)	26700
Background	400
1st Ab only	500
2nd Ab only	13100
% Specific (T-NSB*/ T) signal	51%

Table 5.1. The IR signal characteristics. NSB (non specific binding) was equal to 2nd antibody signal intensity.

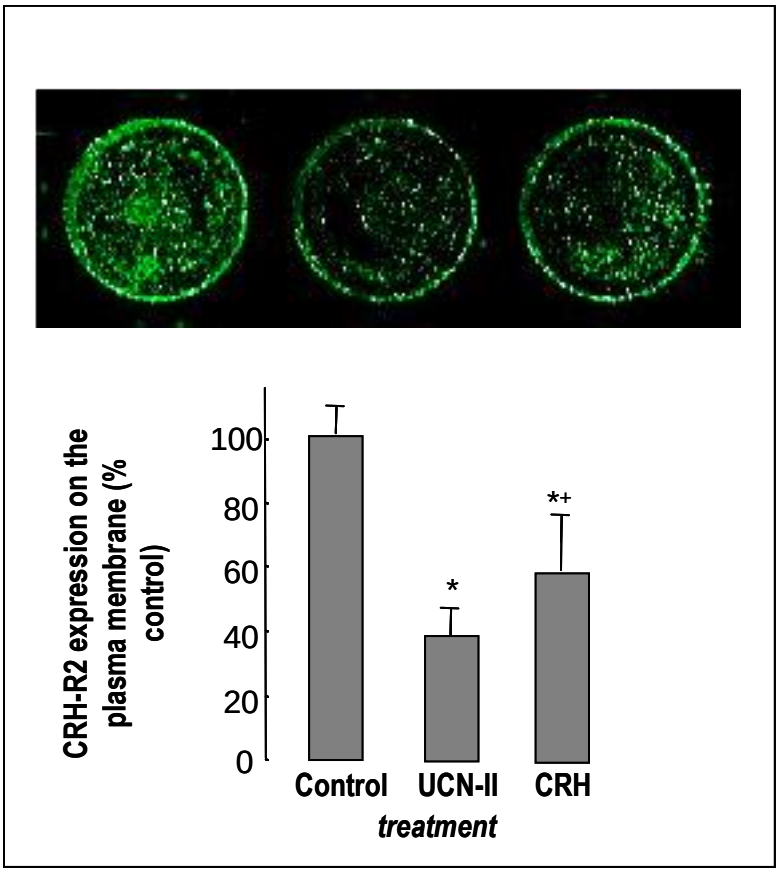

Figure 5.19. Quantification of CRH-R2β expression on the plasma membrane. CRH-R2β loss from the cell-surface following agonist stimulation (UCN-II or CRH, 100 nM) for 30 min, was quantified by an "On-cell Western" assay with near IR dyes in non-permeabilized cells, using antibody against the CRH-R2β N-terminus and the Odyssey infrared (IR) imaging system, as described in the Materials and Methods. Data represent the mean ± SEM of two estimations from three independent experiments. *, P <0.05 compared with cells without pretreatment. +, P <0.05 compared to each other agonist pre-treatment.

5.2.11 Internalization of CRH-R2β is β-arrestin and clathrin dependent

The internalization of most GPCR requires recruitment of β-arrestin and clathrin to the plasma membrane (DeWire SM *et al*., 2007). The fate of CRH-R2β receptors following activation by UCN-II or CRH was investigated by indirect confocal microscopy to monitor the temporal distribution of the receptor. In the absence of agonist, CRH-R2β receptors were exclusively localized on the cell

surface of st.293-R2β cells (Figure 5.20 top row). Immunostaining for β-arrestin (using an antibody that recognises both β-arrestin1 and β-arrestin2) and clathrin (heavy chain) demonstrated widespread distribution, primarily in the cytoplasm. Treatment of cells with 100 nM UCN-II for 2 min induced a rapid redistribution of β-arrestin and clathrin to the plasma membrane that appear to co-localise with CRH-R2β receptors, as this appeared to cause an increase in plasma membrane immunostaining of β-arrestin (green) and clathrin (blue) signal and the appearance of white signals, in the overlap images (Figure 5.20-merge). Within 15 min of UCN-II treatment there was evidence of some receptor trafficking in the cytoplasm and after 30 min of treatment intense receptor fluorescent signal was observed in the cytoplasm, indicative of substantial receptor internalization (Figure 5.20). Interestingly, receptor association with β-arrestin and clathrin was transient and restricted on or near to the plasma membrane since CRH-R2β receptors internalized without any β-arrestin or clathrin.

Use of CRH as the receptor internalization-inducing agonist revealed important agonist-specific temporal differences in CRH-R2β internalization kinetics; although CRH (100 nM) induced β-arrestin and clathrin recruitment to the plasma membrane after 2 min following CRH treatment (Figure 5.20) substantial CRH-R2β internalization was evident only after 30 min of treatment. Similar to UCN-II, CRH-induced internalized CRH-R2β receptors did not co-localize with β-arrestin or clathrin.

Further experiments were performed to characterise β-arrestin activation and membrane translocation in response to agonist-occupied receptor. Distribution of β-arrestin immunoreactivity was monitored in cell membrane fractions prepared from st.293-R2β□cells treated with either 100 nM CRH or UCN-II for various time

intervals (0–15 min). In resting 293-R2β□cells, small amounts of β-arrestin1 (49 kDa) and β-arrestin2 (47 kDa) were detected in the cell membrane fraction. UCN-II or CRH treatment for 2 min resulted in a 3-4 fold increase in the membrane fraction content of both β-arrestin1 and β-arrestin2 (Figure 5.21). This increase was transient and after 10-15 min of UCN-II treatment, membrane levels of both β-arrestins were significantly reduced (by 70%). In contrast, following CRH (100 nM) treatment, substantial membrane levels of β-arrestin1 and β-arrestin2 were observed after 15 min of treatment (2 and 3.5 fold above basal for β-arrestin1 and β-arrestin2, respectively).

The retention of β-arrestin on the plasma membrane following UCN-II or CRH stimulation for 15 min was also assessed with indirect confocal microscopy (Figure 5.22). For this purpose confocal images were taken from the middle and top of the same cell. The results revealed that β-arrestin was not present on the top of unstimulated cells, a weak β-arrestin signal was detected on the top of the cells treated with UCN-II for 15 min, while substantial immunoreactivity corresponding β-arrestin was observed on the top of the cells treated with CRH for 15 min (Figure 5.22).

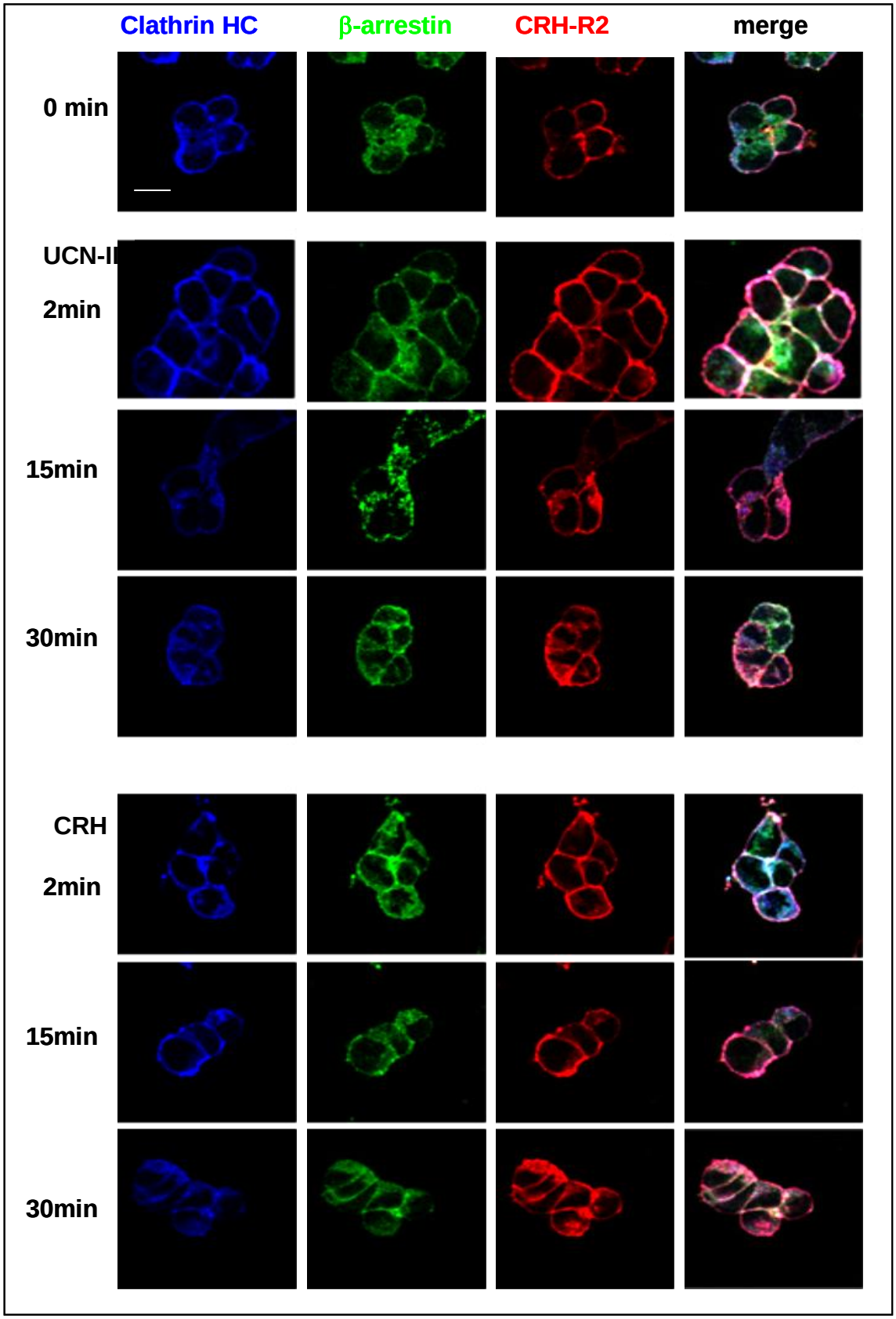

Figure 5.20. CRH-R2β, β-arrestin and clathrin subcellular distribution following CRH or UCN-II treatment: visualization by fluorescent

confocal microscopy. st.293-R2β were stimulated with either UCN-II or CRH (100 nM) for 2-30 min. CRH-R2β, clathrin and β-arrestin distribution was monitored over the ensuing time period by indirect triple immunofluorescence using specific primary antibody and Secondary Alexa-Flour antibody as described in the Material and Methods.. Identical results were obtained from 4 independent experiments. Scale bar is 20 μm.

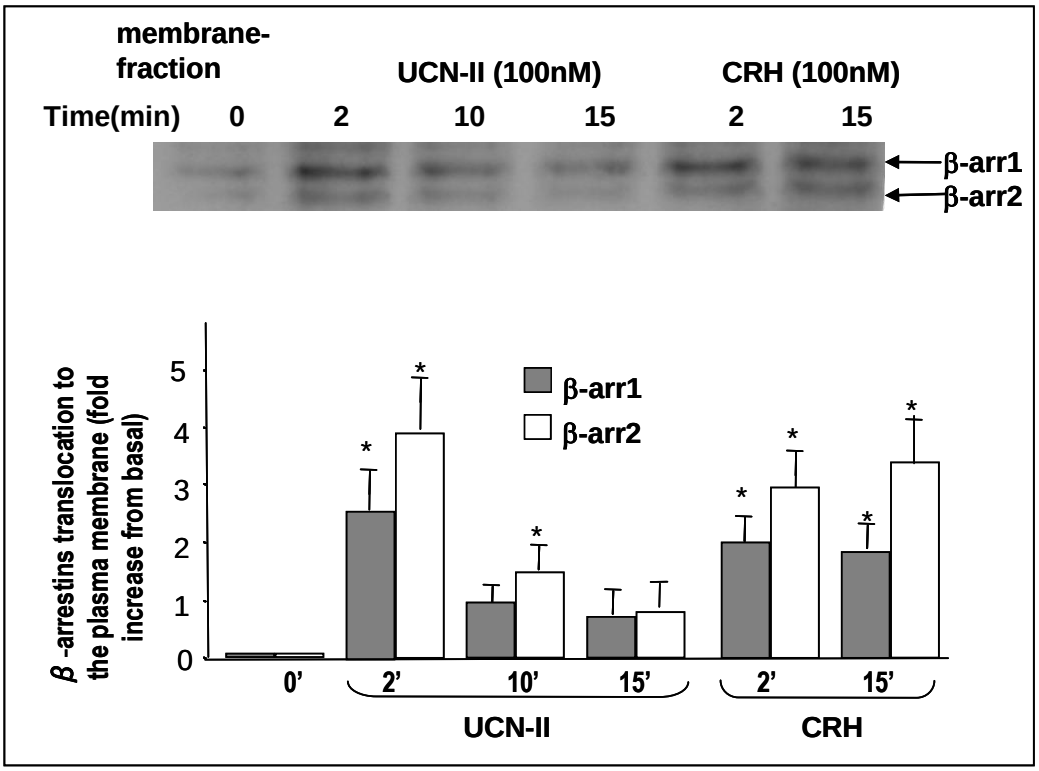

Figure 5.21. Agonist-dependent β-arrestin recruitment to the plasma membrane. Plasma membrane fractions were prepared from st.293-R2β cells, stimulated with or without UCN-II or CRH (100 nM) for various time intervals and proteins were resolved on SDS-PAGE gels, followed by immunoblotting with pan-arrestin antibodies, as described in the Materials and Methods. Densitometry scanning was carried out to quantify agonist-induced β-arrestin translocation to the plasma membrane. Top panel: representative immunoblots and bottom panel: mean ±SEM of three independent experiments; *, $P < 0.05$ compared with basal.

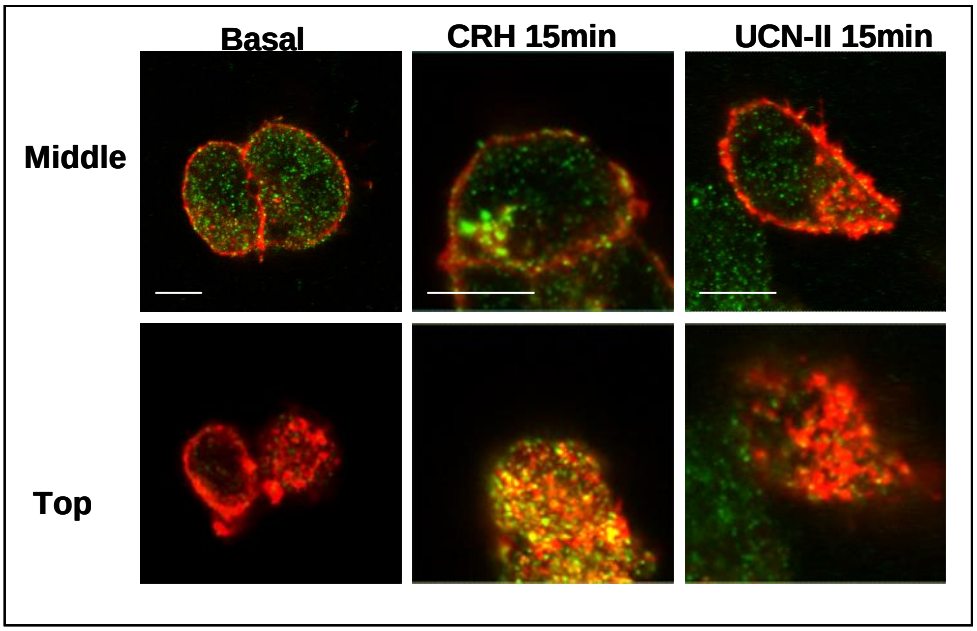

Figure 5.22. Recruitment of β-arrestin by the agonist-activated CRH-R2β in st.293-R2β. Confocal microscopy was used to evaluate the interaction of CRH-R2β (red) with β-arrestin (green). The images were taken from the middle and top of the same cell. The identical results were obtained from three independent experiments. Scale bar is 10 μm.

5.2.12 UCN-II induced MAPK activation is independent of CRH-R2β endocytosis

Since GPCRs internalization can potentially lead to activation of the MAPK signalling cascade, the possibility that CRH-R2β endocytosis is involved in UCN-II-induced activation of ERK1/2 and p38 MAPK signalling cascades was investigated. The receptor internalization was inhibited with conconavalin A (con A), or DN (dominant negative) β-arrestin (319–418). Both of these approaches strongly inhibited agonist-stimulated CRH-R2β internalization (Figure 5.23.).

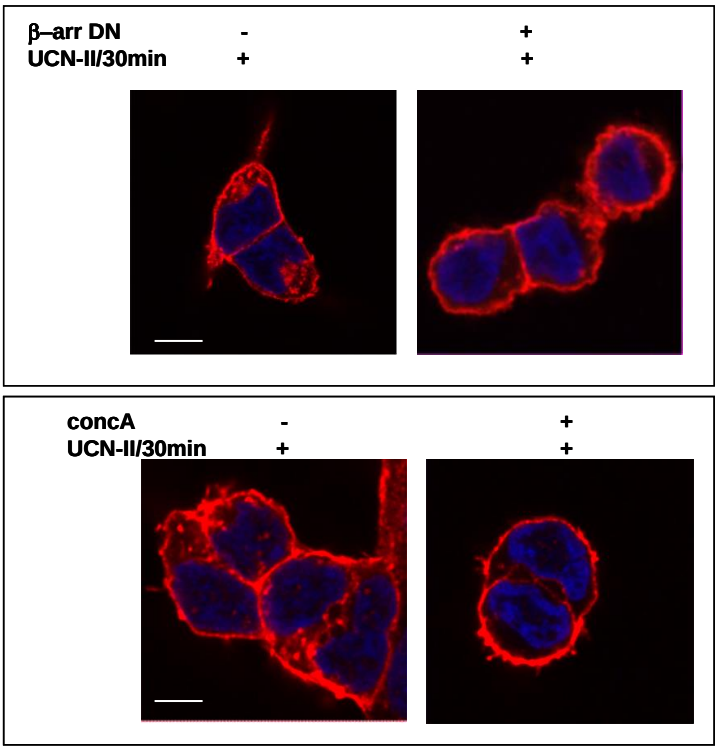

Figure 5.23. Effect of DN β-arrestin and conconavalin A on UCN-II induced CRH-R2β endocytosis in st.293-R2β cells. Cells were pre-treated with or without concanavalin A (conc A) (0.25mg/ml for 40 min) or alternatively transfected with either 5 μg of empty pcDNA3 vector (control) or dominant negative β-arrestin (β-arr DN) (319–418) and the effect on UCN-II (100 nM for 30 min) induced receptor internalization was monitored by indirect confocal microscopy. Identical results were obtained from two independent experiments. Scale bare is 10 μm.

Additionally, the receptor endocytosis was blocked with the transfection of st.293-R2β with siRNA duplexes targeting CHC (clathrin heavy chain) (Figure 5.23), confirming that the internalization of CRH-R2β is a clathrin dependent process. The efficiency of the clathrin silencing was assessed by confocal microscopy (Figure 5.24) and western blot analysis (Figure 5.25). Confocal microscopy revealed that the silencing was 90% efficient; strong immunoreactivity for clathrin was present in approximately 10% of the cells, also in those cells UCN-II induced CRH-R2β endocytosis was detectable (Figure 5.24, the cell pointed by the white arrow).

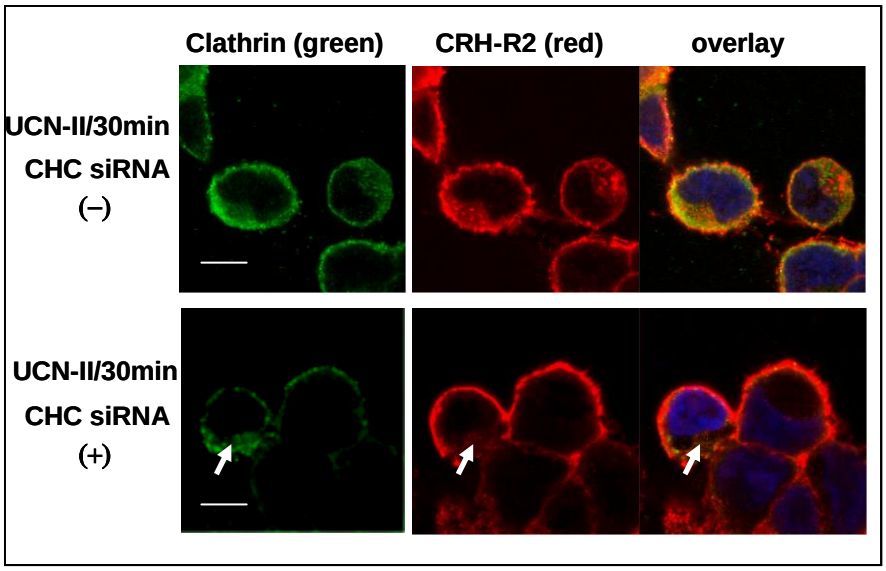

Figure 5.24. Effect of CHC siRNA on UCN-II induced CRH-R2β internalization in st.293-R2β cells. Cells were transfected with 1nmol of CHC siRNA or scrambled oligonucleotide and the effect on UCN-II induced internalization of CRH-R2β were monitored by indirect confocal microscopy using specific primary antibodies and Alexa-Fluor® 594 secondary antibody for CRH-R2β (red) and Alexa-Fluor® 488 secondary antibody for clathrin heavy chain (CHC) (green). The white arrow points to a cell that did not uptake CHC siRNA. Identical results were obtained from 3 independent experiments. At least 10 individual cells in five random fields of view were examined. Scale bar is 10 μm.

Although it has been reported that UCN-I induced ERK1/2 and p38 MAPK phosphorylation was dependent upon internalization of CRH-R1α (Punn A *et al*., 2006); none of the compounds used to inhibit UCN-II induced CRH-R2β internalization did not exert inhibitory effects on ERK1/2 and p38MAPK activation (Figure 5.26). Moreover, disruption of CRH-R2β internalization by β-arrestin (319–418) and CHC siRNA amplified by 70% and 30% respectively, ERK1/2 phosphorylation stimulated by 100 nM UCN-II. Studies on UCN-II-induced

p38MAPK activation showed similar effects (Figure 5.26). These results suggested that an intact receptor endocytosis pathway is not essential for UCN-II-induced MAPK activation.

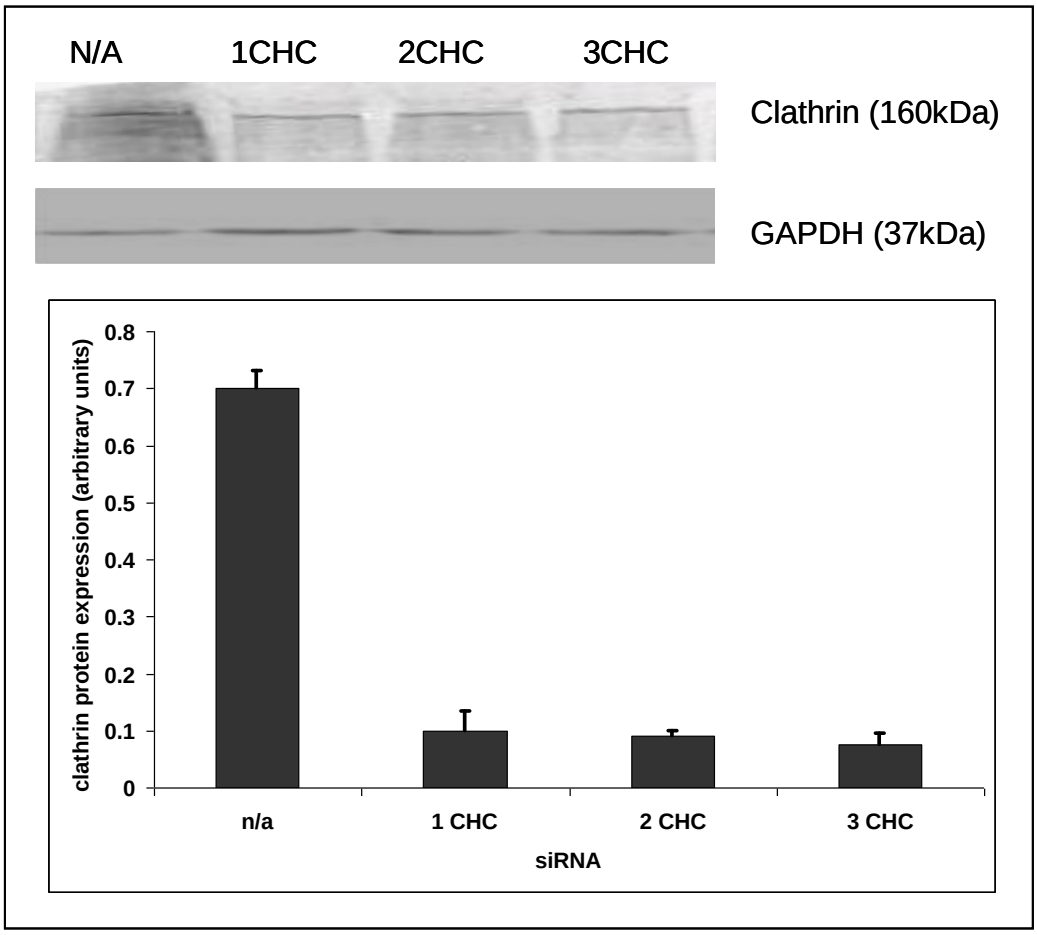

Figure 5.25. Verification of clathrin silencing by CHC siRNA in st.293-R2β cells. Cells were transfected with 1nmol of three pairs of CHC siRNA (1CHC, 2CHC and 3CHC) or scrambled oligonucleotide (N/A). Equal protein levels were confirmed by GAPDH. Representative western blot was shown on the top panel. Data (bottom panel) are represented as the mean ± SEM of three independent transfections.

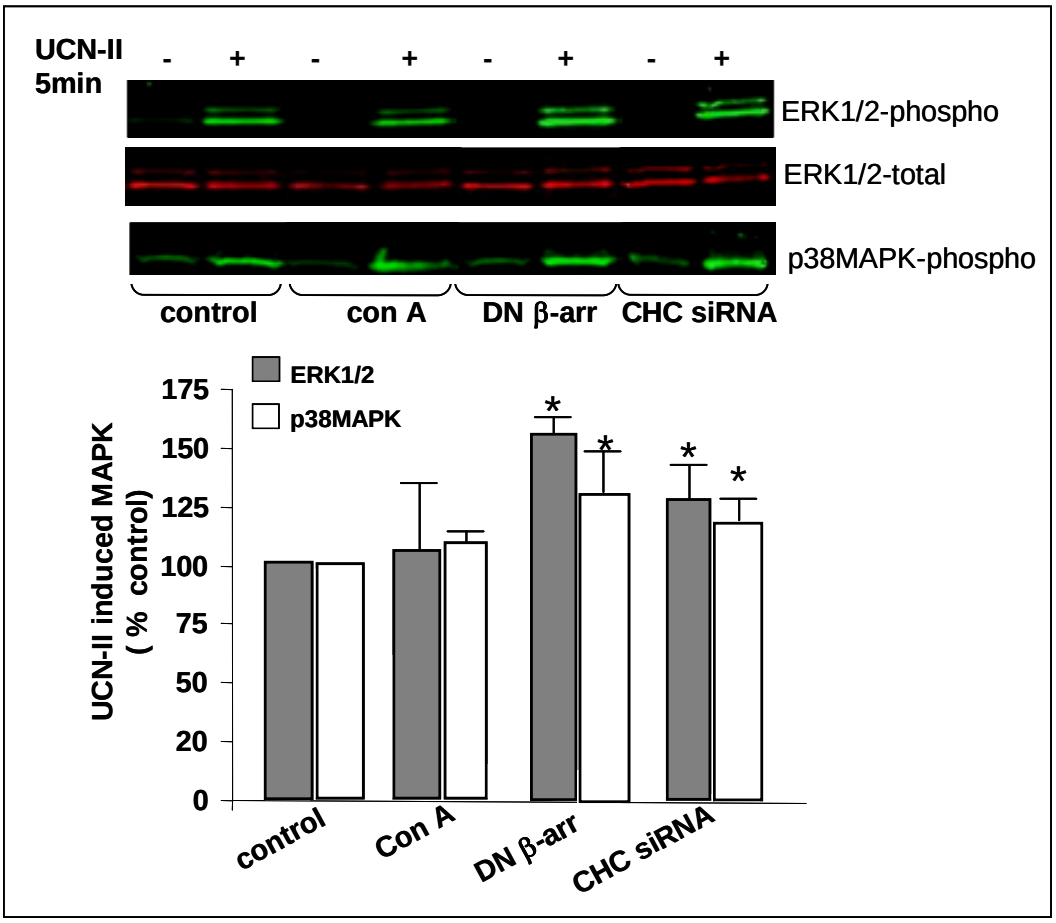

Figure 5.26. Effect of concanavalin A, DN β-arrestin and CHC siRNA on UCN-II induced ERK1/2 and p38MAPK activation in 293-R2β cells. Cells were pre-treated with or without concanavalin A (0.25mg/ml for 40 min) or alternatively transfected with either 5 μg of empty pcDNA3 vector (control) or β-arrestin (319–418) or 1nmol of CHC siRNA or scrambled oligonucleotide and the effect on UCN-II (100 nM for 5 min) stimulation on ERK1/2 and p38MAPK activation was determined, by measurement of ERK1/2 and p38MAPK phosphorylation as described in the methods. Data represent the mean ±SEM from three independent experiments. *, P <0.05 compared with control cells.

5.2.13 UCN-II induced CRH-R2β desensitization is dependent on the CRH-R2β endocytotic machinery

In order to investigate whether the presence of β-arrestin or clathrin is essential for CRH-R2β desensitization, agonist-induced CRH-R2β desensitization in the presence of a DN β-arrestin and CHC siRNA was investigated. In st.293-R2β

cells overexpressing DN β-arrestin, the ability of UCN-II pretreatment (100 nM for 30 min) to desensitize CRH-R2β responsiveness and cAMP activation was significantly impaired (by 50%) (Figure 5.27). Furthermore, UCN-II failed to induce CRH-R2β internalization (Figure 5.23), suggesting that CRH-R2β homologous internalization is β-arrestin–dependent. Significant inhibition by 25-35% of CRH-R2β desensitization was also obtained when RNA interference was employed to deplete cells from CHC, and thus preventing assembly of functional clathrin-coated pits at the plasma membrane (Figure 5.27). Reduction in CHC expression (in excess of 90%) in siRNA transfected cells was confirmed by immunoblotting with antibodies directed against the CHC (Figure 5.25). These data suggest that the retention of the receptor in the plasma membrane leads to impaired receptor desensitisation.

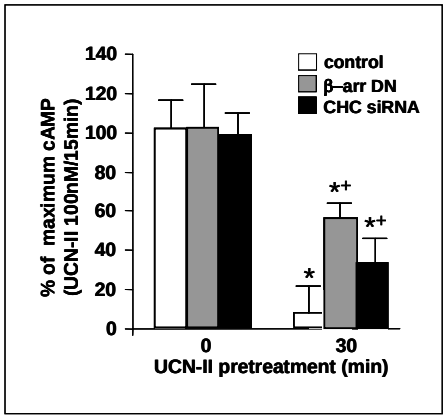

Figure 5.27. Effect of DN β-arrestin and CHC siRNA on UCN-II induced CRH-R2β desensitization in st.293-R2β cells. Cells were transfected with either 5 μg of empty pcDNA3 vector (control) or β-arrestin (319–418) or 1nmol of CHC siRNA or scrambled oligonucleotide and the effect on CRH-R2β homologous desensitization (induced by pretreatment with 100 nM UCN-II for 30 min) was determined, by measurement of UCN-II-induced cAMP production. Data represent the mean ±SEM of two estimations from three independent experiments. *, P <0.05 compared with cells without UCN-II pretreatment; $^{+}$, P <0.05 compared with control cells.

5.2.14 UCN-II induced ERK1/2 phosphorylation negatively regulates CRH-R2β endocytosis via β-arrestin1 phosphorylation

Next, it was investigated whether UCN-II activated ERK1/2 can potentially regulate CRH-R2β internalization through a feedback mechanism previously described (Lin F-Y *et al*., 1999), involving phosphorylation of β-arrestin1 at Ser412. Western blot analysis of cell membrane fractions using β-arrestin1 specific antibody and analysis of total cellular proteins using phospho-β-arrestin1 (Ser412) specific antibody was employed to demonstrate β-arrestin1 trafficking and phosphorylation in the presence or absence of U0126 (MEK inhibitor-10μM for 2 h).

It was confirmed that UCN-II ERK1/2 interactions are MEK dependent (Figure 5.28), since U0126 pre-treatment blocked UCN-II induced ERK1/2 activation.

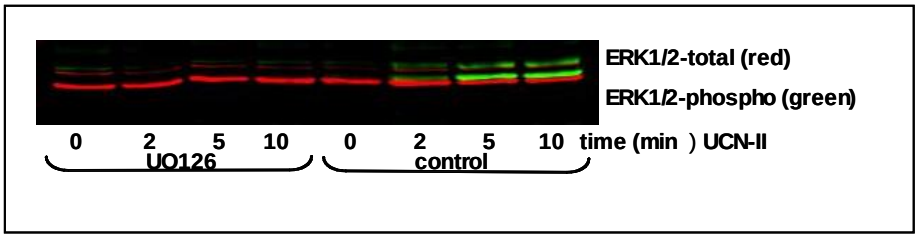

Figure 5.28. UCN-II induced ERK1/2 phosphorylation is MEK dependent. Cells were pre-treated with or without U0126 (10μM) for 2 h to inhibit basal and UCN-II-dependent ERK1/2 activation, before stimulation with UCN-II (100 nM) for various time intervals (0-10 min). The identical results were obtained from three independent experiments.

In section 5.2.11, it was demonstrated that β-arrestin1 was recruited to the plasma membrane following UCN-II treatment. However, in those experiments pan-arrestin antibody that recognises both β-arrestins, β-arrestin1 and β-arrestin2, was used (Figure 5.21). In agreement with those results, use of β-arrestin1 specific antibody showed that in st.293-R2β cells treated with UCN-II for 2 min, β-arrestin1

recruitment to the plasma membrane was significantly increased by 70%-90% above basal. This effect was transient and within 10 min the rise in β-arrestin1 membrane fraction was reduced by 50% (Figure 5.29 A and C). The discrepant values for β-arrestin1 translocation to the plasma membrane shown in figures 5.21 and 5.29 could be due to specificity of the different antibodies, as well as to the detection method (ECL vs. near IR detection system). Both basal and UCN-II induced trafficking of β-arrestin1 appeared to be regulated by ERK1/2, since inhibition of MEK and ERK1/2 by U0126 pretreatment significantly increased (by 50%) basal β-arrestin1 recruitment to the plasma membrane (Figure 2.29 B).The effect of UCN-II was not altered in the absence of active ERK1/2 and levels of membrane-bound β-arrestin1 remained unchanged for the period tested (up to 10 min) (Figure 5.29 C).

The purity of plasma membrane protein isolation was confirmed by probing the PVDF membrane (from the above experiment) with GAPDH antibody. A lack of GAPDH immunoreactive band confirms that the plasma membrane protein preparation did not contain proteins from the cytoplasmic/mitochondrial fraction (Figure 2.29 A). Although 10μg of membrane proteins were separated on a 10% SDS-PAGE, the equal amount of proteins was confirmed by probing PVDF membranes with pan-cadherin antibody which was also used as a plasma membrane protein marker, cadherin (Figure 5.29 A).

Before focusing on β-arrestin1 phosphorylation studies, the specificity of phospho-β-arrestin1 (Ser412) antibody was confirmed with alkaline phosphatase treatment of a PVDF membrane. The membrane was incubated at 37^{o}C overnight in 10mls of alkaline phosphatase buffer and 1000u of alkaline phosphatase. After 18 h the membrane was washed with TBS-T and probed with the phospho-β-arrestin1

(Ser412) and total β-arrestin1 antibodies, resulting in a loss of an immunoreactive band corresponding to phospho-β-arrestin1 (Figure 5.30).

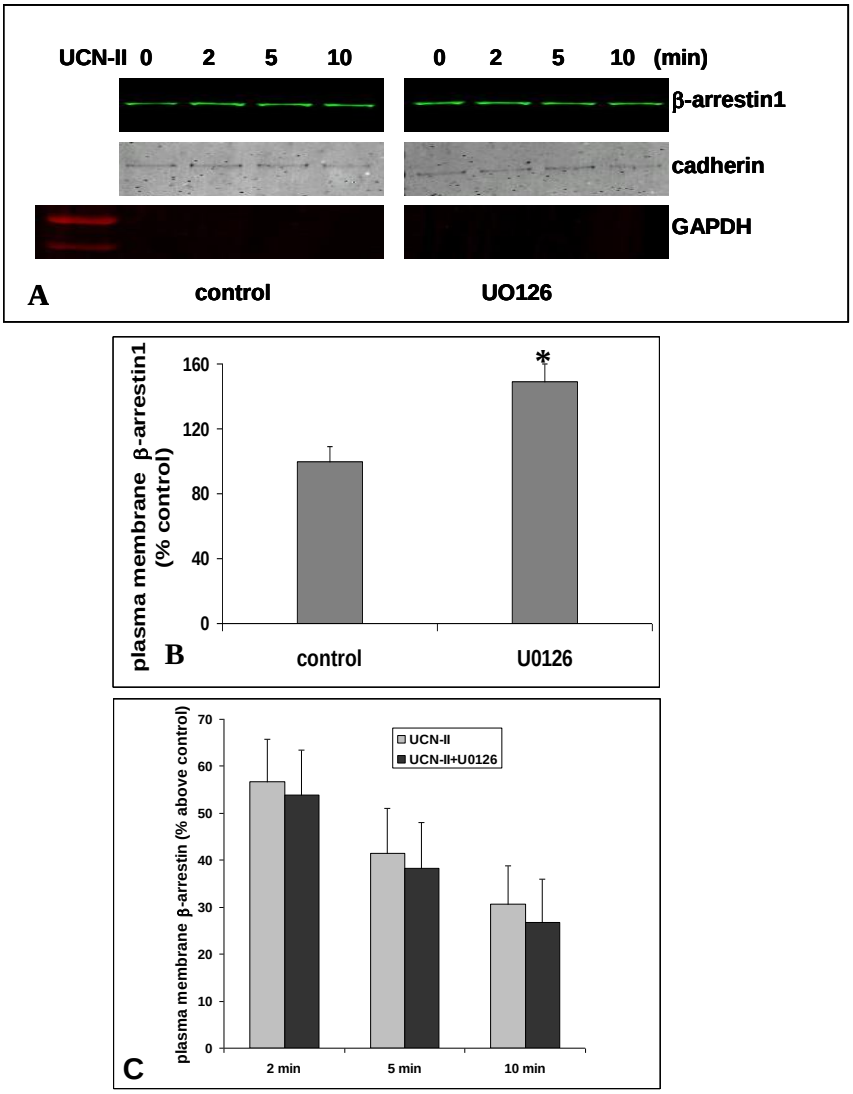

Figure 5.29. Regulation of β-arrestin1 membrane translocation by ERK1/2 in 293-R2β cells. Cells were pre-treated with or without U0126 (10μM) for 2 h to inhibit basal and UCN-II-dependent ERK1/2 activation before stimulation with UCN-II (100 nM) for various time intervals (0-10 min). Following cell lysis and membrane fractionation membrane-bound β-arrestin1 were determined by specific antibodies and Alexa Fluor®680-conjugated goat anti-mouse IgG using the Odyssey Infrared Imaging System. (A) top- representative β-arrestin1 western blot of cells stimulated with the inhibitor and 100 nM UCN-II. middle-representative pan-cadherin western blot, bottom-representative GAPDH western blot. (B) The effect of U0126 on basal β-arrestin1 translocation to the membrane. (C) Quantitative representation of β-arrestin1 translocation. Data represent the mean ±SEM from three independent experiments. *, *P* <0.05 compared with unstimulated cells.

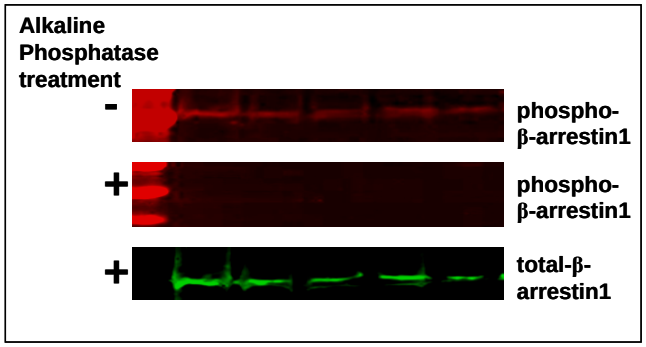

Figure 5.30. Characterisation of phospho-β-arrestin1 (Ser412) antibody. Following cell lysis in RIPA buffer, phospho-β-arrestin1 (Ser412) was determined by specific antibodies Alexa Fluor®680-conjugated goat anti-mouse IgG using the Odyssey Infrared Imaging System (top blot). The membrane was treated with alkaline phosphatase as described in the Materials and Methods, and phospho-β-arrestin1 (Ser412) and total-β-arrestin1 were determined by specific antibodies and IRDye™800-conjugated goat anti-rabbit IgG and/or Alexa Fluor®680-conjugated goat anti-mouse IgG using the Odyssey Infrared Imaging System.

Since Ser412 of β-arrestin1 is the site of ERK1/2 mediated phosphorylation (Lin F-Y *et al*., 1999), UCN-II induced β-arrestin1 phosphorylation in the presence or absence of U0126 was investigated. After an initial rise of 13-20% within 2 min of UCN-II treatment, the prolonged exposure to the peptide led to 45-50% decrease below basal levels in phosphorylation of β-arrestin1 at Ser412. UCN-II induced phosphorylation β-arrestin1 appeared to be regulated by ERK1/2. In the absence of active ERK1/2, UCN-II treatment led to a significant reduction by 40% (compared to basal) of phospho-β-arrestin1 immunoreactivity within 5 min, possibly due to activation of protein phosphatases (Figure 5.31). However, the inhibition of ERK1/2 phosphorylation did not effect the basal levels of β-arrestin1 phosphorylation.

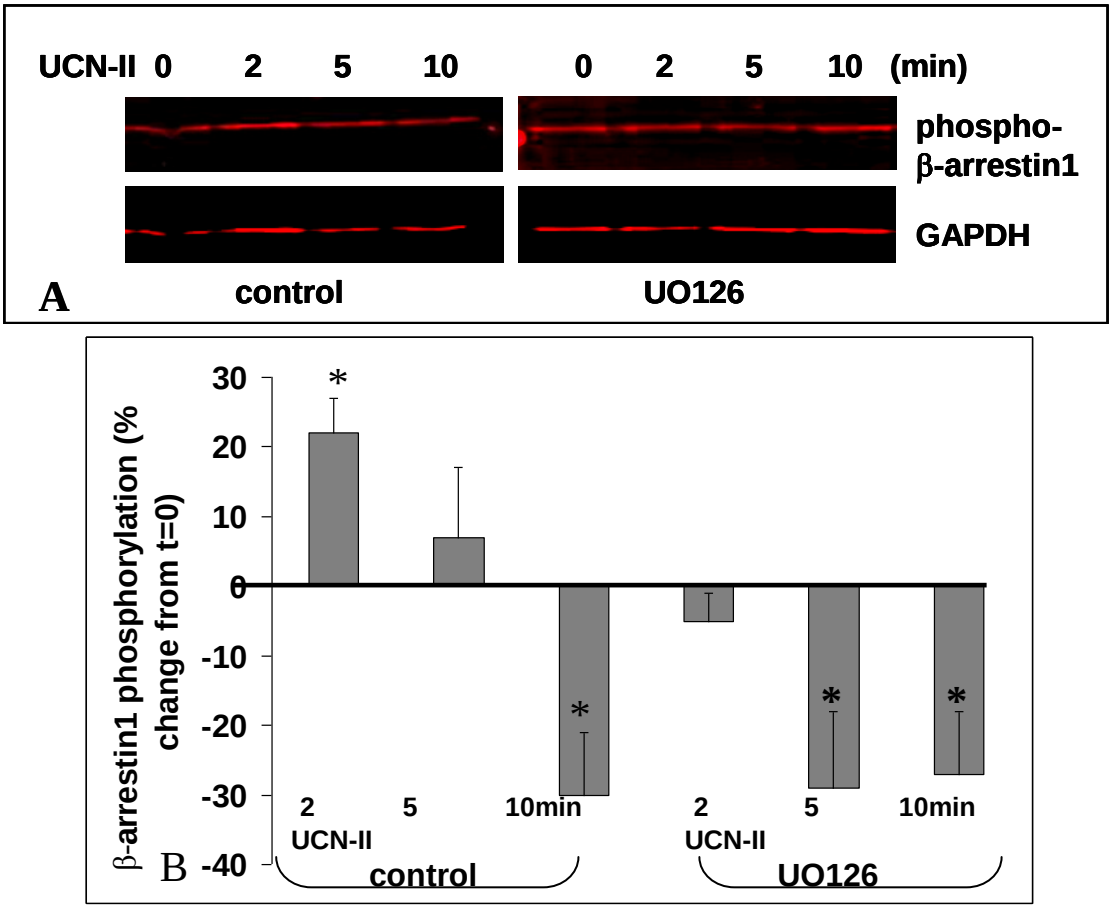

Figure 5.31. Regulation of β-arrestin1 phosphorylation by ERK1/2 in 293-R2β cells. Cells were pre-treated with or without U0126 (10μM) for 2 h to inhibit basal and UCN-II-dependent ERK1/2 activation before stimulation with UCN-II (100 nM) for various time intervals (0-10 min). Following cell lysis in RIPA buffer phospho-β-arrestin1 were determined by specific antibodies and IRDye™800-conjugated goat anti-rabbit IgG using the Odyssey Infrared Imaging System. (A) top-representative phospho-β-arrestin1 western blot of cells stimulated with the inhibitor and 100 nM UCN-II; bottom-GAPDH western blot to demonstrate equal loading. (B) Quantitative representation of β-arrestin1 translocation. Data represent the mean ±SEM from three independent experiments. *, P <0.05 compared with unstimulated cells.

5.2.15 The effect of ERK1/2 on CRH-R2β internalization

Confocal microscopy was used to determine the effect of ERK1/2 in CRH-R2β internalization; in both U0126 pre-treated and control cells incubation with 100

nM UCN-II for 15 min elicited a significant redistribution of cellular immunostaining, indicative of receptor internalization (Figure 5.32). Quantification of red fluorescence in the intracellular space of 20 individual cells that were randomly selected, showed 30-50% increased amount of red fluorescent signal throughout the intracellular space (4–18μm) in U0126 pre-treated cells compared to the control (Figure 5.32), suggesting that ERK1/2 inhibition was associated with increased receptor internalization.

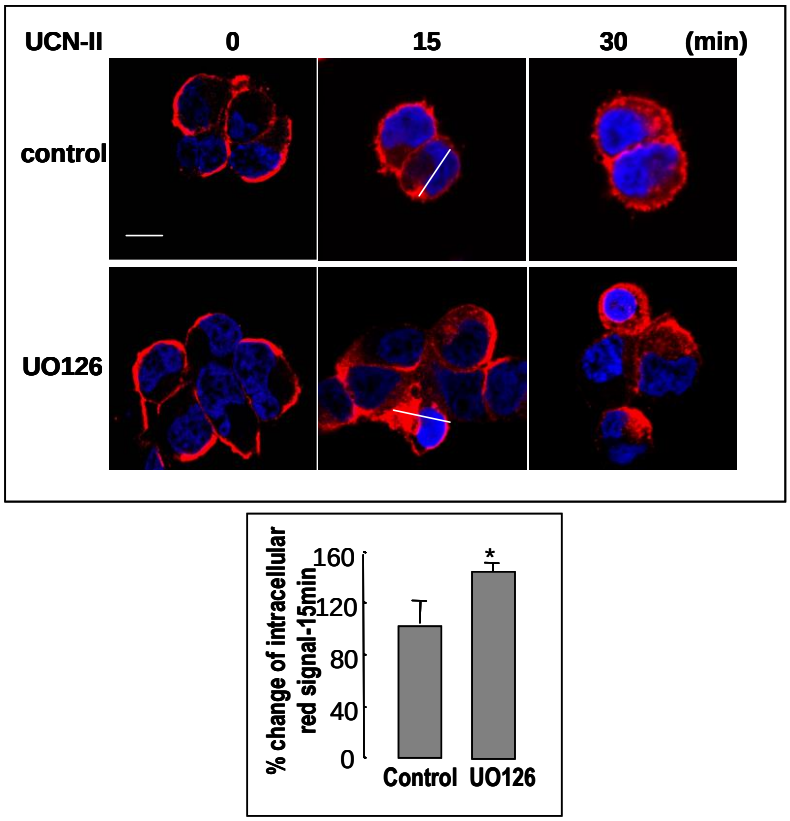

Figure 5.32. The effect of ERK1/2 on CRH-R2β endocytocis. The effect of U0126 on UCN-II induced CRH-R2β internalization was monitored by indirect fluorescent confocal microscopy using specific primary antibodies and Alexa-Fluor 594 secondary antibody for CRH-R2 (red). Quantification of cytoplasmic CRH-R2β distribution was done as described in the Materials and Methods. Scale bar is 10 μm. In the bottom panel the results are expressed as the mean ± S.E.M of three estimations from 20 individual cells. *, $p < 0.05$ compared with unstimulated values.

5.2.16 The role of C-terminus of CRH-R2β in the receptor mediated signalling

The CRH-R1 and R2 receptors share considerable amino acid homology between their C-termini. A notable diversity is found within the last four amino acid residues of the C-terminus (TAAV instead of STAV). In contrast to the CRH-R2, the CRH-R1-MAPK interactions display different spatio-temporal characteristics involving β-arrestin-dependent pathways; therefore the possibility that this amino acid cassette plays a role in determining CRH-R2β-mediated MAPK activation was explored. Site-directed mutagenesis was used to create CRH-R2β receptors, in which the cassette TAAV was replaced by AAAA, STAV, or deleted (DEL) (Figure 5.33).

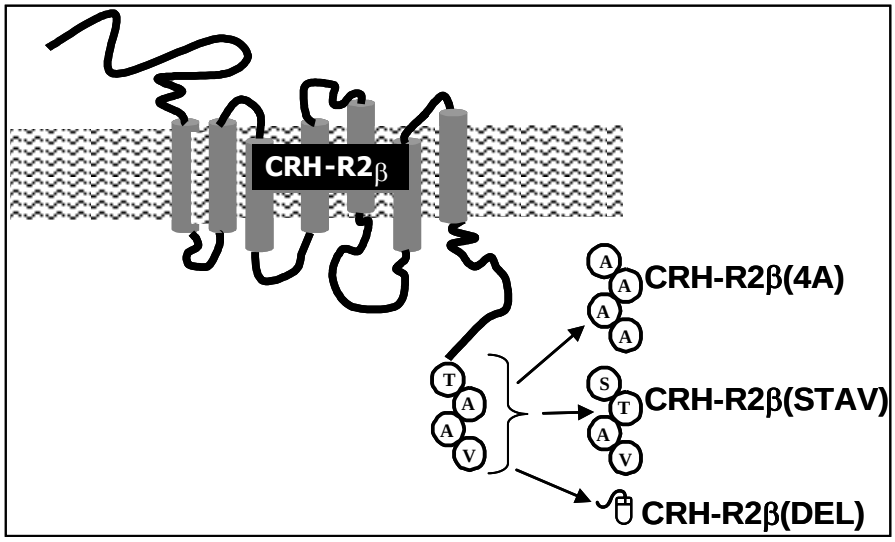

Figure 5.33. Schematic representation of the created CRH-R2β mutant receptors.

Wild-type (w.t) and mutant CRH-R2β receptors, CRH-R2β(STAV), CRH-R2β(4A), and CRH-R2β(Del), were transiently expressed in HEK293 cells. These mutant receptors were expressed normally at the cell membrane (Figure 5.34).

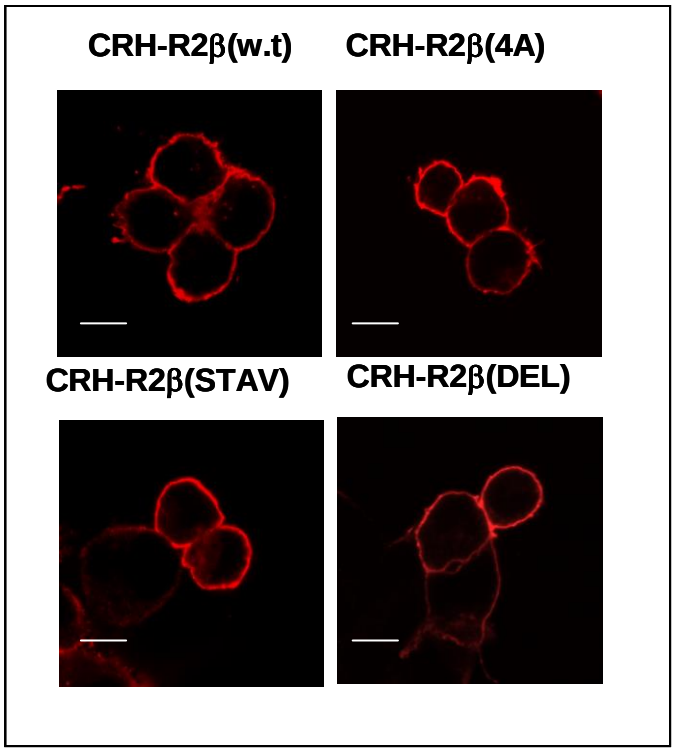

Figure 5.34. Role of CRH-R2β C-terminus amino acid cassette TAAV on receptor expression in the plasma membrane. Receptor (wild type or mutant) expression was monitored by indirect fluorescent confocal microscopy using specific primary antibodies and Alexa-Fluor® 594 secondary antibodies for CRH-R2β (red). Identical results were obtained from 3 independent transfections. Scale bar is 20 μm.

5.2.16.1 The role of CRH-R2β C-terminus in UCN-II induced cAMP production and CRH-R2β desensitization

All mutant receptors were able to stimulate intracellular cAMP production in response to 100 nM UCN-II (Figure 5.35). Interestingly, although CRH-R2β(4A) and CRH-R2β(Del) ability in stimulating cAMP response was comparable to the wild type receptor, the CRH-R2β(STAV) cAMP response was 50% greater than the wild type CRH-R2β. Furthermore, the sensitivity of both wild type and mutant receptors to desensitization, induced by UCN-II (100 nM) pretreatment for 30 min, was comparable (Figure 5.35), and no significant differences were detected.

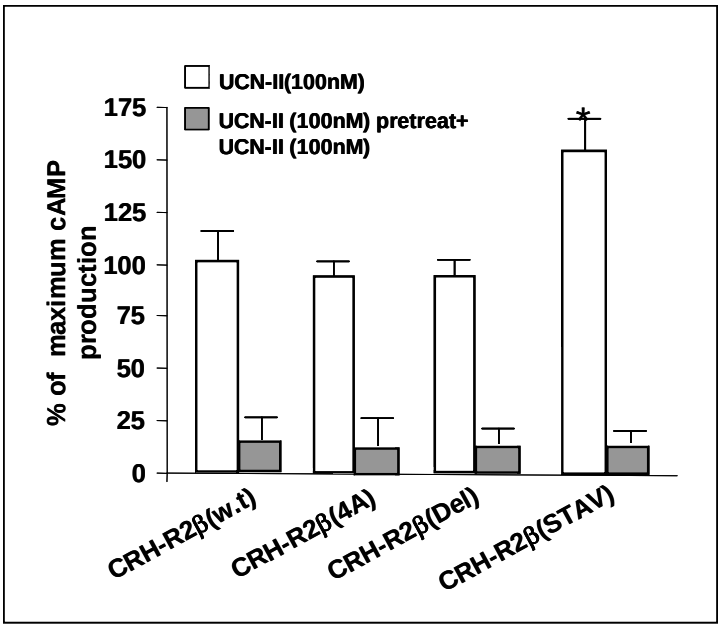

Figure 5.35. Role of CRH-R2β C-terminus amino acid cassette TAAV on UCN-II induced cAMP production and receptor desensitization. Transiently transfected HEK293 were stimulated with 100 nM UCN-II for 15 min, additionally the cells were pretreated with UCN-II (100 nM) for 30 min to induce desensitization. After extensive washing, cAMP response to a second UCN-II stimulus (100 nM for 15 min) was determined. Data represent the mean±SEM of two estimations from three independent experiments. *, P <0.05 compared to wild type CRH-R2 cAMP response.

5.2.16.2 The role of CRH-R2β C-terminus in UCN-II induced CRH-R2β internalization

The confocal microscopy studies showed that the CRH-R2β(4A) and CRH-R2β(Del) mutant receptors exhibited an increased rate of internalization compared to the wild type receptor; receptor (red) fluorescent signal was observed in the cytoplasm after only 5 min of UCN-II (Figure 5.36). All the mutant receptors substantially internalised following 30 min of UCN-II treatment. Additionally, the internalization of all mutant receptors was coincident with β-arrestin recruitment to the plasma membrane, suggesting that the process of internalization was β-arrestin

dependent (Figure 5.37). The intensity of β-arrestin recruitment was slightly impaired in the cells over-expressing the CRH-R2β(Del) mutant receptor.

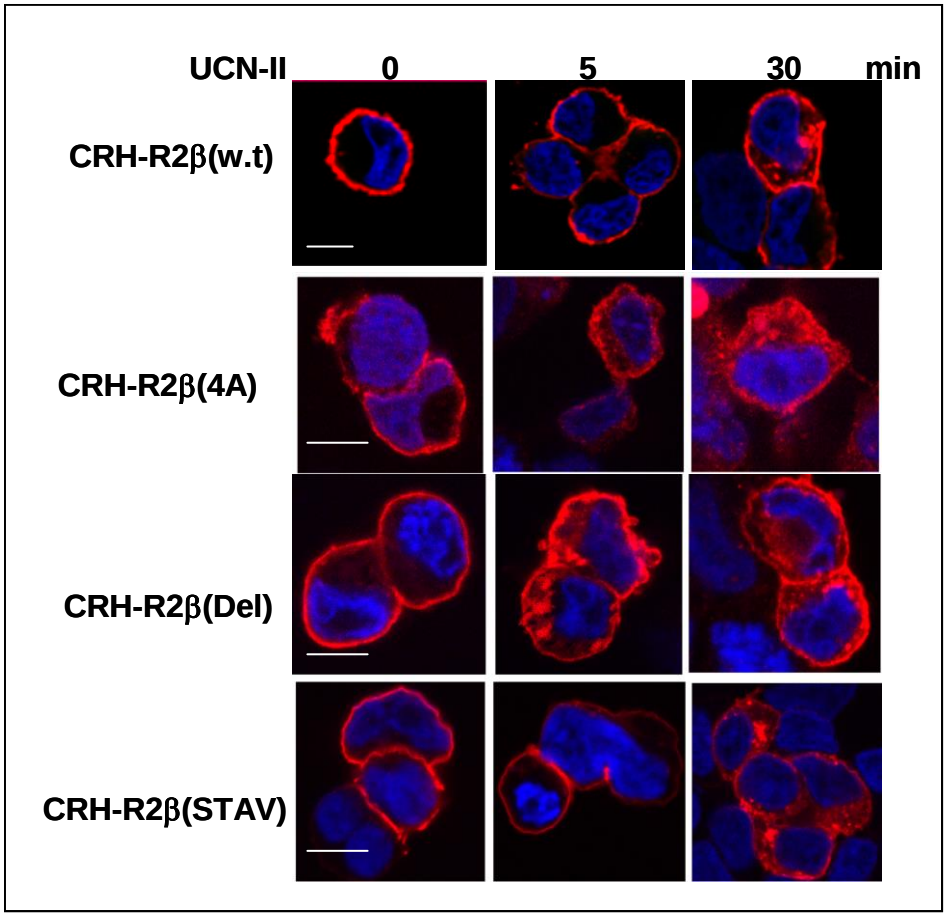

Figure 5.36. Role of CRH-R2β C-terminus amino acid cassette TAAV on receptor endocytosis. Cells were also stimulated with 100 nM UCN-II for various time intervals and CRH-R2β internalization was monitored by indirect confocal microscopy. Cell nuclei were stained with the DNA-specific dye DAPI (*blue*). Identical results were obtained from four independent experiments. Scale bar is 10 μm.

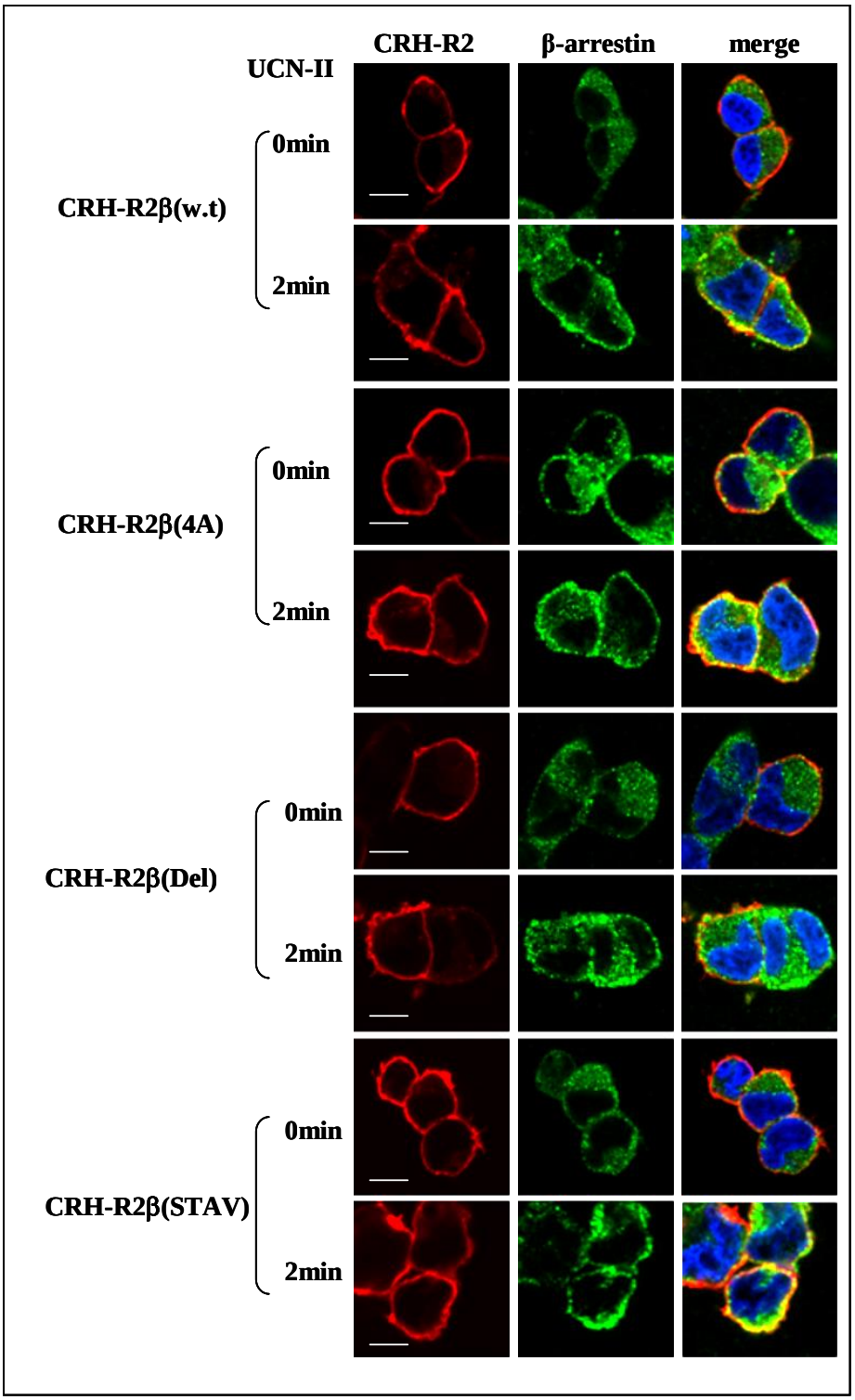

Figure 5.37. Role of CRH-R2β C-terminus amino acid cassette, TAAV, on UCN-II induced β-arrestin recruitment visualization by fluorescent confocal microscopy. Cells were stimulated with UCN-II (100 nM) for 2 min. CRH-R2β and β-arrestin distribution was monitored by indirect immunofluorescence as described in the Materials and Methods. Cell nuclei were visualized with DAPI. Scale bar is 10 μm. Identical results were obtained from 4 independent experiments.

5.2.16.3 The role of CRH-R2β C-terminus in UCN-II induced ERK1/2 and p38 MAPK phosphorylation

The temporal characteristics of ERK1/2 and p38MAPK activation of the CRH-R2β mutant receptors were also determined. HEK293 transiently transfected with the mutant receptors were stimulated with 100 nM UCN-II for 0-30 min. The western blot analysis revealed that the CRH-R2β(STAV) mutant receptor was comparable to the wild type (w.t) receptor, in activating both p38MAPK (Figure 5.38) and ERK1/2 (Figure 5.39) in response to UCN-II. However, the ability of CRH-R2β(4A), and CRH-R2β(Del) to induce ERK1/2 and p38MAPK activation was significantly impaired by 35% and 20% respectively.

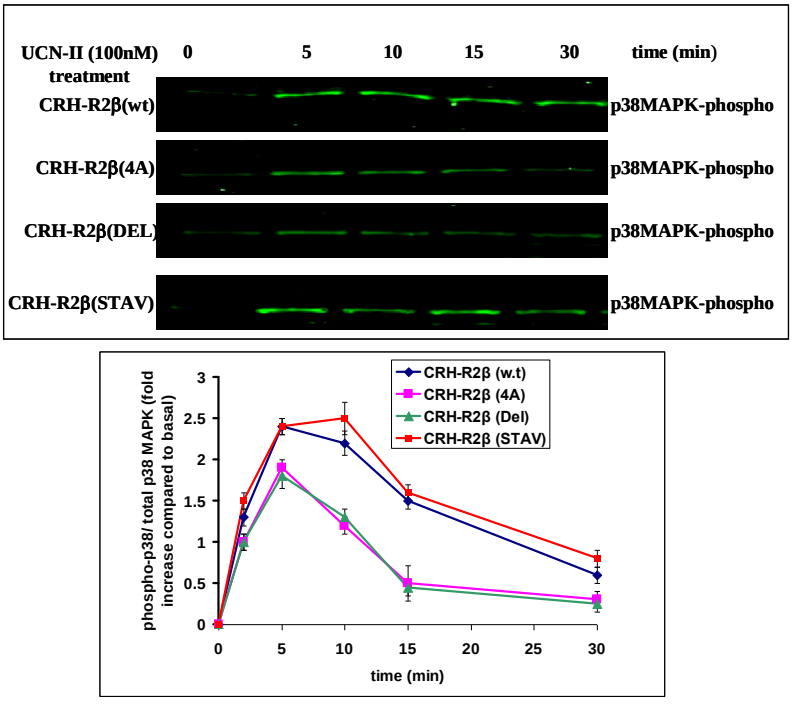

Figure 5.38. Time course of UCN-II stimulated p38 MAPK phosphorylation in HEK293 cells transiently expressing wild type or mutant CRH-R2β. HEK293 cells transiently expressing w.t and mutant CRH-R2β receptors were treated with or without UCN-II (100 nM) for various time intervals to induce MAPK activation. p38 MAPK activation was determined as described in the Materials and Methods. The data represent the mean ± SEM from three independent experiments.

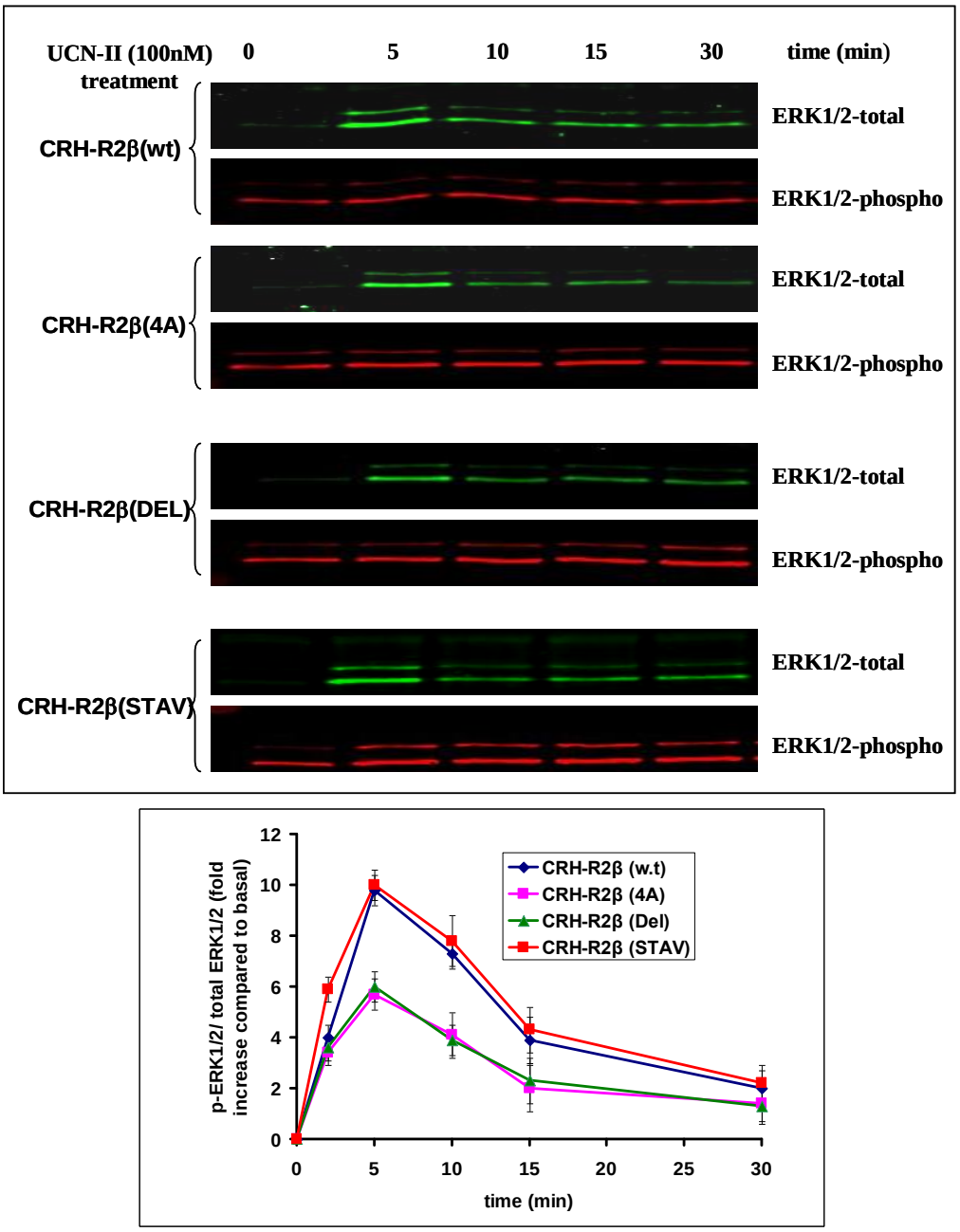

Figure 5.39. Time course of UCN-II stimulated ERK1/2 phosphorylation in HEK293 cells transiently expressing wild type or mutant CRH-R2β. HEK293 cells transiently expressing w.t and mutant CRH-R2β receptors were treated with or without UCN-II (100 nM) for various time intervals to induce MAPK activation. ERK1/2 activation was determined as described in the methods. The data represent the mean ± SEM from three independent experiments.

5.3 DISCUSSION

CRH and CRH-related peptides play a pivotal role in the body's response to stress by integrating and co-ordinating the activity of diverse physiological systems. The action of CRH and CRH-related peptides is mediated though two types of CRH-receptors (CRH-R1 and CRH-R2). The CRH-Rs transduce the signals through the cell membrane leading to the generation of second messengers (cAMP, cGMP, DAG, IP_3, Ca^{2+}), and activation of a plethora of intracellular protein kinases and other important molecules. Although originated from distinct genes, the two types of the receptors share considerable sequential homology (approximately 70%). However, the CRH-R2 gene exhibits a different splicing and distribution pattern than CRH-R1, as elaborated on the general Introduction chapter.

The aim of this part of my project was to investigate the signalling pathways and molecules whose activation was mediated via CRH-R2β, and to determine the intracellular mechanisms regulating CRH-R2 responsiveness to agonist stimulation and its potential link to activation of distinct signalling cascades. Novel evidence that the CRH-R2β functional activity is sensitive to homologous desensitization following UCN-II binding and receptor activation was provided in this chapter. In addition, the internalization properties of CRH-R2β were characterised.

One of the main intracellular mediators of CRH-R2 signalling in tissues is cAMP (Hillhouse EW & Grammatopoulos DK, 2006). In agreement with previous studies (Lewis K *et al*., 2001), this study showed that both UCN-II and UCN-I were equally efficient in inducing adenylyl cyclase activation and were 40% more effective than CRH (Figure 5.6.). Additionally, desensitization of the CRH-R2β appears to be considerably rapid and exposure to UCN-II for 15 min was sufficient

to diminish receptor activity by 80-90% (Figure 5.7). This is remarkably different from the response of the CRH-R1α, which requires agonist (CRH) treatment for 2-3 h to achieve a similar level of desensitization (Teli T *et al*., 2005). This might reflect distinct requirements of the two CRH-Rs signal propagation in mammalian pathophysiology.

Since agonist induced GPCRs desensitization and internalization go hand in hand, my study focused on investigations of the molecular mechanisms downstream of CRH-R2β desensitization. The results demonstrated that UCN-II induced a rapid and transient recruitment of both β-arrestin1 and 2 to the plasma membrane (Figure 5.20, 5.21, 5.22). Many other GPCRs that belong to the subfamily B1 ("brain-gut" neuropeptide receptors) exhibit high affinity for both β-arrestin1 and 2 and although this project did not specifically address the relative contribution of each β-arrestin isoform, it is possible that both β-arrestins are involved in CRH-R2β desensitization and endocytosis. Previous studies (Holmes KD *et al*., 2006) have demonstrated that the CRH-R1α preferentially interacts with β-arrestin2, but β-arrestin1 also translocates to the plasma membrane following CRH-R1α activation.

Translocation of β-arrestin to the plasma membrane is an important step in receptor endocytosis. β-arrestins, by binding to clathrin, promote GPCR endocytosis via clathrin-coated pits (Shenoy SK & Lefkowitz RJ, 2003). The mechanism of CRH-R2β endocytosis also appears to require clathrin, which rapidly translocates to the plasma membrane following CRH-R2β activation, since depletion of clathrin significantly impairs CRH-R2β endocytosis. These findings suggest that CRH-R2β endocytosis might occur via clathrin-coated pits, similar to CRH-R1α (Perry SJ *et al*., 2005). However, no receptor co-localization with β-arrestins inside the cells was observed, which is a characteristic of "class A" GPCRs. This is in contrast to the

"mixed" class A/class B picture previously reported for the CRH-R1α/β-arrestin interactions (Markovic D *et al*., 2006). This might have important consequences on the fate of the internalized receptor, since lack of interaction between β-arrestins and internalized class A GPCRs allows a more rapid recycling and resensitization by facilitating receptor dephosphorylation (Oakley RH *et al*., 1999). In a recent report, Tu H and colleagues (Tu H *et al*., 2007) demonstrated that UCN uptake in HEK293 overexpressing CRH-R1 and CRH-R2 was clathrin and caveolae independent, concluding that CRH-R1 and R2 play a facilitatory role in the non-clathrin, non-caveolae mediated endocytosis (Tu H *et al*., 2007). Interestingly, the authors draw this conclusion not from immunofluorescence or biochemical experiments, but solely from the use of an inhibitor of clathrin coated pits and caveolae formation.

The studies investigating CRH-R2β desensitization and endocytosis also revealed a number of interesting features. Firstly, the efficiency and kinetics of this process appears to be dependent on CRH-R2β-agonist affinity since CRH, which has a low affinity for the receptor, induced a weaker desensitization and delayed receptor endocytosis compared to UCN-II (Figure 5.7, 5.18, 5.19). The temporal characteristics of β-arrestin translocation to the plasma membrane also appeared to be differentially regulated by UCN-II and CRH and although both peptides induced rapid translocation of β-arrestins and clathrin (Figure 5.20, 5.21), CRH actions led to a prolonged association of β-arrestins to the membrane (Figure 5.21, 5.22). At present, the precise functional consequences of these differences are not known, however, it is possible that these distinct characteristics are linked to differences in receptor active conformations in response to UCN-II or CRH that potentially lead to

diverse signalling pathways in agreement with the hypothesis of "agonist-directed trafficking" (Kenakin T, 1997).

It was also showed that UCN-II binding to CRH-R2β led to a robust activation of ERK1/2 and p38MAPK (Figure 5.10-5.14), important signalling cascades for mediating CRH-R2 physiological effects (Dermitzaki E *et al*., 2002, Sananbenesi F *et al*., 2003, Karteris E *et al*., 2004). In particular, in certain cellular models, p38MAPK but not ERK1/2, is capable of modulating CRH-R2β expression and signalling since it has the potential to down-regulate CRH-R2β mRNA levels (Kageyama K *et al*., 2005). In this chapter it was demonstrated that CRH-R2β mediated ERK1/2 and p38MAPK activation was characterized by:

a) transient MAPK phosphorylation responses (Figure 5.12, and 5.13),

b) a lack of association between internalized CRH-R2β receptors and phospho-ERK1/2 or p38MAPK (Figure 5.14),

c) cytoplasmic as well as nuclear distribution of activated ERK1/2 (Figure 5.14).

Current hypotheses on GPCRs-ERK1/2 activation suggest that G protein-dependent pathways produce a transient activation of nuclear ERK1/2 whereas β-arrestin-dependent pathways lead to sustained activation of ERK1/2 that is localized to the cytosol and endosomes (Luttrell DK & Luttrell LM, 2003). Thus the absence of β-arrestin-dependent pathways in CRH-R2β mediated ERK1/2 and p38MAPK activation might explain the distinct spatio- temporal characteristics of CRH-R2β-mediated ERK1/2 phosphorylation. It has been previously reported that CRH-R1α mediates a sustained ERK1/2 activation, which is likely to be β-arrestin dependent, and is restricted primarily to the cytoplasm in stable complex formation with internalized CRH-R1α (Punn A *et al*., 2006). Moreover, data from this chapter

demonstrated that the inhibition of receptor desensitization and endocytosis (by dominant negative β-arrestin and depletion of clathrin) enhanced UCN-II MAPK activation, possibly due to increased amount of accessible active receptors expressed in the cell membrane.

In addition, this project has provided novel evidence that ERK1/2 but not P38MAPK activation is dependent on PKA activity. The interaction between cAMP/PKA and ERK1/2 signalling pathways is very complex and can occur at a number of distinct points and these effects can be tailored in a cell-specific manner (Houslay MD & Baillie GS, 2003). The cell type specific expression of Raf-1 and B-Raf isoforms allows increased cAMP levels to couple either negatively or positively to the activation of ERK. Additionally, PKA catalyses phosphorylation of protein tyrosine phosphatase (PTP) and a serine residue within a docking site on ERK2, preventing coupling between PTP and activated ERK, thus attenuating dephosphorylation of ERK (Houslay MD & Baillie GS, 2003).

It has been reported that PKA negatively regulates CRH-R1α mediated ERK1/2 activation, via phosphorylation of the receptor at Ser-301 (Papadopoulou N *et al*., 2004). In contrast, it has been reported that in various cellular systems the CRH-R1α mediated ERK1/2 activation is either independent or positively regulated by PKA, but not negatively regulated (Brar BK *et al*., 2004). The latter report states that the same pattern is involved in the CRH-R2 mediated ERK1/2 activation (Brar BK *et al*., 2004). Data provided in this chapter paint a complex picture of interactions between these two pivotal pathways in cellular functioning (Figure 5.15 and 5.16). Analysis of only one time point (2, 5 or 10 min) of UCN-II induced ERK1/2 phosphorylation in the absence of PKA activity can be deceptive. However, the detailed time course experiment (Figure 5.16) demonstrated that the interaction

between the PKA and ERK1/2 signalling cascades was not a simple one. At 2 min PKA had a negative effect on ERK1/2 activation, while at 5 and 10 min the effect was positive. This data suggest a complex regulation of ERK1/2 activation. The simplest explanation would be that the inhibition of PKA activity accelerates UCN-II induced ERK1/2 phosphorylation. However, the mechanisms remain unknown.

One of the main downstream targets of ERK1/2 appears to be β-arrestin1 (Lin F-T *et al*., 1999, Hupfeld CJ *et al*., 2005). β-arrestin1 phosphorylation at Ser-412 and function are modulated by an ERK1/2-dependent mechanism that leads to attenuation of GPCRs internalization. Cytosolic β-arrestin1 is phosphorylated at Ser-412, upon activation of GPCRs β-arrestin1 is recruited to the plasma membrane and dephosphorylated. Dephosphorylated β-arrestin1 targets agonist-occupied, GRK-phosphorylated GPCR to the clathrin-coated pits for internalisation. Activated ERK1/2 phosphorylates β-arrestin1 at Ser-412, and reduces it ability to bind certain proteins including clathrin.

The studies presented in this chapter suggested that UCN-II dependent ERK1/2 activation, although endocytosis independent (and potentially β-arrestin independent), could potentially modulate β-arrestin1 phosphorylation and membrane translocation and ultimately CRH-R2β endocytosis. Experimental conditions that diminished ERK1/2 activity, resulted in increased accumulation of β-arrestin1 to the plasma membrane and led to rapid dephoshorylation, thus allowing enhanced interaction with clathrin and an increased rate of CRH-R2β endocytosis. The precise nature of the molecular determinants regulating β-arrestin1 dephoshorylation are unknown; previous studies have shown that protein phosphatase 2A (PP2A) is found in a molecular complex with beta-arrestin1 and phosphatase inhibitors increase Ser-412 phosphorylation (Fan GH *et al*., 2001).

Thus it is possible that PP2A, through induction of β-arrestin1 dephosphorylation, directly modulates β-arrestin1 interaction with clathrin and ultimately receptor endocytosis. Evidence from other GPCR systems suggest that in this signalling assembly of GPCR/β-arrestin1, PP2A is capable of targeting multiple substrates including the receptor protein itself (Fan GH *et al*., 2001).

Interestingly, β-arrestin2 can also act as a signalling intermediate through an Akt/PP2A scaffold that can mediate inactivation of Akt in response to GPCR stimulation (Beaulieu JM *et al*., 2005). Similarly to β-arrestin1, β-arrestin2 is also regulated by phosphorylation. Casein kinase phosphorylates β-arrestin2 on Thr-383 and Ser-361 (DeWire SM *et al*., 2007).

In addition, the importance of the amino acid cassette -TAAV present at the end of the C-terminus of CRH-R2β was investigated. The cassette appears to be important for determining the rate of receptor endocytosis (Figure 5.36, 5.37), but not for receptor desensitization and activation of the cAMP pathway (Figure 5.35). Interestingly, the C-tail of CRH-R1α which exhibits a slower rate of desensitization and endocytosis, contains one extra Ser/Thr residue (-STAV). The mutagenesis studies suggest that lack of potential phospho-acceptor residues in this amino acid cassette results in accelerated receptor endocytosis. The molecular determinants of this are unknown; it is possible that absence of Ser/Thr residues from the end of the C-tail might facilitate interaction and association with signalling molecules involved in receptor endocytosis. Future studies involving RGS12 will test this hypothesis. Additionally, mutant CRH-R2β receptors [CRH-R2β(4A) and CRH-R2β(Del)] that showed a faster internalization rate exhibited a decreased MAPK response to UCN-II (Figure 5.38, 5.39). The potential effect of mutating the CRH-

R2β C-tail on G-protein coupling should also be considered as a contributing factor to the impaired MAPK response to UCN-II.

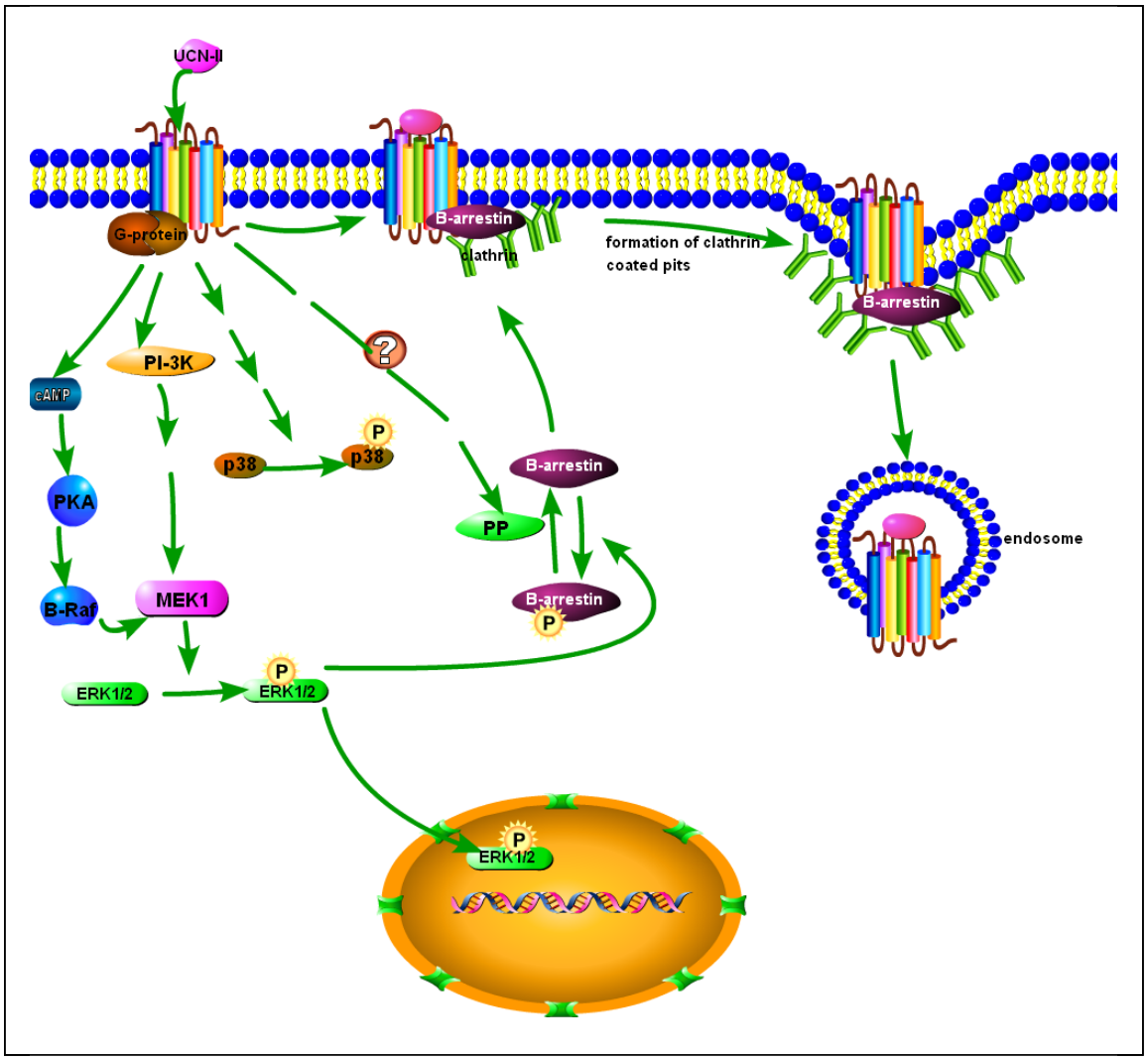

Figure 5.40. Schematic representation of signal transduction pathways activated by CRH-R2β. Binding of UCN-II to the CRH-R2β receptor leads to the activation of PKA and PI-3K which are involved in ERK1/2 activation. Phosphorylated ERK1/2 translocates to the nucleus where it potentially activates genes transcription, also ERK1/2 mediates phosphorylation of β-arrestin1 at Ser-412 leading to the retention of β-arrestin1 in the cytosol. The p38MAPK phosphorylation was independent of PKA and PI-3K activity as well as the receptor endocytic machinery.

In summary, this project demonstrated involvement of PKA and PI-3 kinase in UCN-II induced ERK1/2 activation, and that the activation of p38MAPK was independent of these two kinases. Additionally, novel evidence was demonstrating that the CRH-R2β receptor desensitization involves β-arrestin recruitment to the plasma membrane and depends on the binding and signalling potency of the desensitizing agonist. Subsequently, the receptor internalizes in a manner typical of class A GPCRs via a β-arrestin and clathrin-dependent mechanism. The kinetics and pattern of trafficking partners differs significantly from the corresponding mechanism regulating CRH-R1α functional activity, a finding that might have important implications for the elucidation of CRH and UCNs signal propagation in mammalian pathophysiology. Furthermore, it was shown that this mechanism is not involved in the activation of ERK1/2 and p38MAPK cascades, and this functional independence allows distinct spatio-temporal control of MAPK activity by UCNs and CRH-R2β.The transiently and β-arrestin independently activated ERK1/2 translocates to the nucleus where it possibly activates gene transcription. Moreover, it seems that activated ERK1/2 also regulate CRH-R2β endocytosis via direct phosphorylation of β-arrestin1 at Ser-412 in a mechanism that influences the rate and extent of β-arrestin1 recruitment to the plasma membrane (Figure 5.40).

6 THE REGULATION OF EXPRESSION AND SIGNALLING CHARACTERISTICS OF ENDOGENOUS CRH-Rs IN HUMAN PREGNANT MYOMETRIAL CELLS

6.1 INTRODUCTION

Corticortopin releasing hormone (CRH), a hypothalamic stress peptide, is also produced by the placenta of pregnant primates and released into the circulation, suggesting a potential role of the hormone in reproduction (Linton EA *et al*., 2001). During gestation the uterus remains in a state of quiescence whilst the foetus matures. At term, delivery is facilitated by cervical dilatation and a switch of the uterus from quiescence to a state of co-ordinated contractility (Challis JRG *et al*., 2000). The mechanism controlling myometrial transition from relaxation to active contractions during pregnancy and labour are still unknown. CRH and related peptides, urocortins (UCNs) might play an important role in foetus implantation and endocrinology of pregnancy. CRH, produced by the trophoblast, promotes blastocyst implantation and facilitates immune tolerance of the early pregnancy by killing maternal activated T cells (Carr BR & Rehman KS, 2004). Placentaly derived CRH increases exponentially in maternal plasma throughout pregnancy and peaks during labour and delivery. Levels of CRH at term may be 50- to 100-fold higher than those in non pregnant women. There is also an increase in carrier protein, CRH-binding protein (CRH-BP), which binds CRH and may blunt the

increase in CRH biological activity, protecting against inappropriate stimulation of the HPA axis. However, near the end of normal pregnancy, with the exponential rise in plasma CRH, levels of CRH-BP fall gradually to half of those of earlier pregnancy (Linton EA *et* al., 2001). Elevated levels of maternal plasma CRH have been found in women in preterm labour who are destined to deliver within 24-48 hours, compared with those who continued pregnancy despite threatened preterm labour. Moreover, in preterm labour and pre-eclampsia, maternal plasma CRH levels are higher and CRH-BP levels are lower than in normal pregnancy; but in women who deliver postdate, plasma CRH levels are lower while CRH-BP is higher than in normal pregnancy (McLean M *et al*, 1995). Thus, the plasma concentrations of CRH may act as a predictor or a "placental clock" of the duration of human gestation (McLean M *et al*, 1995).

The precise biological function of CRH and UCNs during pregnancy is not well defined but they appear to play important roles in regulation of myometrial contractility (Grammatopoulos DK & Hillhouse EW, 1999) either directly by inducing myosin light chain phosphorylation that could lead to increased contractility (Karteris E *et al*., 2004) or indirectly by stimulating the production of prostaglandins in the decidua and fetal membrane (Patraglia F *et al*., 1995; Jones SA & Challis JR, 1989). It is likely that placental CRH influences the fetal adrenal cortex by modulating the fetal pituitary-adrenal axis (Mesiano S & Jaffe RB, 1997). It has been proposed that late in gestation, cortisol produced by the fetal adrenal cortex blocks the inhibitory effect of progesterone on placental CRH production (Karelis K *et al*., 1996). As a consequence, the levels of placentaly produced CRH increase in the fetal compartments, leading to the further stimulation of fetal ATCH production, which stimulates cortisol and dehydroepiandrosterone sulphate (DHEA-

S) production. These steroid hormones produced by fetal adrenal cortex regulate intrauterine homeostasis and the maturation of fetal organs (Karelis K *et al*., 1996; Mesiano S & Jaffe RB, 1997).

The human myometrium expresses a plethora of CRH and CRH-related peptides and their respective receptors R1 and R2 (Hillhouse EW & Grammatopoulos DK, 2001). Current evidence suggests that CRH-R1 and R2-activated signalling pathways might exert distinct actions in the regulation of myometrial contractility. The myometrial CRH-Rs exhibit increased affinity for CRH during pregnancy (Hillhouse EW *et al*., 1993) and upon agonist activation stimulate cAMP and cGMP production and nitric oxide synthase (NOS) up-regulation (Aggelidou E *et al*., 2002); thus promoting myometrial quiescence, possibly though activation of CRH-R1 receptors. Recent isometric contractility studies in myometrial tissue strips have confirmed CRH ability to relax the human pregnant myometrium (Mignot TM *et al*., 2005). In contrast, CRH-R2-specific agonists such as UCN-II can activate MAPK and RhoA pathways which actively promote myometrial contractility (Karteris E *et al*., 2004). Furthermore, progression of human pregnancy towards term and active labour is associated with activation of intracellular mechanisms involving uterotonin-activated PKC that reduces the myometrial responsiveness to CRH, an effect mediated through phosphorylation and desensitization of specific CRH-R variants (Grammatopoulos DK & Hillhouse EW, 1999 b, Markovic D *et al*., 2006).

Furthermore, pregnant and non-pregnant myometrium have a different CRH receptors profile. Seven subtypes of the CRH receptors were found in the human pregnant myometrium at term before the onset of labor, R1α, R1β, R1c, R2α, R2β, and R2γ (Grammatopoulos DK *et al*., 1998), and the splice variant R1d

(Grammatopoulos DK *et* al., 1999), whereas only three subtypes, R1α, R1β and R2β were found in the non-pregnant myometrium. This differential expression pattern of the CRH-R during pregnancy suggests that CRH, acting via different receptor subtypes, might be able to exert distinct actions on the human myometrium in the pregnant, compared to the non-pregnant state (Grammatopoulos DK *et al*., 1998).

The human CRH-R1 gene spans over a 50.3-kb region and contains 14 exons (Hillhouse EW & Grammatopoulos DK, 2006); translation of all exons results in a human-specific, 444 amino acid 7TMD protein receptor, termed CRH-R1β, which exhibits impaired agonist-binding and signalling properties. Deletion of exon 6 results in expression of CRH-R1α mRNA, which is the main functional CRH-R1 receptor variant and contains 415 amino acids. Therefore, the CRH-R1β can be considered as a "pro-CRH-R1" receptor variant (Hillhouse EW & Grammatopoulos DK, 2006). The CRH-R1 gene appears to be subject to significant alternative splicing and a growing number of CRH-R1 mRNA splice variants have been described, termed R1c-n (Hillhouse EW & Grammatopoulos DK, 2006). All these variants have exon 6 spliced out together with other deletions. At least 4 distinct CRH-R1 mRNA variants (α, β, c and d) have been identified in human myometrium during pregnancy (Grammatopoulos DK *et al*., 1998); progression towards term is associated with altered expression of myometrial CRH-Rs and the appearance of CRH-R1 variants such as the R1d, with reduced signalling abilities (Grammatopoulos *et al*., 1999). This might have important functional consequences by dampening tissue responsiveness to CRH actions.

The mechanisms regulating myometrial CRH-R1 expression are not well understood. The CRH-R1 promoter contains, amongst others, putative nuclear

factor-kappa B (NF-κB) recognition elements (κBs) (Parham KL *et al*., 2004). Accumulating evidence points towards a role for NF-κB and its major activator IL-1β, in the physiology and pathophysiology of labour (Lindstrom TM & Bennett PR, 2005), since myometrial IL-1β and NF-κB activity increases with the onset of labour and is central to multiple prolabour pathways by stimulating prostaglandin H synthase 2 (PGHS-2), also known as cyclooxygenase 2 (COX-2), expression and prostaglandin (PG) synthesis (Belt AR *et al*., 1999).

NF-κB is a transcription factor, composed of homo- or heterodimeres of the Rel family members including NF-κB1 (p50), NF-κB2 (p52), RelA (p65), RelB, and c-Rel (Chen FE and Ghosh S, 1999). NF-κB is sequestered in the cytoplasm of unstimulated cells via binding to an inhibitor protein, IκB. Following the cell stimulation, the activated IκB kinase (IKK) complex, predominantly acting through IKKβ in an IKKγ-dependent manner, catalyzes the phosphorylation of IκBα at Ser-32 and Ser-36 (DiDonato JA *et al*., 1997) and NF-κB at Ser536 in p65 (Ghosh S & Karin M, 2002). The phosphorylated IκBα undergoes polyubiquitination and subsequent degradation by the 26S proteosome. The released NF-κB dimers (most commonly p65/p50) translocate to the nucleus, bind DNA and regulate gene transcription (Jiang X *et al*., 2003).

In this part of the project, the investigation was focused on the endogenous CRH system in human pregnant myometrial cells. The aim was to characterise the regulation of CRH-R1 gene expression and in particular the effects of IL-1β. In the second part of the chapter, some of the signalling characteristics of CRH-R activated by UCN-II (CRH-R2 specific agonist) were described.

6.2 RESULTS

THE EFFECT OF IL-1β ON MYOMETRIAL CRH-R1 SPLICE VARIANT EXPRESSION

6.2.1 CRH-R mRNA and protein expression in primary myometrial smooth muscle cells

The differential expression levels of CRH–R1 mRNA transcripts in human myometrial biopsies during labour, was investigated in primary myometrial smooth muscle cells. Qualitative RT-PCR studies confirmed the expression of multiple CRH-R1 (including CRH-R1β) mRNAs (Figure 6.2 A) (Markovic D *et al*., 2007). Additionally, the expression of CRH-R2 mRNA was also confirmed (Figure 6.2 B)

Moreover, indirect immunofluorescence with a CRH-R1/2-specific antibody was used to monitor distribution of CRH-R and counterstaining with phalloidin to detect filamentous–actin (F-actin) stress fibres and the nuclear stain DAPI. Confocal microscopy studies demonstrated a strong CRH-R-positive immunostaining in the plasma membrane and the cytoplasm (Figure 6.2 C); significant co-localization between the CRH-R and F-actin immunostaining was observed in the plasma membrane (yellow colour, Figure 6.2 C), suggestive of some common subcellular localization of CRH-R and actin stress fibres. Additionally, strong intracellular staining was observed as well as "hot spots" of the receptor expression on the plasma membrane of myocytes (Figure 6.1 A). The specificity of the signal was confirmed with a pre-absorption of the antibody along with the corresponding blocking peptide when no staining was detected (Figure 6.1 B). Unfortunately, a lack of variant-specific antibody prevented further protein

splice variant characterisation of the expressed CRH-R in primary cell systems (Markovic D *et al*., 2007a).

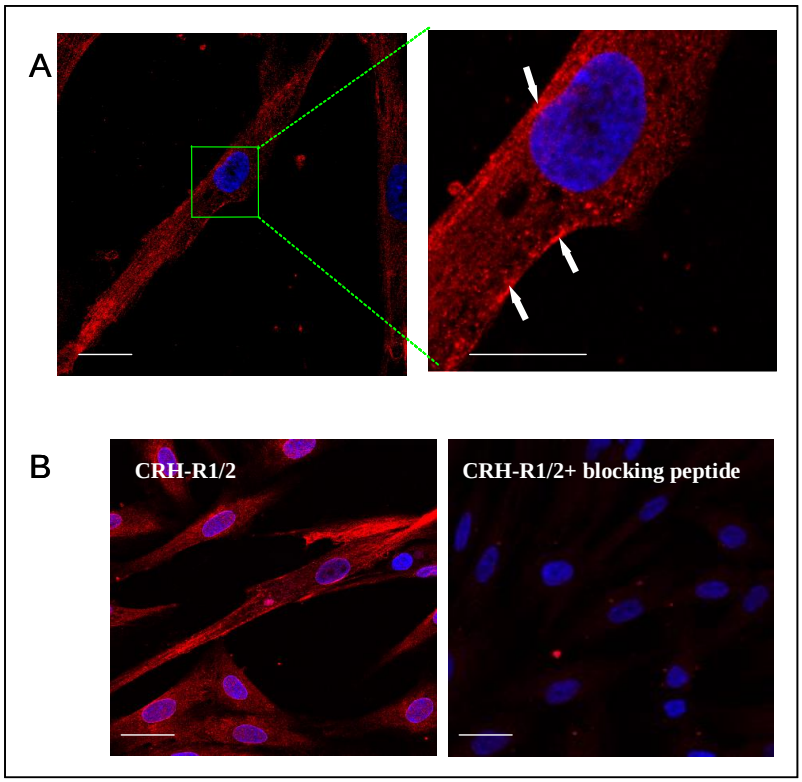

Figure 6.1. Visualization of endogenous CRH-R distribution in primary myometrial cells. Indirect immunofluorescent confocal microscopy and specific primary antibody for CRH-R and Alexa-Fluor®594 (red) were used. A. The CRH-R receptor in primary myometrial smooth muscle cells was expressed in the plasma membrane (white arrows) and in the intracellular compartments (Markovic D *et al*., 2007). B. The specificity of CRH-R antibody was demonstrated with a lack of immunoreactivity following pre-absorption of the antibody with the blocking peptide as described in the Materials and Methods. The cell nuclei were visualised using the DNA specific dye-DAPI. Scale bar is 15µm. Identical results were obtained in three independent experiments.

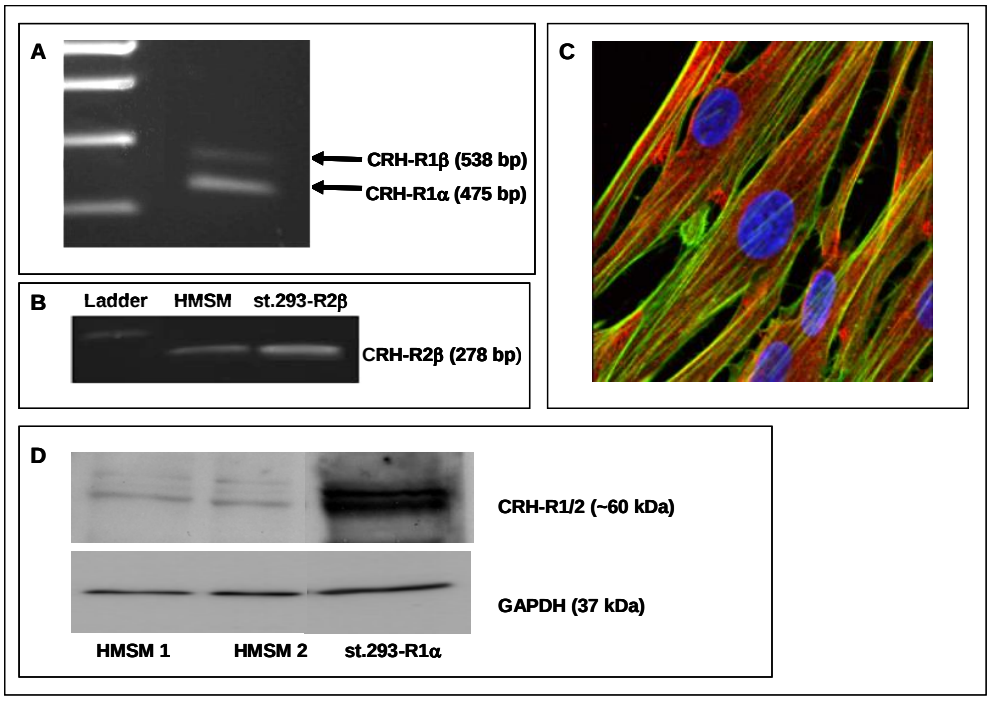

Figure 6.2. Detection of CRH-Rs in HMSM cells. A. RT-PCR amplification of CRH-R1 variants sequences from RNA extracted from primary human myometrial cell cultures. Specific primers able to amplify CRH-R1α, R1β and R1d mRNA were used as described in Methods. Primer sets were designed to amplify a 475-bp fragment, present in CRH-R1α and R1d (but not R1c) mRNA or a 538-bp fragment, present in CRH-R1β mRNA. PCR products were resolved on 1.2% agarose gel and stained with ethidium bromide. The identities of the fragments were confirmed by direct nucleotide sequencing. **B.** RT-PCR amplification of CRH-R2 sequences from RNA extracted from primary human myometrial cell cultures. The primer set was design to amplify all three variants of CRH-R2. **C.** Visualization of CRH-R distribution in HMSM cells by indirect immunofluorescence confocal microscopy using specific primary antibodies for CRH-R and Alexa-Fluor®594 secondary antibody *(red)* and phalloidin (Alexa-Fluor®488 green) as described in Methods. Cell nuclei were stained with the DNA specific dye DAPI (blue). Identical results were obtained from three independent experiments. **D.** Western blot analysis of HMSM cells lysates. The presence of CRH-Rs was identified by using CRH-R1/2 antibody as described in the Materials and Methods (Markovic D *et al*., 2007a).

Using the antibody that recognises both types of CRH-R for a western blot analysis, two immnuoreactive bands with approximate molecular weight of 60 kDa were detected (Figure 6.2 D). These two bands could represent different CRH

receptor types or splice variants, but also could be a result of post-translational modifications such as glycosylation and phosphorylation.

6.2.2 Effects of IL-1β on PGHS-2 mRNA and protein expression in primary myometrial smooth muscle cells.

It is a well established fact that pro-inflammatory cytokines, especially IL-1β are important regulators of myometrial smooth muscle cell gene expression during pregnancy by activating NF-κB, p38 MAPK, and ERK1/2 (Barlett SR *et al*., 1999; Sooranna SR *et al*., 2005). To confirm the functional activity of IL-1β in these cells, experiments were carried out in cells treated with IL-1β for various time-intervals and expression levels of PGHS-2 mRNA and protein were determined by quantitative RT-PCR and immunoblot and immunofluorescent analysis using a specific antibodies.

Results of real-time PCR and semi-quantitative PCR analysis showed that exposure of HMSM cells to IL-1β (1 ng/ml) significantly up-regulated PGHS-2 mRNA levels in a time-dependent manner (Figure 6.3). A semi-quantitative PCR analysis was performed as described in the Materials and Methods. As an internal standard, primers that amplify 18S were used. The PCR reaction was set with both sets of the primers in the same PCR reaction. Two bands were obtained from each PCR reaction (Figure 6.3A). The top band of 525 bp was a product of 18S amplification and a 305 bp band was a product of PGHS-2 amplification. At time point 0 h the levels of PGHS-2 mRNA were barely detectable. After 2 h of IL-1β treatment substantial levels of PGHS-2 mRNA were detected. The effect of IL-1β on PGHS-2 mRNA levels was more profound after 6 and 18 h (Figure 6.3A).

These results were confirmed by quantitative real time PCR: IL-1β significantly increased PGHS-2 mRNA after 2 h of incubation (by 60 fold above basal), and achieved maximal response after 18 h (300 fold above basal) (Figure 6.3 B) (Markovic D *et al*., 2007a).

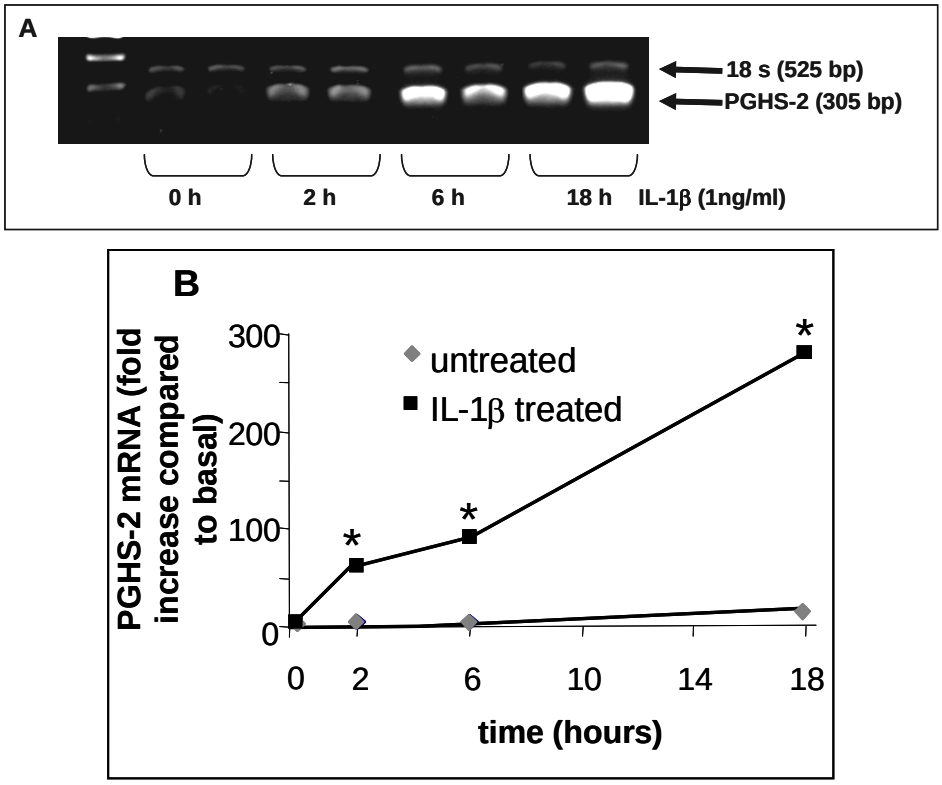

Figure 6.3. Time course of the IL-1β effects on PGHS-2 mRNA expression. HMSM cells isolated from myometrium of non-labouring women (n=6) were treated with IL-1β (1 ng/ml) for various time-intervals and PGHS-2 mRNA analysed by semi-quantitative PCR **(A)** and by real-time quantitative PCR (Lightcycler) **(B)**. On the panel B, data are expressed as the mean ± SEM of relative mRNA expression levels normalised against β-actin mRNA, and compared to basal (t=0). **P*<0·05 compared to basal (time=0 h).

Additionally, the protein levels of PGHS-2 following IL-1β treatments were analysed by Western blot analysis (Figure 6.4). The increase in PGHS-2 protein expression mirrored the increase in the mRNA levels. Treatment of 1 ng/ml IL-1β for 2 h induced a significant increase in PGHS-2 protein expression

(20 fold above basal). The effect of IL-1β was maximal after 18 h when PGHS-2 protein levels were increased by 140 fold above basal (Figure 6.4) (Markovic D *et al*., 2007a).

The IL-1β induced PGHS-2 protein levels were also detected by indirect confocal microscopy studies (Figure 6.5). Prior to IL-1β stimulation, the PGHS-2 protein could not be detected by immunofluorescence; however, after 18 h of IL-1β treatment significant levels of PGHS-2 proteins were detected in the cytoplasm of HMSM cells (Figure 6.5), evident by the appearance of red signal (originated from PGHS-2 specific antibody and Alexa-Fluor®594 secondary antibody).

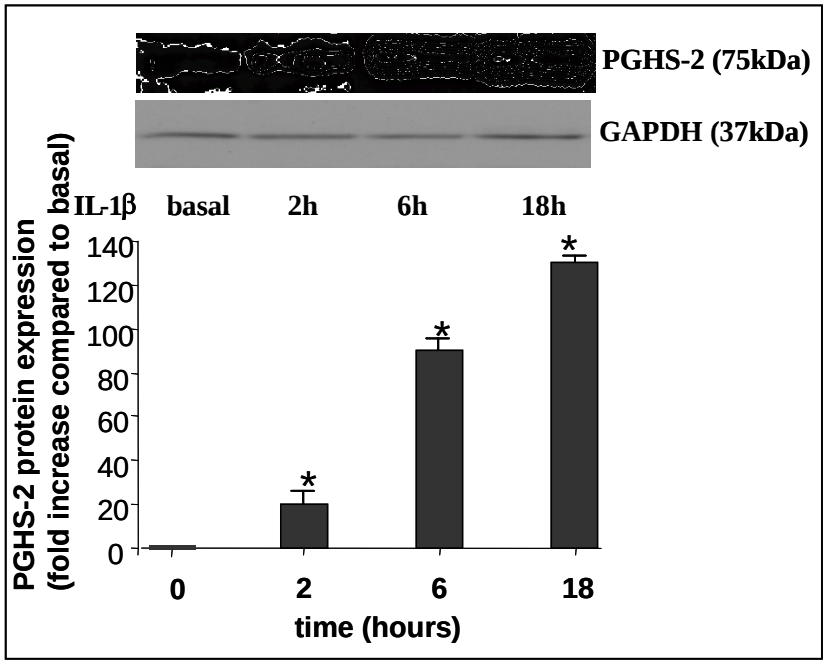

Figure 6.4. Time course of the IL-1β effects on PGHS-2 protein expression. HMSM cells isolated from myometrium of non-labouring women (n=6) were treated with IL-1β (1 ng/ml) for various time-intervals and PGHS-2 proteins were analysed by western blotting. Data are expressed as the mean ± SEM of relative protein expression levels normalised against GAPDH protein levels and compared to basal (t=0). **P*<0·05 compared to basal. A representative western blot was shown on the top part of the figure.

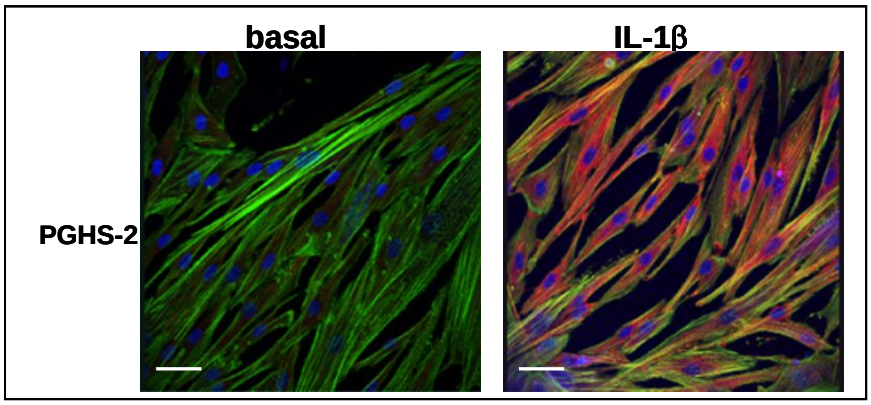

Figure 6.5. The effect of IL-1β on PGHS-2 protein expression monitored by indirect immunofluorescence confocal microscopy. The cells were grown on cover slips and treated with IL-1β (1 ng/ml) for 18 h. The PGHS-2 protein was visualised using specific primary antibodies for PGHS-2 and Alexa-Fluor®594 secondary antibody (red). Distribution of F-actin and stress fibers was also monitored by double staining with Alexa Fluor®488 phalloidin (green). Cell nuclei were stained with the DNA specific dye DAPI (blue). Identical results were obtained from three independent experiments. Scale bar is 20 μm.

6.2.3 Effects of IL-1β on CRH-R1 mRNA and protein expression in primary myometrial smooth muscle cells

The effects of IL-1β treatments on CRH-R1 mRNA and protein levels were also investigated. The semi-quantitative analysis of CRH-R1 mRNA expression suggested that IL-1β (1 ng/ml) treatment for 18 h influenced the expression of CRH-R1α and CRH-R1β mRNA (Figure 6.6 A). At the basal state both splice variants were expressed; however, following the 18 h treatment with IL-1β the CRH-R1 splice variant expression profile changed. The intensity of the top band, CRH-R1β, was significantly reduced, while the intensity of the bottom band (CRH-R1α) was substantially increased (Figure 6.6A).

Moreover, a quantitative real time PCR analysis, performed by Dr Mei Gu, confirmed these observations. IL-1β treatment for 18 h increased myometrial cell CRH-R1$_T$(α) mRNA expression by 3 fold whilst significantly attenuating myometrial CRH-R1β mRNA expression by 40% (Figure 6.6B). In contrast, IL-1β treatments for 2 or 6 h had no effect on myometrial cell CRH-R1 (total) and CRH-R1β mRNA expression levels (Figure 6.6B) (Markovic D *et al*., 2007a).

No significant changes in CRH-R protein expression were detected following IL-1β treatment, as demonstrated by western blot analysis (Figure 6.7A) and indirect confocal microscopy studies (Figure 6.7B). However, these data cannot be correlated to the mRNA data, due to lack of CRH-R1 splice variant specific antibodies.

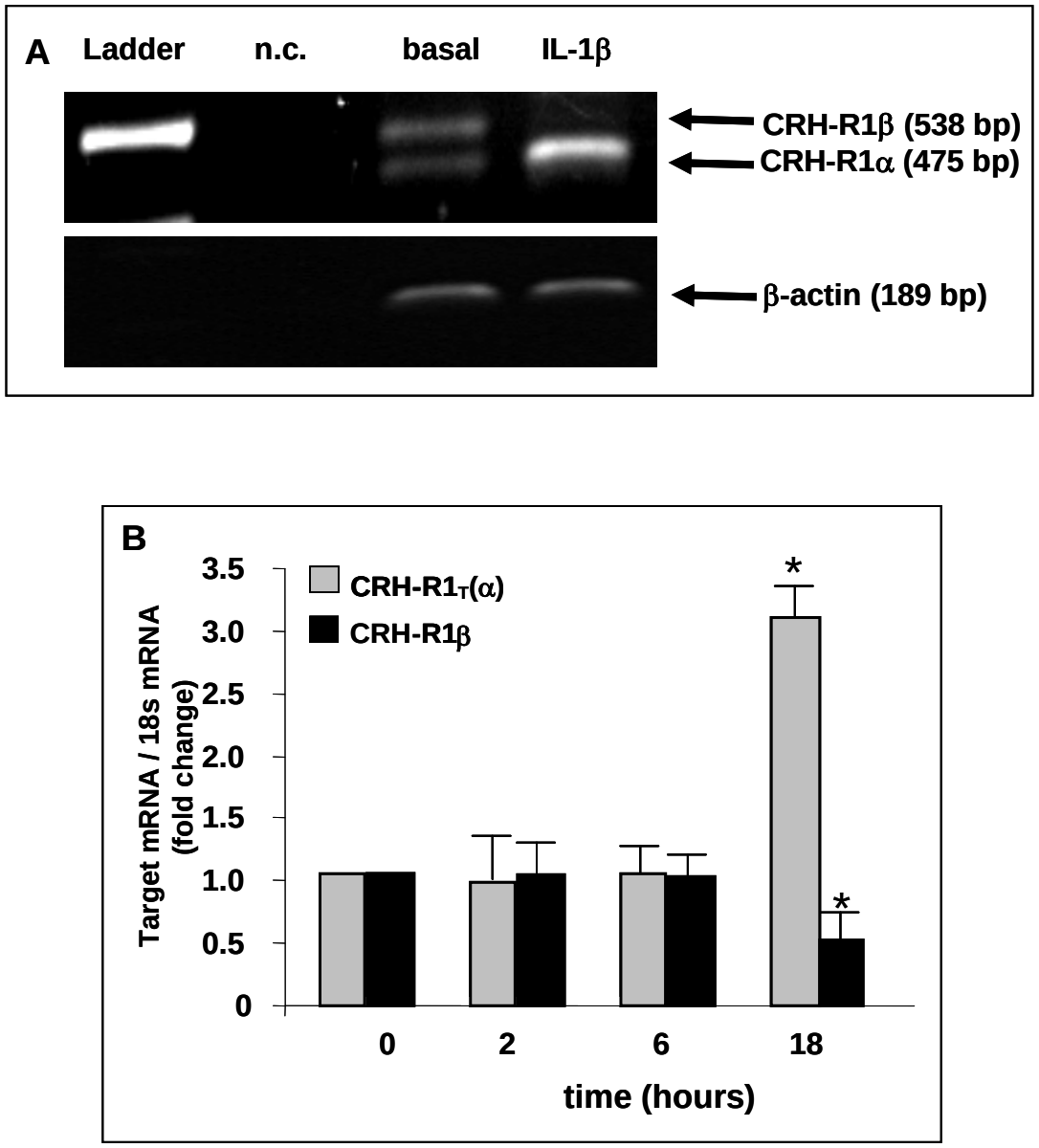

Figure 6.6. The IL-1β effect on CRH-R1 mRNA expression. A. Conventional PCR analysis of IL-1β effects on CRH-R1 mRNA levels following 18 h treatment; n.c, negative control. **B.** Quantitative PCR analysis: time course of the IL-1β effect on CRH-R1 (total) and CRH-R1β mRNA level in human myometrial smooth muscle cells. Cells isolated from myometrium of nonlabouring women (n=6) were treated with IL-1β (1 ng/ml) for various time-intervals and target mRNA were determined by real-time RT-PCR (Taqman) as described in the Materials and Methods. Data are expressed as mean values ± SEM of relative mRNA expression levels normalised against 18S RNA. **P*<0·05 compared to basal (time = 0). The mean results of basal untreated mRNA concentrations were arbitrarily assigned the value 1.

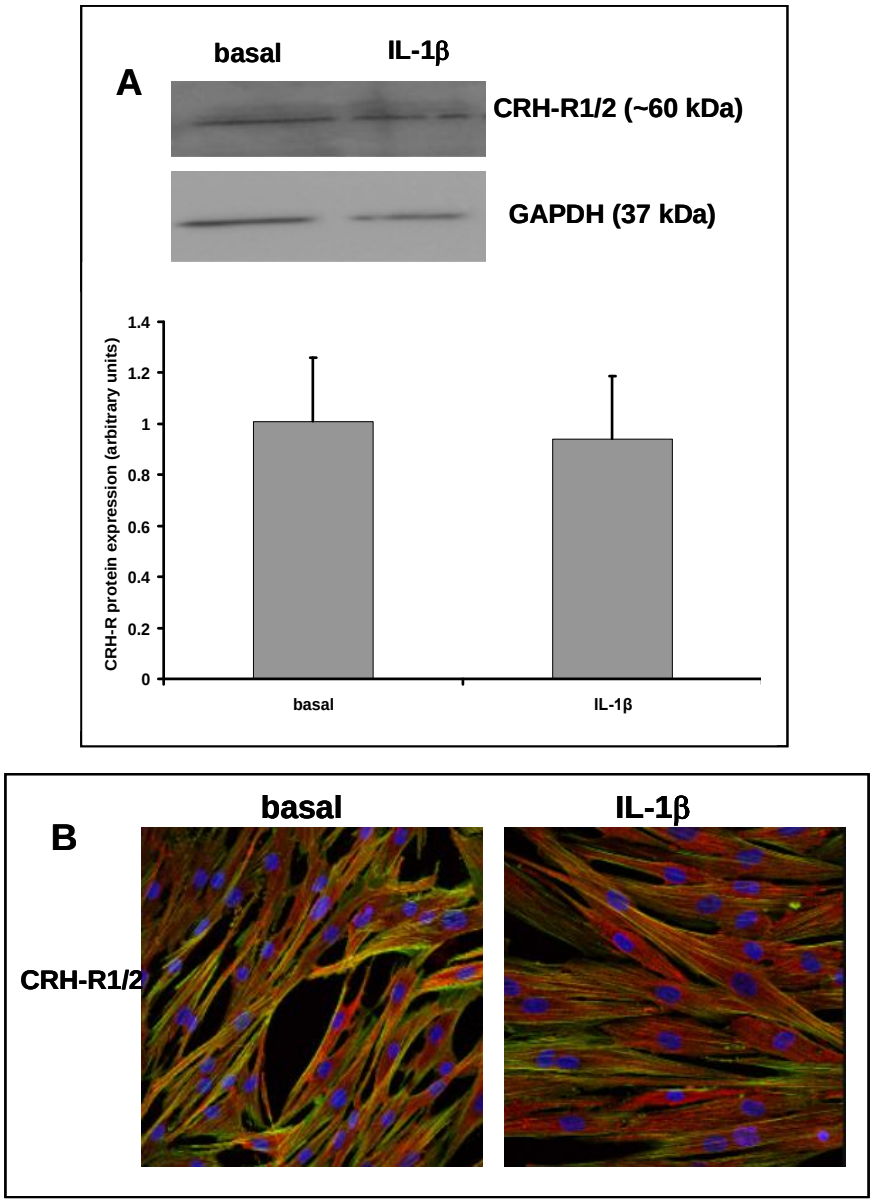

Figure 6.7. The effect of IL-1β on CRH-R protein expression monitored by western blot (A) and indirect immunofluorescence confocal microscopy (B). A. HMSM cells isolated from myometrium of non-labouring women (n=3) were treated with IL-1β (1 ng/ml) for 18 h and CRH-R proteins were analysed by western blotting. Results are presented as the mean ± SEM of three experiments. **B.** The cells were grown on cover slips and treated with IL-1β (1 ng/ml) for 18 h. The CRH-R protein was visualised using specific primary antibodies for CRH-R1/2 and Alexa-Fluor®594 secondary antibody (red). Distribution of F-actin and stress fibers was also monitored by double staining with Alexa Fluor®488 phalloidin (green). Cell nuclei were stained with the DNA specific dye DAPI (blue). Identical results were obtained from three independent experiments.

6.2.4 Signalling pathways mediating IL-1β effects in myometrial cells

NF-κB, a transcription factor composed of homo- or heterodimers of the Rel family members, (p50, p52, p65, RelB and c-Rel) is a major key intermediate of IL-1β actions in myometrial cells (Lindstrom TM & Bennett PR, 2005). Thus, the aim of this study was to investigate the potential role of NF-κB on IL-1β-induced PGHS-2 and CRH-R1 mRNA variant expression. Confocal microscopy studies were employed using a specific p65 (RelA) antibody to demonstrate that in untreated cells p65 immunoreactivity was exclusively found in the cytoplasm (Figure 6.8). Exposure of myometrial cells to IL-1β (1 ng/ml) induced nuclear translocation of p65 within 30min, this response was sustained for at least 1 h (Figure 6.8) (Markovic D *et al*., 2007a).

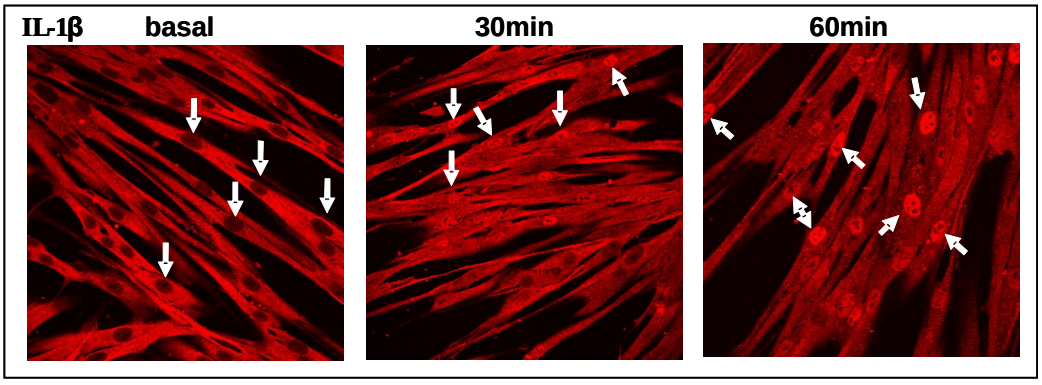

Figure 6.8. IL-1β-induced p65 translocation. Human smooth muscle cells isolated from myometrium of non-labouring women (n=6) were treated with IL-1β (1 ng/ml) for various time-intervals and p65 (RelA) nuclear translocation was monitored by indirect immunofluorescence confocal microscopy using specific primary antibodies for p65 and Alexa-Fluor®594 secondary antibody (red) as described in the Materials and Methods. The white arrows point towards cell nuclei (Markovic D *et al*., 2007a).

IκBα is a protein that retains NFκB in an inactive form through association and masking its nuclear localisation sequence (Lindstrom TM & Bennett PR, 2005). IL-1β induced rapid phosphorylation of IκBα, indicated by the appearance of another

immunoreactive protein with a slightly higher molecular weight (Newton R *et al*., 1998) and subsequent (almost complete) degradation of IκBα within 30 min (Figure 6.9) (Markovic D *et al*., 2007a).

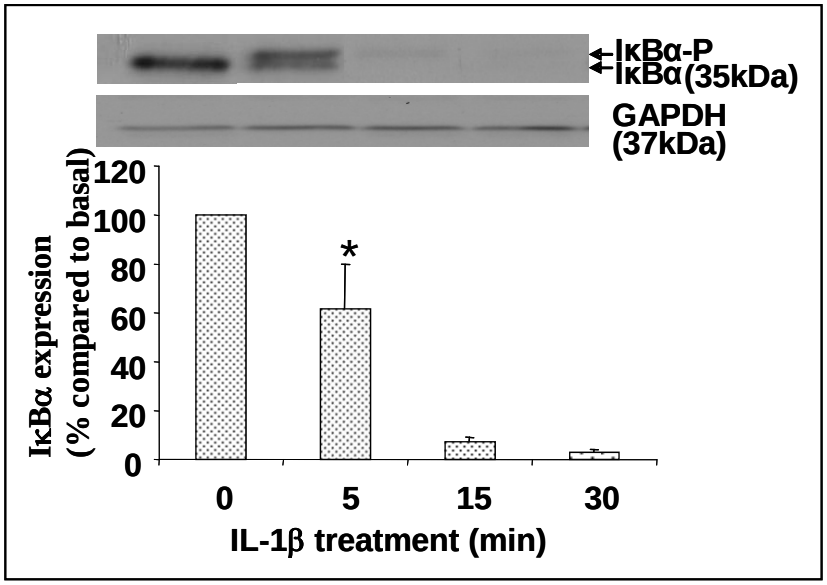

Figure 6.9. IL-1β-induced degradation of IκBα. Representative western blots of IκBα expression of cells stimulated with IL-1β (1ng/ml) for various time-intervals as described in the Materials and Methods. The data are normalized with GAPDH and represented as the mean ± SEM of 3 estimations from three independent experiments. **P*<0.05 compared to basal (Markovic D *et al*., 2007a)

The role of the upstream IκB kinase (IKK) was evaluated by the use of a specific IKK inhibitor II-Wedelolactone (Pande V & Ramos MJ, 2005) and determination of myometrial IκBα degradation following IL-1β treatment. Pretreatment of cells with 25 μM of IKK inhibitor II-Wedelolactone for 4 h abolished IL-1β-induced IκBα degradation and p65 (RelA) nuclear translocation (Figure 6.10).

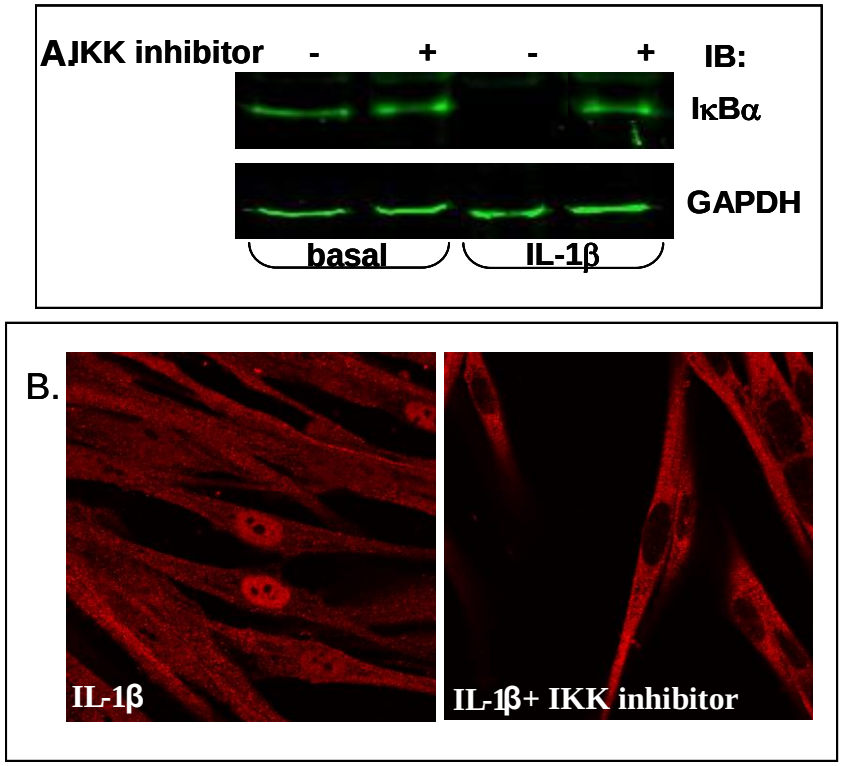

Figure 6.10. The inhibitory effect of IKK inhibitor II on IL-1β induced IκBα degradation and p65 translocation. The cells were pre-treated with or without 25 μM of IKK inhibitor II- Wedelolactone for 4 h, prior to IL-1β addition for 1h. Identical results were obtained from four independent experiments. **A.** Representative western blots of IκBα expression of cells stimulated with IL-1β (1ng/ml) for 1h in the presence and absence of the inhibitor. Immunoreactivity was detected by secondary antibodies conjugated to IRDye 800™ and the Odyssey detection system as described in the Materials and Methods. **B.** Cells were grown on cover slips and treated as above. The translocation of p65 was detected as described at figure 6.8. (Markovic D *et al*., 2007a).

Most importantly, the IKK inhibitor II significantly attenuated IL-1β-induced up-regulation of both PGHS-2 and CRH-R1 mRNA expression (Figure 6.11). Previous investigations have shown that IL-1β effects on myometrial PGHS-2 up-regulation involve ERK and p38 MAPK (Sooranna SR *et al*., 2005). The role of these kinases on IL-1β-induced regulation of myometrial target gene expression was investigated by employing U0126 (a specific MEK1/2 inhibitor) and SB 203580 (a

p38 MAPK inhibitor). Pretreatment of myometrial cells with each inhibitor significantly attenuated by 70-85% IL-1β-effects on PGHS-2 and CRH-R1 mRNA expression (Figure 6.11). A conformation that the effect of the inhibitors on the mRNA levels was specific came from an experiment where the adenylyl cyclase inhibitor (1μM SQ 22536) was used and did not affect IL-1β-induced CRH-R1 and PGHS-2 mRNA transcription. Additionally the presence of U0126 and SB 203580 had no effect on other cellular functions such as cAMP production (data not shown).

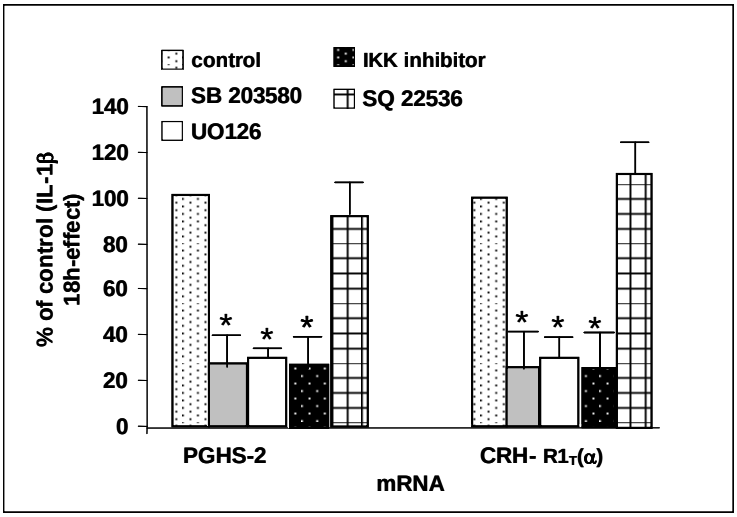

Figure 6.11 Effect of IKK, ERK1/2 and p38 MAPK inhibitors on IL-1β-induced effects on myometrial PGHS-2 and CRH-R1 gene expression. Following pretreatment of cells with either IKK inhibitor II, U0126, SB 203580 and SQ 22536 and stimulation with IL-1β (1ng/ml) for 18h, RNA was extracted and PGHS-2 and CRH-R1 mRNA levels were determined by real-time quantitative RT-PCR (Lightcycler and Taqman, respectively) as described in the Materials and Methods. Data are expressed as mean values ± SEM. of relative mRNA expression levels normalised against β-actin and 18S mRNA. *P<0.05 compared to inhibitor-untreated values.

6.2.5 Effects of IL-1β on CRH-induced myometrial cAMP response

The functional consequences of IL-1β-induced myometrial CRH-R1 up-regulation was investigated by pretreatment of cells with IL-1β for 18 h followed by

determination of cAMP production in response to CRH stimulation. The Gsα-adenylyl cyclase pathway is one of the major signalling pathways mediating CRH effects in human myometrial cells (Grammatopoulos D and Hillhouse EW, 1999c). Surprisingly, although IL-1β treatment increased basal and forskolin-stimulated cAMP levels (by 10x and 2x fold respectively) (Figure 6.12A and B), it significantly impaired CRH-induced cAMP production (by 85±7%) suggesting that myometrial CRH-R1 mRNA up-regulation was not associated with increased functional activity and cAMP production (Figure 6.12A) (Markovic D *et al*., 2007a).

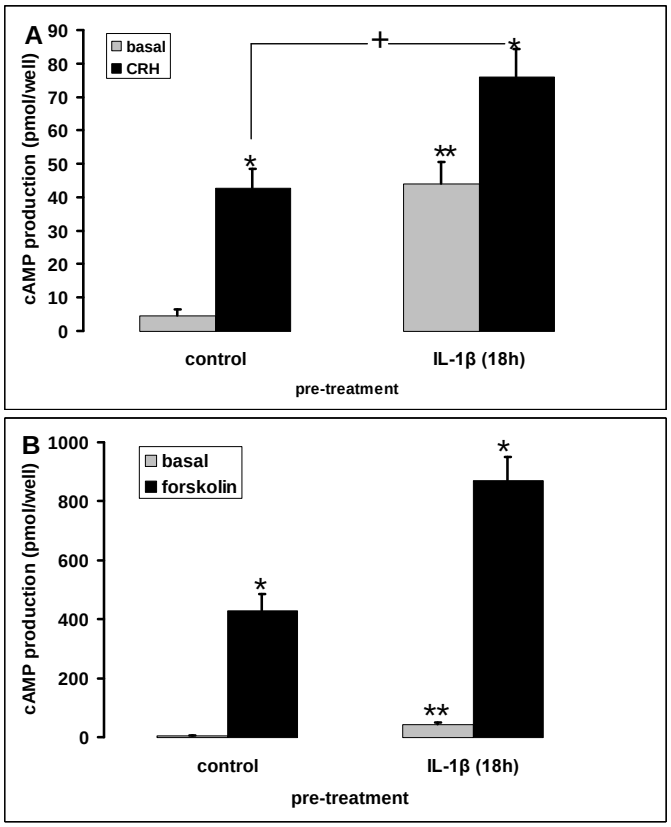

Figure 6.12. Effect of IL-1β on CRH-induced cAMP production from human pregnant myometrial cells. Cells were pretreated with IL-1β (1 ng/ml) for 18 h, followed by incubation with 100nM CRH for 15 min at 37^{o}C. Results are representative of six separate cell culture preparations. Each point is the mean ± SEM of four estimates. * P<0.05 compared to basal; + P<0.05 compared to CRH-stimulated values in cells without IL-1β pre-treatment; ** P<0.05 compared to basal values in cells without IL-1β pre-treatment.

UCN-II INDUCED SIGNALLING PATHWAYS IN MYOMETRIAL SMOOTH MUSCLE CELLS

6.2.6 The effect of UCN-II on cAMP production

As previously mentioned, one of the major signalling pathways mediating CRH effects in human myometrial cells involves activation of the Gsα-adenylyl cyclase pathway which mediates myometrial relaxation (Grammatopoulos D and Hillhouse EW, 1999c). Interestingly, CRH-like peptides such as urocortin-II (a CRH-R2 specific agonist) have been linked to activation of signalling pathways involved in myometrial contractility. When cells were challenged with various concentrations (1 nM -100 nM) of UCN-II no significant cAMP production was detected (Figure 6.13), suggesting that the receptor did not couple to Gs-protein.

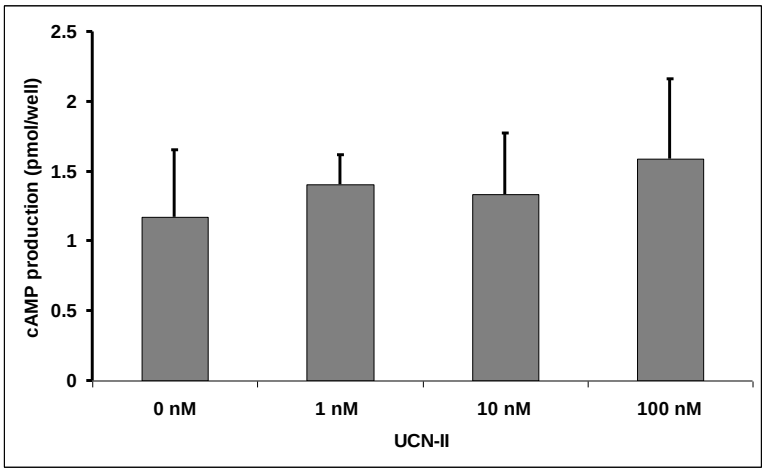

Figure 6.13. The effect of UCN-II on cAMP production in HMSM cells. The cells were treated for 15 min with 1-100 nM UCN-II, supernatants were collected and cAMP levels were determined by a commercially available ELISA kit. Results are representative of three separate cell culture preparations. Each point is the mean ± SEM of three estimates.

6.2.7 The effect of UCN-II on MAPK activation

In various cellular types, another major pathway activated by UCN-II, via CRH-R2β, is the mitogen activated protein kinase (MAPK) signalling cascade. Preliminary studies (Karteris E *et* al., 2004) have implicated the ERK pathway as a signalling cascade mediating UCN-II effects in HSMC. Additional experiments confirmed this finding and also showed that UCN-II induced p38MAPK phosphorylation (Figure 6.14).

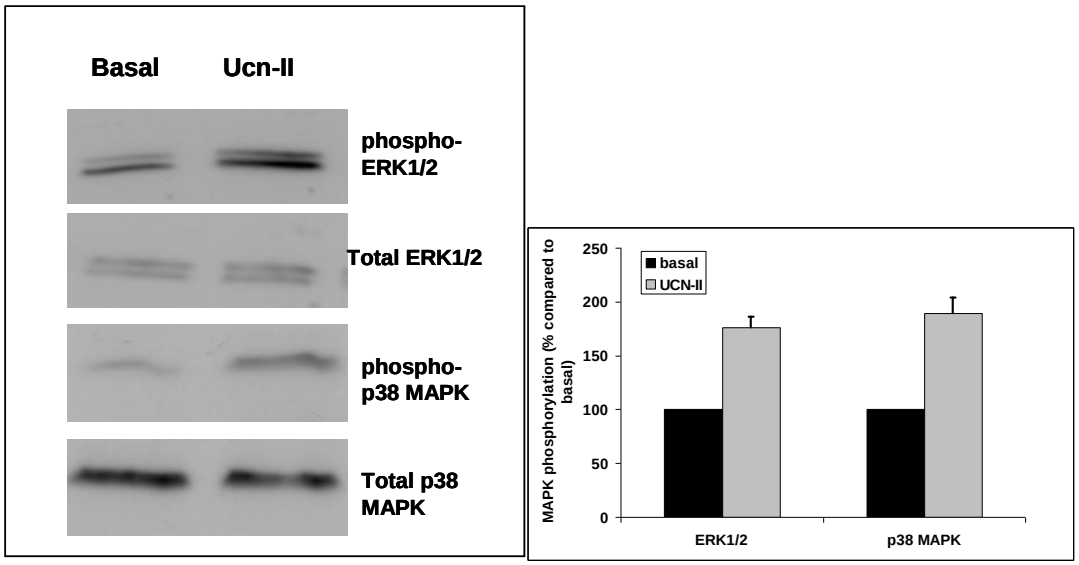

Figure 6.14. UCN-II-induced ERK1/2 and p38MAPK phosphorylation in HMSM cells. The cells were stimulated with 100 nM UCN-II for 5 min. Total cellular proteins were subjected to SDS-PAGE and immunoblotted as described in the Materials and Methods. Representative western blots from three experiments are shown. The results are presented as the mean ± SEM of three experiments.

Activated MAPKs can phosphorylate various cytoplasmic and nuclear targets, some of which are transcription factors including Elk, c-Fos, c-Myc, NF-κB (Roux PP & Blenis J, 2004). Selection of targets is determined by the spatio-temporal characteristics of MAPK activation. Since previous studies demonstrated (Chapter 5) that in st.293-R2β cells, UCN-II activated ERK1/2 translocates to the

nucleus of a cell, it was investigated whether a similar spatial-temporal pattern was present in cells that endogenously express the CRH-R2 receptor, such as HMSM cells.

UCN-II induced ERK1/2 activation was transient and maximal stimulation was observed after 5 min of treatment, and this returned to basal levels after 30 min of treatment (Figure 6.15). Phosphorylation levels of ERK1/2 were determined by normalizing phospho-ERK1/2 signal with GAPDH instead of total ERK1/2, because of technical reasons.

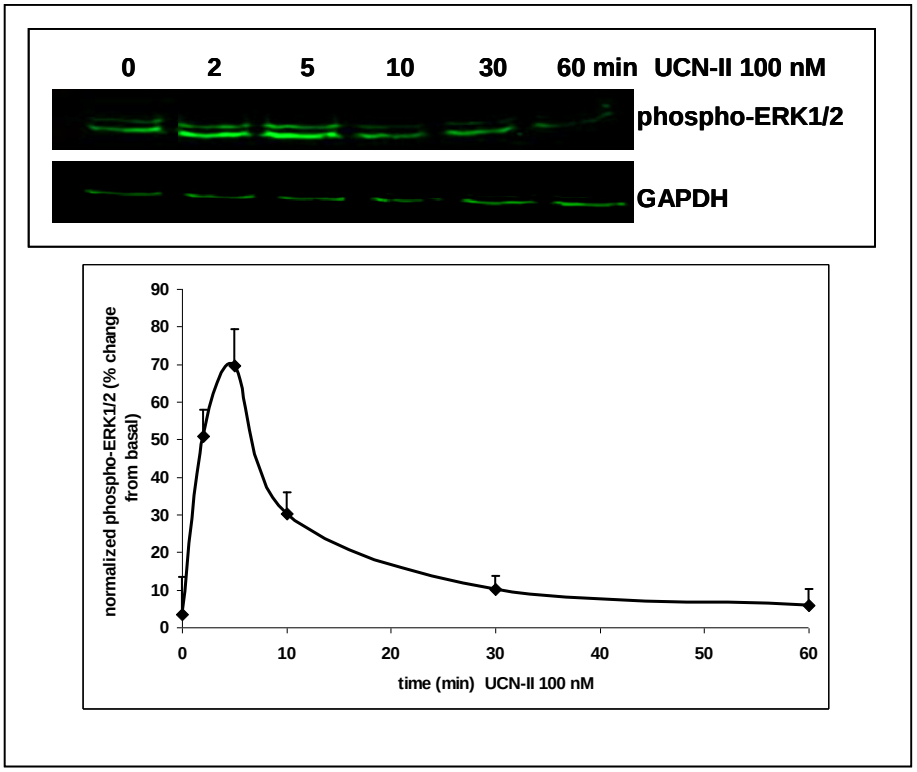

Figure 6.15. Time-dependent ERK1/2 activation by UCN-II in HMSM cells. Top panels are representative Western blots of cells stimulated with UCN-II (100 nM) for various time points (2-60 min). The ERK1/2 phosphorylation was assessed using phospho-spesific-ERK1/2 antibody and GAPDH antibody and secondary antibodies conjugated to IRDye™ 800. Results are expressed as the means±SEM of three independent experiments

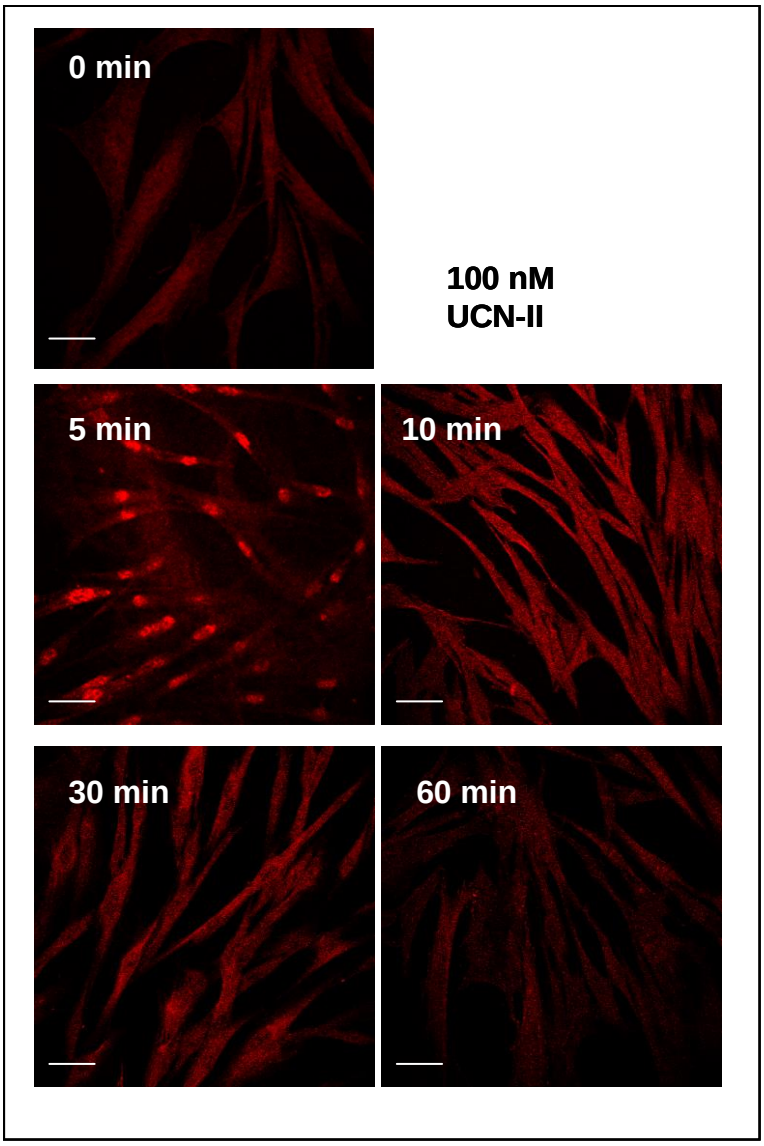

Figure 6.16. Phospho-ERK1/2 subcellular distribution induced by UCN-II in HMSM cells: visualization by confocal microscopy. The cells were stimulated with or without UCN-II (100 nM) for various time intervals (5–60 min). Phospho-ERK1/2 distribution was monitored over the ensuing time period by indirect immunofluorescence using specific primary antibodies for phospho-ERK1/2 and Alexa-Fluor®594 secondary antibody (red). Identical results were obtained from two independent experiments and at least 10 cells were examined in each image. Microscope and laser settings were constant during the experiments. Scale bar is 20 μm.

In unstimulated HMSM cells, low levels of activated (phosphorylated) ERK1/2 were found. UCN-II treatment for 5 min led to a rapid increase in the

amount of fluorescent signal for phospho-ERK1/2, indicating increased activity. The phospho-ERK1/2 immunoreactive signal was wide spread throughout the cytoplasm although the majority of the signal was localized to the cell nuclei. After 10 min of UCN-II treatment phospho-ERK1/2 was evenly widespread throughout the cytoplasm and nucleus. In agreement with the immunoblotting experiments suggesting transient MAPK activation, after prolonged treatment (30 min) with UCN-II (100 nM), only a small increase in the amount of phospho-ERK1/2 was evident. Interestingly, most of the cell nuclei were void of the phospho-ERK1/2 immunoreactive signal, reflecting deactivation of the signaling pathway or possible export of the MAPK outside the nucleus. After 60 min UCN-II treatment there was no significant phospho-ERK1/2 signal in the cells (Figure 6.16).

6.2.8 CRH-R2 mediated RhoA translocation

Furthermore, it was demonstrated that the treatment of HMSM cells with CRH also caused a small but significant increase in RhoA translocation (by 4 fold), which was significantly less than UCN-II-induced RhoA translocation (13 fold increase above basal), implicating a CRH-R2 mediated phenomenon. Interestingly, pre-treatment of UCN-II stimulated cells with CRH attenuated UCN-II effect on RhoA translocation to the plasma membrane, suggesting either desensitization of CRH-R2 or a possible cross talk between the CRH-R1 and R2 receptors. The well-established uterotonin, oxytocin, was used as a positive control; treatment of myocytes with oxytocin induced increased RhoA translocation by 17 fold above basal (Figure 6.17).

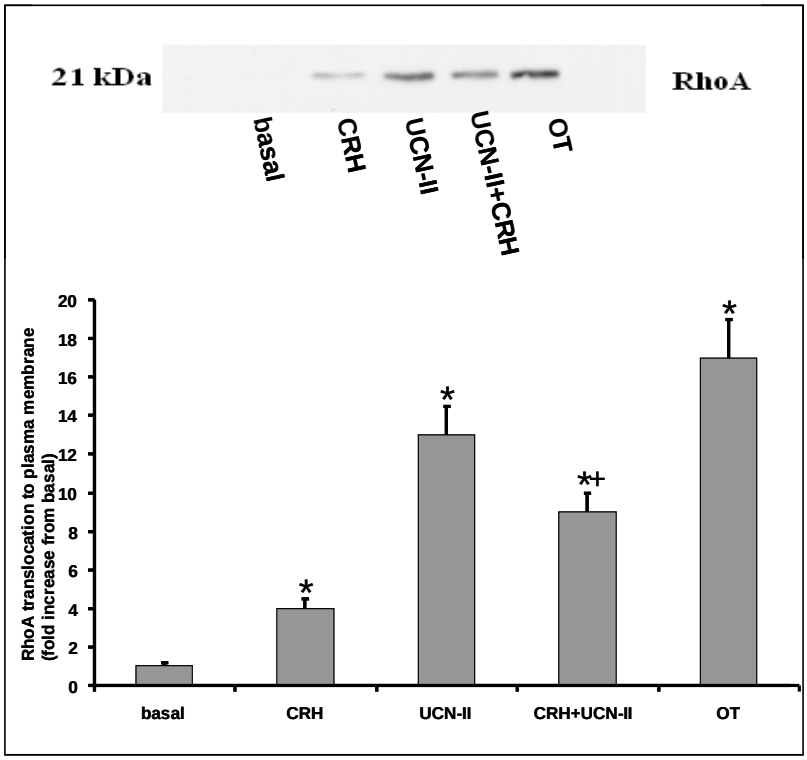

Figure 6.17. Agonist induced RhoA translocation to the plasma membrane in HMSM. Cells were stimulated with agonists for 5 min. The RhoA translocation was determined as described in the Materials and Methods. The results represent the means ± SEM from three independent experiments. *, P<0.05 compared to basal; +, P<0.05 compared to UCN-II treated cells.

6.2.9 Methods for monitoring UCN-II induced RhoA translocation and activation

Previous studies suggested that the activation of ERK1/2 in HMSM cells leads to further activation/ translocation of small GTPase, RhoA (Karteris E *et al*., 2004). The activity of this protein is partially responsible for UCN-II-induced MLC phosphorylation, a key step in induction of contractions in a muscle cell (Karteris E *et al*., 2004). In order to develop better means for the detection of RhoA translocation to the plasma membrane of a single cell and subsequent activation, an

immunofluorescence method previously described by Hayashi K and colleagues (Hayashi K *et al*., 1999) was adapted. The detailed protocol is presented in section 6.1.10. These studies showed that in resting HMSM cells RhoA was evenly distributed thought the cytoplasm, but UCN-II treatment of HMSM cells for a period as short as 5 min induced a robust RhoA translocation from the cytoplasm to the plasma membrane (Figure 6.18).

However, the translocation of RhoA to the plasma membrane is just the first step towards the activation of RhoA. The activation of this small GTPase was monitored by a commercially available kit (described in the section 6.1.8). The treatment of HMSM cells with UCN-II for 5min induced activation of RhoA (Figure 6.19).

Use of these methods provided more conclusive evidence on the effect of UCN-II on RhoA translocation and activation. A big advantage of these techniques over the preparation of membrane proteins, the techniques used by Karteris E *et al*, is the smaller amount of starting material, the cells. This is of pivotal importance, since the pregnant myometrial smooth muscle cells could loose the original properties of primary cells if they are passaged many times. A gradual loss of CRH receptors with successive passage of cultured non-pregnant myocytes was reported, as well as reduced signalling properties (Linton EA *et al*., 2001); it is possible that the same is true for cultured pregnant myocytes.

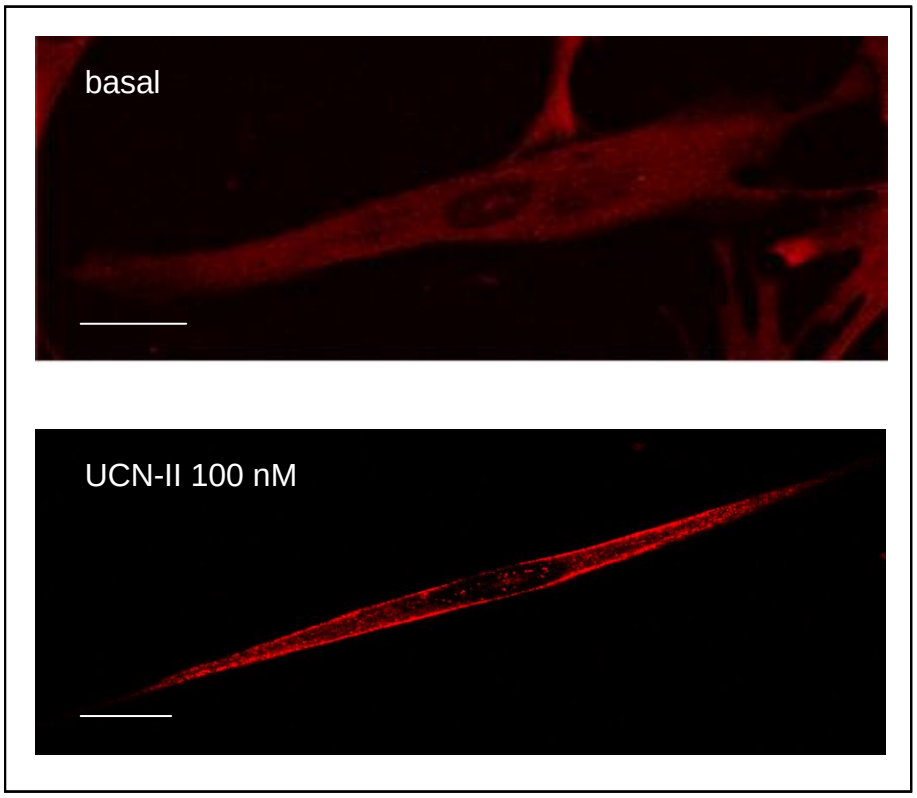

Figure 6.18. UCN-II induced RhoA translocation in HMSM cells. The cells were grown on cover slips and treated with 100 nM UCN-II for 5min. The cells were fixed with TCA as described in the Materials and Methods. RhoA distribution was monitored by indirect immunofluorescence using specific primary antibodies for RhoA and Alexa-Fluor®594 secondary antibody (red). Identical results were obtained from two independent experiments. Microscope and laser settings were constant during the experiments. Scale bar is 20 μm.

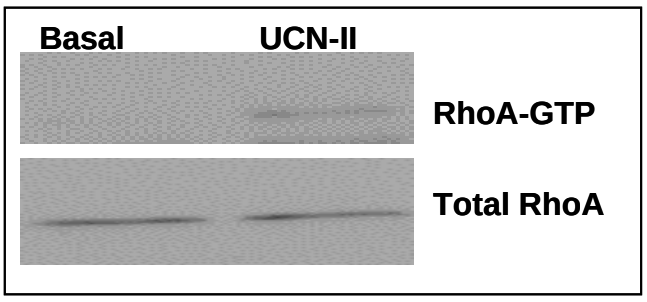

Figure 6.19. UCN-II induced RhoA activation in HMSM cells. The cells were treated with 100 nM UCN-II for 5min, proteins were harvested and the RhoA-GTP pull down assay was performed as described in the Materials and Methods. The identical results were obtained from two independent experiments.

6.2.10 UCN-II induced CRH-R internalization

CRH-R activity, as with the activity of any other GPCR, is controlled by a fine balance between molecular mechanisms mediating receptor signalling, desensitization, internalization and resensitisation. Endocytotic internalization is an important physiological "feedback" mechanism that protects against receptor over-stimulation. As shown on Figure 6.1A and 6.2, "hot spots" of CRH-R expression are present on the surface of HMSM cells. The exposure of HMSM cells to 100 nM UCN-II for 60 mins results in retraction of CRH-R immnunoreactive signal from the cell surface and the appearance of punctuate intracellular staining, indicative of receptor endocytosis.

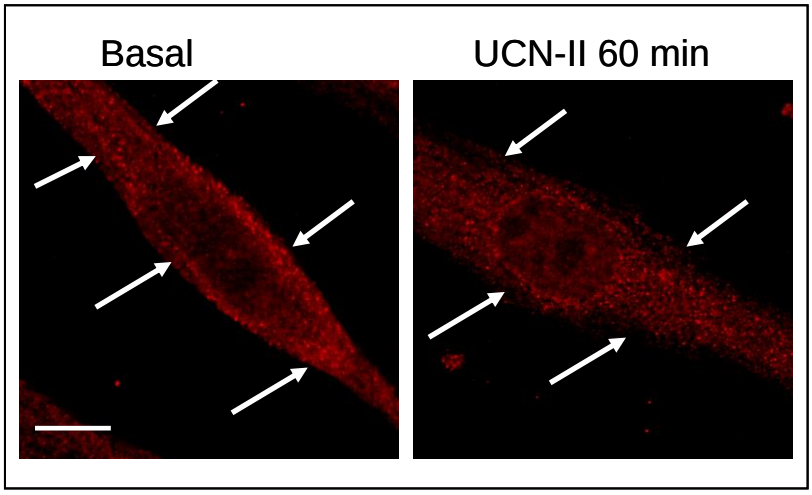

Figure 6.20. UCN-II induced CRH-R internalization in HMSM cells. The cells were treated with 100 nM UCN-II for 60 min and fixed. The CRH-R protein was visualised using specific primary antibodies for CRH-R1/2 and Alexa-Fluor®594 secondary antibody (red). The white arrows indicate CRH-R immunoreactive signal on the edges of the cells. Identical results were obtained from four independent experiments. Scale bar is 10 μm.

6.3 DISCUSSION

CRH and UCNs are expressed in placental and intrauterine tissues during pregnancy and labour (Petraglia F *et al*., 1987). However, the precise biological functions of CRH during human pregnancy are still unknown. There is a wealth of evidence, including myometrial contractility studies, suggesting that CRH plays a "protective" role for the pregnant uterus, by generating intracellular signals (cAMP, NO/cGMP) that maintain the uterus in a state of relaxation and prevent contraction (Grammatopoulos DK, 2007; Vatish M *et al*., 2006). On the other hand, increased maternal plasma CRH levels are used as a predictor of the onset of labour (Korebrits C *et al*., 1998). These two physiological roles of CRH are not necessary contradictory, since it is possible that CRH and myometrial CRH-Rs have distinct and possible opposite roles during different stages of pregnancy (Grammatopoulos DK, 2007). Also it is possible, that the significantly higher levels of maternal plasma CRH in abnormal pregnancy states might be produced in response to premature labouring process, in order to prevent inappropriate contractions (Warren WB *et al*., 1995).

Human pregnancy is associated with changes in the myometrial CRH-R variant expression profile and functional activity, consistent with the important role(s) of CRH and CRH-related peptides in the control of myometrial transition from a state of quiescence to one of increased contractility (Grammatopoulos D & Hillhouse EW, 1999; Hillhouse EW *et al*., 1993; Grammatopoulos D *et al*., 1998; Grammatopoulos D *et al*., 1999; Grammatopoulos D *et al*., 1996). Our recent report utilizing quantitative real-time PCR analysis has demonstrated that as pregnancy progresses towards term, there is an increased transcription of the CRH-R1 gene in

quiescent myometrial tissue (Markovic D *et al*., 2007a). Most importantly, we have suggested that mechanisms activating myometrial contractility and labour, either term or pre-term, induce increased transcription of the CRH-R1 gene and accelerate the (unknown) splicing mechanisms involved in the generation of CRH-R1 mRNA splice variants. Use of quantitative RT-PCR probes capable of distinguishing between different mRNA variants allowed us to investigate expression of individual CRH-R1 mRNA variants. The finding that in labouring myometrium there is decreased mRNA expression of the "pro-CRH-R1" variant, CRH-R1β, with simultaneous increase of the "total"CRH-R1 mRNA (that reflects the fully-active CRH-R1α and the signalling deficient variant CRH-R1d), suggests induction of the two splicing events regulating individual expression of CRH-R1 variants by removing sequentially exons 6 and 13 (Markovic D *et al*., 2007a). These findings expand previous studies employing a semi-quantitative RT-PCR method and showed that the CRH-R1 mRNA in the lower myometrial segment, but not the fundus, is significantly increased in both preterm and term labour (Stevens MY *et al*., 1998).

The mechanisms regulating CRH-R1 alternative splicing are largely unknown. Studies in keratinocytes suggest that environmental stimuli such as UV irradiation as well as intracellular messengers such as cAMP and phorbol esters can induce CRH-R1 splicing (Pisarchik A & Slominski AT, 2001). Furthermore, CRH-R heterogeneity has been previously shown in human myometrial membrane extracts (Grammatopoulos D *et al*., 1995) and the functional activity of some receptor variants appeared to be differentially regulated by oxytocin (Grammatopoulos D & Hillhouse EW, 1999b; Markovic D *et al*., 2006). Unfortunately, the lack of suitable antibodies able to distinguish between different CRH-R1 variants does not allow investigations at the level of individual protein expression and functional response.

Confocal microscopy studies performed on primary myometrial smooth muscle cells (Figure 6.1 and 6.2) have demonstrated that CRH receptors were not uniformly expressed on the plasma membrane, some parts of smooth muscle cell plasma membrane had higher receptor expression than other parts of the cell surface, suggesting "hot spots" of CRH mediated signalling (Markovic D *el at*., 2007). Additionally, strong intracellular and peri-nuclear staining detected in the native systems could represent intracellular receptor variants (such is CRH-R1d) and the newly synthesised CRH-R, respectively. It is very possible that the intracellular CRH-R signal was from the CRH-R1d variant, since other splice variants that might have cytoplasmic expression (such as CRH-R1e1 and CRH-R1h – Table 1.1) do not have the epitope against which the antibody used was raised. Additional evidence for the CRH-R1d intracellular expression came from over-expression studies in HEK293 and primary myometrial smooth muscle cells. The pattern of CRH-R1d over-expression in myocytes showed striking similarity to the endogenous CRH-R intracellular staining. These data provide a novel insight into the CRH-R1 protein expression profile in endogenous systems. Of course, one can not conclude with certainty that the intracellular immunoreactivity is solely due to CRH-R1d expression. Further use of siRNA to knock down CRH-R1d or all the other variants but CRH-R1d would possibly provide more concrete evidence. However, at this point of time, a lack of variant specific antibody prevents any further analysis of CRH-R variant protein localisation in endogenous systems.

In order to further the investigation of the expression of CRH-R1, primary human myometrial cells obtained from term human quiescent myometrial biopsies were used. It was demonstrated that CRH-Rs are un-evenly distributed in the plasma membrane. This finding strongly suggests "hot spots" of receptor expression

probably reflecting "confined" CRH-R signalling networks in specific areas. These experiments also showed significant intracellular staining for CRH-R, potentially indicating newly synthesised unprocessed receptors, internalised mature CRH-R or cytoplasmic forms of specific CRH-R variants.

Moreover, *in vitro* studies of myometrial cells identified IL-1β as a potential regulator of CRH-R1 gene transcription and splicing pattern. IL-1β, like many other pro-inflammatory cytokines, has been proposed to play important roles in the onset of labour and the pathogenesis of infection-induced preterm labour (Muhle RA *et al*., 2001). IL-1β induced PGHS-2 mRNA and protein expression is due to the activation of the NF-κB pathway (Figures 6.3-6.5, 6.8, 6.9, 6.11); but more importantly the data presented in this chapter suggests that IL-1β can potentially mediate CRH-R1 gene transcription and splicing mechanisms targeting the first splicing step (exon 6, but not exon 13, of the CRH-R1 gene) (Figure 6.6). These interactions appeared to involve two members of the MAPK family of proteins, ERK1/2 and p38 MAPK (Figure 6.11). In a variety of cells these kinases exert their effects through phosphorylation of p65 and modulation of the NF-κB transcriptional activity (Viatour P *et al*., 2005). NF-κB is a critical component of pathways mediating IL-1β-actions in human myometrium and other feto-maternal tissues (Soloff MS *et al*., 2004). Moreover, increased p65 (RelA):p50 heterodimer DNA binding has been demonstrated in labouring myometrium and was linked with increased transcriptional activation to specifically modulate changes in expression of genes critical for myometrial activation and contraction (Chapman NR *et al*., 2004). The evidence presented in this chapter point towards an important role for NF-κB in IL-1β effects on CRH-R1 gene regulation and splicing. This is possible since the CRH-R1 promoter contains NF-κB recognition elements (Parham KL *et al*., 2004).

Also it was demonstrated that IL-1β action induced phosphorylation of IκBα through an IKK-mediated mechanism that releases p65 (RelA) and allows its translocation to the nucleus (Figures 6.8-6.10) (Lindstrom TM & Bennett PR, 2005; Markovic D *et al*., 2007).

Surprisingly, increased CRH-R1 gene transcription and generation of receptor splice variants was not associated with increased CRH-R protein levels (Figure 6.7) and CRH signalling activity (Figure 6.12). On the contrary, prolonged exposure of cells to IL-1β significantly impaired CRH-induced cAMP production, although the IL-1β pre-treatment significantly augmented basal adenylyl cyclase activity, in agreement with previous studies (Breuiller-Fouche M *et al*., 2005). It is likely that this is directly related to repression of the myometrial Gαs gene by NF-κB that has been reported (Oger S *et al*., 2002). The possibility that IL-1β pre-treatment might induce expression of signalling-deficient variants of CRH-R1 such as R1c and R1d was excluded by the real-time PCR experiments. Interestingly, the myometrial IL-1β/NF-κB and cAMP/PKA signalling pathways can interact at multiple levels; exposure of myometrial cells to IL-1β results in a significant up-regulation of cAMP-phosphodiesterase 4 (PDE4) which is the predominant family of PDEs expressed in human myometrium (Breuiller-Fouche M *et al*., 2005), through a mechanism involving PGE_2 production and subsequent cAMP augmentation. Also, myometrial p65 appears to be specifically associated with a PKA catalytic subunit (as well as IκBα) through an interaction that potentially involves the phosphorylation of p65 at serine-536 (Chapman NR *et al*., 2004). This association might contribute to the inactive state of p65 until the cell is exposed to a p65 inducing stimulus (*e.g.* IL-1β).

One of the main actions of IL-1β in human myometrium involves the up-regulation of PGHS-2 enzyme and increased production of prostaglandins such as PGE_2 (Sooranna SR *et al*., 2005). The previous studies from our group have shown that short (0.5-2hr) as well as prolonged (8-18hr) treatments with CRH can attenuate myometrial PGE_2 release and only the prolonged effect of CRH can be inhibited by co-incubation with IL-1β (Grammatopoulos D & Hillhouse EW, 1999c). This coupled with the findings of the present study might suggest that IL-1β acts to diminish the CRH-induced cAMP response through modulation of CRH-R1 gene transcription and splicing and/or down-regulation of Gsα, thus implicating the myometrial cAMP/PKA pathway in the inhibition of PGE_2 synthesis and release.

Additionally, this work provided novel evidence that IL-1β is one of the signals involved in the regulation of CRH-R1 gene, through a pathway involving activation of NF-κB, the classical mediator of IL-1β intracellular events, as well as at least two members of the MAPK family of proteins, ERK1/2 and p38MAPK. However, no substantial changes of the CRH-R protein levels following the IL-1β treatment were detected. One possible explanation could be as follows: because an antibody that recognises the C-termini of both types of CRH receptors, R1 and R2, was used, the possible changes in protein levels of different CRH-R1 variants could not have been detected due to the antibody promiscuity. Another possibility is that the changes of CRH-R1 variant mRNA levels are actually not reflected in the protein levels (no translation). However, the most important evidence from this part of the project was that IL-1β actions led to dampening of the CRH-induced cAMP response, an event that might contribute to the pro-contractile intracellular environment required for the onset of labour. It is tempting to speculate that up-regulation of functional CRH-R1s might lead to activation of alternative signalling

cascades that may help in the transition of the uterus from a state of quiescence to one of increased contractility and active labour.

In the second part of this chapter, the investigation was focused on the identification of signalling cascades activated by UCN-II, a CRH-R2 specific agonist. It has been demonstrated that UCN-I acting via both types of CRH receptors, R1 and R2, can potentially promote contractility via activation of the ERK signalling cascade (Grammatopoulos DK *et al*., 2000), and that UCN-II activates MLC phosphorylation via pathways involving sequential activation of PKC, MEK1, ERK1/2, RhoA and ROCK (RhoA associated kinase) (Karteris E *et al*., 2004). In agreement with these observations, it was demonstrated that the activation of CRH-R2 did not lead to production of cAMP (Figure 6.13), the main mediator of myometrial quiescence, suggesting a potential dual role of CRH-Rs in the control of myometrial contractility. Moreover, the data suggested that ERK1/2 and p38MAPK signalling cascades were activated following UCN-II treatment. Particular attention was focused on ERK1/2 activation since it has been demonstrated that the transient activation of ERK1/2 in st293-R2β cells is characterised by nuclear localisation of the phospho-ERK1/2, which is of pivotal importance for the role of ERK1/2 as a regulator of transcription factor activity. The same spatio-temporal characteristics were detected in HMSM cells, suggesting that the activation of endogenous CRH-R2 is important in gene transcription.

The small GTPase Rho family have been reported to regulate many cellular functions such as cell adhesion, cell contraction, cell migration and tumour cell invasion, growth control and survival responses, phospholipids metabolism, MAP kinase activation and gene transcription, endocytosis, exocytosis, glucose transport and ion channels (Wettschureck N and Offermanns S, 2002). RhoA is the best

characterized member of Rho family. The data presented in this chapter suggested that the treatment of HMSM cells with CRH also led to a small but significant increase in RhoA translocation, which was significantly less than UCN-II-induced RhoA translocation, implicating a CRH-R2 mediated phenomenon. Interestingly, pre-treatment of UCN-II stimulated cells with CRH attenuated UCN-II effect on RhoA translocation to the plasma membrane, suggesting either desensitization of CRH-R2 or a possible cross talk between the CRH-R1 and R2 receptors (Figure 6.17).

Taken together, the data presented in this chapter demonstrate a complex molecular network involved in regulation of CRH and UCNs induced signaling, including CRH-R1 gene expression and the activation of various protein kinases.

7 CHARACTERISATION OF CRH RECEPTOR SIGNALLING AND BIOLOGICAL PROPERTIES IN BROWN ADIPOCYTES

7.1 INTRODUCTION

The critical function of CRH and UCNs in energy balance and homeostasis has started to emerge. These peptides exert their effects through activation of two types of CRH receptors, CRH-R1 and R2, leading to attenuation of fasting-induced feeding as well as increased energy expenditure through thermogenesis and lipolysis (Spina M *et al*., 1996; Uehara Y *et al*., 1998; Kalra SP *et al*., 1999). Numerous studies, primarily *in vivo*, demonstrated that CRH administration prevents excessive body weight gain and stimulates sympathetic outflow, resulting in a decrease in basal hyperinsulinemia and hepatic glycogen content, whilst increasing brown adipose tissue (BAT) activity (Arase K *et al*., 1988; Jerova D *et al*., 1999; Smith SR *et al*., 2001; Cullen MJ *et al*., 2001; Tsigos C & Chrousos GP, 2002). CRH and UCNs increase BAT thermogenesis (Rivest S *et al*., 1989), uncoupling protein-1 (UCP-1) expression (Kotz CM *et al*., 2002), and elevate sympathetic nerve activity to BAT (Egawa M *et al*., 1990a; Egawa M *et al*., 1990b) *in vivo*. Studies investigating the role of CRH-R2 in the regulation of regional tissue

thermogenesis and adaptive physiology using CRH-R2 knockout (KO) animal models showed increased sympathetic nervous system (SNS) activity and basal thermogenesis as well as elevated levels of UCP-1 in BAT. CRH-R2-mutant mice also have smaller white and brown adipocytes indicating possible increased sympathetic tone (Bale TL *et al*., 2003). These studies suggested an important role for CRH-R2 in energy homeostasis and adaptive responses to environmental perturbations.

The appearance of BAT in early evolutionary developmental stages gave mammals a survival advantage and allowed them to be active during periods of nocturnal or hibernal cold, and also to survive the cold stress of birth (Cannon B & Nedergaard J, 2004). One of the functions of this highly specified tissue is to transfer energy from food into heat, a process known as thermogenesis (Brooks SL *et al*., 1980). This adaptive thermogenesis is due to the action of UCP-1, which functions as a mitochondrial proton translocator, uncoupling β-oxidative phosphorylation and ATP production, resulting in heat release (Ricquier D *et al*., 1986).

It has long been known that the thermogenic process in brown adipocytes can be mimicked by the addition of fatty acids, suggesting that lipolysis and thermogenesis are linked processes. Indeed, all attempts to induce lipolysis in brown adipocytes also induced thermogenesis, and no thermogenesis can be evoked without simultaneously evoking lipolysis (Cannon B & Nedergaard J, 2004). Lipolysis, the process of breaking down lipids results in glycerol and fatty acid release. In mature brown adipocytes, norepinephine interacts with all three types of adrenergic receptors: β, α_2 and α_1. These receptors are linked with activation of different signalling pathways in the brown adipocytes. The activated β-adrenergic

receptor is involved in increasing lipolysis whereas the activation of α_2-adrenergic receptor inhibits lipolysis (Cannon B & Nedergaard J, 2004).

The best known mechanism mediating lipolysis is the cAMP/PKA pathway. The activated PKA catalyses phosphorylation of perilipin and hormone sensitive lipase (HSL), leading to translocation of perilipin from the lipid droplets and HSL to the lipid droplets, resulting in a breakdown of triglycerides and diglycerides and subsequent release of free fatty acids (FFA) and glycerol (Carmen G-Y & Vicror S-M, 2006). The detailed mechanism of this pathway and its associated proteins is given in the general introduction (section 1.9).

Furthermore, brown adipocytes are also able to secrete leptin (Buyse M *et al*., 2001) and other adipocytokines such as resistin and adiponectin, two adipocyte-specific secretory factors involved in glucose and lipid metabolism (Viengchareun S *et al*., 2002).

However, at the BAT level, neither the type of CRH-R expressed nor signalling pathways employed by CRH and UCNs in the regulation of physiological responses are clearly characterized. To elucidate the biological properties of CRH-R and their agonists in BAT, a brown adipocyte cell line was utilized (T37i). The T37i cell line is derived from a hibernoma (malignant brown adipose tissue tumour) of the transgenic mouse founder 37 carrying a hybrid gene composed of the human mineralocorticoid receptor proximal promoter fused to the SV40 large T antigen (Zennaro MC *et al*., 1998).

7.2 RESULTS

7.2.1 Expression of CRH-R in T37i cells

In agreement with previous studies (Zennaro MC *et al.*, 1998), preliminary experiments confirmed that insulin and triiodothyronine (T3) treatment for more than 8 days induced T37i cell differentiation into mature brown adipocytes, and this was accompanied by morphological and functional changes, such as accumulation of multilocular intracytoplasmic lipid droplets, identified by Oil Red O staining (Figure 7.1) and expression of UCP1 mRNA (Figure 7.2).

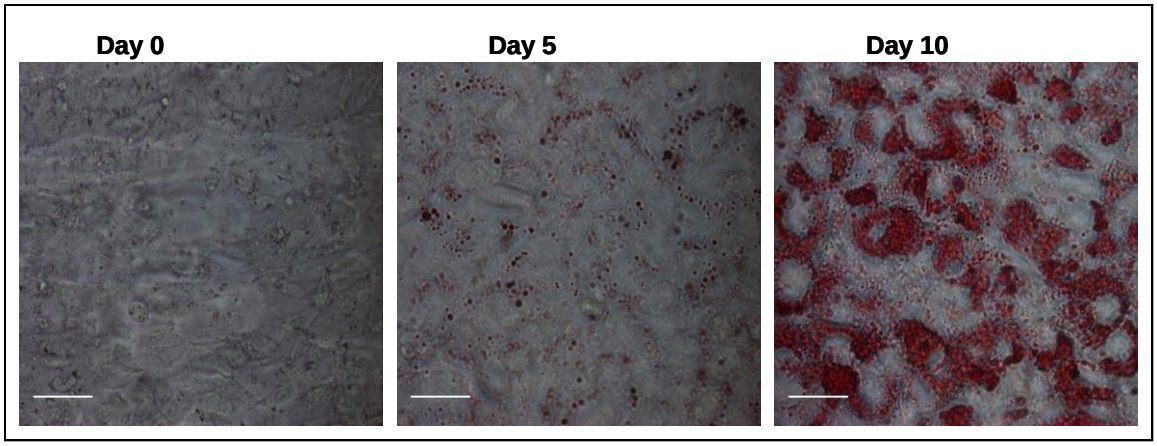

Figure 7.1. Differentiation of T37i fibroblast into adipocytes. T37i cells were incubated with media containing 20 nM insulin and 2 nM T3 for 0-10 days. Cell differentiation was monitored by examining Oil Red O stained cells for lipid droplet (red) formation by a light microscope (40 x magnification). Scale bar is 20 μm. Identical results were obtained in three experiments.

RT-PCR analysis showed that only differentiated cells and BAT expressed UCP-1 mRNA. Additionally both CRH-R1 and R2 mRNAs were expressed in undifferentiated cells, T37i adipocytes and BAT (Figure 7.2).

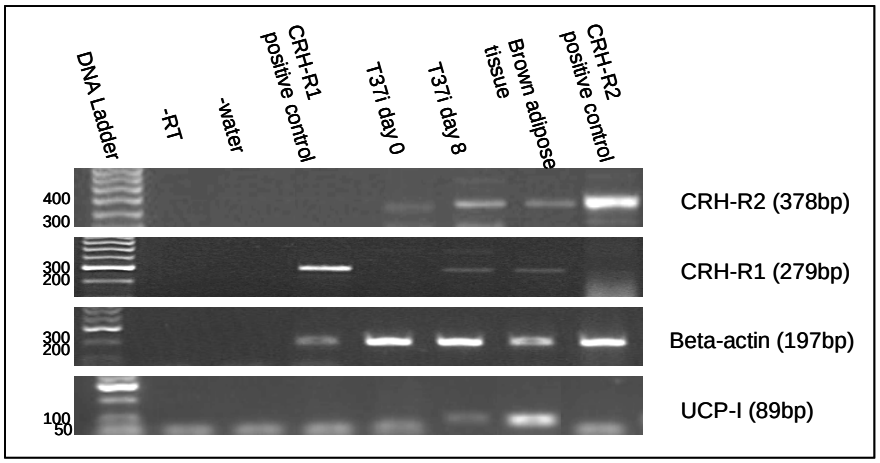

Figure 7.2. RT-PCR analysis of CRH-Rs and UCP-1 mRNA expression. Specific primers for CRH-R1, CRH-R2, UCP-1, and β-actin mRNA were used as described in the Materials and Methods. The PCR products were resolved on 1.2 % agarose gel, purified and sequenced to confirm the authenticity of the products. Identical results were obtained from two experiments.

Furthermore, CRH-R proteins expression in T37i adipocytes was assessed by indirect confocal microscopy and western blotting. Western blot analysis identified multiple bands between 64 and 115 kDa (Figure 7.3). These bands were not detected when the antibody was preabsorbed with the blocking peptide prior to the incubation on the membrane, demonstrating that the detection of multiple bands was not due to non-specific interactions of the antibody and other proteins. The predicted molecular weight of CRH-R protein is approximately 44 kDa. However, differential post-translational glycosylation events might be responsible for the appearance of multiple bands and increased molecular weight of the receptors in the T37i adipocytes (Figure 7.3). Additionally, it is possible that CRH-R could form dimers (the band above 82 kDa) or even trimers (the band above 115 kDa).

In confocal microscopy experiments, cells were also co-stained with the lipid droplet-associated protein, perilipin, CRH-R1/2 and the nuclear stain DAPI. Results

showed a punctuate immunostaining pattern of CRH-R protein, which was not confined to the cell membrane but was widely distributed in specific cytoplasmic areas (Figure 7.4). Interestingly, CRH-R-positive immunostaining was also found near the lipid droplets as well as around the nucleus.

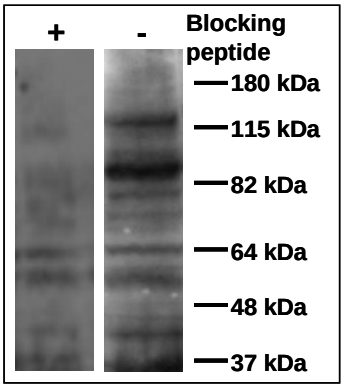

Figure 7.3. Western blot analysis of CRH-R1/2 protein expression. Total cellular proteins were resolved on 10 % SDS-PAGE, electrotransfered onto a nitrocellulose membrane and incubated with CRH-R1/2 specific antibody (+: preabsorbed with the blocking peptide or -: not preabsorbed with the blocking peptide) as described in the Materials and Methods. Identical results were obtained from three experiments.

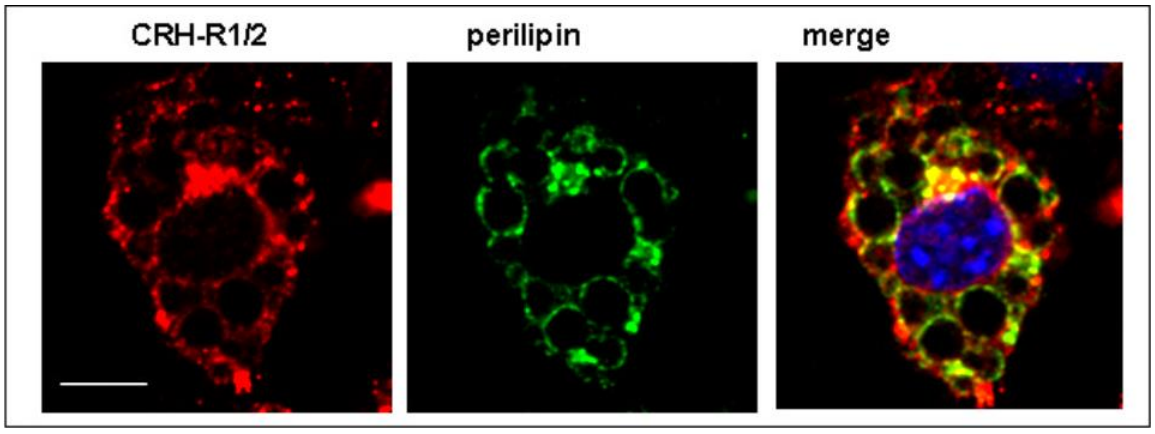

Figure 7.4 Visualization of CRH-Rs and perilipin A in T37i adipocytes by indirect confocal microscopy. Specific primary antibodies were used for CRH-R and Alexa-Fluor®594 secondary antibody (red), and distribution of perilipin A was monitored with antibody for perilipin A and Alexa-Fluor®488 secondary antibody (green). Cell nuclei were stained with the DNA specific dye DAPI (blue). Identical results were obtained from three independent experiments. Scale bar is 10 μm.

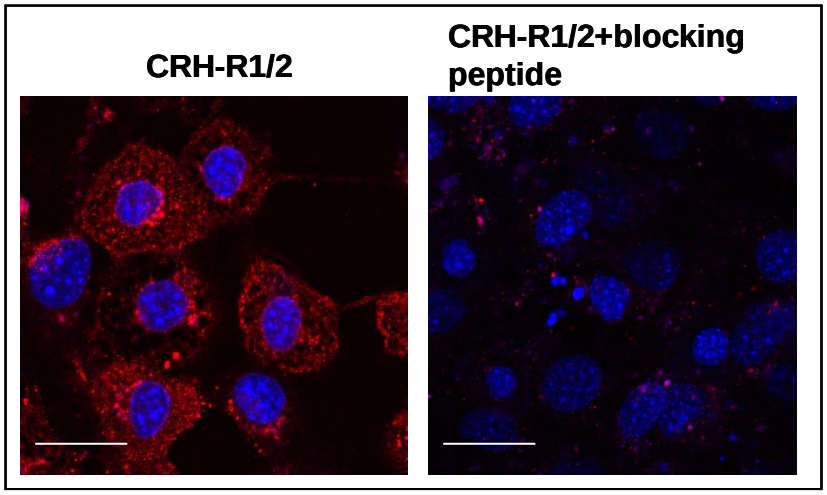

Figure 7.5 Validation of CRH-R immunoreactive in T37i adipocytes by indirect confocal microscopy. Specific primary antibodies were used for CRH-R and Alexa-Fluor®594 secondary antibody (red) in the presence or absence of CRH-R blocking peptide (1 mM) as described in the Material and Methods. Cell nuclei were stained with the DNA specific dye DAPI (blue). Identical results were obtained from three independent experiments. Scale bar is 50 μm.

No staining was detectable in cells in which the primary anti-CRH-R antibody was omitted or when cells were pre-incubated with a specific CRH-R antibody-blocking peptide (Figure 7.5).

7.2.2 Agonist induced cAMP production in T37i adipocytes

Having established the presence of CRH-R in T37i cells, their functional and signalling properties in response to CRH and the CRH-R2 specific agonist, UCN-II were investigated. As mentioned in previous chapters, one of the main signalling cascades activated through CRH-Rs is the cAMP/PKA cascade. Exposure of differentiated T37i cells to 0.1 or 1 nM CRH or UCN-II for 15min led to a significant increase in intracellular cAMP levels in a dose-dependent manner (Figure

7.6). These low concentration of agonists are close to the receptor binding affinity (Kd=1 nM). CRH was significantly more efficient than UCN-II in inducing cAMP accumulation (maximum stimulation, 2.5 vs 0.9 fold above basal). Moreover, for both agonists the maximum response was observed at low concentrations of 0.1 and 1 nM and treatment of cells with higher concentrations (10-1000 nM) resulted in small or insignificant changes in cAMP levels. Interestingly, the higher doses of UCN-II (100 and 1000 nM) reduced cAMP compared to the basal levels, suggesting possible coupling of CRH-R2 with Gi protein or other pathways leading to inhibition of adenylyl cyclase activity (Figure 7.6).

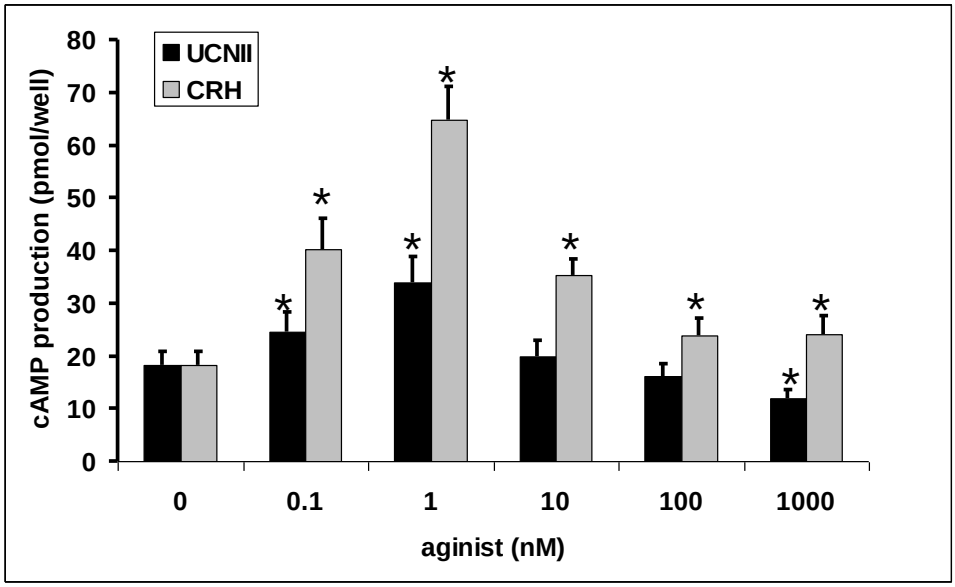

Figure 7.6. Agonist induced cAMP production in T37i adipocytes. Cells were stimulated with various concentrations of CRH and UCN-II (0.1 to 1000 nM) for 15 min. The samples were collected and cAMP determined as described in the Materials and Methods. Data represent the mean ± SEM of three independent experiments. *, P<0.05 compared to basal (0).

7.2.3 Agonist induced MAPK activation in T37i adipocytes

Another pathway under investigation was the MAPK signalling cascades. The functional coupling of CRH-R to these cascades was evaluated by determining the levels of phosphorylated ERK1/2 and p38 MAPK in response to CRH and UCN-II treatment. UCN-II induced a time- and concentration-dependent increase in both ERK1/2 (p-ERK1/2) and p38 MAPK phosphorylation (p-p38 MAPK). As seen in Figure 7.7, the UCN-II effect on both ERK1/2 and p38 MAPK activation was significant at concentrations greater than 10nM and was maximal at a concentration of 100nM; maximal ERK1/2 activation was 6 fold above basal levels, whereas maximal p38 MAPK activation was found to be 3.5-4 fold above basal. In addition, UCN-II induced ERK1/2 activation was transient, maximal stimulation was observed after 5min of treatment and returned to near basal levels after 60 min of treatment (Figure 7.8). UCN-II effect on p38 MAPK phosphorylation showed a similar response with maximal stimulation after 5min of treatment and which returned to basal levels after 30 min of treatment (Figure 7.8). Interestingly, CRH exerted a weaker effect by 70-80% on ERK1/2 and p38 MAPK activation that reached a plateau at a concentration of 10nM (Figure 7.7).

To examine the spatial characteristics of ERK1/2 activation, indirect immunofluorescence confocal microscopy was employed with phospho-specific ERK1/2 antibodies, to monitor the relative subcellular distribution of activated MAPK after agonist stimulation (Figure 7.9). In unstimulated T37i cells, low levels of activated (phosphorylated) ERK1/2 were found. UCN-II treatment for 5-10 min led to rapid increase in the amount of fluorescent signal for phospho-ERK1/2, indicating increased activity of the kinase. Phospho-ERK1/2 immunoreactive signal was widespread throughout the intracellular space. Interestingly, the activation of

ERK1/2 was not consistent in all cells, in some of the cells the MAPK was not activated at all (Figure 7.9 5 and 10 min treatments). In agreement with the immunoblotting experiments suggesting transient MAPK activation (Figure 7.8), prolonged treatment (15-30 min) with UCN-II (100 nM), caused only a small increase in the amount of phospho-ERK1/2 reflecting deactivation of the signalling pathway (Figure 7.9).

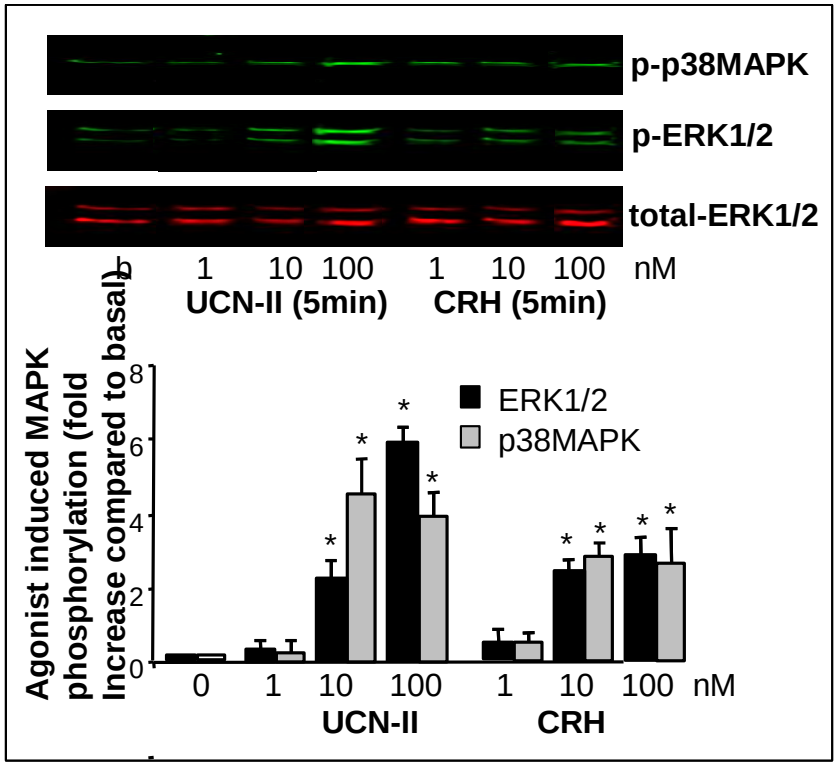

Figure 7.7. Agonist dose dependent MAPK activation in T37i adipocytes. Cells were stimulated with various concentration of CRH and UCN-II (1-100 nM) for 5 min. ERK1/2 and p38 MAPK phosphorylation was determined by SDS-PAGE and immunoblotting as described in the Materials and Methods. Representative western blots are shown. Results were normalised with total-ERK1/2 and presented as the mean ± SEM of three independent experiments. $P<0.05$ compared to basal.

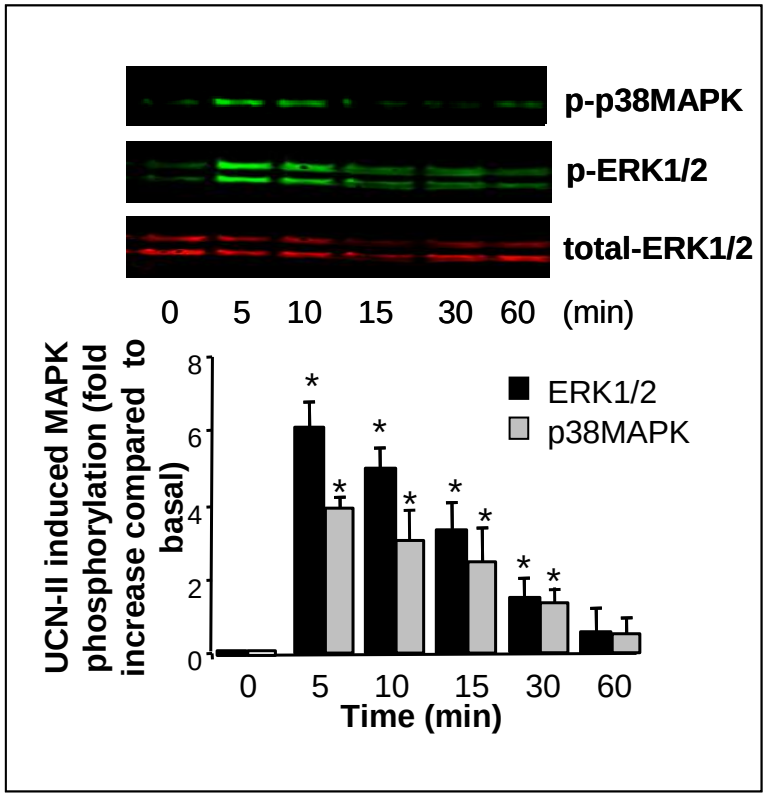

Figure 7.8. Time course of UCN-II induced MAPK activation in T37i adipocytes. Cells were stimulated with 100 nM UCN-II for various time periods (0-60 min). ERK1/2 and p38 MAPK phosphorylation was determined by SDS-PAGE and immunoblotting as described in the Materials and Methods. Representative western blots are shown. Data normalized with total ERK1/2 represent the mean ± SEM of three independent experiments.*, $P<0.05$ compared to basal (time=0).

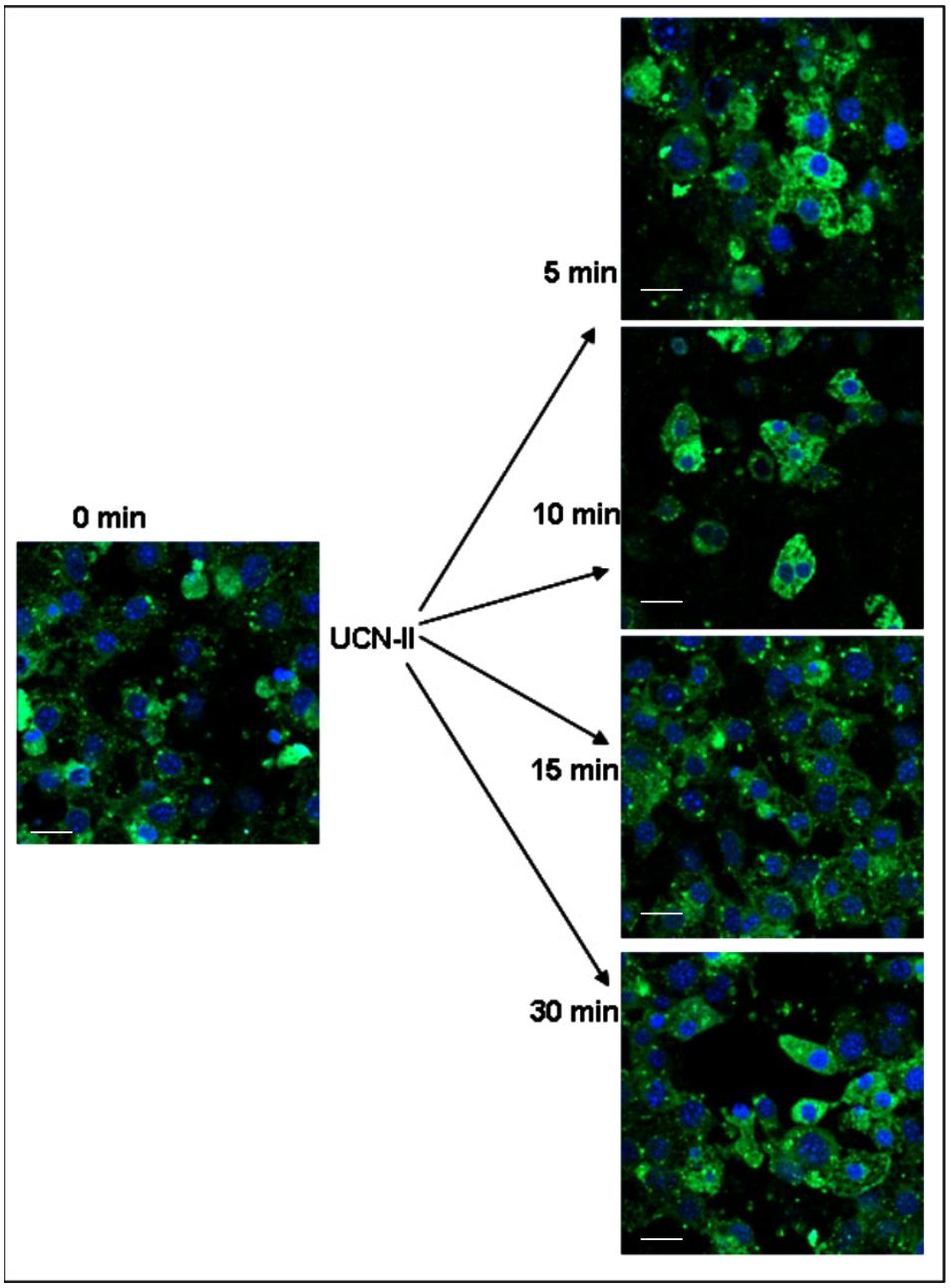

Figure 7.9. Phospho-ERK1/2 MAPK subcellular distribution induced by UCN-II in T37i adipocytes: visualization by confocal microscopy. Cells were stimulated with or without UCN-II (100 nM) for various time intervals (5–30 min). Phospho-ERK1/2 distribution was monitored over the ensuing time period by indirect immunofluorescence using specific primary antibodies for phospho-ERK1/2 and Alexa-Fluor®488 secondary antibody (green) as described in the Materials and Methods. Cell nuclei were stained with the DNA-specific dye DAPI (*blue*). Identical results were obtained from two independent experiments.

7.2.4 The involvement of PKA and PI(3)-kinase in UCN-II induced MAPK activation

Further studies identified some of the signalling molecules involved in CRH-R-MAPK interactions. Previous studies have identified PI(3)-kinase as a crucial kinase in UCN-II-induced MAPK activation (Brar BK *et al*., 2004). Additionally in Chapter 5, it has been demonstrated that PI(3)-kinase is involved in UCN-II induced ERK1/2 activation, but inhibition of the kinase did not effect UCN-II induced p38 MAPK phosphorylation in st.293-R2β cells.

The role of PI(3)-kinase in T37i adipocytes was determined by the use of a specific PI3-K inhibitor LY294002. Pretreatment of T37i cells with LY294002 (50 μM) for 30 min significantly attenuated by 75% UCN-II induced ERK1/2 activation; in contrast, UCN-II induced p38 MAPK activation was augmented by 1.5 fold (Figure 7.10).

Potential cross-talk between the cAMP/PKA and MAPK signalling cascades was also investigated by using a selective PKA inhibitor (myr-PKAi) and st-Ht31 peptide which prevents binding between PKA regulatory subunits and A-kinase anchoring proteins (AKAP). The results showed that basal ERK1/2 and p38 MAPK activity in brown adipocytes is under the negative regulation of the PKA signalling cascade since pre-treatment with either PKAi or st-Ht31 enhanced phospho-ERK1/2 and p38 MAPK levels by 50% and 40% respectively. In contrast, these compounds had no effect on UCN-II induced ERK1/2 and p38 MAPK phosphorylation compared to the UCN-II effect without the inhibitors; (Figure 7.10), which is expected, since 100 nM UCN-II fail to induce production cAMP, the main regulator of PKA activity, in T37i adipocytes (Figure 7.6).

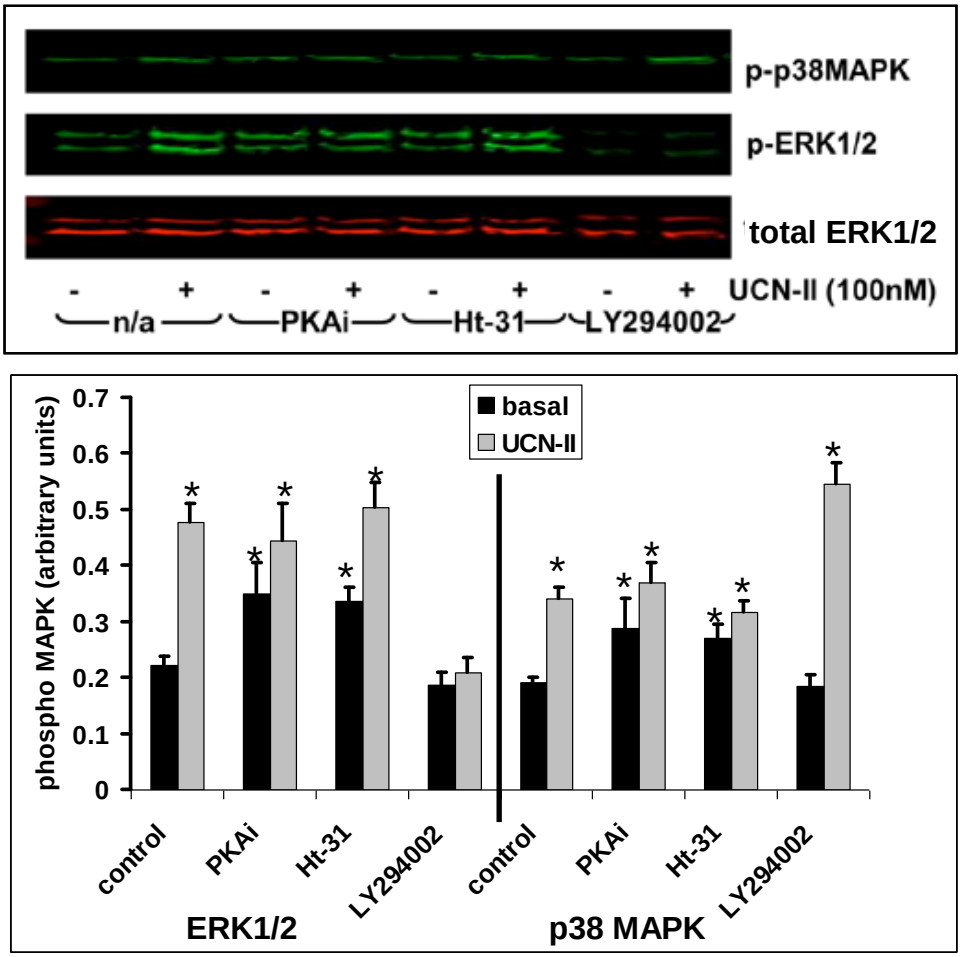

Figure 7.10. The role of PKA, AKAP and PI(3)-kinase on UCN-II induced ERK1/2 and p38 MAPK activation in T37i adipocytes. Cells were pretreated with or without 1 μM PKAi, 10 μM Ht-31, or 50 μM LY294002 for 30 min prior to agonist stimulation and the effect on UCN-II (100 nM for 5 min) stimulation on ERK1/2 and p38 MAPK activation was determined, by measuring ERK1/2 and p38 MAPK phosphorylation as described in the Materials and Methods. Results are normalized for total ERK1/2 and expressed as arbitrary units. Data represent the mean ± SEM from three independent experiments. *, $P<0.05$ compared to control (no inhibitors) basal.

7.2.5 Agonist induced proliferation of T37i fibroblasts

Given that one of the main biological functions of the MAPK cascade is to promote cellular differentiation and proliferation, the role of CRH and UCN-II in T37i fibroblasts proliferation was evaluated. Incubation of cells with UCN-II or

CRH (1-100nM) for 48h, but not 24h, significantly increased cell proliferation as assessed by the number of viable cells; UCN-II was the more efficient of the two agonists used and increased fibroblast proliferation by 50% in a dose-dependent manner (Figure 7.11), whereas maximum CRH effect (30% increase compared to untreated) was observed at 10nM CRH. Incubation with higher concentrations of CRH did not significantly alter this effect (Figure 7.11).

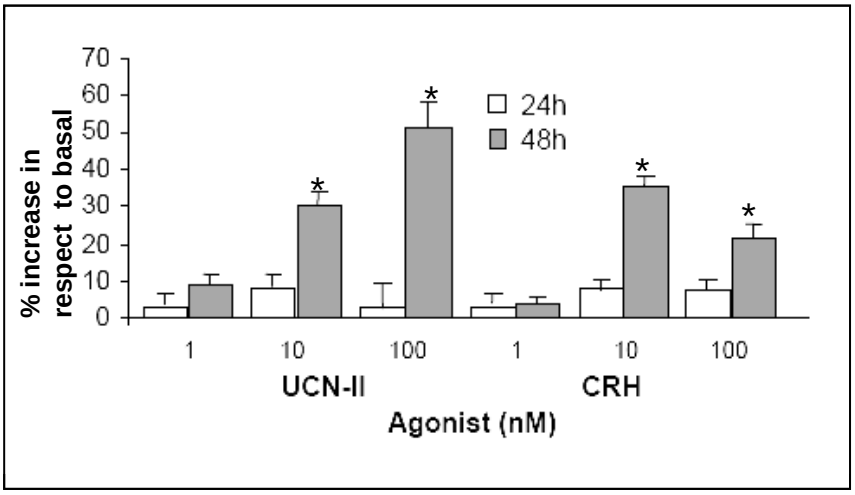

Figure 7.11. Effect of CRH and UCN-II on T37i fibroblast numbers. Cells were stimulated with various concentrations of CRH or UCN-II (1-100 nM) for 24 and 48 h. Cell proliferation was determined as described in the Materials and Methods. Data are representative of two independent experiments and are expressed as the mean ± SEM of 4 estimations.

7.2.6 Agonist induced lipolysis in T37i adipocytes

The potential link between CRH and UCN-II induced cAMP production in directly modulating lipolysis in T37i adipocytes was further investigated. To assess the lipolysis rate in adipocytes in response to CRH, UCN-II or isoproterenol, which was used as a positive control (Tebar F *et* al., 1996), glycerol release was measured. It was demonstrated that within 1h of isoproterenol treatment (1 μM), significant lipolysis was evident (Figure 7.12); this effect was time-dependent and 2h-treatment

with isoproterenol induced a further increase of glycerol release of 2.5 fold. Similar results were obtained when CRH or UCN-II were used as lipolysis-inducing agonists (Figure 7.12). Moreover, CRH was significant more potent than UCN-II in inducing lipolysis, although both CRH-R agonists were weaker than isoproterenol in inducing lipolysis. Analysis of the dose-dependent characteristics of CRH/UCN-II-induced lipolysis revealed that the maximum effect was achieved at low (1nM) agonist concentrations and that the lipolytic effect was diminished or abolished with higher (10-100nM) CRH or UCN-II concentrations. Use of specific signalling molecule inhibitors (PKAi and U0126) demonstrated that PKA, but not ERK1/2, was required for both CRH and UCN-II-induced glycerol release and lipolysis (Figure 7.13).

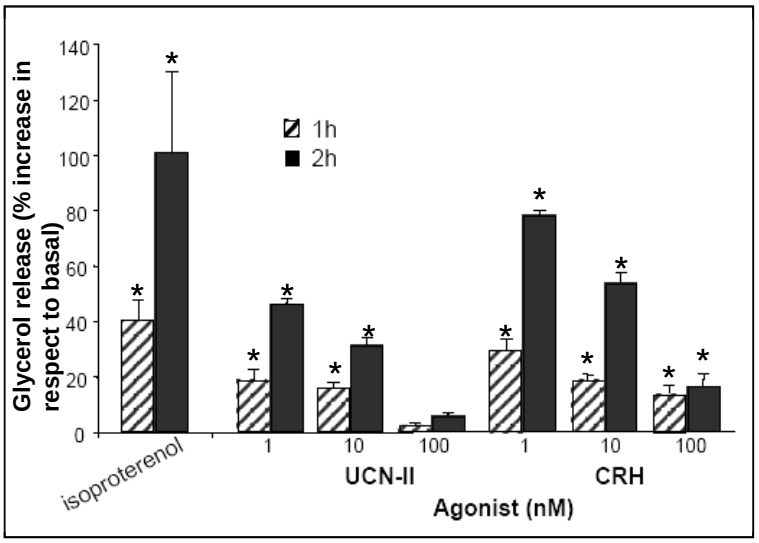

Figure 7.12. CRH and UCN-II induced lipolysis in T37i adipocytes. Cells were stimulated with isoproterenol (1 μM) or various concentrations of CRH or UCN-II (1-100 nM) for 1 or 2 hours and released glycerol was determined as described in methods. Data represents the mean ± SEM of three estimations from three independent experiments. *, P<0.05 compared to untreated cells.

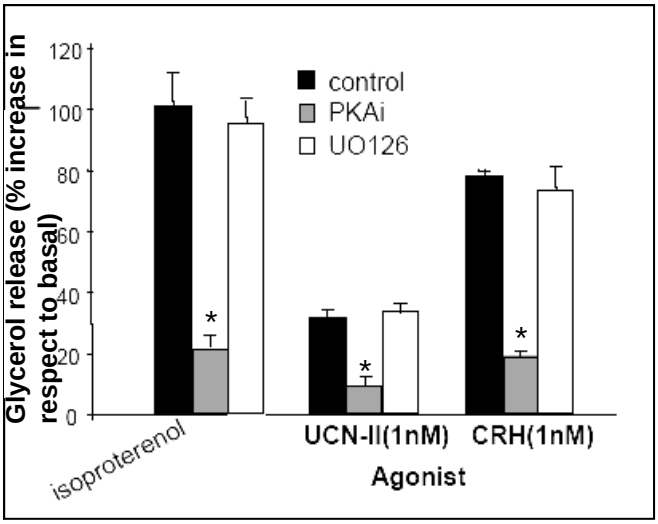

Figure 7.13. CRH and UCN-II induced lipolysis in T37i adipocytes is PKA dependent. Cells were pretreated with 1 μM PKAi for 30min or 10 μM U0126 for 40 min and then stimulated with isoproterenol (1 μM) or CRH or UCN-II (1 nM) for 2 hours and released glycerol was determined as described in the Materials and Methods. Data represents the mean±SEM of three estimations from three independent experiments. *, $P<0.05$ compared to the control treatments (no inhibitors)

7.2.7 The effect of CRH on perilipin and HSL translocation in T37i adipocytes

Lipolysis requires at least phosphorylation of perilipin and its translocation from lipid droplets, and phosphorylation of HSL and translocation to the droplets. In order to further dissect the lipolytic effect of CRH on T37i adipocytes, I investigated the effect of 1 nM CRH on possible translocation of perilipin and HSL.

Indirect confocal microscopy studies showed that prior to stimulation, perilipin was distributed exclusively around lipid droplets, evident as a "full circle" immunoreactive signal around the droplets. However, isoproterenol (1μM) or CRH (1nM) stimulation of the cells resulted in redistribution of perilipin signal from the

droplets to the cytoplasm. In addition, the perilipin signal on the droplet surface became diffuse and punctuate, suggesting redistribution of the protein. (Figure 7.14).

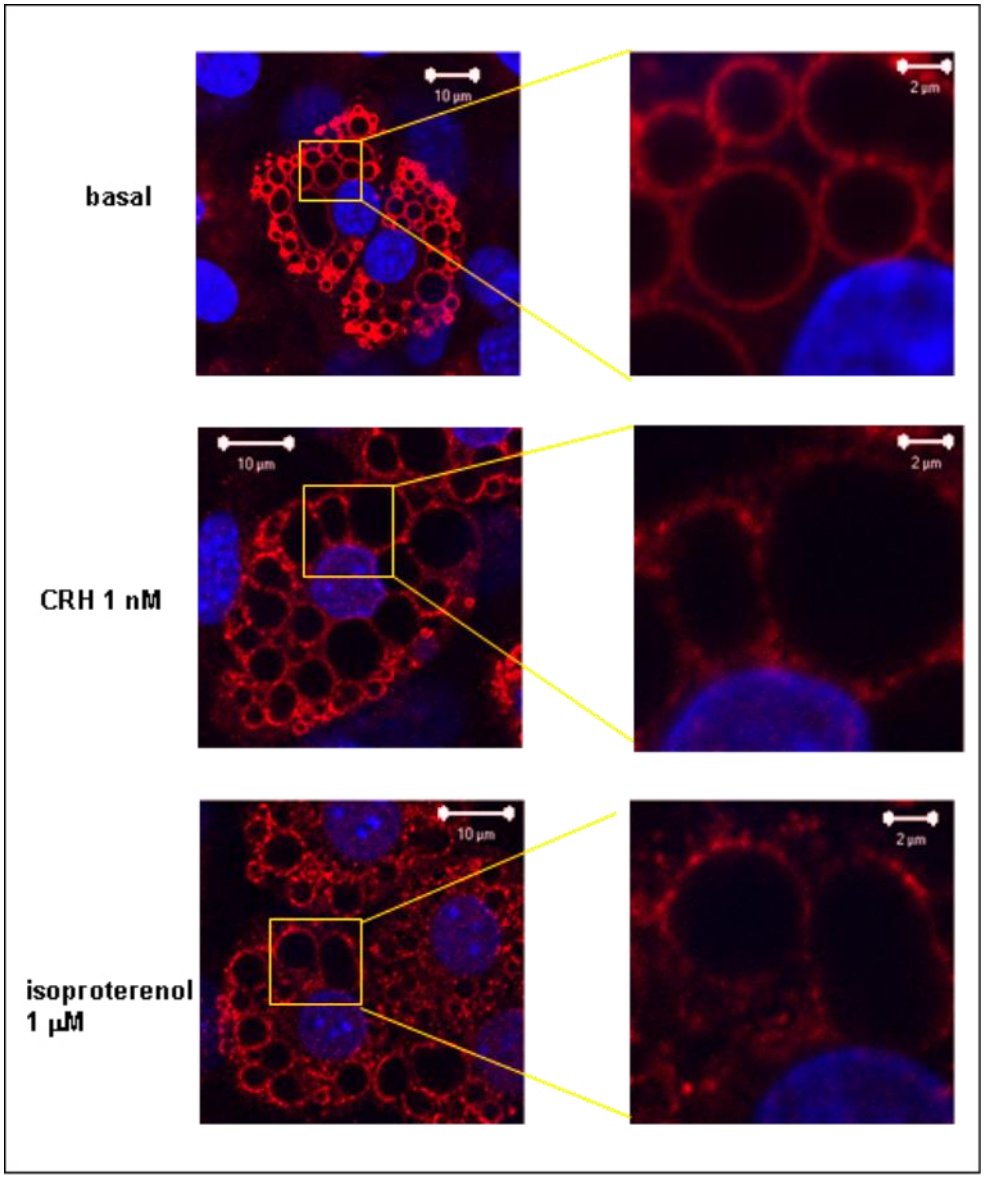

Figure 7.14. Visualization of perilipin A/B distribution in T37i adipocytes by indirect confocal microscopy. Cells were treated with 1 nM CRH or 1 µM isoproterenol for 15 min. Following fixation with 4 % PFA (in PBS) and blocking, the specific primary antibodies were used for perilipin A/B and Alexa-Fluor®594 secondary antibody (red). Cell nuclei were stained with the DNA specific dye DAPI (blue). Identical results were obtained in three independent experiments.

The cellular distribution of HSL was also monitored by indirect confocal microscopy. In unstimulated adipocytes, the protein was spread throughout the

cytoplasm and no staining around lipid droplets was detected. Following isoproterenol or CRH stimulation punctuate staining appeared around the droplets, suggesting the translocation of HSL to the site of lipolysis (Figure 7.15).

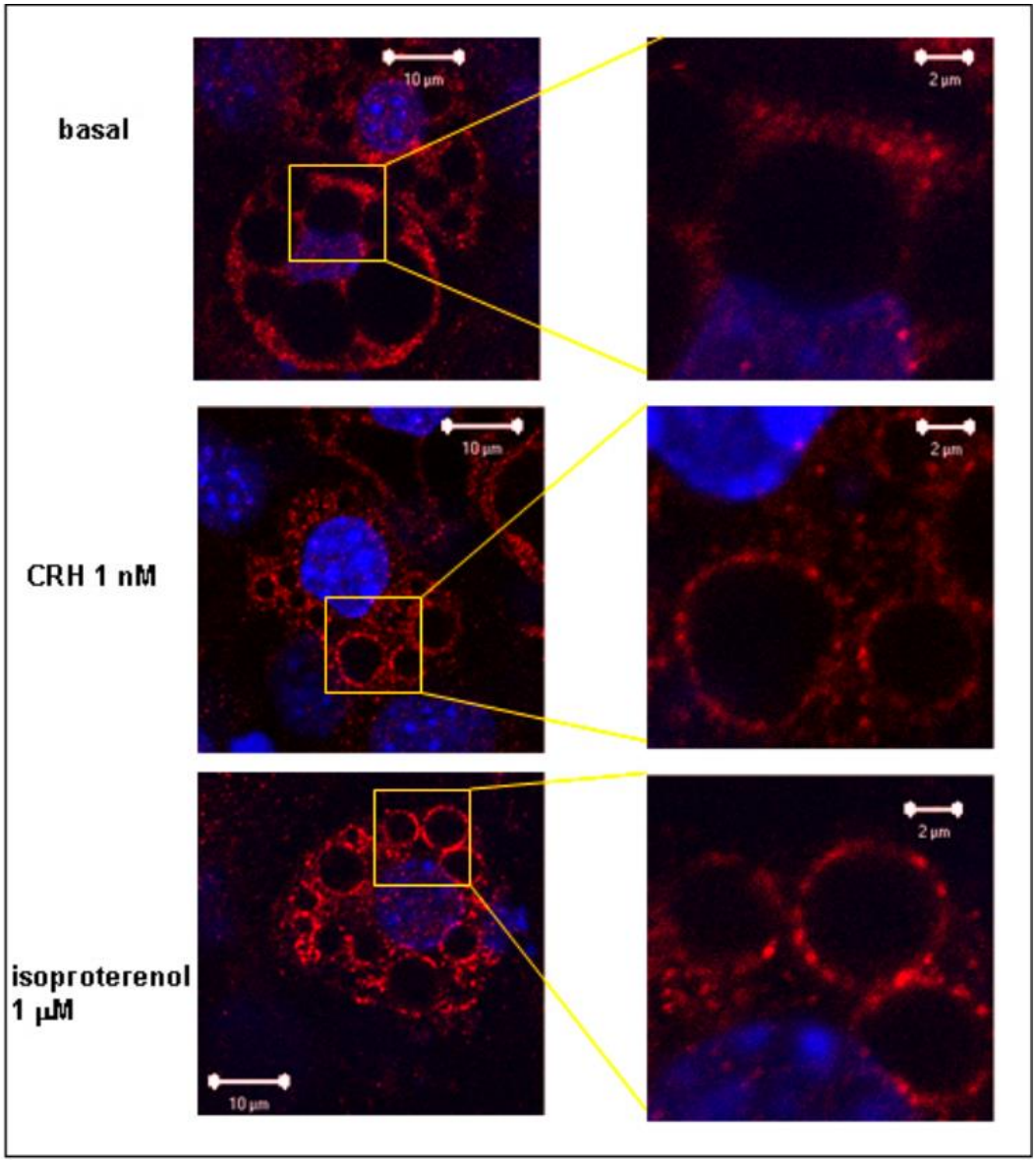

Figure 7.15. Visualization of HSL distribution in T37i adipocytes by indirect confocal microscopy. Cells were treated with 1 nM CRH or 1 µM isoproterenol for 15 min. Following fixation with 4 % PFA (in PBS) and blocking, the specific primary antibodies were used for HSL and Alexa-Fluor®594 secondary antibody (red). Cell nuclei were stained with the DNA specific dye DAPI (blue). Identical results were obtained in three independent experiments.

In addition, a preliminary data set suggested that 15 minutes treatment with 1 nM CRH leads to phosphorylation of HSL at the Ser-563. This residue as well as Ser-660 are the residues primarily targeted by PKA mediated phosphorylation and lead to the activation of HSL, and further lipolysis.

7.3 DISCUSSION

CRH and UCNs are potent regulators of mammalian thermogenesis and their effects on BAT have been primarily attributed to modulation of brain centres controlling sympathetic outflow; however potentially direct effects of CRH and UCNs' on brown adipocytes have not been investigated. In this chapter, it was demonstrated for the first time that the T37i cell line, a cellular model for BAT, expresses functional CRH-R that can influence lipolytic and other biological properties through activation of multiple signalling cascades.

The expression of both CRH-R1 and R2 receptor mRNA in brown adipocytes and BAT (Figure 7.2), suggests the presence of a wide receptor network that potentially can respond to multiple agonists and modulate diverse biological functions. Interestingly, using indirect confocal microscopy it has been shown that the CRH-R receptors are not uniformly distributed over the entire cell membrane, and that their localization is not restricted to the plasma membrane, as one might expect from GPCR. Immunofluorescence confocal microscopy experiments showed a punctuate pattern of extensive staining in the cytoplasm and around the nucleus potentially indicative of newly synthesised unprocessed receptors, internalised mature CRH-R or "cytoplasmic" forms of specific CRH-R variants (Figure 7.4).

A more detailed study employing different experimental approaches would be appropriate to determine the real nature of the CRH-R localisation in these model cells. The use of inhibitors of protein synthesis such as cycloheximide, would demonstrate whether perinuclear staining was indeed from newly synthesised CRH-Rs. Additionally, co-staining and potential co-localisation of CRH-R with protein markers of various cellular compartments would reveal the intracellular localisation of the receptor. The possibility of constitutive CRH-R endocytosis could be addressed by knocking down β-arrestins (as demonstrated in previous chapters, the internalization of both CRH-R1 and R2 requires the recruitment of β-arrestin to the plasma membrane), overexpressing dominant negative dynamin (K44A) which would inhibit clathrin mediated endocytosis, or using chemical inhibitors of internalisation such is ConconovalinA. All these three agents would block any constitutive receptor endocytosis and keep it trapped within the lipid bilayar of plasma membrane, which would result in increased CRH-R signal on the membrane.

The possibility that the cytoplasmic staining comes from the intracellular forms of the CRH-Rs, such as CRH-R1d, would be more difficult to assess because of a lack of splice variant specific antibodies. The specific silencing of certain types of the receptors would be possible with a careful consideration of the siRNA sequences, but a validation of silencing on the protein levels would be impossible, at least at this moment.

One of the most interesting features of CRH-Rs is their ability to activate diverse G-protein dependent and independent signalling pathways (Collins S *et* al., 2004; Hillhouse EW & Grammatopoulos DK, 2006). The results presented in this chapter demonstrated that in T37i adipocytes similarly to other cellular systems, CRH-R activation leads to downstream activation of at least two signalling cascades:

the adenylyl cyclase/cAMP and the MAPK (ERK1/2 and p38 MAPK) cascades (Hillhouse EW & Grammatopoulos DK, 2006).

These results also showed that CRH-R signalling characteristics exhibit another interesting feature not previously described: agonist concentration-dependent selectivity of the activated signalling pathway. At low agonist concentrations (close to the receptor binding affinity-Kd) intracellular cAMP levels are increased whereas high concentrations prevent cAMP increase (Figure 7.6) and instead induce transient ERK1/2 and p38 MAPK activation that appears to modulate primarily cytoplasmic targets (Figure 7.7-7.9). The precise nature of the molecular mechanisms mediating this signalling "switch" are unknown. Given that previous studies reviewed in Hillhouse and Grammatopoulos, 2006, have shown the potential of the receptor to activate Gi-proteins, one can hypothesise that agonist concentrations sufficient to induce substantial CRH-R-Gi-protein coupling might lead to inhibition of adenylyl cyclase activity and simultaneous MAPK phosphorylation through Gi-, Gq- or other pathways. This could be tested in future studies by implemented techniques for GPCR coupling to G-proteins. Additionally, use of siRNA to knock down individual G-proteins or dominant negative G-protein constructs would be an intriguing way to dissect the promiscuous signalling properties of CRH-R

In addition, the relative potencies of the CRH-R agonist tested could suggest that the CRH-R1 is primarily responsible for cAMP production, whereas the CRH-R2 is more efficiently linked to the MAPK pathway. This could be tested in the future by silencing the specific type of the CRH receptors, R1 or R2.

In mature brown adipocytes, norepinephrine interaction with β3-adrenergic receptor activates the adenylyl cyclase/cAMP cascade leading to activation of PKA

and consequent lipolysis (Cannon B & Nedergarrd J, 2004). Perilipin, a protein located on the lipid droplets, is phosphorylated by PKA and translocates from the droplets. At the same time HSL protein translocates from cytoplasmic compartments to its site of action, the lipid droplets (Egan JJ *et al*., 1992; Clifford GM *et al*., 2000). I have provided evidence that both CRH and UCN-II appear to induce lipolysis in T37i adipocytes through a PKA-dependent mechanism (Figure 7.12 and 7.13). The agonist concentration appeared to be one of the main determinants of lipolysis induction; however, at present the precise reason for this is not known. It is possible that this tight regulation of lipolysis prevents uncontrolled lipolysis and thermogenesis in conditions of excess CRH secretion such as in response to stressful stimuli. Additionally, the stimulation of T37i adipocytes with 1 nM CRH led to significant translocation of perilipin from and HSL towards the lipid droplets as demonstrated by indirect confocal microscopy (Figure 7.14 and 7.15).

Although an accessory role of the ERK1/2 pathway has been linked to lipolysis (Greenberg AS *et al*., 2001) in adipocytes, CRH-R-induced lipolysis appears to be ERK1/2 independent since it occurs at low concentrations of the agonists, considerably less than the concentrations required for MAPK activation.

It has been demonstrated that activation of ERK1/2 is important in cell proliferation and differentiation (Chang L & Karin M, 2001). It would be of interest that future studies determine the potency of CRH and UCN-II on MAPK activation during different stages of the cell differentiation. During the course of this study, most experiments were performed on cells composed of 85-90% adipocytes and 10-15% fibroblasts, however the proliferation assay was performed on T37i fibroblasts. It was demonstrated that CRH and UCN-II were potent proliferatory agents, most likely via activation of MAPK signalling cascade.

The data on the signalling pathways involved in T37i adipocyte CRH-R2-MAPK interactions suggest a critical role of PI(3)-kinase, a signalling molecule previously identified as being important for CRH-R2-stimulated thermogenesis in skeletal muscle (Solinas G *et al*., 2006). Use of a specific inhibitor showed that PI(3)-kinase is involved in selective activation of ERK1/2 in T37i adipocytes. Another interesting feature of the CRH-R2-MAPK interactions in T37i cells is that it occurs independently of the cAMP/PKA and AKAP pathway, at the tested concentration of agonist (100 nM), since the specific pathway inhibitors failed to alter UCN-II stimulated ERK1/2 or p38MAPK phosphorylation, although some inhibition was seen on basal activity. For agonist induced MAPK activation this is not surprising since the ERK1/2 and p38MAPK activation occurs at agonist concentration that are unable to induce cAMP production (Figure 7.10).

In summary, it was demonstrated for the first time that low levels of CRH and UCN-II can exert direct effects on brown adipocytes to induce lipolysis, and subsequent thermogenesis. This effect is mediated through the cAMP/PKA cascade, and involves phosphorylation and translocation of perilipin and HSL. However, at the higher concentration of the agonist the effect is reduced or abolished. This could be of potential physiological importance in mammals that rely on thermogenesis, such as rodents, hibernating animals and (even) human newborns. It is possible that in highly stressful situations when CRH is excessively secreted, the BAT lipolysis is shut down, whereas during the physiological states of low stress, such as hibernation and sleep, when CRH levels are lower, this peptide induces thermogenesis.

8 CONCLUSION

In addition to its traditional role as an activator of the HPA axis and a coordinator of autonomic, behavioural, emotional, immune, and cognitive responses to stress, corticortopin releasing hormone (CRH) and the related peptides (UCN-I, UCN-II and UCN-III) have been implicated in mediating diverse peripheral functions (i.e. in reproduction, cancer biology, metabolism and energy homeostasis). The regulation of these various central and peripheral functions is mediated via activation of one or both CRH receptors, R1 and R2. In many tissues endogenously expressing CRH-R stimulation of the receptor by CRH or CRH-related peptides leads to the activation of adenylyl cyclase (AC) and increases cAMP levels. However, other signalling cascades such as the MAPK signalling pathway, are also targeted by CRH-R activation. The distinct response of CRH-R activation has been attributed to differential and multiple G-protein activation. The peripheral expression of CRH-R1 and R2 exhibits a species dependent pattern with R2 receptor as the main functional receptor in animal peripheral tissues, most peripheral human tissues express both types of CRH receptors, indicating higher levels of complexity and more subtle roles for CRH and UCNs in human physiology.

Tables 8.1 and 8.2 summarize the characteristics of the receptor studied in this thesis.

CRH-R1	Homologous internalizat i-on	β-arrestin recruitment to the PM	Co-localization (R1 and β-arrestin) in cytoplasm	Heterologous internalization (PKC dependent)	β-arrestin recruitment to the PM	Co-localization (R1 and β-arrestin) in cytoplasm
R1α	Yes	Yes	Yes	No	No	No
R1β	Yes	Yes	Yes	Yes	No	No
R1d	Yes	Yes	No	----------	----------	----------

Table 8.1. Internalization characteristics of CRH-R1 splice variants.

Receptor	Desensitization	Internalization	MAPK activation
CRH-R2β	Fast (15 min)	β-arrestin recruited to the plasma membrane. No co-localization in the cytoplasmic compartments	β-arrestin and internalization independent
CRH-R1α	Slow (2-3h) (Teli T *et al.*,2005)	β-arrestin recruited to the plasma membrane. Partial co-localization in the cytoplasmic compartments	β-arrestin and internalization dependent (Punn A *et al.*, 2006)

Table 8.2. Internalization and signalling characteristics of CRH receptors type 1 and 2.

This study was the first to demonstrate that although sharing 70% sequence homology, the CRH-R1 and R2 receptors have different desensitization, internalization and signalling characteristics. Desensitization of CRH-R2 is remarkably different from the response of the CRH-R1α, which requires CRH treatment for 2-3 h to achieve a similar level of desensitization as CRH-R2β after

just 15 min. This might reflect distinct requirements of the two CRH receptors' signalling propagation in mammalian pathophysiology. Moreover, this could be of pivotal importance in physiological conditions accompanied by the changes in the receptor expression patterns (i.e. in uterus during pregnancy). In addition, the co-expression studies have provided evidence that CRH-R1d attenuates effects of UCN-II induced CRH-R2β activation. This is of potential importance in understanding how the action of urocortins via activation of CRH-R2 are controlled in peripheral tissues, such as skin, muscle and adipose tissue, that express both types of receptors.

Tissue sensitivity to agonists is determined by the availability of receptor in the plasma membrane. The immunofluorescence studies investigating the cellular expression of CRH-R1 variants have provided novel evidence that in HEK293 over-expressing CRH-R1α and R1β, the receptor protein is localised in the plasma membrane, while another splice variant termed CRH-R1d is primarily expressed intracellularly.

The mechanisms regulating CRH-R1 alternative splicing are largely unknown. *In vitro* studies in myometrial cells identified IL-1β, a pro-inflammatory cytokines implicated in the onset of labour and the pathogenesis of infection-induced preterm labour, as a potential regulator of CRH-R1 gene transcription and splicing pattern. However, increased CRH-R1 gene transcription and generation of receptor splice variants was not associated with increased CRH-R protein levels and CRH signalling activity, implicating a complex regulation of CRH biological action.

CRH and UCNs are potent regulators of mammalian thermogenesis and their effects on BAT have been primarily attributed to modulation of brain centers controlling sympathetic outflow; however direct effects of CRH and UCNs on

brown adipocytes have not been investigated. During the course of this study, it was demonstrated that both types of CRH-Rs are expressed in mice BAT and T37i cells. CRH-R activation led to downstream activation of at least two signalling cascades: the adenylyl cyclase/cAMP/PKA and the MAPK (ERK1/2 and p38MAPK) cascades. CRH mediated activation of PKA led to lipolysis in adipocytes; on the other hand, UCN-II stimulation of T37i preadipocytes led to increased proliferation. The efficiency of the CRH-R agonist tested could suggest that the CRH-R1 is primarily responsible for cAMP production, while the CRH-R2 is linked to the MAPK pathway. It would be intriguing to determine if CRH-Rs are expressed and functional in human infant BAT, and to investigate the potential link between increased maternal CRH levels and newborn BAT activity.

9 BIBLIOGRAPHY

Aggelidou E, Hillhouse EW, Grammatopoulos DK (2002) Up-regulation of nitric oxide synthase and modulation of the guanylate cyclase activity by corticotropin-releasing hormone but not urocortin II or urocortin III in cultured human pregnant myometrial cells.*Proc Natl Acad Sci U S A.* **99(5):**3300-5.

Albright AL, Stern JS (1998) http://www.sportsci.org/encyc/adipose/adipose.html

Anthonsen MW, Rönnstrand L, Wernstedt C, Degerman E, Holm C (1998) Identification of novel phosphorylation sites in hormone-sensitive lipase that are phosphorylated in response to isoproterenol and govern activation properties in vitro.*J Biol Chem.* **273(1):**215-21

Arai M, Assil IQ, Abou-Samra AB (2001) Characterization of three corticotropin-releasing factor receptors in catfish: a novel third receptor is predominantly expressed in pituitary and urophysis. *Endocrinology*. **142(1):**446-54.

Arase K, York DA, Shargill NS, Bray GA (1989) Interaction of adrenalectomy and fenfluramine treatment on body weight, food intake and brown adipose tissue.*Physiol Behav.* **45(3):**557-64.

Arase K, York DA, Shimizu H, Shargill N, Bray GA (1988) Effects of corticotropin-releasing factor on food intake and brown adipose tissue

thermogenesis in rats.*Am J Physiol*. **255(3 Pt 1):**E255-9.

Ardati A, Goetschy V, Gottowick J, Henriot S, Valdenaire O, Deuschle U, Kilpatrick GJ (1999) Human CRF2 alpha and beta splice variants: pharmacological characterization using radioligand binding and a luciferase gene expression assay. *Neuropharmacology*. **38(3):**441-8.

Arenzana-Seisdedos F, Turpin P, Rodriguez M, Thomas D, Hay RT, Virelizier JL, Dargemont C (1997) Nuclear localization of I kappa B alpha promotes active transport of NF-kappa B from the nucleus to the cytoplasm.*J Cell Sci.* **110 (Pt 3):**369-78

Asakura H, Zwain IH, Yen SS (1997) Expression of genes encoding corticotropin-releasing factor (CRF), type 1 CRF receptor, and CRF-binding protein and localization of the gene products in the human ovary. *J Clin Endocrinol Metab.* **82(8):**2720-5

Austgen L (2002)
http://www.vivo.colostate.edu/hbooks/pathphys/misc_topics/brownfat.html

Baeuerle PA, Henkel T (1994) Function and activation of NF-kappa B in the immune system. *Annu Rev Immunol*. **12**:141-79

Bale TL, Anderson KR, Roberts AJ, Lee KF, Nagy TR, Vale WW (2003) Corticotropin-releasing factor receptor-2-deficient mice display abnormal homeostatic responses to challenges of increased dietary fat and cold. *Endocrinology*. **144(6):**2580-7.

Bale TL, Picetti R, Contarino A, Koob GF, Vale WW, Lee KF.(2002) Mice deficient for both corticotropin-releasing factor receptor 1 (CRFR1) and CRFR2

have an impaired stress response and display sexually dichotomous anxiety-like behavior. *J Neurosci.* **22(1):**193-9.

Bale TL, Contarino A, Smith GW, Chan R, Gold LH, Sawchenko PE, Koob GF, Vale WW, Lee KF (2000) Mice deficient for corticotropin-releasing hormone receptor-2 display anxiety-like behaviour and are hypersensitive to stress. *Nat Genet.* **24(4):**410-4

Barnes PJ, Karin M (1997) Nuclear factor-kappaB: a pivotal transcription factor in chronic inflammatory diseases. *N Engl J Med.* **336(15):**1066-71

Barnes WG, Reiter E, Violin JD, Ren XR, Milligan G, Lefkowitz RJ (2005) beta-Arrestin 1 and Galphaq/11 coordinately activate RhoA and stress fiber formation following receptor stimulation.*J Biol Chem.* **280(9):**8041-50

Bartlett SR, Sawdy R, Mann GE (1999) Induction of cyclooxygenase-2 expression in human myometrial smooth muscle cells by interleukin-1beta: involvement of p38 mitogen-activated protein kinase. *J Physiol*. **520 Pt 2:**399-406.

Beaulieu JM, Sotnikova TD, Marion S, Lefkowitz RJ, Gainetdinov RR, Caron MG. (2005) An Akt/beta-arrestin 2/PP2A signaling complex mediates dopaminergic neurotransmission and behavior. *Cell*. **122(2):**261-73.

Beg AA, Sha WC, Bronson RT, Ghosh S, Baltimore D (1995) Embryonic lethality and liver degeneration in mice lacking the RelA component of NF-kappa B.*Nature* **376(6536):**167-70.

Behan DP, Linton EA, Lowry PJ (1989) Isolation of the human plasma corticotrophin-releasing factor-binding protein.*J Endocrinol*. **122(1):**23-31

Behan DP, Potter E, Lewis KA, Jenkins NA, Copeland N, Lowry PJ, Vale WW (1993) Cloning and structure of the human corticotrophin releasing factor-binding protein gene (CRHBP) *Genomics.* **16(1):**63-8.

Belt AR, Baldassare JJ, Molnár M, Romero R, Hertelendy F (1999) The nuclear transcription factor NF-kappaB mediates interleukin-1beta-induced expression of cyclooxygenase-2 in human myometrial cells. *Am J Obstet Gynecol.* **181(2):**359-66

Benovic JL, DeBlasi A, Stone WC, Caron MG, Lefkowitz RJ (1989) Beta-adrenergic receptor kinase: primary structure delineates a multigene family. *Science* **246(4927):**235-40.

Benovic JL, Onorato JJ, Arriza JL, Stone WC, Lohse M, Jenkins NA, Gilbert DJ, Copeland NG, Caron MG, Lefkowitz RJ (1991) Cloning, expression, and chromosomal localization of beta-adrenergic receptor kinase 2. A new member of the receptor kinase family. *J Biol Chem.* **266(23):**14939-46.

Benovic JL, Gomez J (1993) Molecular cloning and expression of GRK6. A new member of the G protein-coupled receptor kinase family. *J Biol Chem* **268(26):**19521-7.

Bernlohr DA, Simpson MA, Hertzel AV, Banaszak LJ (1997) Intracellular lipid-binding proteins and their genes.*Annu Rev Nutr.***17:**277-303

Betuing S, Daviaud D, Pages C, Bonnard E, Valet P, Lafontan M, Saulnier-Blache JS (1998) Gbeta gamma-independent coupling of alpha2-adrenergic receptor to p21(rhoA) in preadipocytes.*J Biol Chem.***273(25):**15804-10.

Bhattacharya M, Babwah AV, Ferguson SS (2004) Small GTP-binding protein-coupled receptors.*Biochem Soc Trans.* **32(Pt 6):**1040-4

Blank T, Nijholt I, Grammatopoulos DK, Randeva HS, Hillhouse EW, Spiess J (2003) Corticotropin-releasing factor receptors couple to multiple G-proteins to activate diverse intracellular signaling pathways in mouse hippocampus: role in neuronal excitability and associative learning. *J Neurosci.* **23(2):**700-7.

Boutillier AL, Sassone-Corsi P, Loeffler JP (1991) The protooncogene c-fos is induced by corticotropin-releasing factor and stimulates proopiomelanocortin gene transcription in pituitary cells. *Mol Endocrinol.* **5(9):**1301-10.

Bonizzi G, Karin M (2004) The two NF-kappaB activation pathways and their role in innate and adaptive immunity. *Trends Immunol.* **25(6):**280-8.

Bonnard M, Mirtsos C, Suzuki S, Graham K, Huang J, Ng M, Itie A, Wakeham A, Shahinian A, Henzel WJ, Elia AJ, Shillinglaw W, Mak TW, Cao Z, Yeh WC (2000) Deficiency of T2K leads to apoptotic liver degeneration and impaired NF-kappaB-dependent gene transcription. *EMBO J*. **19(18):**4976-85.

Brar BK, Jonassen AK, Egorina EM, Chen A, Negro A, Perrin MH, Mjos OD, Latchman DS, Lee KF, Vale W (2004) Urocortin-II and urocortin-III are cardioprotective against ischemia reperfusion injury: an essential endogenous cardioprotective role for corticotropin releasing factor receptor type 2 in the murine heart.*Endocrinology***145(1):**24-35

Brar BK, Chen A, Perrin MH, Vale W (2004) Specificity and regulation of extracellularly regulated kinase1/2 phosphorylation through corticotropin-releasing factor (CRF) receptors 1 and 2beta by the CRF/urocortin family of peptides. *Endocrinology***145(4):**1718-29

Breuiller-Fouche M, Moriniere C, Dallot E, Oger S, Rebourcet R, Cabrol D, Leroy MJ (2005) Regulation of the endothelin/endothelin receptor system by interleukin-

1{beta} in human myometrial cells. *Endocrinology***146(11):**4878-86

Brooks SL, Rothwell NJ, Stock MJ, Goodbody AE, Trayhurn P (1980) Increased proton conductance pathway in brown adipose tissue mitochondria of rats exhibiting diet-induced thermogenesis. *Nature* **286(5770):**274-6.

Cao J, Papadopoulou N, Kempuraj D, Boucher WS, Sugimoto K, Cetrulo CL, Theoharides TC (2005) Human mast cells express corticotropin-releasing hormone (CRH) receptors and CRH leads to selective secretion of vascular endothelial growth factor. *J Immunol.* **174(12):**7665-75.

Cannon B, Nedergaard J. Brown adipose tissue: function and physiological significance (2004) *Physiol Rev.* **84(1):**277-359

Carlin KM, Vale WW, Bale TL (2006) Vital functions of corticotropin-releasing factor (CRF) pathways in maintenance and regulation of energy homeostasis. *Proc Natl Acad Sci U S A.* **103(9):**3462-7.

Carmen GY, Víctor SM (2006) Signalling mechanisms regulating lipolysis.*Cell Signal.* **(4):**401-8

Carr BR, Rehman KS (2004) Fertilization, Implantation, and Endocrinology of Pregnancy *Textbook of Endocrine Physiology* **249-274**

Challis JRG, Matthews SG, Gibb W, Lye SJ (2000) Endocrine and paracrine regulation of birth at term and preterm. *Endocr Rev.* **21(5):**514-50

Chalmers DT, Lovenberg TW, De Souza EB (1995) Localization of novel corticotropin-releasing factor receptor (CRF2) mRNA expression to specific

subcortical nuclei in rat brain: comparison with CRF1 receptor mRNA expression. *J Neurosci.* **15(10):**6340-50.

Chang L, Karin M. Mammalian MAP kinase signalling cascades (2001) *Nature*. **410(6824):**37-40.

Chapman NR, Europe-Finner GN, Robson SC (2004) Expression and deoxyribonucleic acid-binding activity of the nuclear factor kappaB family in the human myometrium during pregnancy and labor. *J Clin Endocrinol Metab*. **89(11):**5683-93.

Chen A, Brar B, Choi CS, Rousso D, Vaughan J, Kuperman Y, Kim SN, Donaldson C, Smith SM, Jamieson P, Li C, Nagy TR, Shulman GI, Lee KF, Vale W (2006) Urocortin 2 modulates glucose utilization and insulin sensitivity in skeletal muscle. *Proc Natl Acad Sci U S A.* **103(44):**16580-5

Chen FE, Ghosh G (1999) Regulation of DNA binding by Rel/NF-kappaB transcription factors: structural views. *Oncogene.* **18(49):**6845-52

Chen F, Demers LM, Shi X (2002) Upstream signal transduction of NF-kappaB activation. *Curr Drug Targets Inflamm Allergy*. **1(2):**137-49.

Chen R, Lewis KA, Perrin MH, Vale WW (1993) Expression cloning of a human corticotropin-releasing-factor receptor. *Proc Natl Acad Sci U S A.* **90(19):**8967-71.

Chen ZJ, Parent L, Maniatis T (1996) Site-specific phosphorylation of IkappaBalpha by a novel ubiquitination-dependent protein kinase activity. *Cell* **84(6):**853-62.

Cerione RA, Codina J, Benovic JL, Lefkowitz RJ, Birnbaumer L, Caron MG (1984)

The mammalian beta 2-adrenergic receptor: reconstitution of functional interactions between pure receptor and pure stimulatory nucleotide binding protein of the adenylate cyclase system. *Biochemistry.* **23(20):**4519-25

Claing A, Laporte SA, Caron MG, Lefkowitz RJ (2002) Endocytosis of G protein-coupled receptors: roles of G protein-coupled receptor kinases and beta-arrestin proteins. *Prog Neurobiol.* **66(2):**61-79.

Clifford GM, Londos C, Kraemer FB, Vernon RG, Yeaman SJ (2000) Translocation of hormone-sensitive lipase and perilipin upon lipolytic stimulation of rat adipocytes. *J Biol Chem.* **275(7):**5011-5.

Collins S, Cao W, Robidoux J (2004) Learning new tricks from old dogs: beta-adrenergic receptors teach new lessons on firing up adipose tissue metabolism. *Mol Endocrinol.* **18(9):**2123-31

Colledge M, Scott JD (1999) AKAPs: from structure to function. *Trends Cell Biol.* **9(6):**216-21.

Cooper JR, Bloom FE, Roth RH (1991) The Biochemical Basis of Neuropharmacology, Oxford Press, New York

Craft CM, Whitmore DH, Wiechmann AF (1994)Cone arrestin identified by targeting expression of a functional family. *J Biol Chem.* **269(6):**4613-9

Cullen MJ, Ling N, Foster AC, Pelleymounter MA (2001) Urocortin, corticotropin releasing factor-2 receptors and energy balance. *Endocrinology* **142(3):**992-9.

Dautzenberg FM, Hauger RL (2002) The CRF peptide family and their receptors: yet more partners discovered. *Trends Pharmacol Sci.* **23(2):**71-7

Dautzenberg FM, Braun S, Hauger RL (2001) GRK3 mediates desensitization of CRF1 receptors: a potential mechanism regulating stress adaptation. *Am J Physiol Regul Integr Comp Physiol* **280(4):**R935-46.

Deckert CM, Heiker JT, Beck-Sickinger AG (2006) Localization of novel adiponectin receptor constructs. *J Recept Signal Transduct Res.* **26(5-6):**647-57.

Degerman E, Smith CJ, Tornqvist H, Vasta V, Belfrage P, Manganiello VC (1990) Evidence that insulin and isoprenaline activate the cGMP-inhibited low-Km cAMP phosphodiesterase in rat fat cells by phosphorylation. *Proc Natl Acad Sci U S A.* **87(2):**533-7.

Dermitzaki E, Tsatsanis C, Gravanis A, Margioris AN (2002) Corticotropin-releasing hormone induces Fas ligand production and apoptosis in PC12 cells via activation of p38 mitogen-activated protein kinase. *J Biol Chem.* **277(14):**12280-7

DeWire SM, Ahn S, Lefkowitz RJ, Shenoy SK (2007) Beta-arrestins and cell signaling. *Annu Rev Physiol.* **69**:483-510

Ding C, Racusen L, Wilson P, BurrowC, Levine MA (1995) *J Bone Miner Res* **10 (Suppl 1):**S484

Di Blasio AM, Pecori Giraldi F, Vigano P, Petraglia F, Vignali M, Cavagnini F (1997) Expression of corticotropin-releasing hormone and its R1 receptor in human endometrial stromal cells. *J Clin Endocrinol Metab*. **82(5):**1594-7.

Diviani D, Soderling J, Scott JD (2001) AKAP-Lbc anchors protein kinase A and nucleates Galpha 12-selective Rho-mediated stress fiber formation. *J Biol Chem.* **276(47):**44247-57

Egan JJ, Greenberg AS, Chang MK, Wek SA, Moos MC Jr, Londos C (1992) Mechanism of hormone-stimulated lipolysis in adipocytes: translocation of hormone-sensitive lipase to the lipid storage droplet. *Proc Natl Acad Sci U S A.* **89(18):**8537-41.

Egawa M, Yoshimatsu H, Bray GA (1990) Preoptic area injection of corticotropin-releasing hormone stimulates sympathetic activity. *Am J Physiol.* **259(4 Pt 2):**R799-806

Egawa M, Yoshimatsu H, Bray GA (1990b) Effect of corticotropin releasing hormone and neuropeptide Y on electrophysiological activity of sympathetic nerves to interscapular brown adipose tissue. *Neuroscience.* **34(3):**771-5.

Eckart K, Jahn O, Radulovic J, Tezval H, van Werven L, Spiess J (2001) A single amino acid serves as an affinity switch between the receptor and the binding protein of corticotropin-releasing factor: implications for the design of agonists and antagonists *Proc Natl Acad Sci U S A.* **98(20):**11142-7.

Engqvist-Goldstein AE, Zhang CX, Carreno S, Barroso C, Heuser JE, Drubin DG (2004) RNAi-mediated Hip1R silencing results in stable association between the endocytic machinery and the actin assembly machinery. *Mol Biol Cell.* **15(4):**1666-79

Ermak G, Slominski A (1997) Production of POMC, CRH-R1, MC1, and MC2 receptor mRNA and expression of tyrosinase gene in relation to hair cycle and dexamethasone treatment in the C57BL/6 mouse skin. *J Invest Dermatol.* **108(2):**160-5.

Fan GH, Yang W, Wang XJ, Qian Q, Richmond A (2001) Identification of a motif

in the carboxyl terminus of CXCR2 that is involved in adaptin 2 binding and receptor internalization. *Biochemistry.* **40(3):**791-800.

Ferguson SS (2001) Evolving concepts in G protein-coupled receptor endocytosis: the role in receptor desensitization and signaling. *Pharmacol Rev*. **53(1):**1-24.

Garton AJ, Yeaman SJ (1990) Identification and role of the basal phosphorylation site on hormone-sensitive lipase. *Eur J Biochem* **191(1):**245-50.

Ghosh S, May MJ, Kopp EB (1998) NF-kappa B and Rel proteins: evolutionarily conserved mediators of immune responses. *Annu Rev Immunol.* **16:**225-60.

Ghosh S, Karin M (2002) Missing pieces in the NF-kappaB puzzle.*Cell.* **109** Suppl:S81-96.

Gliemann J (1970) on the action of insulin on isolated fat cells. *Horm Metab Res*. **2:**Suppl 2:116-9.

Gilmore TD (1999) The Rel/NF-kappaB signal transduction pathway: introduction. *Oncogene* **18(49):**6842-4.

Glowa JR, Gold PW (1991) Corticotropin releasing hormone produces profound anorexigenic effects in the rhesus monkey. *Neuropeptides.***18(1):**55-61.

Gohla A, Harhammer R, Schultz G (1998) The G-protein G13 but not G12 mediates signaling from lysophosphatidic acid receptor via epidermal growth factor receptor to Rho.*J Biol Chem*.**273(8):**4653-9.

Gomes I, Jordan BA, Gupta A, Rios C, Trapaidzen N, Devi LA. (2001). G protein coupled receptor dimerization: implication in modulating receptor function. *J. Mol. Med* **79(5-6):**226-42.

Goodman OB Jr, Krupnick JG, Santini F, Gurevich VV, Penn RB, Gagnon AW, Keen JH, Benovic JL (1996) Beta-arrestin acts as a clathrin adaptor in endocytosis of the beta2-adrenergic receptor. *Nature*.**383(6599)**:447-50.

Grammatopoulos DK (2007)The role of CRH receptors and their agonists in myometrial contractility and quiescence during pregnancy and labour. *Front Biosci.* **12**:561-71.

Grammatopoulos DK, Chrousos GP (2002) Functional characteristics of CRH receptors and potential clinical applications of CRH-receptor antagonists. *Trends Endocrinol Metab.***13(10):**436-44.

Grammatopoulos DK, Randeva HS, Levine MA, Kanellopoulou KA, Hillhouse EW. (2001) Rat cerebral cortex corticotropin-releasing hormone receptors: evidence for receptor coupling to multiple G-proteins. *J Neurochem.***76(2):**509-19.

Grammatopoulos DK, Randeva HS, Levine MA, Katsanou ES, Hillhouse EW. (2000) Urocortin, but not corticotropin-releasing hormone (CRH), activates the mitogen-activated protein kinase signal transduction pathway in human pregnant myometrium: an effect mediated via R1alpha and R2beta CRH receptor subtypes and stimulation of Gq-proteins.Mol Endocrinol. 14(12):2076-91.

Grammatopoulos DK, Hillhouse EW. (1999a) Activation of protein kinase C by oxytocin inhibits the biological activity of the human myometrial corticotropin-releasing hormone receptor at term. *Endocrinology*. **140(2):**585-94.

Grammatopoulos DK, Hillhouse EW. (1999b) Basal and interleukin-1beta-stimulated prostaglandin production from cultured human myometrial cells: differential regulation by corticotropin-releasing hormone. *J Clin Endocrinol Metab*.**84(6):**2204-11.

Grammatopoulos DK, Hillhouse EW.(1999c) Role of corticotropin-releasing hormone in onset of labour. *Lancet.* **354(9189):**1546-9.

Grammatopoulos DK, Dai Y, Randeva HS, Levine MA, Karteris E, Easton AJ, Hillhouse EW.(1999) A novel spliced variant of the type 1 corticotropin-releasing hormone receptor with a deletion in the seventh transmembrane domain present in the human pregnant term myometrium and fetal membranes. *Mol Endocrinol.13* **(12):**2189-202.

Grammatopoulos D, Hillhouse EW (1998a). Solubilization and biochemical characterization of the human myometrial corticotrophin-releasing hormone receptor.
Mol Cell Endocrinol. **138(1-2):**185-98.

Grammatopoulos D, Dai Y, Chen J, Karteris E, Papadopoulou N, Easton AJ, Hillhouse EW. (1998b) Human corticotropin-releasing hormone receptor: differences in subtype expression between pregnant and nonpregnant myometria. *J Clin Endocrinol Metab*. **83(7):**2539-44.

Grammatopoulos D, Stirrat GM, Williams SA, Hillhouse EW. (1996) The biological activity of the corticotropin-releasing hormone receptor-adenylate cyclase complex in human myometrium is reduced at the end of pregnancy. *J Clin Endocrinol Metab*. **81(2):**745-51.

Grammatopoulos D, Thompson S, Hillhouse EW.(1995) The human myometrium

expresses multiple isoforms of the corticotropin-releasing hormone receptor. *J Clin Endocrinol Metab.* **80(8):**2388-93.

Grammatopoulos D, Milton NG, Hillhouse EW.(1994) The human myometrial CRH receptor: G proteins and second messengers. *Mol Cell Endocrinol.* **99(2):**245-50.

Granzin J, Wilden U, Choe HW, Labahn J, Krafft B, Buldt G. (1998) X-ray crystal structure of arrestin from bovine rod outer segments. *Nature.* **391(6670):**918-21.

Grigoriadis DE, De Souza EB. (1989) Heterogeneity between brain and pituitary corticotropin-releasing factor receptors is due to differential glycosylation. *Endocrinology.* **125(4):**1877-88

Grinninger C, Wang W, Oskoui KB, Voice JK, Goetzl EJ. A natural variant type II G protein-coupled receptor for vasoactive intestinal peptide with altered function. J Biol Chem. 2004 Sep 24;279(39):40259-62.

Greenberg AS, Shen WJ, Muliro K, Patel S, Souza SC, Roth RA, Kraemer FB. (2001) Stimulation of lipolysis and hormone-sensitive lipase via the extracellular signal-regulated kinase pathway. *J Biol Chem*. **276(48):**45456-61

Hamann A, Benecke H, Le Marchand-Brustel Y, Susulic VS, Lowell BB, Flier JS. (1995) Characterization of insulin resistance and NIDDM in transgenic mice with reduced brown fat. *Diabetes.* **44(11):**1266-73.

Harhammer R, Gohla A, Schultz G. (1996) Interaction of G protein Gbetagamma dimers with small GTP-binding proteins of the Rho family. *FEBS Lett* **399(3):**211-4.

Hayashi K, Yonemura S, Matsui T, Tsukita S. (1999) Immunofluorescence detection of ezrin/radixin/moesin (ERM) proteins with their carboxyl-terminal threonine phosphorylated in cultured cells and tissues. *J Cell Sci.* **112 (Pt 8):**1149-58

Hayden MS, Ghosh S.(2004) Signaling to NF-kappaB. *Genes Dev.* **18(18):**2195-224.

Higuchi R, Krummel B, Saiki RK.(1988) A general method of in vitro preparation and specific mutagenesis of DNA fragments: study of protein and DNA interactions.
Nucleic Acids Res. **16(15):**7351-67.

Hillhouse EW, Grammatopoulos DK. (2006) The molecular mechanisms underlying the regulation of the biological activity of corticotropin-releasing hormone receptors: implications for physiology and pathophysiology. *Endocr Rev.* **27(3):**260-86.

Hillhouse EW, Grammatopoulos DK.(2002) Role of stress peptides during human pregnancy and labour. *Reproduction.* **124(3):**323-9.

Hillhouse EW, Grammatopoulos DK (2001). Control of intracellular signalling by corticotropin-releasing hormone in human myometrium. *Front Horm Res*. **27:**66-74.

Hillhouse EW, Grammatopoulos D, Milton NG, Quartero HW.(1993) The identification of a human myometrial corticotropin-releasing hormone receptor that increases in affinity during pregnancy. *J Clin Endocrinol Metab.* **76(3):**736-41.

Hisatomi O, Matsuda S, Satoh T, Kotaka S, Imanishi Y, Tokunaga F.(1998) A novel subtype of G-protein-coupled receptor kinase, GRK7, in teleost cone photoreceptors. *FEBS Lett.* **424(3):**159-64

Hoare SR, Sullivan SK, Fan J, Khongsaly K, Grigoriadis DE. (2005) Peptide ligand binding properties of the corticotropin-releasing factor (CRF) type 2 receptor: pharmacology of endogenously expressed receptors, G-protein-coupling sensitivity and determinants of CRF2 receptor selectivity. *Peptides.* **26(3):**457-70.

Holm C, Osterlund T, Laurell H, Contreras JA. (2000) Molecular mechanisms regulating hormone-sensitive lipase and lipolysis. *Annu Rev Nutr*. **20**:365-93

Holmes KD, Babwah AV, Dale LB, Poulter MO, Ferguson SS. (2006) Differential regulation of corticotropin releasing factor 1alpha receptor endocytosis and trafficking by beta-arrestins and Rab GTPases. *J Neurochem.* **96(4):**934-49.

Houslay MD, Baillie GS. (2003) The role of ERK2 docking and phosphorylation of PDE4 cAMP phosphodiesterase isoforms in mediating cross-talk between the cAMP and ERK signalling pathways. *Biochem Soc Trans*.**31(Pt 6):**1186-90.

Hsu SY, Hsueh AJ. (2001) Human stresscopin and stresscopin-related peptide are selective ligands for the type 2 corticotropin-releasing hormone receptor. *Nat Med.* **7(5):**605-11.

Huising MO, Vaughan JM, Grillot K, Shah S, Flik G, Vale WV (2007) CRF and Urocortin 1 Require Different Contact Sites for High Affinity Binding to CRF-Binding Protein (CRF-BP). [P3-63] 89th annual meeting, endo 07, toronto-june 2-5.

Hupfeld CJ, Resnik JL, Ugi S, Olefsky JM. (2005) Insulin-induced beta-arrestin1 Ser-412 phosphorylation is a mechanism for desensitization of ERK activation by Galphai-coupled receptors. *J Biol Chem.* **280(2):**1016-23.

Inglese J, Koch WJ, Caron MG, Lefkowitz RJ.(1992) Isoprenylation in regulation of signal transduction by G-protein-coupled receptor kinases. *Nature*.**359(6391):**147-50.

Jahn O, Eckart K, Brauns O, Tezval H, Spiess J. (2002) The binding protein of corticotropin-releasing factor: ligand-binding site and subunit structure. *Proc Natl Acad Sci U S A.* **99(19):**12055-60.

Jezek P, Orosz DE, Modriansky M, Garlid KD. (1994) Transport of anions and protons by the mitochondrial uncoupling protein and its regulation by nucleotides and fatty acids. A new look at old hypotheses. *J Biol Chem.* **269(42):**26184-90.

Jezek P, Hanus J, Semrad C, Garlid KD.(1996) Photoactivated azido fatty acid irreversibly inhibits anion and proton transport through the mitochondrial uncoupling protein.*J Biol Chem.* **271(11):**6199-205.

Jezova D, Ochedalski T, Glickman M, Kiss A, Aguilera G.(1999) Central corticotropin-releasing hormone receptors modulate hypothalamic-pituitary-adrenocortical and sympathoadrenal activity during stress. *Neuroscience.* **94(3):**797-802.

Jones SA, Challis JR. (1989) Local stimulation of prostaglandin production by corticotropin-releasing hormone in human fetal membranes and placenta. *Biochem Biophys Res Commun*.**159(1):**192-9.

Karalis K, Goodwin G, Majzoub JA. (1996) Cortisol blockade of progesterone: a

possible molecular mechanism involved in the initiation of human labor. *Nat Med.* **2(5):**556-60.

Karin M, Ben-Neriah Y. (2000) Phosphorylation meets ubiquitination: the control of NF-[kappa]B activity. *Annu Rev Immunol*. **18**:621-63.

Kalra SP, Dube MG, Pu S, Xu B, Horvath TL, Kalra PS. (1999) Interacting appetite-regulating pathways in the hypothalamic regulation of body weight. *Endocr Rev.* **20(1):**68-100

Karteris E, Vatish M, Hillhouse EW, Grammatopoulos DK.(2005) Preeclampsia is associated with impaired regulation of the placental nitric oxide-cyclic guanosine monophosphate pathway by corticotropin-releasing hormone (CRH) and CRH-related peptides. *J Clin Endocrinol Metab.* **90(6):**3680-7.

Karteris E, Hillhouse EW, Grammatopoulos D.(2004) Urocortin II is expressed in human pregnant myometrial cells and regulates myosin light chain phosphorylation: potential role of the type-2 corticotropin-releasing hormone receptor in the control of myometrial contractility. *Endocrinology.* **145(2):**890-900.

Karteris E, Goumenou A, Koumantakis E, Hillhouse EW, Grammatopoulos DK. (2003) Reduced expression of corticotropin-releasing hormone receptor type-1 alpha in human preeclamptic and growth-restricted placentas. *J Clin Endocrinol Metab.* **88(1):**363-70.

Karteris E, Randeva HS, Grammatopoulos DK, Jaffe RB, Hillhouse EW. (2001a) Expression and coupling characteristics of the CRH and orexin type 2 receptors in human fetal adrenals. *J Clin Endocrinol Metab. 86(9):*4512-9.

Karteris E, Grammatopoulos DK, Randeva HS, Hillhouse EW.(2001b) The role of

corticotropin-releasing hormone receptors in placenta and fetal membranes during human pregnancy. *Mol Genet Metab.* **72(4):**287-96.

Karteris E, Grammatopoulos D, Randeva H, Hillhouse EW. (2000) Signal transduction characteristics of the corticotropin-releasing hormone receptors in the feto-placental unit. *J Clin Endocrinol Metab.* **85(5):**1989-96.

Karteris E, Grammatopoulos D, Dai Y, Olah KB, Ghobara TB, Easton A, Hillhouse EW.(1998) The human placenta and fetal membranes express the corticotropin-releasing hormone receptor 1alpha (CRH-1alpha) and the CRH-C variant receptor. *J Clin Endocrinol Metab.* **83(4):**1376-9

.

Kenakin T. (1997) Agonist-specific receptor conformations. *Trends Pharmacol Sci.* **18(11):**416-7.

Kirchhausen T. (1999) Adaptors for clathrin-mediated traffic. *Annu Rev Cell Dev Biol*. **15**:705-32.

Kopp EB, Ghosh S. (1995) NF-kappa B and rel proteins in innate immunity.*Adv Immunol*.**58**:1-27.

Kohout TA and Lefkowitz RJ. (2003) Regulation of G protein-coupled receptor kinases and arrestins during receptor desensitization. *Mol. Pharmacol.* **63(1):**9-18

Korebrits C, Ramirez MM, Watson L, Brinkman E, Bocking AD, Challis JR. (1998) Maternal corticotropin-releasing hormone is increased with impending preterm birth. *J Clin Endocrinol Metab.* **83(5):**1585-91.

Kostich WA, Chen A, Sperle K, Largent BL. (1998)Molecular identification and

analysis of a novel human corticotropin-releasing factor (CRF) receptor: the CRF2gamma receptor. *Mol Endocrinol*. **12(8):**1077-85.

Kotz CM, Wang C, Levine AS, Billington CJ. (2002) Urocortin in the hypothalamic PVN increases leptin and affects uncoupling proteins-1 and -3 in rats. *Am J Physiol Regul Integr Comp Physiol.* **282(2):**R546-51.

Kozasa T, Jiang X, Hart MJ, Sternweis PM, Singer WD, Gilman AG, Bollag G, Sternweis PC. (1998) p115 RhoGEF, a GTPase activating protein for Galpha12 and Galpha13. *Science.* **280(5372):**2109-11.

Krappmann D, Hatada EN, Tegethoff S, Li J, Klippel A, Giese K, Baeuerle PA, Scheidereit C. (2000) The I kappa B kinase (IKK) complex is tripartite and contains IKK gamma but not IKAP as a regular component. *J Biol Chem.* **275(38):**29779-87.

Kraetke O, Wiesner B, Eichhorst J, Furkert J, Bienert M, Beyermann M. (2005) Dimerization of corticotropin-releasing factor receptor type 1 is not coupled to ligand binding. *J Recept Signal Transduct Res.* **25(4-6):**251-76.

Kunapuli P, Benovic JL. (1993) Cloning and expression of GRK5: a member of the G protein-coupled receptor kinase family. *Proc Natl Acad Sci U S A*. **90(12):**5588-92.

Kunapuli P, Gurevich VV, Benovic JL. (1994b) Phospholipid-stimulated autophosphorylation activates the G protein-coupled receptor kinase GRK5. *J Biol Chem*.**269(14):**10209-12.

Ladds G, Davis K, Hillhouse EW, Davey J. (2003) Modified yeast cells to investigate the coupling of G protein-coupled receptors to specific G proteins. *Mol Microbiol*.**47(3):**781-92.

Laporte SA, Oakley RH, Zhang J, Holt JA, Ferguson SS, Caron MG, Barak LS. (1999) The beta2-adrenergic receptor/betaarrestin complex recruits the clathrin adaptor AP-2 during endocytosis. *Proc Natl Acad Sci U S A.* **96(7):**3712-7

Lawrence KM, Latchman DS. (2006) The Urocortins: mechanisms of cardioprotection and therapeutic potential. *Mini Rev Med Chem.* **6(10):**1119-26.

Lee KB, Pals-Rylaarsdam R, Benovic JL, Hosey MM. (1998) Arrestin-independent internalization of the m1, m3, and m4 subtypes of muscarinic cholinergic receptors. *J Biol Chem.* **273(21):**12967-72.

Lenardo MJ, Baltimore D. (1989) NF-kappa B: a pleiotropic mediator of inducible and tissue-specific gene control. *Cell.* **58(2):**227-9.

Lewis K, Li C, Perrin MH, Blount A, Kunitake K, Donaldson C, Vaughan J, Reyes TM, Gulyas J, Fischer W, Bilezikjian L, Rivier J, Sawchenko PE, Vale WW. (2001) Identification of urocortin III, an additional member of the corticotropin-releasing factor (CRF) family with high affinity for the CRF2 receptor. *Proc Natl Acad Sci U S A.* **98(13):**7570-5

Li C, Chen P, Vaughan J, Blount A, Chen A, Jamieson PM, Rivier J, Smith MS, Vale W. (2003) Urocortin III is expressed in pancreatic beta-cells and stimulates insulin and glucagon secretion. *Endocrinology.* **144(7):**3216-24.

Lin FT, Krueger KM, Kendall HE, Daaka Y, Fredericks ZL, Pitcher JA, Lefkowitz RJ. (1997) Clathrin-mediated endocytosis of the beta-adrenergic receptor is regulated by phosphorylation/dephosphorylation of beta-arrestin1. *J Biol Chem.* **272(49):**31051-7.

Lin FT, Miller WE, Luttrell LM, Lefkowitz RJ. (1999) Feedback regulation of beta-arrestin1 function by extracellular signal-regulated kinases. *J Biol Chem.* **274(23):**15971-4.

Lin FT, Chen W, Shenoy S, Cong M, Exum ST, Lefkowitz RJ.(2002) Phosphorylation of beta-arrestin2 regulates its function in internalization of beta(2)-adrenergic receptors. *Biochemistry.* **41(34):**10692-9.

Lindstrom TM, Bennett PR.(2005) The role of nuclear factor kappa B in human labour. *Reproduction.* **130(5):**569-81.

Linton EA, Woodman JR, Asboth G, Glynn BP, Plested CP, Bernal AL.(2001) Corticotrophin releasing hormone: its potential for a role in human myometrium. *Exp Physiol*. **86(2):**273-81.

Linton EA, Behan DP, Saphier PW, Lowry PJ. (1990)Corticotropin-releasing hormone (CRH)-binding protein: reduction in the adrenocorticotropin-releasing activity of placental but not hypothalamic CRH. *J Clin Endocrinol Metab.* **70(6):**1574-80.

Lohse MJ, Benovic JL, Codina J, Caron MG, Lefkowitz RJ. (1990) beta-Arrestin: a protein that regulates beta-adrenergic receptor function. *Science.* **248(4962):**1547-50.

Lohse MJ. (1993) Molecular mechanisms of membrane receptor desensitization. *Biochim Biophys Acta.* **1179(2):**171-88.

Londos C, Brasaemle DL, Gruia-Gray J, Servetnick DA, Schultz CJ, Levin DM, Kimmel AR. Perilipin: unique proteins associated with intracellular neutral lipid droplets in adipocytes and steroidogenic cells. Biochem Soc Trans. 1995

Aug;23(3):611-5. Review.

Lorenz W, Inglese J, Palczewski K, Onorato JJ, Caron MG, Lefkowitz RJ. (1991) The receptor kinase family: primary structure of rhodopsin kinase reveals similarities to the beta-adrenergic receptor kinase. *Proc Natl Acad Sci U S A*. **88(19):**8715-9

Lovenberg TW, Liaw CW, Grigoriadis DE, Clevenger W, Chalmers DT, De Souza EB, Oltersdorf T. (1995) Cloning and characterization of a functionally distinct corticotropin-releasing factor receptor subtype from rat brain. *Proc Natl Acad Sci U S A.* **92(3):**836-40.

Lovenberg TW, Chalmers DT, Liu C, De Souza EB. (1995) CRF2 alpha and CRF2 beta receptor mRNAs are differentially distributed between the rat central nervous system and peripheral tissues. *Endocrinology.* **136(9):**4139-42.

Lowell BB, Flier JS. (1997) Brown adipose tissue, beta 3-adrenergic receptors, and obesity. *Annu Rev Med.* **48:**307-16.

Lowell BB, S-Susulic V, Hamann A, Lawitts JA, Himms-Hagen J, Boyer BB, Kozak LP, Flier JS.(1993) Development of obesity in transgenic mice after genetic ablation of brown adipose tissue. *Nature*. **366(6457):**740-2.

Luttrell LM, Lefkowitz RJ. (2002) The role of beta-arrestins in the termination and transduction of G-protein-coupled receptor signals. *J Cell Sci.* **115(Pt 3):**455-65

Malbon CC, Tao J, Shumay E, Wang HY. (2004) AKAP (A-kinase anchoring protein) domains: beads of structure-function on the necklace of G-protein signalling. *Biochem Soc Trans.* **32(Pt 5):**861-4.

Markovic D, Vatish M, Gu M, Slater D, Newton R, Lehnert H, Grammatopoulos DK. (2007a) The onset of labor alters corticotropin-releasing hormone type 1 receptor variant expression in human myometrium: putative role of interleukin-1beta. *Endocrinology.* **148(7):**3205-13.

Markovic D, Papadopoulou N, Teli T, Randeva H, Levine MA, Hillhouse EW, Grammatopoulos DK. (2006) Differential responses of corticotropin-releasing hormone receptor type 1 variants to protein kinase C phosphorylation. *J Pharmacol Exp Ther.* **319(3):**1032-42.

Maya-Nunez G, Castro-Fernandez C, Mendez JP.(2005) CRH-stimulation of cyclic adenosine 5'-monophosphate pathway is partially inhibited by the coexpression of CRH-R1 and CRH-R2alpha. *Endocrine.* **27(1):**67-73.

McDonald PH, Chow CW, Miller WE, Laporte SA, Field ME, Lin FT, Davis RJ, Lefkowitz RJ.(2000) Beta-arrestin 2: a receptor-regulated MAPK scaffold for the activation of JNK3. *Science.***290(5496):**1574-7

McEvoy AN, Bresnihan B, Fitzgerald O, Murphy EP.(2002) Corticotropin-releasing hormone signaling in synovial tissue vascular endothelium is mediated through the cAMP/CREB pathway. *Ann N Y Acad Sci.* **966**:119-30.

McLean M, Bisits A, Davies J, Woods R, Lowry P, Smith R.A (1995) A placental clock controlling the length of human pregnancy. *Nat Med.* **1(5):**460-3.

Mesiano S, Jaffe RB. (1997) Developmental and functional biology of the primate fetal adrenal cortex. *Endocr Rev.* **18(3):**378-403.

Meyer AH, Ullmer C, Schmuck K, Morel C, Wishart W, Lübbert H, Engels P. (1997) Localization of the human CRF2 receptor to 7p21-p15 by radiation hybrid

mapping and FISH analysis. *Genomics.* **40(1):**189-90

Mignot TM, Paris B, Carbonne B, Vauge C, Ferre F, Vaiman D.(2005) Corticotropin-releasing hormone effects on human pregnant vs. nonpregnant myometrium explants estimated from a mathematical model of uterine contraction. *J Appl Physiol.* **99(3):**1157-63.

Miller JW (2004) Tracking G protein-coupled receptor trafficking using Odyssey imaging. Published August by LI-COR Biosciences

(http://www.licor.com/bio/PDF/Miller_GPCR.pdf accession date Jan 12 2007)

Muhle RA, Pavlidis P, Grundy WN, Hirsch E.A (2001) A high-throughput study of gene expression in preterm labor with a subtractive microarray approach. *Am J Obstet Gynecol.* **185(3):**716-24

Munford RS (2004) Immune-Endocrine Interactions, *Textbook of Endocrine Physiology;* 89-101, Oxford University Press, USA

Murakami A, Yajima T, Sakuma H, McLaren MJ, Inana G. (1993) X-arrestin: a new retinal arrestin mapping to the X chromosome. *FEBS Lett.* **334(2):**203-9

Murthy KS, Zhou H, Grider JR, Makhlouf GM. (2003) Inhibition of sustained smooth muscle contraction by PKA and PKG preferentially mediated by phosphorylation of RhoA. *Am J Physiol Gastrointest Liver Physiol.* **284(6):**G1006-16.

Newton R, Seybold J, Kuitert LM, Bergmann M, Barnes PJ. (1998) Repression of cyclooxygenase-2 and prostaglandin E2 release by dexamethasone occurs by transcriptional and post-transcriptional mechanisms involving loss of

polyadenylated mRNA. *J Biol Chem.* **273(48):**32312-21.

Nnodim JO, Lever JD. (1988) Neural and vascular provisions of rat interscapular brown adipose tissue. *Am J Anat.* **182(3):**283-93.

Oakley RH, Olivares-Reyes JA, Hudson CC, Flores-Vega F, Dautzenberg FM, Hauger RL. (2007) Carboxyl-terminal and intracellular loop sites for CRF1 receptor phosphorylation and beta-arrestin-2 recruitment: a mechanism regulating stress and anxiety responses. *Am J Physiol Regul Integr Comp Physiol.* **293(1):**R209-22.

Oakley RH, Laporte SA, Holt JA, Barak LS, Caron MG. (2001) Molecular determinants underlying the formation of stable intracellular G protein-coupled receptor-beta-arrestin complexes after receptor endocytosis. *J Biol Chem.* **276(22):**19452-60.

Oakley RH, Laporte SA, Holt JA, Caron MG, Barak LS. (2000) Differential affinities of visual arrestin, beta arrestin1, and beta arrestin2 for G protein-coupled receptors delineate two major classes of receptors. *J Biol Chem*.**275(22):**17201-10.

Ojeda SR (2004) The Anterior Pituitary and Hypothalamus, *Textbook of Endocrine Physiology;* 120-147 Oxford University Press, USA

Orth DN, Mount CD.Specific (1987) A high-affinity binding protein for human corticotropin-releasing hormone in normal human plasma. *Biochem Biphys Res Commun.* **143(2):**411-7.

Pahl HL. (1999) Activators and target genes of Rel/NF-kappaB transcription factors. *Oncogene.* **18(49):**6853-66.

Papadopoulou N, Chen J, Randeva HS, Levine MA, Hillhouse EW, Grammatopoulos DK. (2004) Protein kinase A-induced negative regulation of the corticotropin-releasing hormone R1alpha receptor-extracellularly regulated kinase signal transduction pathway: the critical role of Ser301 for signaling switch and selectivity. *Mol Endocrinol.* **18(3):**624-39.

Pande V, Ramos MJ.(2005) NF-kappaB in human disease: current inhibitors and prospects for de novo structure based design of inhibitors. *Curr Med Chem*. **12(3):**357-74.

Parham KL, Zervou S, Karteris E, Catalano RD, Old RW, Hillhouse EW. (2004) Promoter analysis of human corticotropin-releasing factor (CRF) type 1 receptor and regulation by CRF and urocortin. *Endocrinology.* **145(8):**3971-83.

Perona R, Montaner S, Saniger L, Sanchez-Perez I, Bravo R, Lacal JC. (1997) Activation of the nuclear factor-kappaB by Rho, CDC42, and Rac-1 proteins. *Genes Dev.* **11(4):**463-75.

Perrin M, Donaldson C, Chen R, Blount A, Berggren T, Bilezikjian L, Sawchenko P, Vale W. (1995) Identification of a second corticotropin-releasing factor receptor gene and characterization of a cDNA expressed in heart. *Proc Natl Acad Sci U S A.* **92(7):**2969-73.

Perrin MH, Sutton SW, Cervini LA, Rivier JE, Vale WW. (1999) Comparison of an agonist, urocortin, and an antagonist, astressin, as radioligands for characterization of corticotropin-releasing factor receptors. *J Pharmacol Exp Ther.* **288(2):**729-34.

Perry SJ, Junger S, Kohout TA, Hoare SR, Struthers RS, Grigoriadis DE, Maki RA (2005). Distinct conformations of the corticotropin releasing factor type 1 receptor adopted following agonist and antagonist binding are differentially regulated.

J Biol Chem. **280(12):**11560-8.

Perry SJ, Baillie GS, Kohout TA, McPhee I, Magiera MM, Ang KL, Miller WE, McLean AJ, Conti M, Houslay MD, Lefkowitz RJ. (2002) Targeting of cyclic AMP degradation to beta 2-adrenergic receptors by beta-arrestins. *Science*. **298(5594):**834-6.

Perry SJ, Junger S, Kohout TA, Hoare SR, Struthers RS, Grigoriadis DE, Maki RA (2005). Distinct conformations of the corticotropin releasing factor type 1 receptor adopted following agonist and antagonist binding are differentially regulated. *J Biol Chem.* **280(12):**11560-8.

Petraglia F, Benedetto C, Florio P, D'Ambrogio G, Genazzani AD, Marozio L, Vale W.(1995) Effect of corticotropin-releasing factor-binding protein on prostaglandin release from cultured maternal decidua and on contractile activity of human myometrium in vitro. *J Clin Endocrinol Metab*. **80(10):**3073-6.

Pisarchik A, Slominski A. (2002) Corticotropin releasing factor receptor type 1: molecular cloning and investigation of alternative splicing in the hamster skin. *J Invest Dermatol.***118(6):**1065-72.

Pisarchik A, Slominski AT. (2001) Alternative splicing of CRH-R1 receptors in human and mouse skin: identification of new variants and their differential expression. *FASEB J.* **15(14):**2754-6.

Pitcher JA, Inglese J, Higgins JB, Arriza JL, Casey PJ, Kim C, Benovic JL, Kwatra MM, Caron MG, Lefkowitz RJ.(1992) Role of beta gamma subunits of G proteins in targeting the beta-adrenergic receptor kinase to membrane-bound receptors. *Science*. **257(5074):**1264-7.

Pitcher JA, Payne ES, Csortos C, DePaoli-Roach AA, Lefkowitz RJ. (1995) The G-protein-coupled receptor phosphatase: a protein phosphatase type 2A with a distinct subcellular distribution and substrate specificity. *Proc Natl Acad Sci U S A.* **92(18):**8343-7.

Pomerantz JL, Baltimore D. (1999) NF-kappaB activation by a signaling complex containing TRAF2, TANK and TBK1, a novel IKK-related kinase. *EMBO J.* **18(23):**6694-704.

Potter E, Sutton S, Donaldson C, Chen R, Perrin M, Lewis K, Sawchenko PE, Vale W.(1994) Distribution of corticotropin-releasing factor receptor mRNA expression in the rat brain and pituitary. *Proc Natl Acad Sci U S A.* **91(19):**8777-81.

Premont RT, Koch WJ, Inglese J, Lefkowitz RJ.(1994) Identification, purification, and characterization of GRK5, a member of the family of G protein-coupled receptor kinases. *J Biol Chem*. **269(9):**6832-41.

Punn A, Levine MA, Grammatopoulos DK. (2006) Identification of signaling molecules mediating corticotropin-releasing hormone-R1alpha-mitogen-activated protein kinase (MAPK) interactions: the critical role of phosphatidylinositol 3-kinase in regulating ERK1/2 but not p38 MAPK activation. *Mol Endocrinol*. **20(12):**3179-95.

Rasmussen TN, Novak I, Nielsen SM. (2004) Internalization of the human CRF receptor 1 is independent of classical phosphorylation sites and of beta-arrestin 1 recruitment. *Eur J Biochem.* **271(22):**4366-74

Reiter E and Lefkowitz RJ (2006) GRKs and beta-arrestins: roles in receptor silencing, trafficking and signalling. *Trends Endocrinol. Metab*. **17(4)**:159-65

Reyes TM, Lewis K, Perrin MH, Kunitake KS, Vaughan J, Arias CA, Hogenesch JB, Gulyas J, Rivier J, Vale WW, Sawchenko PE. (2001) Urocortin II: a member of the corticotropin-releasing factor (CRF) neuropeptide family that is selectively bound by type 2 CRF receptors. *Proc Natl Acad Sci U S A.* **98(5):**2843-8.

Ricquier D, Bouillaud F, Toumelin P, Mory G, Bazin R, Arch J, Penicaud L. (1986) Expression of uncoupling protein mRNA in thermogenic or weakly thermogenic brown adipose tissue. Evidence for a rapid beta-adrenoreceptor-mediated and transcriptionally regulated step during activation of thermogenesis *J Biol Chem*. **261(30):**13905-10

Rivest S, Deshaies Y, Richard D. (1989) Effects of corticotropin-releasing factor on energy balance in rats are sex dependent. *Am J Physiol.* **257(6 Pt 2):**R1417-22.

Rodbell M, (1964) Metabolism of isolated fat cells: Effects of hormones on glucose metabolism and lipolysis. *J Biol Chem.* **239:**375-80.

Romashkova JA, Makarov SS. (1999) NF-kappaB is a target of AKT in anti-apoptotic PDGF signalling. *Nature*. **401(6748):**86-90.

Rothwell NJ. (1989) CRF is involved in the pyrogenic and thermogenic effects of interleukin 1 beta in the rat. *Am J Physiol.* **256(1 Pt 1):**E111-5.

Roux PP, Blenis J.(2004) ERK and p38 MAPK-activated protein kinases: a family of protein kinases with diverse biological functions. *Microbiol Mol Biol Rev*.**68(2):**320-44.

Samaj J, Baluska F, Voigt B, Schlicht M, Volkmann D, Menzel D.(2004) Endocytosis, actin cytoskeleton, and signaling. *Plant Physiol*. **135(3):**1150-61.

Sananbenesi F, Fischer A, Schrick C, Spiess J, Radulovic J.(2003) Mitogen-activated protein kinase signaling in the hippocampus and its modulation by corticotropin-releasing factor receptor 2: a possible link between stress and fear memory. *J Neurosci.* **23(36):**11436-43.

Sanz E, Monge L, Fernandez N, Climent B, Dieguez G, Garcia-Villalon AL. (2003) Mechanisms of relaxation by urocortin in renal arteries from male and female rats. *Br J Pharmacol.* **140(5):**1003-7.

Sato H, Nagashima Y, Chrousos GP, Ichihashi M, Funasak Y. (2002) The expression of corticotropin-releasing hormone in melanoma. *Pigment Cell Res*. **15(2):**98-103

Sawchenko PE, Arias C. (1995) Evidence for short-loop feedback effects of ACTH on CRF and vasopressin expression in parvocellular neurosecretory neurons. *J Neuroendocrinol.* **7(9):**721-31

Schwartz MW, Baskin DG, Kaiyala KJ, Woods SC. (1999) Model for the regulation of energy balance and adiposity by the central nervous system. *Am J Clin Nutr.* **69(4):**584-96.

Seachrist JL, Anborgh PH, Ferguson SS.(2000) beta 2-adrenergic receptor internalization, endosomal sorting, and plasma membrane recycling are regulated by rab GTPases. *J Biol Chem.* **275(35):**27221-8.

Seck T, Pellegrini M, Florea AM, Grignoux V, Baron R, Mierke DF, Horne WC.(2005) The delta e13 isoform of the calcitonin receptor forms a six-transmembrane domain receptor with dominant-negative effects on receptor surface expression and signaling. *Mol Endocrinol.* **19(8):**2132-44.

Seck T, Baron R, Horne WC.(2003) The alternatively spliced deltae13 transcript of the rabbit calcitonin receptor dimerizes with the C1a isoform and inhibits its surface expression. *J Biol Chem.* **278(25):**23085-93.

Sen R, Baltimore D. (1986) Multiple nuclear factors interact with the immunoglobulin enhancer sequences. *Cell.* **46(5):**705-16.

Seres J, Bornstein SR, Seres P, Willenberg HS, Schulte KM, Scherbaum WA, Ehrhart-Bornstein M. (2004) Corticotropin-releasing hormone system in human adipose tissue. *J Clin Endocrinol Metab.* **89(2):**965-70.

Shen WJ, Sridhar K, Bernlohr DA, Kraemer FB. (1999) Interaction of rat hormone-sensitive lipase with adipocyte lipid-binding protein. *Proc Natl Acad Sci U S A.* **96(10):**5528-32.

Shenoy SK, Lefkowitz RJ. (2003) Trafficking patterns of beta-arrestin and G protein-coupled receptors determined by the kinetics of beta-arrestin deubiquitination. *J Biol Chem.* **278(16):**14498-506.

Shyu JF, Inoue D, Baron R, Horne WC. (1996) The deletion of 14 amino acids in the seventh transmembrane domain of a naturally occurring calcitonin receptor isoform alters ligand binding and selectively abolishes coupling to phospholipase C.*J Biol Chem*. **271(49):**31127-34

Sibley DR, Strasser RH, Benovic JL, Daniel K, Lefkowitz RJ. (1986) Phosphorylation/dephosphorylation of the beta-adrenergic receptor regulates its functional coupling to adenylate cyclase and subcellular distribution. *Proc Natl Acad Sci U S A.* **83(24):**9408-12.

Siebenlist U, Franzoso G, Brown K. (1994) Structure, regulation and function of

NF-kappaB. *Annu Rev Cell Biol*. **10:**405-55.

Simon MI, Strathmann MP, Gautam N. (1991) Diversity of G proteins in signal transduction. *Science*. **252(5007):**802-8.

Simoncini T, Apa R, Reis FM, Miceli F, Stomati M, Driul L, Lanzone A, Genazzani AR, Petraglia F. (1999) Human umbilical vein endothelial cells: a new source and potential target for corticotropin-releasing factor. *J Clin Endocrinol Metab.* **84(8):**2802-6.

Shenoy SK, McDonald PH, Kohout TA, Lefkowitz RJ.(2001) Regulation of receptor fate by ubiquitination of activated beta 2-adrenergic receptor and beta-arrestin. *Science.* **294(5545):**1307-13.

Shinohara T, Dietzschold B, Craft CM, Wistow G, Early JJ, Donoso LA, Horwitz J, Tao R. (1987) Primary and secondary structure of bovine retinal S antigen (48-kDa protein). *Proc Natl Acad Sci U S A.* **84(20):**6975-9.

Solinas G, Summermatter S, Mainieri D, Gubler M, Montani JP, Seydoux J, Smith SR, Dulloo AG. (2006) Corticotropin-releasing hormone directly stimulates thermogenesis in skeletal muscle possibly through substrate cycling between de novo lipogenesis and lipid oxidation. *Endocrinology.* **147(1):**31-8.

Slominski A, Ermak G, Mazurkiewicz JE, Baker J, Wortsman J.(1998) Characterization of corticotropin-releasing hormone (CRH) in human skin. *J Clin Endocrinol Metab.* **83(3):**1020-4.

Slominski A, Ermak G, Hwang J, Chakraborty A, Mazurkiewicz JE, Mihm M.(1995) Proopiomelanocortin, corticotropin releasing hormone and corticotropin releasing hormone receptor genes are expressed in human skin. *FEBS Lett.* **374(1):**113-6.

Soloff MS, Cook DL Jr, Jeng YJ, Anderson GD.(2004) In situ analysis of interleukin-1-induced transcription of cox-2 and il-8 in cultured human myometrial cells. *Endocrinology.* **145(3):**1248-54.

Smith RD, Hunyady L, Olivares-Reyes JA, Mihalik B, Jayadev S, Catt KJ. (1998) Agonist-induced phosphorylation of the angiotensin AT1a receptor is localized to a serine/threonine-rich region of its cytoplasmic tail. *Mol Pharmacol.* **54(6):**935-41.

Smith SR, de Jonge L, Pellymounter M, Nguyen T, Harris R, York D, Redmann S, Rood J, Bray GA. (2001) Peripheral administration of human corticotropin-releasing hormone: a novel method to increase energy expenditure and fat oxidation in man. *J Clin Endocrinol Metab.* **86(5):**1991-8.

Somlyo AP, Somlyo AV. (2003) Ca2+ sensitivity of smooth muscle and nonmuscle myosin II: modulated by G proteins, kinases, and myosin phosphatase. *Physiol Rev.* **83(4):**1325-58.

Sooranna SR, Engineer N, Loudon JA, Terzidou V, Bennett PR, Johnson MR. (2005) The mitogen-activated protein kinase dependent expression of prostaglandin H synthase-2 and interleukin-8 messenger ribonucleic acid by myometrial cells: the differential effect of stretch and interleukin-1{beta}. *J Clin Endocrinol Metab.* **90(6):**3517-27.

Spina M, Merlo-Pich E, Chan RK, Basso AM, Rivier J, Vale W, Koob GF. (1996) Appetite-suppressing effects of urocortin, a CRF-related neuropeptide. *Science.* **273(5281):**1561-4

Stevens MY, Challis JR, Lye SJ. (1998) Corticotropin-releasing hormone receptor subtype 1 is significantly up-regulated at the time of labor in the human myometrium. *J Clin Endocrinol Metab.* **83(11):**4107-15

Stoffel RH, Randall RR, Premont RT, Lefkowitz RJ, Inglese J.(1994) Palmitoylation of G protein-coupled receptor kinase, GRK6. Lipid modification diversity in the GRK family. *J Biol Chem.* **269(45):**27791-4.

Stoffel RH 3rd, Pitcher JA, Lefkowitz RJ. (1997) Targeting G protein-coupled receptor kinases to their receptor substrates. *J Membr Biol.* **157(1):**1-8.

Stoffel RH, Inglese J, Macrae AD, Lefkowitz RJ, Premont RT. (1998) Palmitoylation increases the kinase activity of the G protein-coupled receptor kinase, GRK6. *Biochemistry.* **37(46):**16053-9.

Suda T, Tozawa F, Dobashi I, Horiba N, Ohmori N, Yamakado M, Yamada M, Demura H.(1993) Corticotropin-releasing hormone, proopiomelanocortin, and glucocorticoid receptor gene expression in adrenocorticotropin-producing tumors in vitro. *J Clin Invest.* **92(6):**2790-5.

Sun Y, Cheng Z, Ma L, Pei G. (2002) Beta-arrestin2 is critically involved in CXCR4-mediated chemotaxis, and this is mediated by its enhancement of p38 MAPK activation. *J Biol Chem.* **277(51):**49212-9.

Swanson LW, Sawchenko PE, Lind RW. (1986) Regulation of multiple peptides in CRF parvocellular neurosecretory neurons: implications for the stress response. *Prog Brain Res*. **68:**169-90.

Tansey JT, Sztalryd C, Hlavin EM, Kimmel AR, Londos C. (2004) The central role of perilipin a in lipid metabolism and adipocyte lipolysis. *IUBMB Life*. **56(7):**379-85.

Tebar F, Soley M, Ramirez I. (1996) The antilipolytic effects of insulin and

epidermal growth factor in rat adipocytes are mediated by different mechanisms. *Endocrinology.***137(10):**4181-8.

Teli T, Markovic D, Levine MA, Hillhouse EW, Grammatopoulos DK. (2005) Regulation of corticotropin-releasing hormone receptor type 1alpha signaling: structural determinants for G protein-coupled receptor kinase-mediated phosphorylation and agonist-mediated desensitization. *Mol Endocrinol.* **19(2):**474-90.

Tjuvajev J, Kolesnikov Y, Joshi R, Sherinski J, Koutcher L, Zhou Y, Matei C, Koutcher J, Kreek MJ, Blasberg R.(1998) Anti-neoplastic properties of human corticotropin releasing factor: involvement of the nitric oxide pathway. *In Vivo.* **12(1):**1-10.

Tohgo A, Pierce KL, Choy EW, Lefkowitz RJ, Luttrell LM. (2002) beta-Arrestin scaffolding of the ERK cascade enhances cytosolic ERK activity but inhibits ERK-mediated transcription following angiotensin AT1a receptor stimulation. *J Biol Chem.* **277(11):**9429-36.

Touhara K, Inglese J, Pitcher JA, Shaw G, Lefkowitz RJ.(1994) Binding of G protein beta gamma-subunits to pleckstrin homology domains. *J Biol Chem.* **269(14):**10217-20.

Tsigos C, Chrousos (2002) GP.Hypothalamic-pituitary-adrenal axis, neuroendocrine factors and stress. *J Psychosom Res.* **53(4):**865-71.

Tu H, Kastin AJ, Pan W. (2007) Corticotropin-releasing hormone receptor (CRHR)1 and CRHR2 are both trafficking and signaling receptors for urocortin. Mol Endocrinol. **21(3):**700-11.

Turnbull AV, Rivier C.(1997) Corticotropin-releasing factor (CRF) and endocrine responses to stress: CRF receptors, binding protein, and related peptides. *Proc Soc Exp Biol Med*. **215(1):**1-10.

Uehara Y, Shimizu H, Ohtani K, Sato N, Mori M.(1998) Hypothalamic corticotropin-releasing hormone is a mediator of the anorexigenic effect of leptin. *Diabetes.* **47(6):**890-3

Uehata M, Ishizaki T, Satoh H, Ono T, Kawahara T, Morishita T, Tamakawa H, Yamagami K, Inui J, Maekawa M, Narumiya S.(1997) Calcium sensitization of smooth muscle mediated by a Rho-associated protein kinase in hypertension. *Nature*. **389(6654):**990-4.

Valdenaire O, Giller T, Breu V, Gottowik J, Kilpatrick G. (1997)A new functional isoform of the human CRF2 receptor for corticotropin-releasing factor. *Biochim Biophys Acta.* **1352(2):**129-32.

Vale W, Spiess J, Rivier C, Rivier J. (1981) Characterization of a 41-residue ovine hypothalamic peptide that stimulates secretion of corticotropin and beta-endorphin. *Science*. **213(4514):**1394-7.

Vamvakopoulos NC, Sioutopoulou TO. (1994) Human corticotropin-releasing hormone receptor gene (CRHR) is located on the long arm of chromosome 17 (17q12-qter).*Chromosome Res.* **2(6):**471-3.

Vatish M, Randeva HS, Grammatopoulos DK.(2006) Hormonal regulation of placental nitric oxide and pathogenesis of pre-eclampsia. *Trends Mol Med.* **12(5):**223-33.

Vaughan J, Donaldson C, Bittencourt J, Perrin MH, Lewis K, Sutton S, Chan R,

Turnbull AV, Lovejoy D, Rivier C, et al. (1995) Urocortin, a mammalian neuropeptide related to fish urotensin I and to corticotropin-releasing factor. *Nature*. **378(6554):**287-92.

Viengchareun S, Zennaro MC, Pascual-Le Tallec L, Lombes M.(2002) Brown adipocytes are novel sites of expression and regulation of adiponectin and resistin. *FEBS Lett*. **532(3):**345-50.

Waeber G, Thompson N, Chautard T, Steinmann M, Nicod P, Pralong FP, Calandra T, Gaillard RC. (1998) Transcriptional activation of the macrophage migration-inhibitory factor gene by the corticotropin-releasing factor is mediated by the cyclic adenosine 3',5'- monophosphate responsive element-binding protein CREB in pituitary cells. *Mol Endocrinol*. **12(5):**698-705.

Wang HY, Tao J, Shumay E, Malbon CC. (2006) G-Protein-coupled receptor-associated A-kinase anchoring proteins: AKAP79 and AKAP250 (gravin). *Eur J Cell Biol*. **85(7):**643-50.

Warren WB, Gurewitsch ED, Goland RS. (1995) Corticotropin-releasing hormone and pituitary-adrenal hormones in pregnancies complicated by chronic hypertension. *Am J Obstet Gynecol.* **172(2 Pt 1):**661-6.

Weber WA. (2004) Brown adipose tissue and nuclear medicine imaging. *J Nucl Med.* **45(7):**1101-3.

Webster EL, De Souza EB. (1988) Corticotropin-releasing factor receptors in mouse spleen: identification, autoradiographic localization, and regulation by divalent cations and guanine nucleotides. *Endocrinology.* **122(2):**609-17

Webster EL, Battaglia G, De Souza EB.(1989) Functional corticotropin-releasing factor (CRF) receptors in mouse spleen: evidence from adenylate cyclase studies. *Peptides.* **10(2):**395-401.

Wellhoner P, Welzel M, Rolle D, Dodt C. (2007) In vivo effects of corticotropin-releasing hormone on femoral adipose tissue metabolism in women. *Int J Obes (Lond).* **31(4):**718-22.

Wettschureck N, Offermanns S.(2002) Rho/Rho-kinase mediated signaling in physiology and pathophysiology. *J Mol Med.* **80(10):**629-38.

Wettschureck N, Offermanns S. (2005) Mammalian G proteins and their cell type specific functions. *Physiol Rev.* **85(4):**1159-204.

Woods RJ, Kennedy KM, Gibbins JM, Behan D, Vale W, Lowry PJ. (1994) Corticotropin-releasing factor binding protein dimerizes after association with ligand. *Endocrinology.* **135(2):**768-73

Woods RJ, Kemp CF, David J, Sumner IG, Lowry PJ.(1999) Cleavage of recombinant human corticotropin-releasing factor (CRF)-binding protein produces a 27-kilodalton fragment capable of binding CRF. *J Clin Endocrinol Metab.* **84(8):**2788-94.

Xiao G, Harhaj EW, Sun SC. (2001) NF-kappaB-inducing kinase regulates the processing of NF-kappaB2 p100. *Mol Cell*. **7(2):**401-9.

Xiong Y, Xie LY, Abou-Samra AB.(1995) Signaling properties of mouse and human corticotropin-releasing factor (CRF) receptors: decreased coupling efficiency of human type II CRF receptor. *Endocrinology.* **136(5):**1828-34

Yamazaki S, Muta T, Takeshige K. (2001) A novel IkappaB protein, IkappaB-zeta, induced by proinflammatory stimuli, negatively regulates nuclear factor-kappaB in the nuclei. *J Biol Chem.* **276(29):**27657-62.

Yeaman SJ. (2004) Hormone-sensitive lipase--new roles for an old enzyme. Biochem J. **379(Pt 1):**11-22.

Young SF, Griffante C, Aguilera G. (2007) Dimerization between vasopressin v1b and corticotropin releasing hormone type 1 receptors. *Cell Mol Neurobiol.* **27(4):**439-61.

Zbytek B, Pfeffer LM, Slominski AT.(2003) Corticotropin-releasing hormone inhibits nuclear factor-kappaB pathway in human HaCaT keratinocytes. *J Invest Dermatol*.**121(6):**1496-9.

Zbytek B, Pfeffer LM, Slominski AT. (2004) Corticotropin-releasing hormone stimulates NF-kappaB in human epidermal keratinocytes. *J Endocrinol.* **181(3):**R1-7.

Zennaro MC, Le Menuet D, Viengchareun S, Walker F, Ricquier D, Lombes M. (1998) Hibernoma development in transgenic mice identifies brown adipose tissue as a novel target of aldosterone action. *J Clin Invest.* **101(6):**1254-60.

Zhang J, Barak LS, Anborgh PH, Laporte SA, Caron MG, Ferguson SS. (1999) Cellular trafficking of G protein-coupled receptor/beta-arrestin endocytic complexes. *J Biol Chem.* **274(16):**10999-1006.